Evidence-Based Complementary and Alternative Medicine

Rapid Discovery on the Material Basis of Traditional Chinese Medicine

Lead Guest Editor: Lifeng Han
Guest Editors: Li-Ping Kang, Huihui Xiao, Youcai Zhang, and Yingqiu Xie

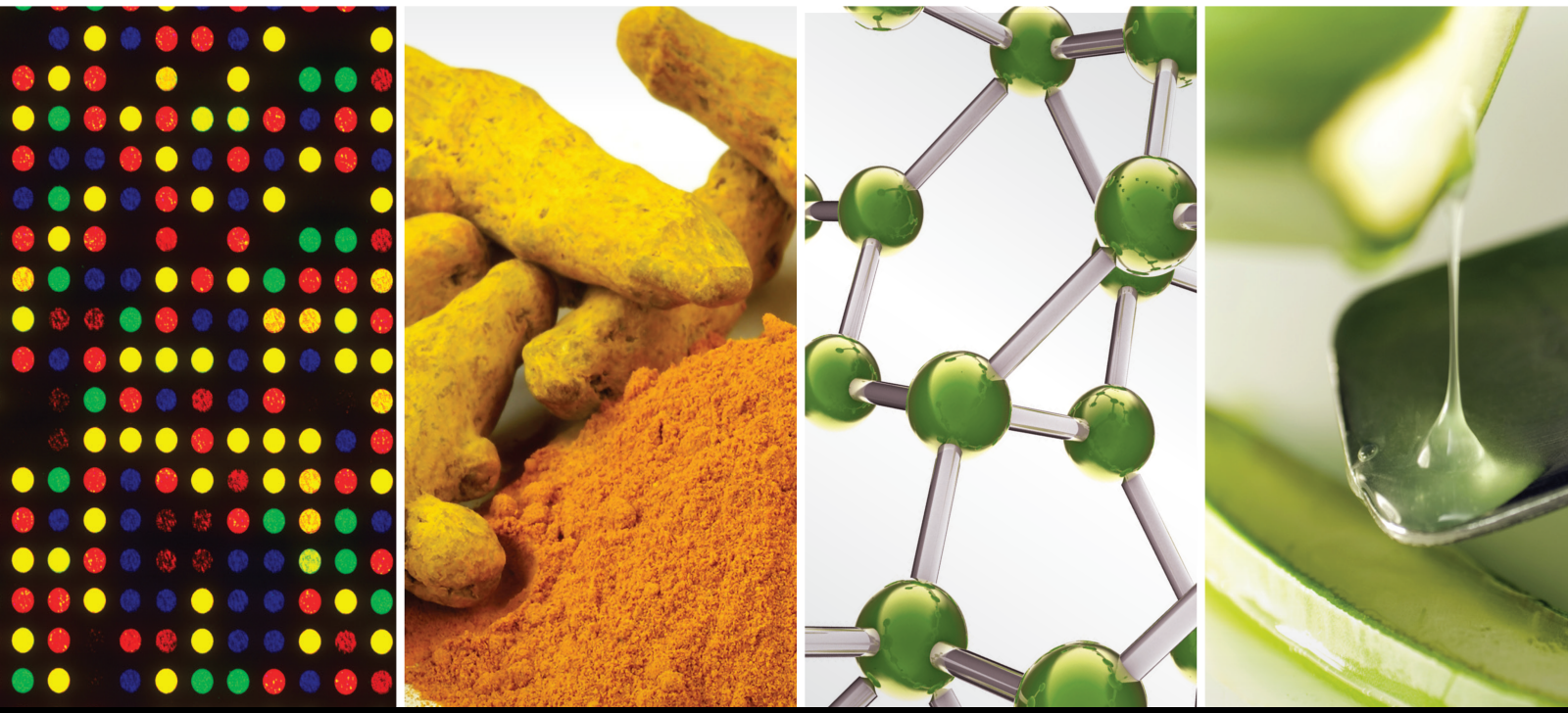

Rapid Discovery on the Material Basis of Traditional Chinese Medicine

Evidence-Based Complementary and Alternative Medicine

Rapid Discovery on the Material Basis of Traditional Chinese Medicine

Lead Guest Editor: Lifeng Han
Guest Editors: Li-Ping Kang, Huihui Xiao, Youcai Zhang, and Yingqiu Xie

Chief Editor

Associate Editors

Academic Editors

Contents

Hindawi
Evidence-Based Complementary and Alternative Medicine
Volume 2022, Article ID 2823315, 13 pages
https://doi.org/10.1155/2022/2823315

Research Article

Shenhuang Plaster Application Improves Gastrointestinal Motility in Mice with Postoperative Ileus through Intestinal Microbiota

Yanan Shi,[1] **Xiao Xu**,[1] **Ting Liu**,[1] **Rongyun Wang**,[1] **Jingming Xu**,[2] **Yujing Wu**,[1] **Bin Ding**,[3] **and Qiuhua Sun**[1]

[1]*The College of Nursing, Zhejiang Chinese Medical University, Hangzhou 310053, China*
[2]*The First Clinical Medical College, Zhejiang Chinese Medical University, Hangzhou 310053, China*
[3]*College of Life Science, Zhejiang Chinese Medical University, Hangzhou 310053, China*

Correspondence should be addressed to Bin Ding; db@zcmu.edu.cn and Qiuhua Sun; sunqiuhua@zcmu.edu.cn

Received 2 November 2021; Revised 31 January 2022; Accepted 25 February 2022; Published 8 August 2022

Academic Editor: Lifeng Han

Postoperative ileus (POI) is a common surgical complication, and its incidence remains high. Shenhuang Plaster (SHP) is a famous traditional Chinese medicine with a definite curative effect on postoperative intestinal dysfunction; however, the mechanisms involved in these effects are unclear. Accordingly, in this study, we constructed a POI mouse model and used the intestinal flora as the target to explore the regulatory effect of SHP on gastrointestinal motility. The results illustrated that SHP applied at the Shenque acupoint promoted the recovery of gastrointestinal motility, relieved intestinal villus atrophy and basal damage caused by POI, protected the integrity of intestinal tissue morphology, and alleviated the inflammatory response in the intestinal tissue of POI model mice. In addition, we clarified the role of the intestinal flora in the occurrence and development of POI, further evaluated the changes in the intestinal flora in each group of mice, and analysed the regulatory effect of SHP on the intestinal flora in mice with POI. The results suggested that SHP might improve gastrointestinal motility disorder in POI mice by effectively regulating intestinal flora.

1. Introduction

Postoperative ileus (POI) is a common complication of abdominal and nonabdominal surgery. It often manifests as various degrees of abdominal pain, abdominal distension, nausea and vomiting, and weakened or disappeared bowel sounds, and it can lead to further complications such as anastomoses and abdominal infections [1]. With the development of rapid rehabilitation surgery in recent years, POI has been considered the core component that affects patients' postoperative recovery because of the prolonged hospitalisation time and increased hospitalisation costs [2]. At present, the pathogenesis of POI is unclear. Hence, there is a lack of clinically effective treatment methods and drugs. The generally applied treatments, such as gastrointestinal decompression, anti-inflammatory rehydration, and additional nutritional supplements, are not effective [3, 4].

Intestinal inflammation is a major factor that induces POI after surgery. Intestinal surgery can induce intestinal myometrial dendritic cells to produce interleukin (IL)-12 and activate M1 macrophages [5], which can release cytokines and inflammatory mediators such as tumour necrosis factor-α (TNF-α), IL-1β, IL-6, and IL-8 and promote the migration of leukocytes to the intestinal muscle layer [6]. It has been elucidated that surgical procedures often induce dysfunction of the intestinal barrier, which could lead to the translocation of microorganisms and variation of their metabolites [7]. Because the occurrence and development of POI are closely related to intestinal microbes and their metabolites [8], the intestinal flora has become a potential target for the treatment of POI.

At present, the intestinal flora is attracting increasing attention as a drug target for disease prevention and treatment, and traditional Chinese medicine has been

increasingly recognised to affect host metabolism and function by regulating the intestinal flora. Our previous studies illustrated that the external treatment Shenhuang Plaster (SHP) applied at the Shenque acupoint (CV8) could effectively promote gastrointestinal transmission and reduce inflammation in the small intestinal smooth muscle [9], and it has already been applied clinically to treat POI [10]. In our previous research, UPLC-MS was applied to identify the main effective components of SHP, including emodin, tanshinone, ginsenoside, and magnolol [11]. Meanwhile, we also found some ingredients of SHP, such as rhein and magnolol, in the sera of rabbits with POI [12]. The prebiotic effects of these active ingredients have been elucidated. In detail, some of these components can enhance the abundance of some probiotics, such as lactic acid bacteria and bifidobacteria, and decrease that of opportunistic bacteria such as *Enterococcus* and *Escherichia shigella* [13–15]. Therefore, we speculated that the application of SHP at CV8 could exert an effect on POI by regulating the structure and function of the intestinal flora. In this study, we revealed the bacterial composition in the small intestine of a mouse model of POI, which may provide new ideas for the clinical application of SHP.

2. Materials and Methods

2.1. Chemical and Biochemical Materials. Paraformaldehyde was purchased from Tianjin Chemical Reagent Research Institute (Tianjin, China). PBS was purchased from Beijing Zhongshan Jinqiao Biotechnology Co., Ltd (Beijing, China). Ammonia was purchased from Hangzhou Changzheng Chemical Plant (Hangzhou, China). Hydrogen peroxide was purchased from Shanghai Yuanda Peroxide Co., Ltd (Shanghai, China). Methanol was purchased from Shanghai Zhenxing Chemical No. 1 Plant (Shanghai, China). Anhydrous ethanol was purchased from Hangzhou Chemical Reagent Co., Ltd (Hangzhou, China). Ethanol (95%) was purchased from Anhui Ante Biochemical Co., Ltd (Suzhou, China). SHP was previously prepared, and the chemical constituents were identified using UPLC-MS/MS [11].

2.2. Animal Treatment. C57BL/6 mice (8 weeks old, 18–20 g) were purchased from the Shanghai Laboratory Animal Centre (Shanghai, China) and handled under a specific pathogen-free condition in the animal experimental centre of Zhejiang Chinese Medical University with a strict light/dark cycle (12 h of light), temperature controlled at 20°C, and free access to food and water. All animal experiments were approved by the ethics committee of Zhejiang Chinese Medical University Animal Research Centre (accepted Nr. 10632). All mice were adaptively fed for 1 week to construct a POI model and randomly divided into the control (Ctrl), model (POI), and intervention groups (POI + SHP), with eight mice per group. After the mice were anaesthetised via isoflurane inhalation, the abdomen of each animal was shaved, disinfected, and covered with sterile gauze, and a 2-cm-long incision was made in the middle of the lower abdomen. The cecum and a part of the small intestine were removed and cleaned using saline-soaked cotton balls for 30 s. The small intestine was then returned to the abdominal cavity, dripped with 1 mL of sterile normal saline, and sutured layer-by-layer while paying attention to protect the intestine from ischaemia and necrosis. After the POI model was established, the animals were fed in separate cages, and SHP was applied at CV8 of mice in the POI + SHP group twice a day.

2.3. Gastrointestinal Transmission. Mice were fasted for 24 h and intragastrically administered 6.25 mg/mL FITC-labelled dextran 70 kDa (200 μL) via a gastric tube. After 30 min, the mice were anaesthetised and sacrificed, and the entire gastrointestinal tract was immediately removed by laparotomy and divided into 15 segments (stomach, one segment; small intestine, 10 segments; cecum, one segment; and colon, three segments). Each intestinal cavity was rinsed with saline, and an FITC-labelled glucan cleaning solution was collected. After centrifugation at 12,000 rpm for 15 min, the supernatant was collected, and the absorbance at 494 nm was measured. The percentage and geometric mean of absorbance were calculated for each segment. Gastrointestinal transport function was expressed as the geometric mean and percentage distribution of FITC-labelled glucan absorbance in each segment. The percent absorbance was calculated as follows: percent absorbance = absorbance per section/total absorbance × 100. The geometric mean was calculated as follows: geometric mean = Σ (percentage of absorbance per segment × number of segments)/100.

2.4. Morphological and Pathological Observation of Intestinal Tissue. At the end of the experiment, the mice were sacrificed via excessive inhalation of carbon dioxide, and the intestinal tissue (colon and ileum) of mice in each group was collected for morphological and immunohistochemical studies. After formaldehyde fixation for 24 h, 10% formalin-fixed tissue was dehydrated using an alcohol/xylene solution concentration gradient. Then, these dehydrated tissues were embedded in paraffin and cut into 4 μm thick slices. These slices were separated into two groups for histological observation and immunohistochemical studies. One group of slices was stained with haematoxylin and eosin (H&E) and observed under a microscope. Moreover, the ileum and colon of each mouse were hybridised with specific antibodies to detect various proteins.

2.5. Real-Time PCR. An RNA extraction kit (TRIzol/chloroform method) was used to extract total RNA from intestinal wall tissue according to the manufacturer's instructions (purchased from American Invitrogen Life Technology Co., Ltd., California, USA). The quality and concentration of the separated mRNA were determined by the ratio of absorbance at 260 and 280 nm. The extracted total RNA was quantitatively detected using a NanoDrop (Thermo Fisher Scientific, USA) and then reverse-transcribed into cDNA with SuperScript III (Invitrogen). The

cDNA was used as the template for real-time PCR. The PCR protocol consisted of template denaturation at 95°C for 5 min followed by 45 amplification cycles of 95°C for 10 s, 55°C for 30 s, and 72°C for 10 s. The melting curve was monitored as the temperature increased from 65 to 95°C. β-actin was used as an internal reference gene. The relative expression of the target gene of each sample was calculated using the $2^{-\Delta\Delta Ct}$ method. The specific primer pairs for target quantification are listed in Table 1.

2.6. 16S rRNA Gene Sequencing and Intestinal Flora Characterisation. A faecal DNA extraction kit was used to extract DNA from 200 mg of frozen faeces. The extracted DNA was quantified using a NanoDrop and purified by 1.0% agarose gel electrophoresis. A Phusion Hot Start Flex 2 × Master Mix was used to amplify the V3-V4 regions of the 16S rDNA gene by PCR with a universal primer pair (341F, 5′-CCTACGGGNGGCWGCAG-3′; 805R, 5′- GACTACHVGGGTATCTAATCC-3′) [9]. The sequencing library was constructed, and the Qubit and Agilent 2100 analyzers were used to quantify the library and evaluate the quality of the library. A 275–450-bp insertion sequence was selected for sequencing on the Illumina NovaSeq platform. The low-quality sequences and contaminating sequences from the host were deleted to obtain the clean data. SOAP de novo (v2.04) was used to assemble and analyse clean data. MetaGeneMark was used for gene prediction and nonredundant gene set construction. MyTaxa and related databases were used to obtain the species annotation information of each gene and species abundance tables at different taxonomic levels. Based on the species abundance table and functional abundance table, linear discriminant analysis effect size (LEfSe), principal component analysis (PCA)/principal coordinate analysis, and sample cluster analysis were performed.

2.7. Statistical Analysis. In this research, the measurement data were expressed as the mean ± SD, and SPSS 22.0 statistical software was used for analysis and processing. The least significant difference test was used for pairwise comparisons between groups, analysis of variance was used for comparisons of homogeneity of variance among multiple groups, and the Kruskal–Wallis H test was used for comparisons of uneven variance among multiple groups. $P < 0.05$ denotes statistical significance.

3. Results

3.1. SHP Alleviated POI-Induced Body Weight Loss. The mice in the Ctrl group had a good mental and physical status throughout the experiment, including smooth and shiny hair and normal food consumption. The mice in the POI group were dull and sluggish, they huddled up in the corner, and they rarely ate. After SHP administration, the mental state, activity, glossiness, and food intake of POI mice were improved. Simultaneously, we monitored the body weight of the mice every other day. As presented in Table 2, the weight gain of mice in the POI group was significantly lower than that of mice in the Ctrl group ($P < 0.001$), whereas mice in the POI + SHP group gained significantly more weight than mice in the POI group ($P < 0.05$), suggesting that SHP could effectively restore the food intake and body weight of mice.

3.2. SHP Improved POI-Induced Gastrointestinal Motility Dysfunction. The gastrointestinal motility of mice was compared according to the fluorescence of various parts of the gastrointestinal tract. As presented in Figure 1(a), fluorescently labelled dextran (70 kDa) was rapidly transmitted in the Ctrl group, and the greatest fluorescence was detected in SI9 (terminal ileum). In the POI group, fluorescent dextran accumulation was greatest in SI1 (the first segment of the ileum), indicating accumulation at the beginning of the gastrointestinal tract, and the transmission of fluorescence was severely hindered. In the POI + SHP group, fluorescent glucan accumulated in SI8 (ileum) at a significantly faster rate than observed in the POI group and a similar rate as that in the Ctrl group. The geometric mean (geometric centre (GC)) of gastrointestinal transmission in each group is presented in Figure 1(b). The GC values of the Ctrl, POI, and POI + SHP groups were 8.34 ± 0.52, 3.11 ± 0.45, and 6.40 ± 0.30, respectively. Compared with the findings in the Ctrl group, the GC value was significantly lower in the POI group ($P < 0.001$), whereas the value was significantly higher in the POI + SHP group ($P < 0.001$). The aforementioned results fully demonstrated that POI could cause obvious gastrointestinal motility dysfunction, and gastrointestinal transmission function was significantly reduced. The topical application of SHP significantly improved the dysfunction induced by POI.

The length of the villus and thickness of the mucosal layer are the two main intestinal morphological parameters for evaluating intestinal health. Therefore, this study performed H&E staining of the colon and ileum of different mice and measured the villus length and mucosal layer thickness. As presented in Figure 2, the colon and ileum tissues in mice in the Ctrl group were intact, with no obvious oedema, congestion, and obvious inflammatory cell infiltration, and the villus and mucosal layer were intact and undamaged. Extensive inflammatory cell infiltration was observed in the colon and ileum in mice in the POI group, in addition to muscle layer damage in some tissues, intestinal structure disorder, villus and muscle layer damage, villus atrophy and basal damage. The changes in the villus and mucosal layer were significantly different from those in the Ctrl group ($P < 0.001$). The histopathological performance of the colon and ileum in POI + SHP mice was significantly better than that of POI mice, including significantly reduced inflammatory cell infiltration and villus and mucosal layer damage and improved villus length and mucosal layer thickness ($P < 0.05$), suggesting that SHP could improve the morphology and function of intestinal tissue.

The results of immunohistochemistry illustrated that the expression and distribution of cyclooxygenase (COX)-2 protein in the colon and ileum of mice in each group were significantly different (Figure 3(a)). The expression and distribution of COX-2 in the colon and ileum of POI mice

Table 1: Primer sequences.

Target cytokines	Forward (5′ to 3′)	Reverse (5′ to 3′)	Gene loci
IL-1β	TCATGGGATGATGATAACCTGCT	CCCATACTTTAGGAAGACACGGATT	Chromosome 2, NC_000068.8 (129206490.129213059, complement)
IL-6	CTTTTGAIATATGGAAT	CCAGTTTGGTAGGCATCCATC	Chromosome 5, NC_000071.7 (30218112.30224973)
Tbx21	CAAGTGGGTGCAGTGTGGAAAG	TGGAGAGACTGCAGGACGATC	Chromosome 11, NC_000077.7 (96988833.97006157, complement)
TNF-α	CCCTCACACTCAGATCATCTTC	GTTGGTTGTCTTTGAGATCCAT	Chromosome 17, NC_000083.7 (35418343.35420983, complement)
COX-2	CAACTCTATATTGCTGGAACATGGA	TGGAAGCCTGTGATACTTTCTGTACT	Chromosome 1, NC_000067.7 (149975782.149983985)
iNOS	CAGCTGGGCTGTACAAACCTT	CATTGGAAGTGAAGCGTTTGG	Chromosome 11, NC_000077.7 (78811613..78851052)
β-Actin	TTCCAGCGTTCCTTCTTGGGT	GTTGGCATAGAGGTGTTTACG	Chromosome 5, NC_000071.7 (142888870.142892509, complement)

IL, interleukin; TNF, tumour necrosis factor; COX, cyclooxygenase; iNOS, inducible nitric oxide synthase.

Table 2: Changes in body weight in each group (g).

Group	Initial weight	Final weight	Body weight gain
Ctrl	21.65 ± 1.47	23.05 ± 1.62	2.23 ± 0.94
POI	22.22 ± 1.53	21.02 ± 1.46	$-1.20 \pm 0.46^{***}$
POI + SHP	21.04 ± 0.66	20.4 ± 0.61	$0.64 \pm 0.24^{\Delta\Delta\Delta}$

Note. The significant differences, marked with * and $^{\Delta}$, were compared with that of the Ctrl and POI groups, respectively, in this study. The significant differences between the POI and Ctrl groups are indicated by asterisks ($^{***}P < 0.001$ and $^{\Delta\Delta\Delta}P < 0.001$). Ctrl, control group; POI postoperative ileus group; POI + SHP, Shenhuang Plaster-treated POI group.

were significantly increased (especially the colon), and the positive area was significantly larger than that of Ctrl mice ($P < 0.001$). The expression and distribution of COX-2 were significantly lower in the POI + SHP group than in the POI group, and the positive area (relative value) was significantly lower than that in the POI group ($P < 0.001$). In addition, as presented in Figure 3(b), the expression and distribution of inducible nitric oxide synthase (iNOS) protein, which plays an important role in the formation of nitric oxide (NO), were also significantly different in the colon and ileum among the groups. The expression and distribution of iNOS in the intestinal tissue of mice were significantly higher in the POI group than in the Ctrl group (especially in the colon), and the positive area was significantly larger in the former group ($P < 0.001$). Compared with the results in the POI group, the expression and distribution of iNOS were reduced, and the positive area (relative value) was smaller in the POI + SHP group (colon, $P < 0.05$; ileum, $P < 0.001$). The aforementioned results indicated that SHP could effectively inhibit the expression and distribution of COX-2 and iNOS, thereby inhibiting the inflammatory response of intestinal tissues.

In this study, qRT-PCR was used to detect the mRNA expression of inflammatory mediators (IL-1β, IL-6, tumour necrosis factor (TNF)-α, T-bet, COX-2, and iNOS) in the smooth muscle of the small intestine tissue. As presented in Figure 3(c), the expression of IL-1β ($P < 0.001$), IL-6 ($P < 0.001$), TNF-α ($P < 0.001$), T-bet ($P < 0.01$), COX-2 ($P < 0.001$), and iNOS ($P < 0.001$) was significantly higher in the POI group than in the Ctrl group, suggesting that the intestinal tissue of POI model mice had obvious inflammation. After treatment with SHP, the expression of IL-1β ($P < 0.05$), IL-6 ($P < 0.01$), TNF-α ($P < 0.001$), COX-2 ($P < 0.001$), and iNOS ($P < 0.01$) in the intestinal tissue of mice was significantly decreased, indicating that the topical use of SHP at CV8 could reduce the mRNA expression of inflammatory mediators in the smooth muscle of the small intestine and relieve the intestinal inflammation caused by POI.

3.3. SHP Regulated POI-Induced Intestinal Flora Imbalance. In this study, the effect of SHP on intestinal flora was determined by sequencing the V3-V4 regions of 16S rDNA. In total, 20 samples were sequenced (Ctrl group, five samples; POI group, six samples; POI + SHP group, nine samples). A total of 1,422,245 Raw_Tags were obtained. After data processing and filtering, clean data were obtained, and the effective sequence length was 1,140,229. The average effective rate of sequencing data was 80%. The final feature average value was 764, including averages of 997, 506, and 806 in the Ctrl, POI, and POI + SHP groups, respectively. All values met the minimum value required for sequencing.

The alpha diversity analysis results (Figure 4(a)) revealed in the intestinal flora of mice among the groups. POI reduced the alpha diversity in the intestinal flora, including species richness and uniformity, whereas these changes were reversed by SHP supplementation. In this study, the Shannon value was used to represent the richness and uniformity of the species, with higher values indicating greater diversity. The beta diversity analysis results illustrated that in PCA (Figure 4(b)), there was a clear separation among the groups. The samples of the Ctrl and POI groups were distributed separately without any intersection. Six samples in the POI + SHP group were clustered closer to the

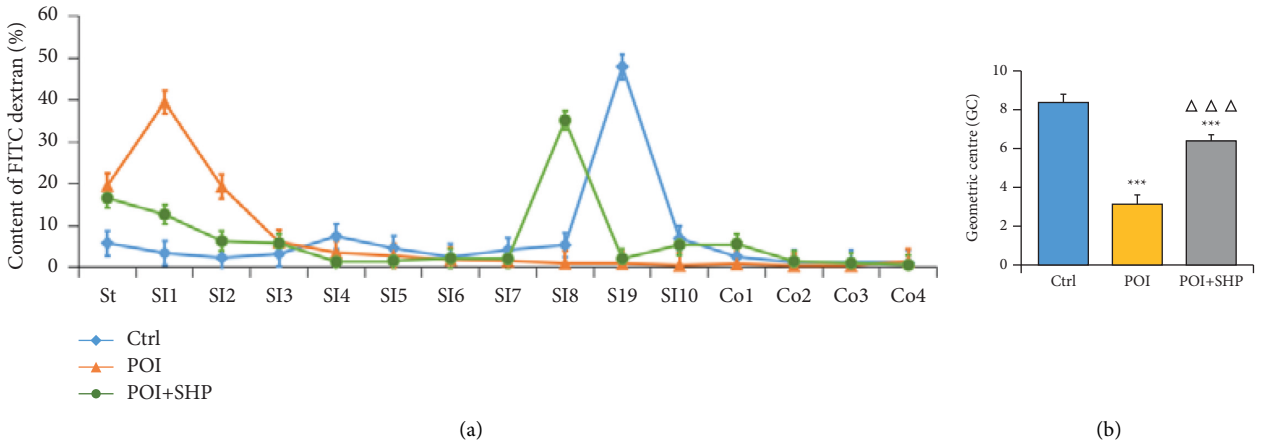

(a) (b)

Figure 1: Intestinal motility evaluation. (a) Gastrointestinal transmission curves: the distribution of fluorescein-labelled dextran in the gastrointestinal tract (St, stomach; SI, small intestinal segments 1–10; Co, colon segments 1–4) of mice in each group. (b) Derived geometric centre of mice in each group. The significant differences, marked with asterisks, were in comparison with the Ctrl ($^{***}P < 0.001$), and the significant differences, marked with triangles, were in comparison with the POI ($^{\Delta\Delta\Delta}P < 0.001$). Ctrl, control group; POI, postoperative ileus group; POI + SHP, Shenhuang Plaster-treated POI group. SHP protected the integrity of intestinal morphology.

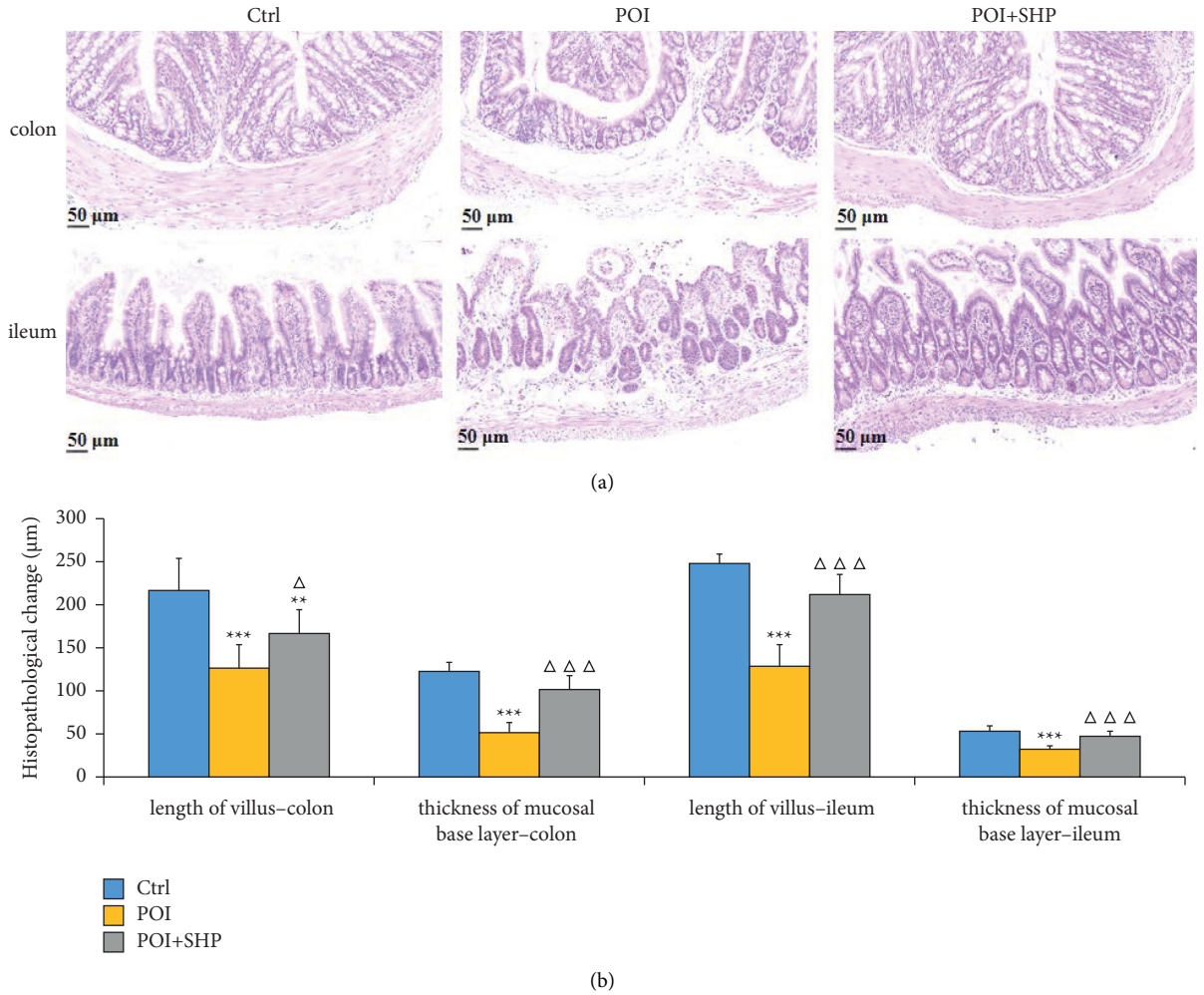

Figure 2: Histological analysis of the intestine. (a) Image of haematoxylin and eosin-stained colon and ileum of Ctrl, POI, and POI + SHP mice. (b) Average length of the intestinal villus and thickness of the mucosal layer in the colon and ileum of mice in each group as measured using NDP view software. The significant differences between the POI and Ctrl groups are indicated with asterisks ($^{***}P < 0.001$), and the significant differences marked with triangles was in comparison between the POI + SHP and the POI groups ($^{\Delta\Delta\Delta}P < 0.001$). Ctrl, control group; POI, postoperative ileus group; POI + SHP, Shenhuang Plaster-treated POI group. SHP inhibited POI-induced inflammation of intestinal tissue.

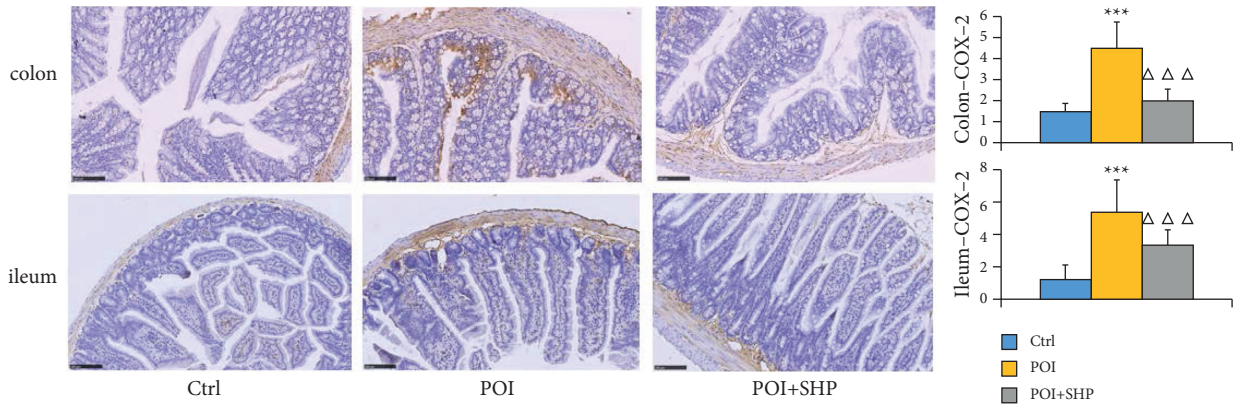

(a)

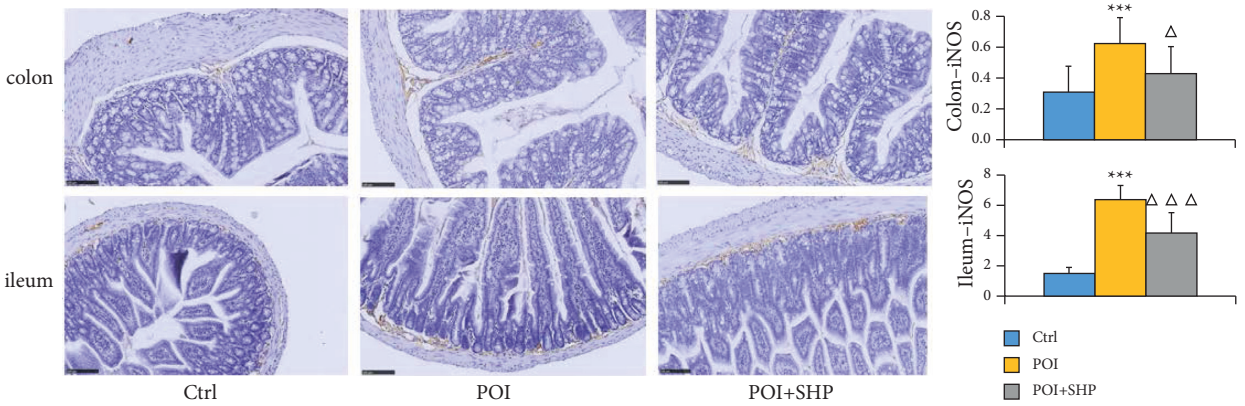

(b)

Figure 3: Continued.

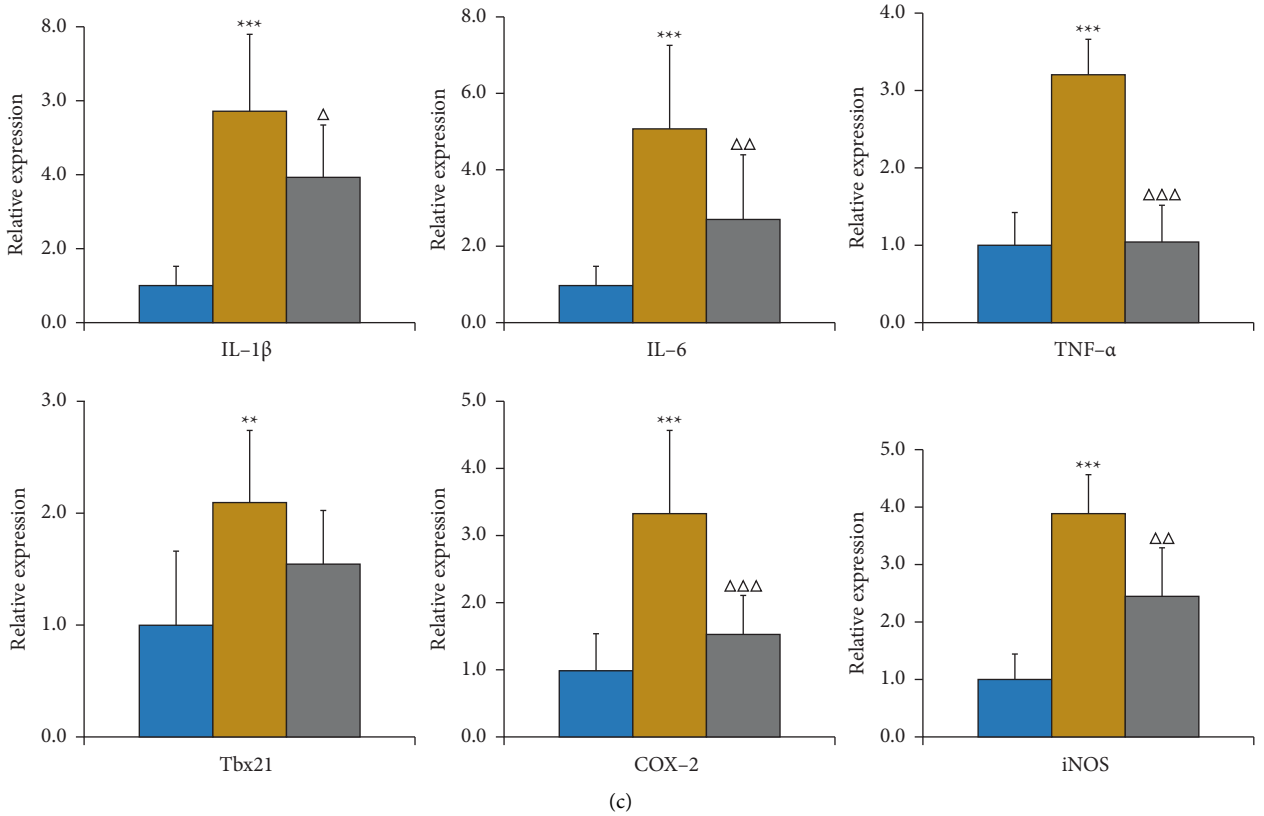

Figure 3: Measurement of inflammatory responses in intestinal tissue via immunohistochemistry. (a) The expression and distribution of COX-2 protein in the colon and ileum in each group. (b) The expression and distribution of iNOS protein in the colon and ileum in each group. (c) Relative expression of some inflammatory cytokines in the ileum and colon of mice in different groups. Data are presented as fold changes compared with that of the Ctrl group. Differences between the POI and Ctrl groups are indicated by asterisks ($^{*}P < 0.05$, $^{**}P < 0.01$, $^{***}P < 0.001$), and differences between the POI + SHP and POI groups are indicated by triangles ($^{\Delta}P < 0.05$, $^{\Delta\Delta}P < 0.01$, $^{\Delta\Delta\Delta}P < 0.001$). Ctrl, control group; POI, postoperative ileus group; POI + SHP, Shenhuang Plaster-treated POI group; IL, interleukin; TNF, tumour necrosis factor; COX, cyclooxygenase; iNOS, inducible nitric oxide synthase.

Ctrl samples, and three samples were clustered with the POI samples. The difference in community composition among the groups was statistically significant ($P < 0.05$).

In terms of the structure and composition of the intestinal flora at the phylum level (Figure 4(c)), the abundance of Bacteroidetes and Firmicutes was highest in the Ctrl group, and their abundance was significantly lower in the POI group. Meanwhile, the abundance of Proteobacteria increased from 4.39% in the Ctrl group to 35.97% in the POI group. The relative abundance of Bacteroidetes and Firmicutes was higher in the POI + SHP group than in the POI group, and the abundance of Proteobacteria decreased to 11.67% in the POI + SHP group. At the genus level (Figure 4(d)), the abundance of Muribaculaceae_unclassified was the highest in the Ctrl group. The relative abundance of the pathogen *Klebsiella* was highest in the POI group, whereas its relative abundance was extremely low in the Ctrl and POI + SHP groups (0.01 and 0.05%, respectively). The abundance of Muribaculaceae_unclassified was significantly lower in the POI group than in the Ctrl group. The abundance of Muribaculaceae_unclassified was higher in the POI + SHP group than in the POI group, whereas that of *Klebsiella* and *Parabacteroides* was significantly lower.

The results of LEfSe (Figure 4(e)) indicated that at the phylum level, Proteobacteria was significantly enriched and Firmicutes was significantly suppressed in the POI group, whereas Firmicutes was significantly enriched and Proteobacteria was significantly depressed in the intestines of mice in the POI + SHP group. At the genus level, pathogenic bacteria, such as *Klebsiella*, *Enterobacter*, and *Enterococcus*, were significantly enriched in the intestinal flora of POI model mice but significantly suppressed in the POI + SHP group. The relative abundance of probiotics such as Lachnospiraceae_NK4A136_group, Eubacterium__xylanophilum_group, *Muribaculum*, Ruminococcus_1, Ruminococcaceae_UCG_014, Ruminiclostridium_6, *Oscillibacter*, and *Paramuribaculum* was significantly decreased in the POI group and significantly enriched in the POI + SHP group.

Correlation analysis of intestinal flora and intestinal function evaluation indices of POI model mice revealed that the enrichment of the intestinal flora in POI model mice had significantly negative correlations with intestinal function evaluation indices (D-value of body weight, GC value, intestinal villus height, and basal thickness). Meanwhile, the enrichment of the intestinal flora in POI model mice was

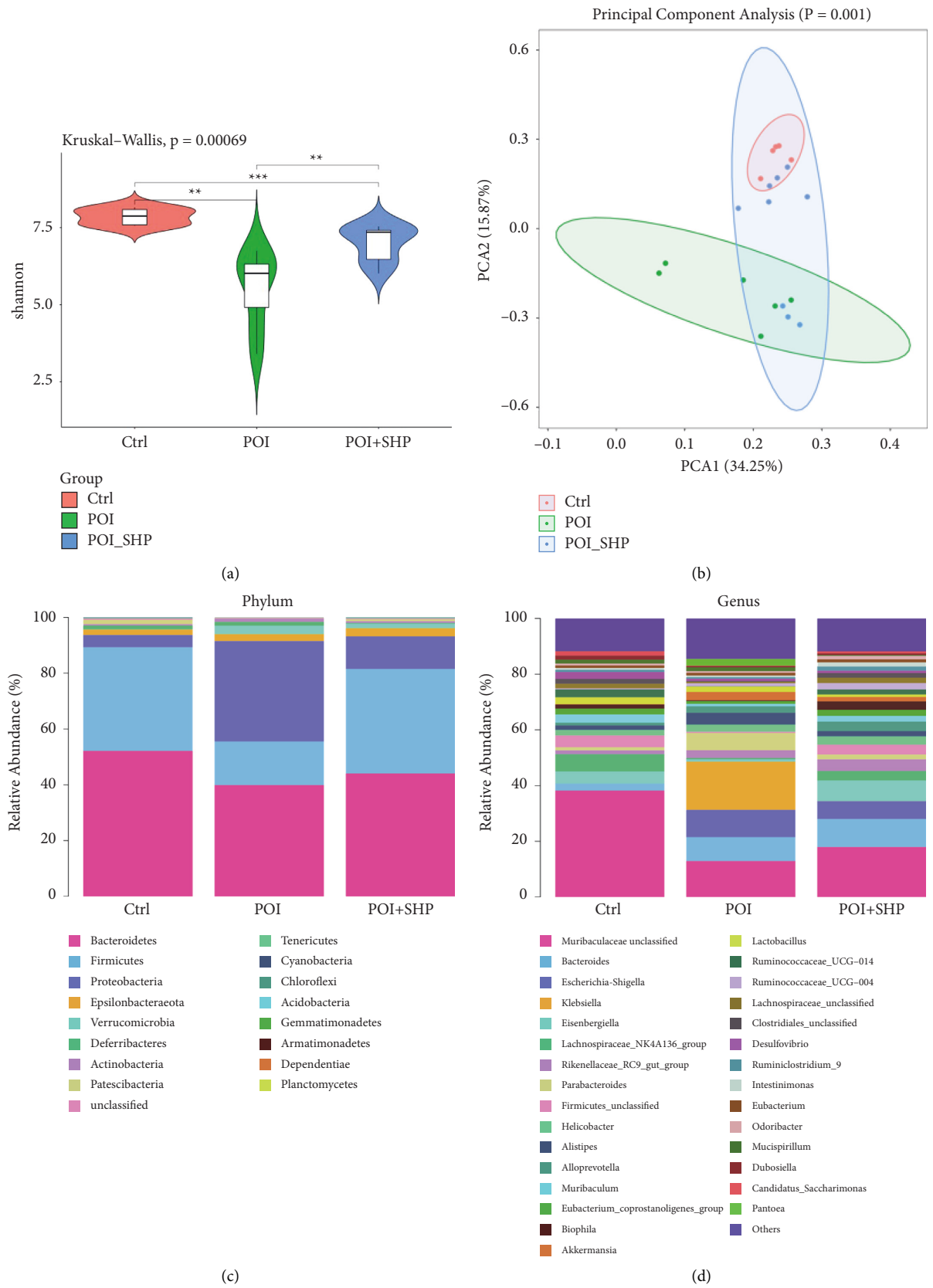

Figure 4: Continued.

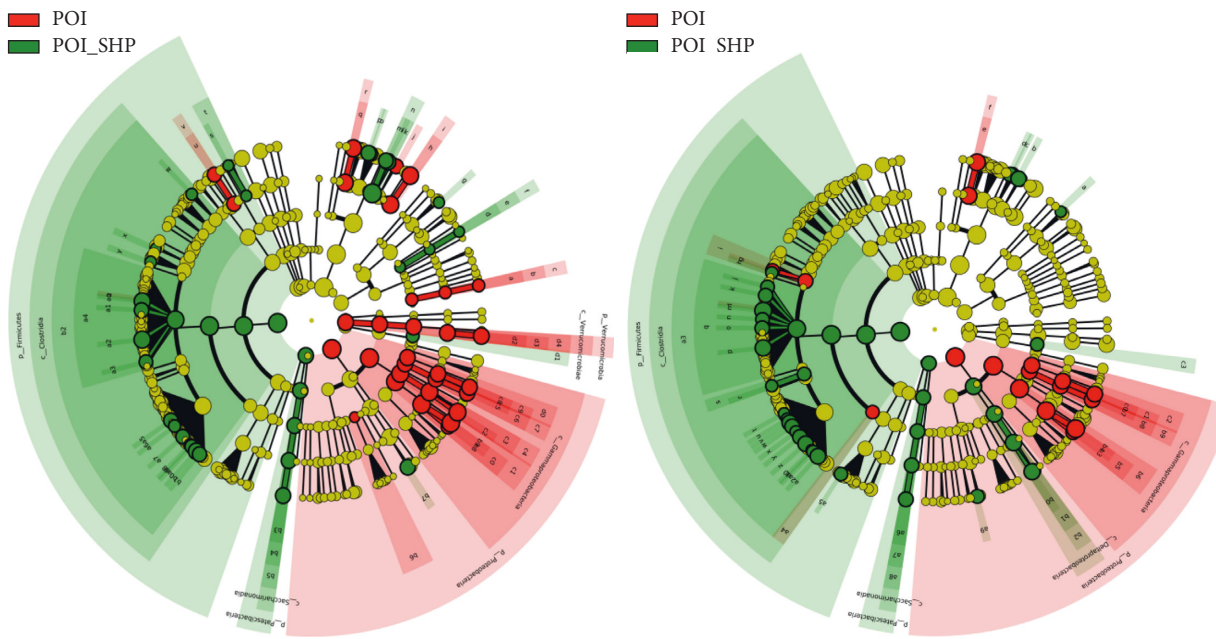

a: g_Bifidobacterium
b: f_Bifidobacteriaceae
c: o_Bifidobacteriales
d: g_Saccharomonospora
e: f_Pseudonocardiaceae
f: o_Pseudonocardiales
g: g_DNF00809
h: g_Bacteroides
i: f_Bacteroidaceae
j: g_Butyricimonas
k: g_Duncaniella
l: g_Muribaculum
m: g_Paramuribaculum
n: f_Muribaculaceae
o: g_Prevotellaceae_NK3B31_group
p: g_Prevotellaceae_UCG_001
q: g_Parabacteroides
r: f_Tannerellaceae
s: g_Gracilibacillus
t: f_Bacillaceae
u: g_Enterococcus
v: f_Enterococcaceae
w: g_Catabacter
x: g_Garciella
y: g_Family_XIII_UCG_001
z: g_Dorea
a0: g_Eisenbergiella
a1: g_Eubacterium_xylanophilum_group
a2: g_Lachnospiraceae_NK4A136_group
a3: g_Roseburia
a4: f_Lachnospiraceae
a5: g_Oscillibacter
a6: g_Papillibacter
a7: g_Ruminiclostridium_6
a8: g_Ruminococcaceae_UCG_007
a9: g_Ruminococcaceae_UCG_009
a0: g_Ruminococcaceae_UCG_014
b1: g_Ruminococcus_1
b2: o_Clostridiales
b3: g_Candidatus_Saccharimonas
b4: f_Saccharimonadaceae
b5: o_Saccharimonadaceae
b6: o_Sphingomonadales
b7: g_Bilophila
b8: g_Enterobacter
b9: g_Klebsiella
c0: f_Enterobacteriaceae
c1: o_Enterobacterales
c2: g_Escherichia_Shigella
c3: f_Enterobacteriaceae
c4: o_Enterobacteriales
c5: g_Rodentibacter
c6: f_Pasteurellaceae
c7: o_Pasteurellales
c8: g_Acinetobacter
c9: f_Moraxellaceae
d0: o_Pseudomonadales
d1: o_Mollicutes_RF39
d2: g_Akkermanslia
d3: f_Akkermansiaceae
d4: o_verrucomicrobiales
a: g_ Parvibacter
b: g_Odoribacter
c: g_Muribaculum
d: g_Paramuribaculum
e: g_Parabacteroides
f: f_Tannerellaceae
g: g_Family_XIII_AD3011_group
h: g_Family_XIII_UCG_001
i: f_Family_XIII
j: g_ Acetatifactor
k: g_Anaerotignum
i: g_Dorea
m: g_Eisenbergiella
n: g_ Eubacterium_xylanophilum_group
o: g_ GCA_900066575
p: g_Lachnospiraceae_NK4A136_group
q: f_Lachnospiraceae
r: g_Peptococcus
s: f_Peptococcaceae
t: g_Flavonifractor
u: g_Harryflintia
v: f_Intestinimonas
w: g_Oscillibacter
x: g_Papillibacter
y: g_Ruminiclostridium
z: g_Ruminiclostridium_9
a0: g_Ruminococcaceae_UCG_007
a1: g_Ruminococcaceae_UCG_009
a2: g_Ruminococcaceae_UCG_014
a3: o_Clostridiales
a4: o_ DTU014
a5: g_Allobaculum
a6: g_Candidatus_Saccharimonas
a7: f_Saccharimonadaceae
a8: o_Saccharimonadales
a9: g_Insolitispirillum
b0: g_Bilophila
b1: f_Desulfovibrionaceae
b2: o_Desulfovibrionales
b3: g_Enterobacter
b4: g_ Klebsiella
b5: f_ Enterobacteriaceae
b6: o_Enterobacterales
b7: g_Rodentibacter
b8: f_Pasteurellaceae
b9: o_Pasteurellales
c0: g_Acinetobacter
c1: f_Moraxellaceae
c2: o_Pseudomonadales
c3: o_Mollicutes_Rf39

(e)

Figure 4: Continued.

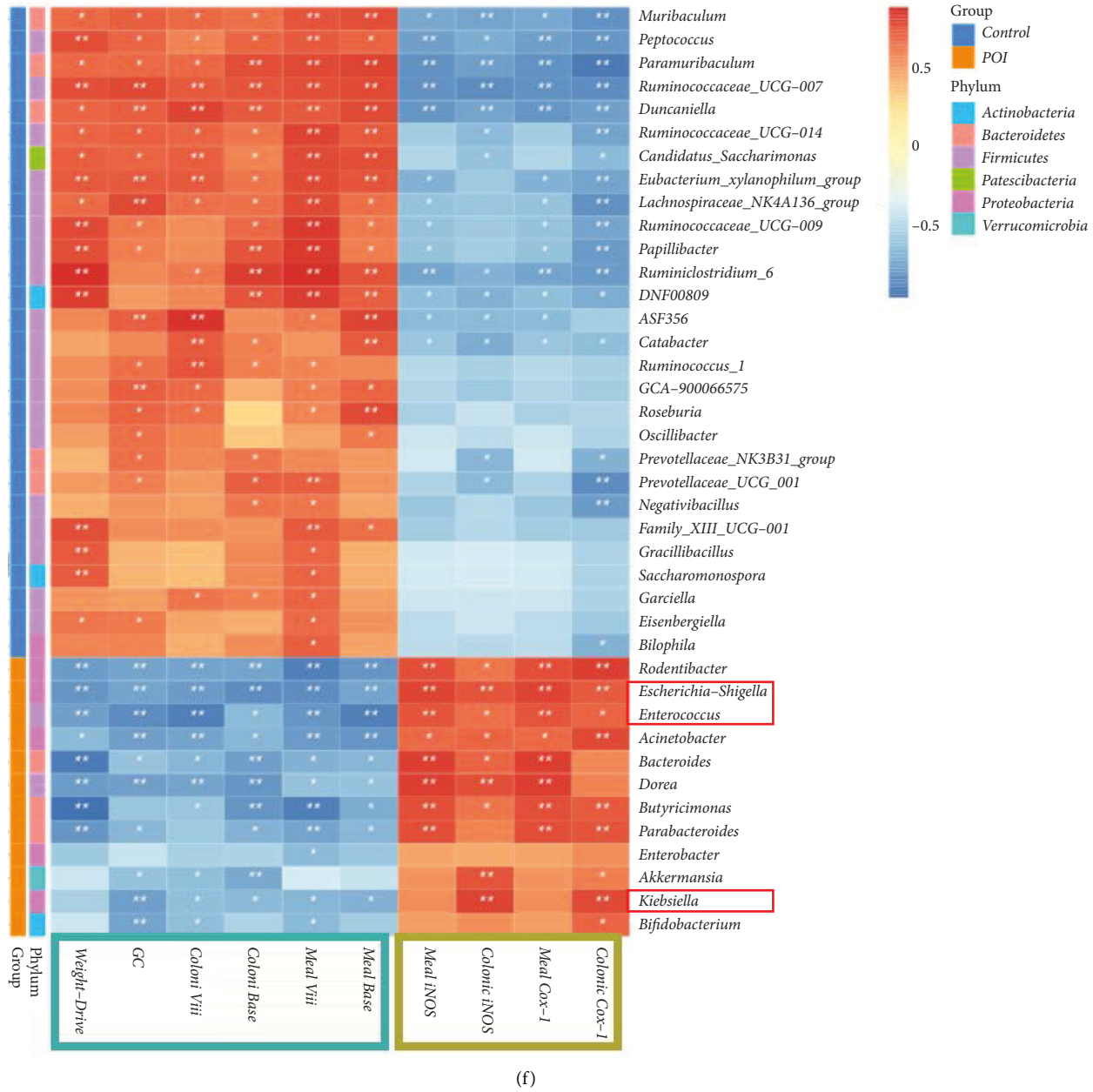

(f)

Figure 4: Changes in the intestinal flora of mice in each group. (a) Analysis of alpha diversity. (b) Analysis of beta diversity. (c) Histogram of the structure and composition of the intestinal flora at the phylum level. (d) Histogram of the structure and composition of the intestinal flora at the genus level. (e) Differential species evolutionary branch diagram of the intestinal flora. (f) Correlation analysis of the intestinal flora and intestinal function evaluation indices of POI model mice. Ctrl, control group; POI, postoperative ileus group; POI + SHP, Shenhuang Plaster-treated POI group.

positively correlated with iNOS and COX-2 expression in the colon and ileum. Specific to the flora, the abundance of *Klebsiella* and *Enterococcus* was positively correlated with iNOS and COX-2 expression in the colon, and the abundance of *Enterococcus* was negatively correlated with the GC value, D-value of body weight, and villus height.

4. Discussion

POI is a common complication of surgery that seriously affects patients' postoperative recovery, prolongs the treatment cycle, reduces patients' quality of life, and exerts a certain amount of economic pressure on patients' families as well as society [16]. To prepare POI model mice in this study, the small intestine of C57BL/6 mice was wiped with a saline-soaked cotton ball, and the application of SHP at CV8 in POI model mice produced obvious improvements. In detail, the application of SHP at CV8 significantly promoted gastrointestinal transport function in POI mice, reduced the damage of intestinal tissue caused by wiping, and alleviated the inflammatory reaction in intestinal tissue. In addition, SHP significantly reversed the dysbiosis of intestinal flora

and protected intestinal homeostasis by increasing the diversity of intestinal flora, promoting the growth of intestinal probiotics, and inhibiting the growth of intestinal pathogens.

In this study, the gastrointestinal transmission capacity and GC value were significantly decreased in POI model mice, highlighting serious damage to gastrointestinal motility, which also verified the feasibility of the POI model in this experiment. This was consistent with previous studies, which suggested that POI mice had serious dysfunction of gastrointestinal transmission [17]. At the same time, the intestine of POI mice displayed severe damage including obvious intestinal villus and basal layer atrophy. Identity to that of our previous studies [11], SHP significantly promoted the recovery of gastrointestinal motility and protected the integrity of intestinal histomorphology in POI mice, and these effects may be attributable to both the effects of the drug and stimulation of the acupoint.

Inflammation of small intestinal smooth muscle is a key factor leading to POI. It has been demonstrated that the release of inflammatory factors in small intestinal smooth muscle is the crucial pathological change of POI [18]. Intestinal macrophages can mediate the inflammatory response, and their dysfunction induces an imbalance of this response. In detail, intestinal injury promotes the activation of macrophages, which release inflammatory mediators such as IL-6, TNF-α, IL-1β, and T-bet that can induce iNOS and COX-2 expressions. Although some published literature suggests that many ingredients in SHP can reduce the expression of inflammatory mediators in intestinal tissue, the present work initially validated the regulative capability of SHP application on the expression of these proteins, which might be related to the anti-inflammatory effect of its multiple effective components [19, 20]. Actually, physcion can inhibit the release of NO [21]. Aloe–emodin and emodin can suppress the mRNA expression of TNF-α [17, 22]. Rhein has good anti-inflammatory effects, and it can alleviate gastrointestinal reactions [23]. And these ingredients in SHP have been previously identified [11].

The intestinal flora is a critical factor influencing the fitness of the intestine and body health, which could be affected by not only food or medicine intake but also massage, acupuncture [24, 25]. Previous studies suggested that the intestinal flora plays a crucial role in wound healing, which is one of the major aetiological factors of POI. It has been commonly recognised that postoperative complications, such as postoperative infection or delayed postoperative intestinal motility disorder, might be related to an imbalance of the intestinal flora [26, 27]. The pathogens, *Klebsiella*, *Enterobacter*, and *Enterococcus*, which were significantly enriched in the intestinal flora of POI mice in our study, highly correlated with many infectious diseases of humans [28, 29]. In addition, expression of iNOS and COX-2 in colon cells has been observed with the enrichment of *Klebsiella* and *Enterococcus*, which had negative correlations with the GC value, D-value of body weight, and intestinal villus height [30]. SHP application selectively inhibited the enrichment of *Enterococcus*, *Klebsiella*, and *Enterobacter*. This result indicated that SHP application on CV8 could also influence the gut microbiota. Unfortunately, the further biomechanisms of SHP's efficacy has not been clarified in this study. The published literature suggests that some ingredients, such as emodin, a prebiotic that is beneficial for the growth of lactic acid bacteria and bifidobacteria [13, 31], could be transdermally absorbed. Otherwise, the umbilical application of rhubarb (an ingredient in SHP) can significantly improve the recovery of postoperative bowel and reduce the incidence of postoperative abdominal distension [32]. Magnolol in SHP can improve gastrointestinal qi stagnation and inhibit intestinal muscle spasm [33]. Meanwhile, we hypothesised that these ingredients in SHP were percutaneous absorbed and improved the postoperative recovery and disorder of the immune response of the intestine, as well as the gastrointestinal microflora.

5. Conclusion

The intestinal flora plays a key role in the occurrence and development of POI. The external application of SHP at CV8 significantly promoted the recovery of intestinal motility and downregulated the expression of inflammatory mediators in POI model mice, by improving the regeneration of intestinal epithelial cells, inhibiting the intestinal inflammation, and maintaining intestinal immune homeostasis, which might relate to the intestinal flora.

Data Availability

All data used to support the findings of this study are included within the article, and these data can also be accessible on website https://fairsharing.org/collection/ShenhuangPlaster Application Improves Gastrointestinal Motility in Mice with Postoperative Ileus through Instestinal Microbiota or requested from the corresponding author of this manuscript (sunqiuhua@zcmu.edu.cn).

Disclosure

Ms. Yanan Shi and Mr. Xiao Xu contributed equally as first authors because they equally completed most of the experiments and data analysis.

Conflicts of Interest

The authors declare that there are no conflicts of interest regarding the publication of this paper.

Authors' Contributions

Yanan Shi and Xiao Xu contributed equally to this work.

Acknowledgments

This study was designed and guided by Qiuhua Sun and Bin Ding, and therefore, they contributed equally as corresponding authors. Ms. Jingming Xu and Ting Liu helped to finish the rat model and SHP application. Rongyun Wang helped with animal anaesthesia treatment. This work was supported by the National Natural Science Foundation of China (No. 81973756), Zhejiang Province Public Welfare

Technology Application Research Project (grant number LGF19H270002), School-level scientific research project (talent special) of Zhejiang Chinese Medical University (grant number 2021RCZXZK19), and Public Platform of Medical Research Center, Academy of Chinese Medical Science, Zhejiang Chinese Medical University.

References

[1] J. Cai, Y. Duan, J. Yu, J. Chen, M. Chao, and M. Ji, "Bone-targeting glycol and NSAIDs ester prodrugs of rhein: synthesis, hydroxyapatite affinity, stability, anti-inflammatory, ulcerogenicity index and pharmacokinetics studies," *European Journal of Medicinal Chemistry*, vol. 55, pp. 409–419, 2012.

[2] J. Chiang, Y. C. Shen, Y. H. Wang et al., "Honokiol protects rats against eccentric exercise-induced skeletal muscle damage by inhibiting NF-kappaB induced oxidative stress and inflammation," *European Journal of Pharmacology*, vol. 610, no. 1–3, pp. 119–127, 2009.

[3] E. A. Deitch, "Simple intestinal obstruction causes bacterial translocation in man," *Archives of Surgery. (Chicago, III)*, vol. 124, no. 6, pp. 699–701, 1989.

[4] M. Endo, M. Hori, H. Ozaki, T. Oikawa, and T. Hanawa, "Daikenchuto, a traditional Japanese herbal medicine, ameliorates postoperative ileus by anti-inflammatory action through nicotinic acetylcholine receptors," *Journal of Gastroenterology*, vol. 49, no. 6, pp. 1026–1039, 2014.

[5] S. Gaines, C. Shao, N. Hyman, and J. C. Alverdy, "Gut microbiome influences on anastomotic leak and recurrence rates following colorectal cancer surgery," *The British Journal of Surgery*, vol. 105, no. 2, pp. e131–e141, 2018.

[6] W. Huo, Y. Zhang, Y. Liu et al., "Dehydrocorydaline attenuates bone cancer pain by shifting microglial M1/M2 polarization toward the M2 phenotype," *Molecular Pain*, vol. 14, Article ID 1744806918781733, 2018.

[7] C. Jacobs, E. Coss Adame, A. Attaluri, J. Valestin, and S. S. C. Rao, "Dysmotility and proton pump inhibitor use are independent risk factors for small intestinal bacterial and/or fungal overgrowth," *Alimentary Pharmacology & Therapeutics*, vol. 37, no. 11, pp. 1103–1111, 2013.

[8] J. Keller, G. Bassotti, J. Clarke et al., "Advances in the diagnosis and classification of gastric and intestinal motility disorders," *Nature Reviews Gastroenterology & Hepatology*, vol. 15, no. 5, pp. 291–308, 2018.

[9] J. B. Logue, C. A. Stedmon, A. M. Kellerman et al., "Experimental insights into the importance of aquatic bacterial community composition to the degradation of dissolved organic matter," *ISME Journal*, vol. 10, no. 3, pp. 533–545, 2016.

[10] H. X. Yu, X. Ying, H. S. Qiu, and W. Xing, "Clinical study on Shenhuang point application of Shenhuang powder to promote early recovery of gastrointestinal insufficiency after gastric cancer surgery," *Zhonghua Journal of Traditional Chinese Medicine*, vol. 28, no. 10, pp. 3131–3133, 2013.

[11] Y. Shi, J. Xu, B. Ding et al., "Gastrointestinal motility and improvement efficacy of Shenhuang plaster application on Shenque: identification, evaluation, and mechanism," *Journal of Immunology Research*, vol. 2020, Article ID 2383970, 13 pages, 2020.

[12] M. Mylonaki, N. B. Rayment, D. S. Rampton, B. N. Hudspith, and J. Brostoff, "Molecular characterization of rectal mucosa-associated bacterial flora in inflammatory bowel disease," *Inflammatory Bowel Diseases*, vol. 11, no. 5, pp. 481–487, 2005.

[13] N. Morita, E. Umemoto, S. Fujita et al., "GPR31-dependent dendrite protrusion of intestinal CX3CR1^{+}cells by bacterial metabolites," *Nature*, vol. 566, no. 7742, 2019.

[14] J.-M. Pohl, S. Gutweiler, S. Thiebes et al., "Irf4-dependent CD103 (+) CD11b (+) dendritic cells and the intestinal microbiome regulate monocyte and macrophage activation and intestinal peristalsis in postoperative ileus," *Gut*, vol. 66, no. 12, pp. 2110–2120, 2017.

[15] M. Shaw, C. Pediconi, D. McVey et al., "Safety and efficacy of ulimorelin administered postoperatively to accelerate recovery of gastrointestinal motility following partial bowel resection," *Diseases of the Colon & Rectum*, vol. 56, no. 7, pp. 888–897, 2013.

[16] N. Stakenborg, P. J. Gomez-Pinilla, and G. E. Boeckxstaens, "Postoperative ileus: pathophysiology, current therapeutic approaches," *Handbook of Experimental Pharmacology*, vol. 239, pp. 39–57, 2017.

[17] G. Stavrou and K. Kotzampassi, "Gut microbiome, surgical complications and probiotics," *Annals of Gastroenterology*, vol. 30, no. 1, pp. 45–53, 2017.

[18] Y. P. Chen, "The mechanistic study of rhubarb for modulation of gut micro-ecology and prohibition of breast cancer-related gene expression in mice," *Guangzhou University of Chinese Medicine*, in Chinese, 2018.

[19] J. Xun, J. W. Luo, W. J. Yao, X. T. Luo, C. L. Su, and Y. H. Wei, "Effect of emodin on gut microbiota of rats with acute kidney failure," *China Journal of Chinese Materia Medica*, vol. 44, no. 04, pp. 758–764, 2019, in Chinese.

[20] M. S. Wen, "TCM viscera and meridians fundamentals of umbilical therapy," *Journal of External Therapy of Traditional Chinese Medicine*, vol. 21, no. 05, p. 33, 2012, in Chinese.

[21] M. H. Ding, Y. Wu, H. F. Wan et al., "Pharmacokinetic comparison of Shenque (CV8) point application and non-acupoint application with Shenhuang powder in rabbit plasma," *China Journal of Traditional Chinese Medicine & Pharmacy*, vol. 33, no. 06, pp. 2321–2326, 2018, in Chinese.

[22] A. H. Huang, Y. G. Chi, Y. E. Zeng, and L. P. Lu, "Influence of fructus aurantii immaturus flavonoids on gastrointestinal motility in rats with functional dyspepsia," *Traditional Chinese Drug Research & Clinical Pharmacology*, vol. 23, no. 06, pp. 612–615, 2012, in Chinese.

[23] X. H. Li, Y. Qi, R. L. Cai, M. Li, X. Wang, and C. Peng, "Effect of lipopolysaccharide-induced expression of inducible nitric oxide synthase by aloe-emodin in RAW264.7 cells," *Chinese Pharmacological Bulletin*, vol. 26, no. 04, pp. 488–492, 2010, in Chinese.

[24] H. Chen, P.-S. Tan, C.-P. Li et al., "Acupoint massage therapy alters the composition of gut microbiome in functional constipation patients," *Evidence-Based Complementary and Alternative Medicine*, vol. 2021, Article ID 1416236, 9 pages, 2021.

[25] X. Ouyang, H. Duan, Q. Jin et al., "Moxibustion may delay the aging process of wistar rats by regulating intestinal microbiota," *Biomedicine & Pharmacotherapy*, vol. 146, Article ID 112147, 2021.

[26] X. F. Xiong, "On the main active ingredient of TCM-Rhubard in pharmacology," *Clinical Journal of Chinese Medicine*, vol. 6, no. 10, pp. 143–146, 2014, in Chinese.

[27] X. H. Xu, Y. L. Chen, X. Wei, J. Q. Kong, H. S. Qiu, and Q.H. Sun, "Effect of Senhuang Powder on gastrointestinal motility and expression of ICAM-1, iNOS, IL-1β and IL-10 in the rat model of postoperative ileus," *Journal of Zhejiang Chinese Medical University*, vol. 39, no. 11, pp. 777–781, 2015, in Chinese.

[28] S. X. Yu, "Quality evaluation of magnolia bark based on analysis of water-soluble components," *China Academy of Chinese Medical Sciences*, in Chinese, 2011.

[29] Q. R. Zhang, L. Ding, X. M. Zhao, X. D. Guo, and L. Li, "Effects of magnolia bark on isolated gastrointestinal motility in rabbits," *Shaanxi Medical Journal*, vol. 06, pp. 656–659, 2007, in Chinese.

[30] J. Zhao, "Interaction between magnesium Lithospermate B and gut microbiota," *Chinese Academy of Sciences (Shanghai Institute of Materia Medica)*, in Chinese, 2018.

[31] C. M. Zhu, Y. Wang, F. L. Ye, and J. Zhou, "Clinical observation on moxibustion and rhubarb umbilical area applying to prevent and treat abdominal distension after cesarean section," *Chinese Journal of Traditional Medical Science & Technology*, vol. 27, no. 06, pp. 962–964, 2020, in Chinese.

[32] A. Swidsinski, A. Ladhoff, A. Pernthaler et al., "Mucosal flora in inflammatory bowel disease," *Gastroenterology*, vol. 122, no. 1, pp. 44–54, 2002.

[33] S. Wehner, T. O. Vilz, B. Stoffels, and J. C. Kalff, "Immune mediators of postoperative ileus," *Langenbeck's Archives of Surgery*, vol. 397, no. 4, pp. 591–601, 2012.

Hindawi
Evidence-Based Complementary and Alternative Medicine
Volume 2022, Article ID 8158699, 14 pages
https://doi.org/10.1155/2022/8158699

Research Article

Flos Carthami Exerts Hepatoprotective Action in a Rat Model of Alcoholic Liver Injury via Modulating the Metabolomics Profile

Xiaojing Fan,[1] **Xiye Wang**,[2] **Jie Lian**,[3] **Zhili Pei**,[3] **Mingyang Jiang**,[3] **and Meirong Bai**[4]

[1]*College of Engineering, Key Laboratory of Intelligent Manufacturing Technology, Inner Mongolia Minzu University, Tongliao 028000, China*
[2]*College of Chemistry and Chemical Engineering, Inner Mongolia Minzu University, Tongliao 028000, China*
[3]*College of Computer Science and Technology, Key Laboratory of Mongolian Medicine Big Data Research and Applications, Inner Mongolia Minzu University, Tongliao 028000, China*
[4]*Key Laboratory of Mongolian Medicine Research and Development Engineering, Ministry of Education, Tongliao 028000, China*

Correspondence should be addressed to Mingyang Jiang; jiang_ming_yang@163.com and Meirong Bai; baimeirong@126.com

Received 18 November 2021; Revised 22 February 2022; Accepted 5 April 2022; Published 30 April 2022

Academic Editor: Lifeng Han

This study was intended to identify the shifts in the metabolomics profile of the hepatic tissue damaged by alcohol consumption and verify the potential restorative action of flos carthami (the flowers of *Carthamus tinctorius*, FC) in the protection of alcohol-induced injury by attenuating the level of identified metabolites. Rats were treated with FC and subsequently subjected to alcohol administration. The serum samples were subjected to liquid chromatography-mass spectrometry (LC-MS)-based metabolomics followed by statistical and bioinformatics analyses. The clustering of the samples showed an obvious separation in the principal component analysis (PCA) plot, and the scores plot of the orthogonal partial least squares-discriminant analysis (OPLS-DA) model allowed the distinction among the three groups. Among the 3211 total metabolites, 1088 features were significantly different between the control and alcohol-treated groups, while 367 metabolites were identified as differential metabolites between the alcohol- and FC-treated rat groups. Time series clustering approach indicated that 910 metabolites in profile 6 were upregulated by alcohol but subsequently reversed by FC treatment; among them, the top 10 metabolites based on the variable importance in projection (VIP) scores were 1-methyladenine, phenylglyoxylic acid, N-acetylvaline, mexiletine, L-fucose, propylthiouracil, dopamine 4-sulfate, isoleucylproline, (R)-salsolinol, and monomethyl phthalate. The Pearson correlation analysis and network construction revealed 96 hub metabolites that were upregulated in the alcohol liver injury model group but were downregulated by FC. This study confirmed the hepatoprotective effects of FC against alcohol-induced liver injury and the related changes in the metabolic profiles, which will contribute to the understanding and the treatment of alcohol-induced acute liver injury.

1. Introduction

Acute hepatic failure is a syndrome characterized by the sudden and severe loss of normal liver function [1–3]. The prevalence of acute liver failure in the international population is high [1–3]. Acute liver failure is often the direct or secondary consequence of drugs, toxins, and infections with hepatitis viruses [1–3]. Alcohol drinking is the foremost cause of the disease and death from liver damage [4–6]. Despite the efforts of so many years of research, the pathogenesis and physiopathology of acute alcoholic liver failure still remain unclear; this makes its diagnosis and prognosis difficult and requires careful studies from different angles and aspects. Moreover, the management of liver failure remains an enormous challenge in hospitals; options offered include supportive measures, N-acetylcysteine for paracetamol poisoning and, in the most extreme cases, liver transplantation [7, 8]. Therefore, it is necessary to find replacement therapeutic approaches.

Flos carthami (the flowers of *Carthamus tinctorius*, FC) is a group of bioactive compounds that have been shown to be of therapeutic benefit in traditional Chinese medicine

[9–12]. FC has been primarily used for the treatment of cardiovascular diseases like thrombosis and coronary artery disease and improves blood flow in the bloodstream [13, 14]. Research also potentiates FC as a key adjuvant for reversing drug resistance in cancer therapy [12]. FC has been also demonstrated to be efficient in treating liver diseases, liver damage, and liver metabolic disorders, demonstrating its probable value in the treatment of liver failure [15]. However, how FC works in the treatment of hepatic failure remains unknown, requiring further studies.

Metabolomics is a science that emerged in recent decades [16–19]. It makes it possible to image at a given moment all the metabolites present or secreted in an organ or tissue under given conditions [16–19]. The application of the metabolomics helped to clarify the metabolic disorders that occur in various diseases [16–19]. With regard to liver diseases, metabolomics was applied to find the metabolites involved in acute liver injury and hepatotoxicity [20–23]. However, no studies demonstrating the effect of FC on the metabolic profile involved in alcoholic acute liver injury have yet been reported elsewhere.

Thus, our present study aims to explore the metabolic profile responsive to the treatment of acute liver injury by FC, the ultimate objective being to elucidate the mechanism of action of FC in the treatment of hepatic injury and potentially in the treatment of acute hepatic failure.

2. Materials and Methods

2.1. Chemicals and Reagents. FC was acquired from the Mongolian Medicine Manufacturing Room of the Affiliated Hospital of Mongolia University for the Nationalities (Tongliao, China). FC is a well-characterized traditional Chinese medicine, and its content in ingredients has been deposited in the Traditional Chinese Medicine Database and Analysis Platform (TCMSP) database (https://tcmsp-e.com/). The list of ingredients contained in FC was downloaded from TCMSP and is supplemented in Additional File S1. FC (1 g) was soaked in 10 mL water for 30 min and extracted at 60°C for three times, 30 min each time. The solutions were filtered using a filter with a membrane pore size of 0.22 μm. The filtrates were combined, recovered, and concentrated at 65°C, and the extract was obtained by freeze-drying. Ethanol (56°) was provided by the Niulanshan distillery of Beijing Shunxin Agriculture Co., Ltd. (Beijing, China). Formic acid and methanol (Fisher Scientific, UK) were of HPLC grade. The kits for ALT, AST, and TG were purchased from Roche Diagnostics Co., Ltd. (Shanghai, China).

2.2. Ethanol-Induced Acute Liver Injury Model Establishment and Treatment. The study obtained approval from the Ethics Committee of the Medicine College of Inner Mongolia Minzu University (IMMNMCEC20210722 [1]). YiSi Laboratory Animal Technology Co., Ltd. (Changchun, China) provided male Wistar rats weighing 200 ± 10 g. The rats were kept in the Affiliated Hospital under standard conditions at 21 ± 2°C with daily exposure to sunshine for 14 hours and had free access to water and rodent chow. The acclimation was achieved for 1 week in metabolism cages prior to experiment. Eight rats were assigned to each of the following groups: control group (CG), model group (MG), FC treatment groups (FC-low (0.4767 g/kg), FC-medium (1.4301 g/kg), and FC-high (4.2903 g/kg) groups), and control drug (paeonol at 60 mg/kg bw orally [24]) group. The dose of 4.2903 g/kg was calculated by extrapolation from the daily human dose of FC. According to the book of Qi Chen [25], the daily human dose of FC is 15 g, the extraction rate of FC is 37.08%, and the daily human dose of FC extract is 5.562 g for the human body weight of 70 kg. The body surface area of rats is 6 times larger than that of humans. Thus, using the following conversion formula, we were able to calculate the dose for rats: dose administered to rats = dose administrated to human/rat body weight × 6 times. This dose is the clinical equivalent, that is, 15 g × 37.08%/70 kg × 6 = 0.4767 g/kg. The dose of 4.2903 g/kg is 9 times the clinically equivalent amount.

On day 1, the rats in the CG and MG were given normal saline, while the rats in the FC groups were given FC extract orally once a day at low, medium, and high doses for 14 successive days. On day 15, the rats in the MG, FC-low, FC-medium, FC-high, and control drug groups were given alcohol by gavage at doses of 8 mL/kg to establish the acute alcoholic liver injury model of rats. After 20 hours, the animals were euthanized prior to blood collection from the hepatic portal vein and subsequent centrifugation at 4°C for 10 min at 3500 rpm. The collected supernatants were frozen instantly, conserved at −80°C, and thawed prior to analysis. The right lobe of liver was fixed in 10% formaldehyde solution for HE pathological section.

2.3. Biochemical Indexes. The determination of ALT, AST, and TG was performed in strict conformity with the instruction provided by the vendor of the kits.

2.4. Detection of Oxidation Markers in Hepatocytes. The hepatic tissue was mixed in PBS buffer using a Teflon homogenizer (Tissue-Tearor; BioSpec Products Inc.). The homogenate was centrifuged 10 min at 4°C at 1800 × g, and the supernatants were collected for subsequent assays. The hepatic ROS level was determined by incubating 2′,7′-dichlorofluorescin (DCF) diacetate (Sigma-Aldrich; Merck KGaA) with 50 μL of the homogenate mixed with 4.85 mL of potassium phosphate buffer (100 mmol/L) (Cayman Chemical) in methanol at 37°C for 15 min. The ROS content was calculated as the level of DCF deduced from an established DCF standard curve. The malondialdehyde (MDA) content and the activity of superoxide dismutase (SOD) and alcohol dehydrogenase (ADH) and glutathione (GSH) levels were detected using kits purchased from NanJing JianCheng Bioengineering Institute in accordance with the provided manual.

2.5. UPLC-MS Conditions. After thawing of the stored serum samples, an aliquot of 100 μL was taken and put in 400 μL acetonitrile. Next, after vortexing for 30 s, the aliquot

was centrifuged for 10 min at 12,000 rpm at 4°C and the supernatant was finally passed through filter membrane (0.22 μm). Metabolomics analysis was achieved using a Thermo Dionex UltiMate 3000 UHPLC system associated with a *Q* Exactive Focus Orbitrap mass spectrometer (Thermo, USA). The elution was done at 40°C with a flow rate of 0.3 mL·min^{-1} using the Waters Acquity UPLC BEH C_{18} column (1.7 μm, 2.1 mm × 50 mm; Waters, UK). The mobile phase *A* composed of 0.1% formic acid in deionized water and the mobile phase *B* constituted of methanol were used. The program of gradient elution using mobile phase *B* was as follows: 0–0.5 min with 8% *B*, 0.5–1.5 min with 8–60% *B*, 1.5–6 min with 60–100% *B*, 6–8 min with 100% *B*, 8–9 min with 100–8% *B*, and 9–10 min with 8% *B*. The volume of sample injected was 10 μL.

For the UHPLC high-definition MS (HDMS) analysis, the sheath used was nitrogen, while the aux gas flow rates were 40 and 5 bar, respectively. The aux gas and capillary heater temperature values were 320°C and 300°C, respectively. The spray voltage was fixed to 4.0 kV.

The MS data were acquired by switching between negative and positive spectra, and the mass range was 100–1000 Da. The full-MS resolution was 70,000. The resolution in the dd-MS^2 detection mode was 17,500 with an isolation gap of 3.0 *m*/*z*. The MS^2 collision energy of 35 eV was applied.

2.6. Data Analysis. A pooled quality control (QC) sample was obtained by combining 20 μL of respective samples for controlling instrument steadiness. Daily, six QC samples were examined to evaluate the steadiness of the device. The peak discovery, normalization, and alignment of peak areas were achieved using Compound Discoverer 2.0 software.

2.7. Bioinformatics Analysis. The *R* package ROPL was used for principal component analysis (PCA), OPLS-DA, and PLS-DA of the samples. The permutation test and cross-validation tests including the root mean square error of cross validation (RMSECV) were performed for the validation of the OPLS-DA and PLS-DA models. The permutation tests were at least 100 iterations of permutation. The variable importance in the projection (VIP) values were obtained from the PLS-DA model for the identification of important metabolites. The edgeR package in *R* was used for differential metabolite expression analysis. Significant differential metabolites were obtained with the following criteria: log2 (fold change) > 1.2 and adjusted *p*value <0.05. The complex heatmap and ggplot2 packages were used for the heatmap and volcano plot visualization of the metabolites' expression profiles. MetaboAnalyst software was used for functional enrichment and pathway analysis. The Hmisc *R* library was used for correlation analysis and generation of the network nodes. Cytoscape software was used for network visualization, and the plugin MCODE in Cytoscape was used for identification of hub metabolites. Detailed information of each metabolite can be retrieved by searching with its name as keyword at https://hmdb.ca/metabolites/HMDB0008642.

3. Results

3.1. FC Pretreatment Alleviates Acute Ethanol-Induced Liver Damage. To explore the action of FC on acute liver injury, a model of acute alcoholic liver injury was established in rats pretreated with FC. Latency to drunkenness (Figure 1(a)) and sleep time (Figure 1(b)) were significantly decreased in the model group (MG) compared with the control group (CG). Pretreatment with different doses of FC was accompanied by an increase in latency to drunkenness (Figure 1(a)) and a reduction in sleep time (Figure 1(b)) in the FC group compared with the MG in a dose-dependent manner, indicating that FC might mitigate the alcoholic hangover effect. Detection of markers of liver damage (ALT and AST) in serum indicated that induction with ethanol (MG) led to a remarkable elevation of serum ALT and AST levels, which was counteracted by treatment with different doses of FC (Figures 1(c) and 1(d)). *H*&*E* staining for histopathologic examination of liver tissue showed the occurrence of fatty liver characterized by disorganization of liver tissue, disordered structure of hepatic lobules, expanded liver sinus, liver cell swelling, and incomplete necrosis and steatosis in rats with acute liver damage (MG) compared with the CG, but this effect was attenuated by pretreatment of FC in the FC group (Figure 1(e)). In addition, the detection of TG in blood (Figure 1(f)) and liver (Figure 1(g)) showed a considerable dose-dependent decrease in TG in rats pretreated with FC and subjected to ethanol gavage (FC group) compared with rats with acute liver injury (MG). These observations show that FC can inhibit acute liver injury induced by ethanol.

3.2. FC Regulates Oxidative Stress Induced by Ethanol. As shown in Figure 2(a), compared with the control group, the gavage of rats with ethanol was followed by an increase in the level of ROS in liver tissue, while the pretreatment of FC was followed by a palpable decrease in ROS compared with the ethanol group. Similarly, compared with the model group of liver damage, pretreatment of FC was accompanied by a significant decrease in malondialdehyde (MDA) in liver tissue and serum (Figure 2(b)). The activation of alcohol dehydrogenase (ADH), an important enzyme involved in the first oxidation reaction, was also tested, and the results showed that FC had significantly decreased the activation of ADH induced by the ethanol (Figure 2(c)). In addition, detection of antioxidant enzymes indicated that the activities of SOD and GSH were decreased by the gavage of ethanol compared with the control groups, but this effect was abrogated by treatment with FC (Figures 2(d) and 2(e)). These observations suggest that FC can significantly alleviate lipid peroxidation in liver tissue and improve antioxidant capacity to enable resistance to alcohol exposure.

3.3. FC Restored the Alcohol-Altered Metabolic Profile of Rat Serum. After confirmation of ethanol-induced acute liver injury and the protective effects of FC, we performed metabolomics analysis to uncover changes in the global metabolic profile. The PCA (Figure 3(a)) and the PLS-DA

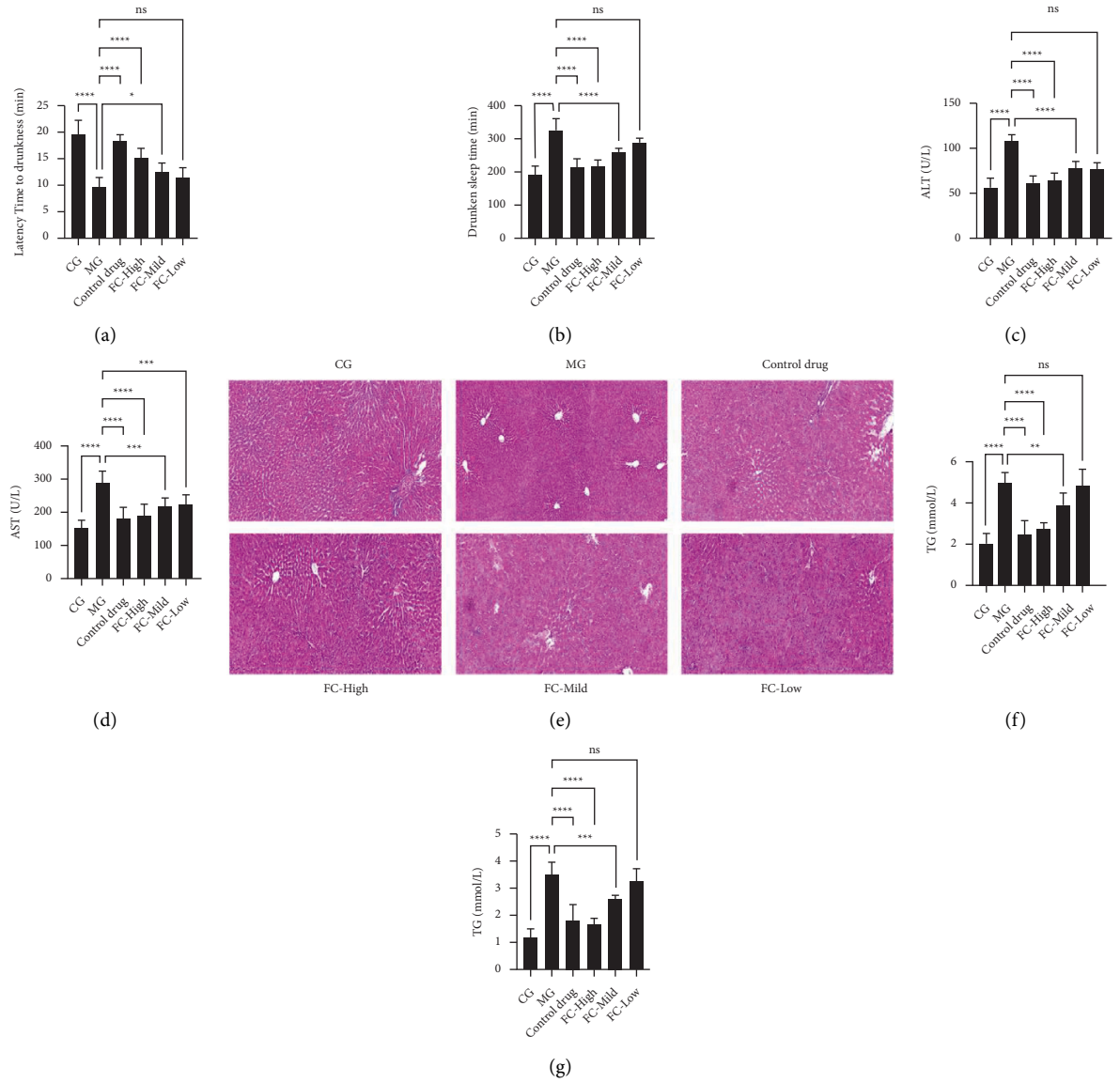

Figure 1: FC pretreatment alleviates acute ethanol-induced liver damage. (a) Effect of FC on the latency to drunkenness. (b) Effect of FC on the reduction in sleep. (c) Effect of FC on the serum level of ALT. (d) Effect of FC on the serum level of AST. (e) *H&E* staining for histopathologic examination of liver tissue. (f) Effect of FC on the serum level of TG. (g) Effect of FC on the liver tissue level of TG. ns = nonsignificant, $^{*}p < 0.05$, $^{**}p < 0.01$, $^{***}p < 0.001$, and $^{****}p < 0.0001$ among the compared groups. Scale bar = 100 μm.

(Figures 3(b)–3(e)) of the serum metabolomics showed a neat separation among the CG, MG, and FC groups (Figure 3(e)), indicating that the metabolic patterns of the three groups were completely separated. In the permutation test of the PLS-DA, we found that the R^2Y value was 0.991, while the Q2 value was 0.905 (Figure 3(c)). The PLS-DA results were further confirmed in the cross-validation (CV) analysis (Figure 3(f)). Next, pairwise comparisons were performed. The OPLS-DA indicated complete separation between the CG and MG with the R^2Y value of 1 and the Q2 value of 0.938 in the permutation testing, showing that alcoholic liver injury altered the metabolic profile (Figures 4(a)–4(e)). This result was confirmed by the results of the cross-validation test as indicated in Figure 4(e) showing root mean square error of cross validation (RMSECV) of >0.73 in the first five components. Moreover, as shown in Figures 4(f)–4(i), treatment of the model rats with FC was followed with significant alteration of the metabolic profile, which was reflected by the complete separation of metabolites from both the groups in the OPLS-DA (Figure 4(i)); the OPLS-DA result was also confirmed by the results of the RMSECV test showing RMSECV >0.72 (Figure 4(j)). No result was obtained in the comparison between the CG and the FC groups in the OPLS-DA; this might be due to the similarity of the metabolite profiles of these groups. Further, differential expression analysis of the metabolites indicated that 1088 metabolites were differentially expressed between the CG and MG, with 573 of them being downregulated (Figures 5(a) and 5(b), Additional File S2). As shown in

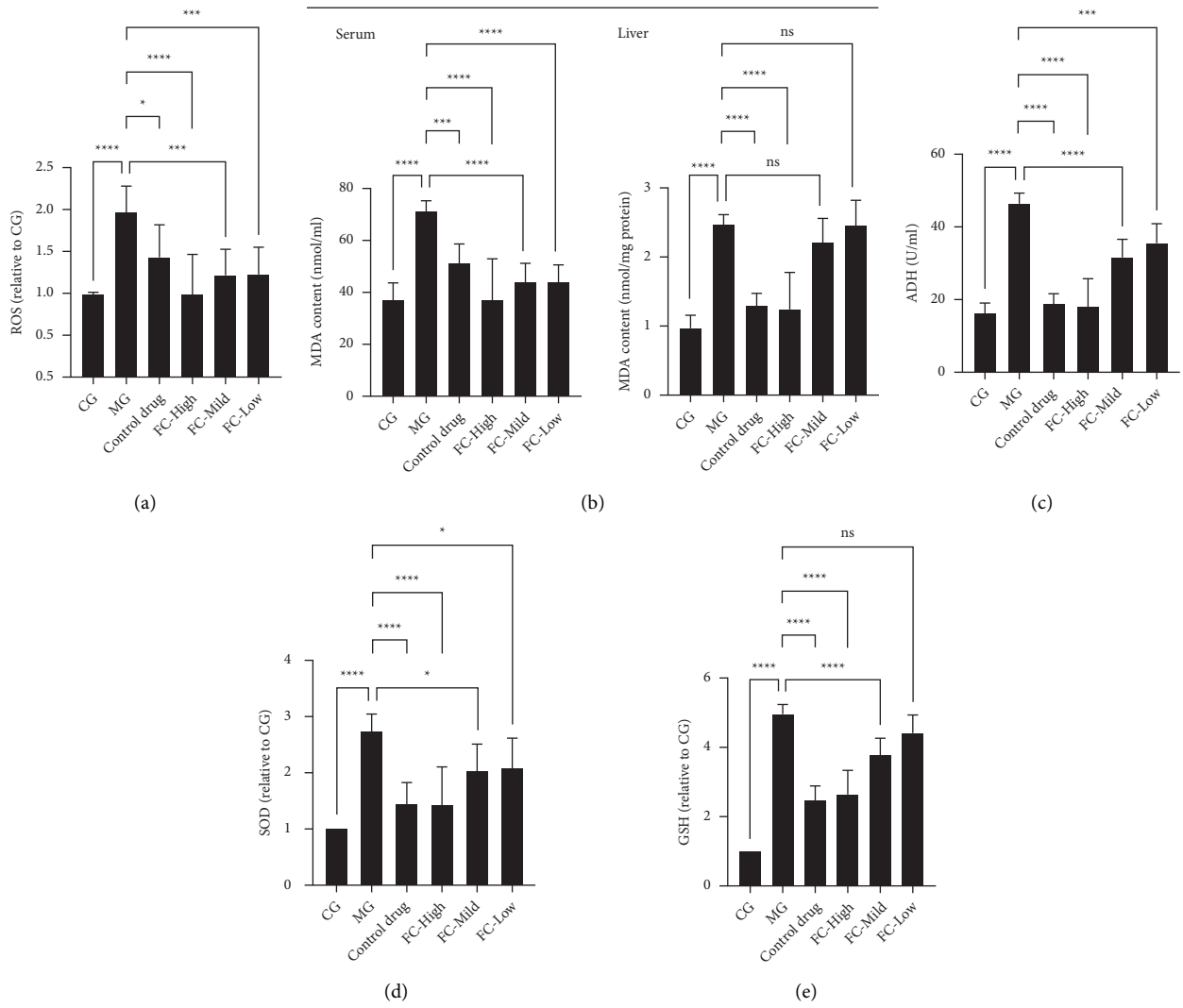

Figure 2: FC regulates oxidative stress induced by ethanol. (a) ROS production in the liver tissue of rats. (b) MDA level in the serum and liver tissue of rats. (c) ADH activity in the liver tissue of rats. (d) SOD activity in the liver tissue of rats. (e) GSH activity in the liver tissue of rats. ns = nonsignificant, $^{*}p < 0.05$, $^{***}p < 0.001$, and $^{****}p < 0.0001$ among the compared groups.

Additional Figure S1, the enrichment analysis of the differential metabolites between the control and model groups indicated that the most overrepresented pathways were "phenylalanine, tyrosine, and tryptophan metabolism," linoleic acid metabolism, terpenoids and other terpenoid-quinone metabolism, and thiamine metabolism. In the MG, the top ten upregulated and top ten downregulated metabolites with their metabolic profiles are presented Figure 5(b). Among the model and FC treatment groups, we identified 367 differentially expressed metabolites encompassing 224 downregulated and 143 upregulated metabolites (Figures 5(c) and 5(d), Additional File S3). The top 20 differentially expressed metabolites and their profiles are presented in Figure 5(d). The enrichment analysis indicated that the metabolites differentially expressed between the model and FC treatment groups were prevalently enriched in thiamine metabolism, sphingolipid metabolism, and "ubiquinone and other terpenoid-quinone metabolism" (Additional Figure S2).

3.4. Identification of FC-Responsive Metabolites in Alcoholic Liver Injury. To identify the metabolites that were altered by the alcoholic liver injury and restored by the FC treatment, we performed the time series clustering analysis. A shown in Figures 6(a) and 6(b), the metabolites could be clustered into eight profiles with 3 of them being significant. Profile 6 was the most significant and was characterized by the upregulation of the metabolites in the model group followed by their downregulation by the FC treatment. This profile contained 910 metabolites (Additional File S4). The top 20 most important metabolites on the basis of their VIP scores obtained from the PLS-DA were 1-methyladenine, phenylglyoxylic acid, N-acetylvaline, mexiletine, L-fucose, propylthiouracil, dopamine 4-sulfate, isoleucylproline, (R)-salsolinol, monomethyl phthalate, asymmetric dimethylarginine, carbimazole, 1,1-dimethylethyl heptanoic acid, 5-hydroxyphenylpropionylglycine, biotin sulfone, 3-methyladenine, D-xylulose, PC(22 : 4 (7Z, 10Z, 13Z, 16Z)/20 : 1(11Z)), and PC(15 : 0/15 : 0) (Figure 6(c)). It is worth noting

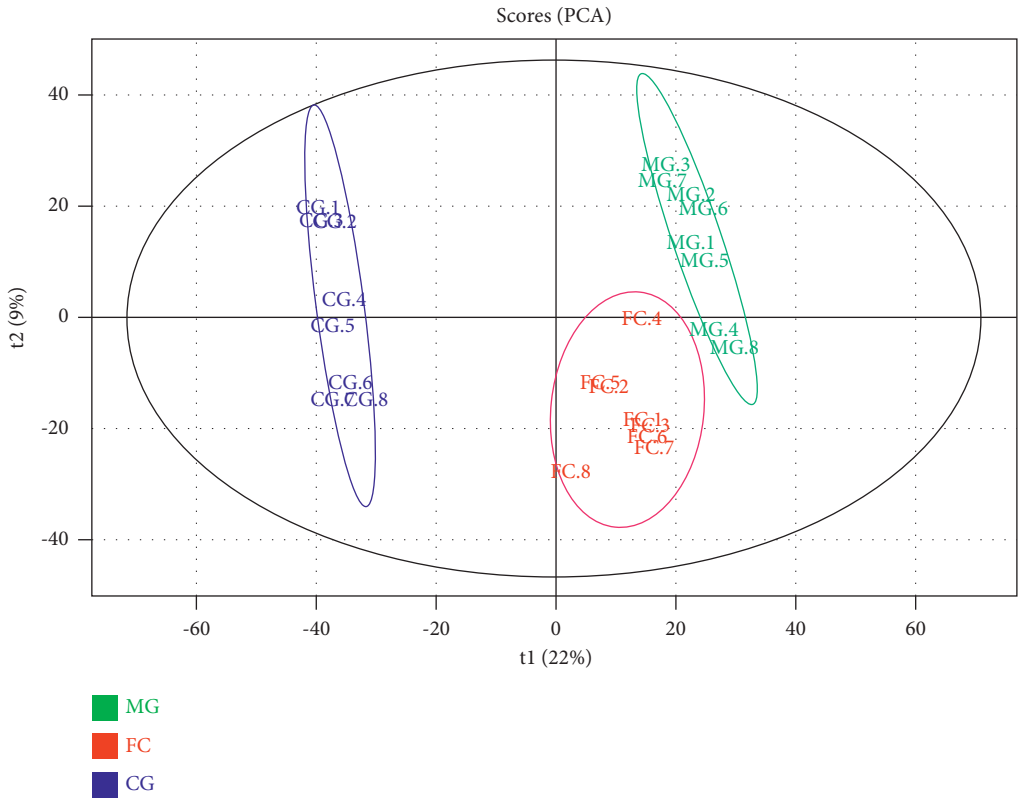

(a)

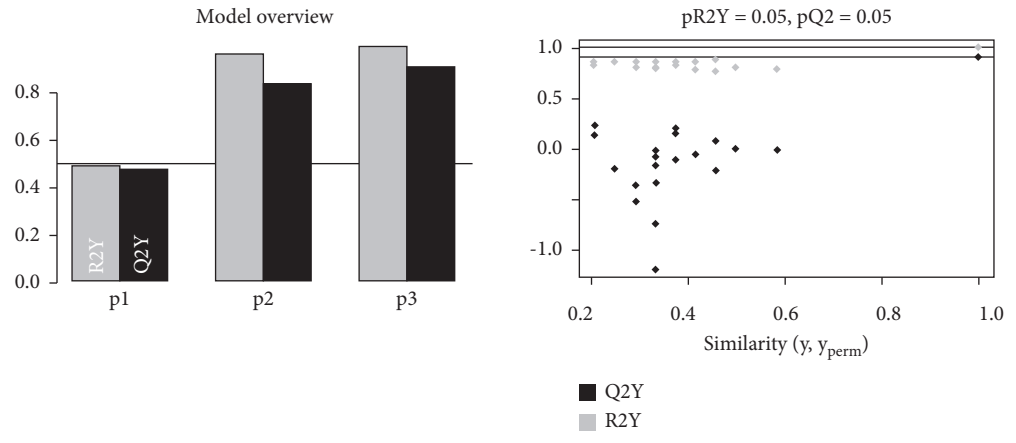

(b) (c)

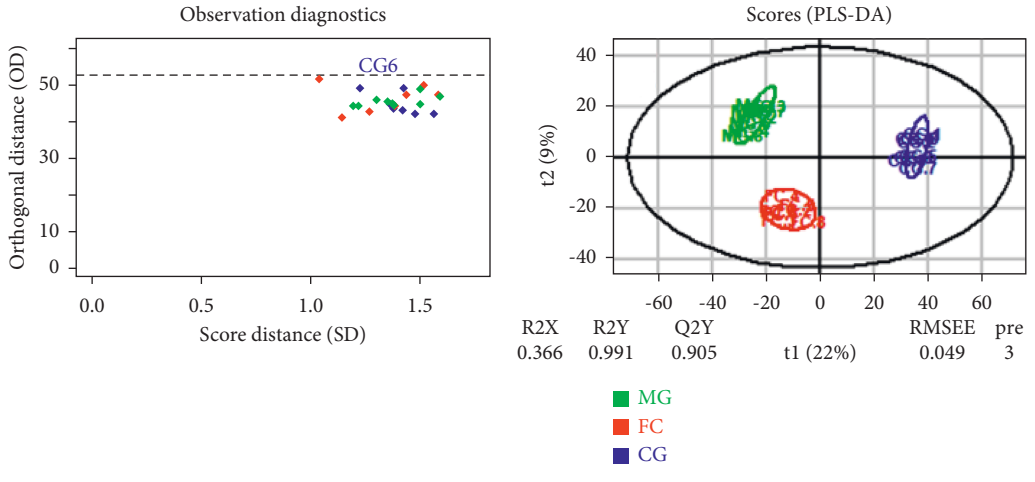

(d) (e)

Figure 3: Continued.

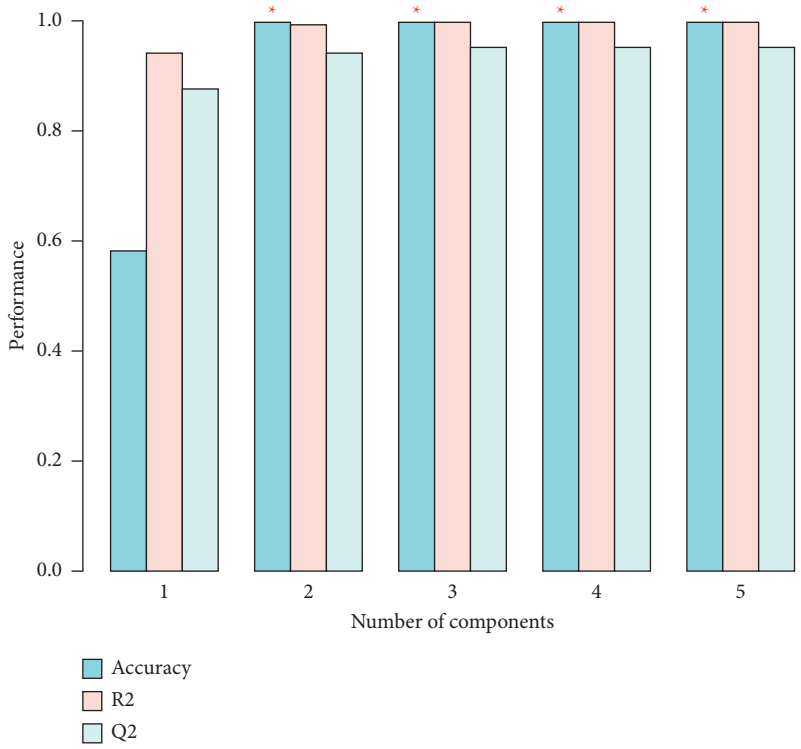

(f)

Figure 3: PCA and PLS-DA of samples based on serum metabolomics. (a) PCA of samples based on the serum metabolomics. (b) Overview of the PLS-DA model of samples based on the serum metabolomics. (c) Permutation test of the PLS-DA model of samples based on the serum metabolomics. (d) Observation diagnostics. (e) Score plot of the PLS-DA model based on the first and second components. (f) Cross-validation (CV) analysis of PLS-DA model.

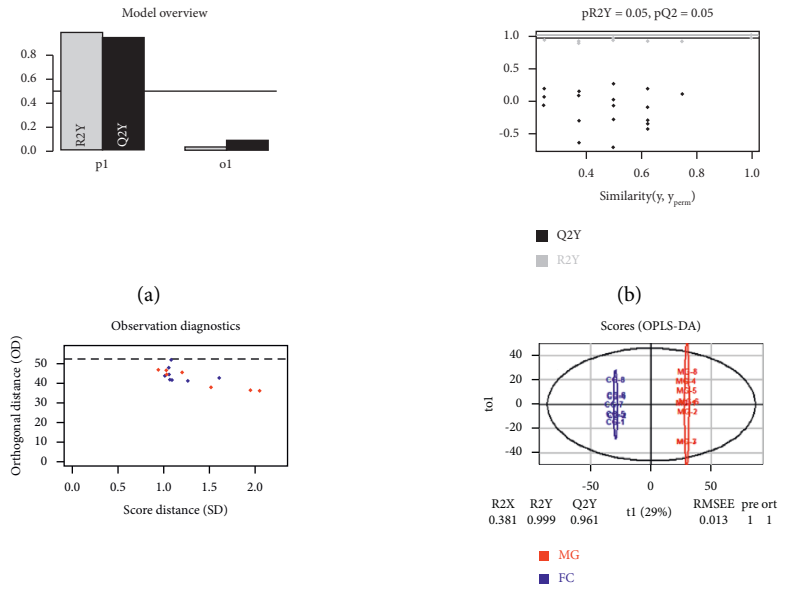

Figure 4: Continued.

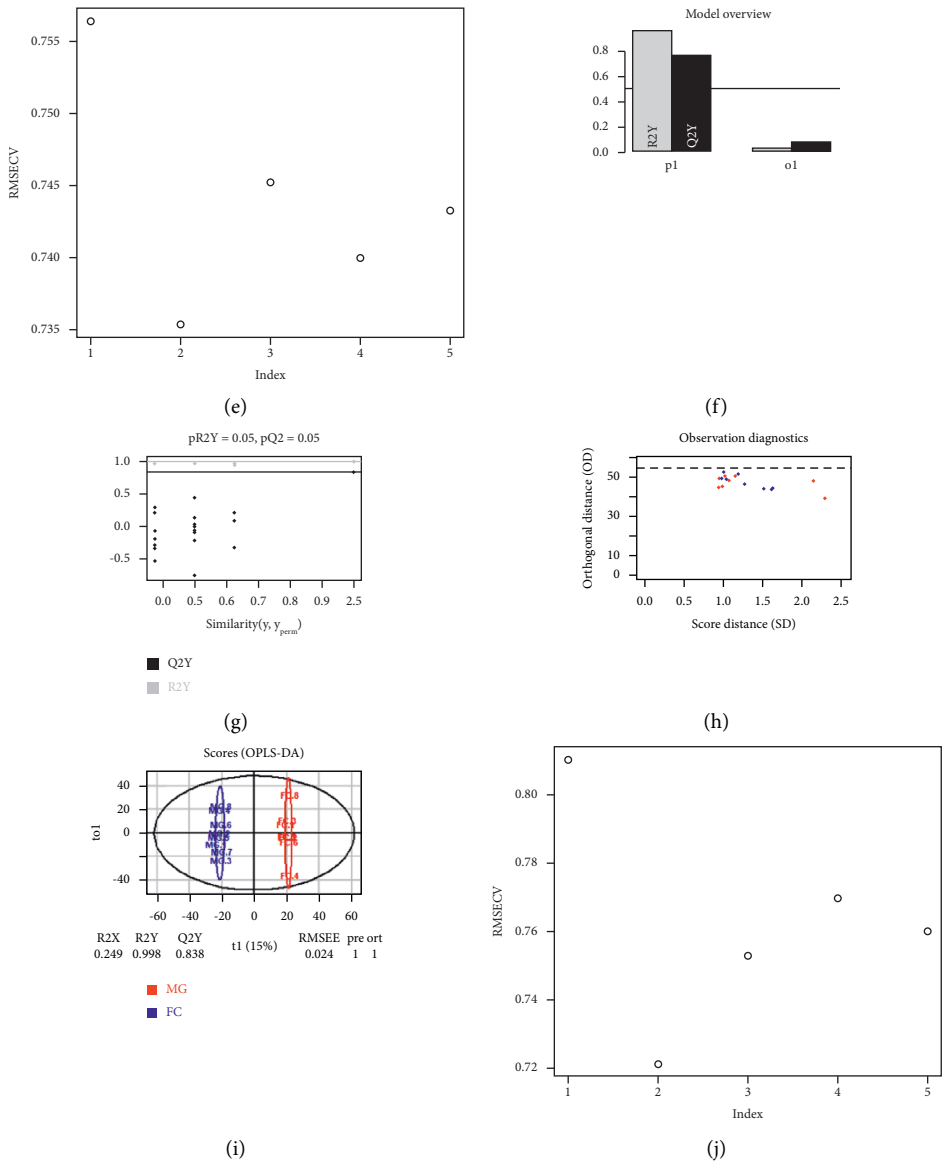

Figure 4: OPLS-DA of samples based on serum metabolomics. (a) Overview of the OPLS-DA model of CG and MG samples based on the serum metabolomics. (b) Permutation test of the OPLS-DA model of CG and MG samples based on the serum metabolomics. (c) Observation diagnostics of the OPLS-DA model of CG and MG samples. (d) Score plot of the OPLS-DA model based on the first and second components. (e) Root mean square error of cross validation (RMSECV) of the OPLS-DA model of CG and FC samples. (f) Overview of the OPLS-DA model of FC and MG samples based on the serum metabolomics. (g) Permutation test of the OPLS-DA model of FC and MG samples based on the serum metabolomics. (h) Observation diagnostics of the OPLS-DA model of FC and MG samples. (i) Score plot of the OPLS-DA model of FC and MG samples based on the first and second components. (j) Root mean square error of cross validation (RMSECV) of the OPLS-DA model of MG and FC samples.

that 1-methyladenine and phenylglyoxylic acid were the metabolites with the highest VIP scores considering all the metabolites. Functional analysis of the metabolites in profile 6 indicated their enrichment in metabolic pathways of lactose degradation, *de novo* triacylglycerol biosynthesis, pyruvaldehyde degradation, glucose-alanine cycle, and glycerol phosphate shuttle (Figure 7).

3.5. Metabolic Correlation Network of FC-Responsive Metabolites in Alcoholic Liver Injury and Identification of Hub Metabolites. In order to identify the interactions between the FC-responsive metabolites clustered in profile 6 and the hub metabolites, the Pearson correlation analysis was performed. The correlation result is summarized in Additional File S5. The metabolites with a correlation coefficient absolute value higher than 0.8 were selected as the interaction network, which was visualized in Cytoscape. The constructed network (Additional Figure S3) contained 634 nodes and 13,549 edges. The average number of neighbors was 45.379, while the network diameter and radius were 10 and 5, respectively. Using the MCODE plugin, we identified 22 hub clusters. The cluster with the highest score contained 103 metabolites, which were considered as the hub

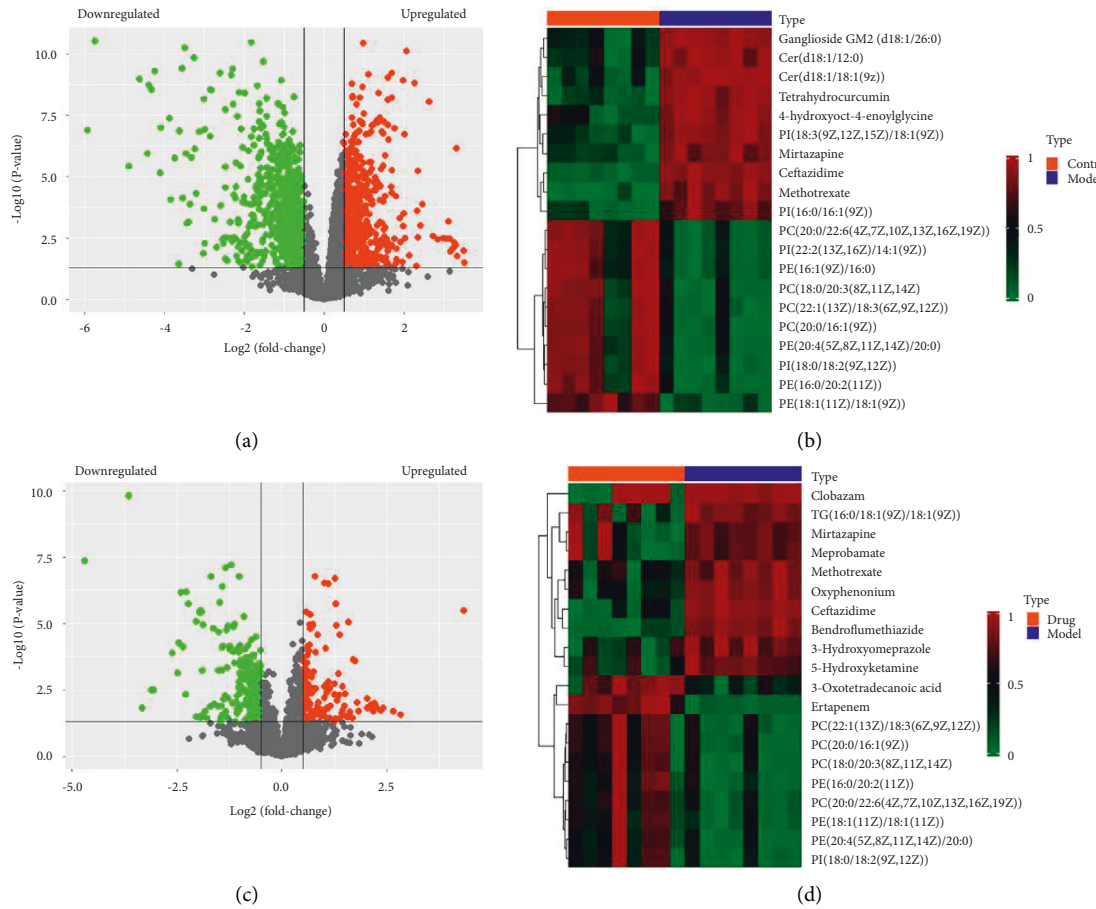

Figure 5: Differential expression analysis of the metabolites. (a) Volcano plot showing the profile of metabolites differentially expressed between the CG and MG. (b) Heatmap showing the profile of the top 20 metabolites differentially expressed between the CG and MG. (c) Volcano plot showing the profile of metabolites differentially expressed between the FC and MG. (d) Heatmap showing the profile of the top 20 metabolites differentially expressed between the FC and MG.

metabolites that are deregulated in alcoholic liver injury and responsive to FC (Figure 8(a)). The enrichment analysis of hub metabolites indicated their involvement in the pathways of nicotinate and nicotinamide metabolism, retinol metabolism, "alanine, aspartate, and glutamate metabolism," tryptophan metabolism, and aminoacyl tRNA-biosynthesis (Figure 8(b)).

4. Discussion

In the present study, we established a rat model of acute alcoholic liver injury and explored the hepatoprotective effect of FC on the injured liver. Moreover, we performed metabolomics analysis to uncover the metabolites that are deregulated in alcohol-induced liver injury and the FC-responsive metabolites in these conditions. We found that alcohol induced significant damage in the liver of rats as indicated by deregulation of liver function markers and histopathological analysis. Alcohol also induced ROS production in the liver of rats. All these deleterious effects were attenuated by FC treatment, indicating the protective role of FC on the hepatocyte. Furthermore, we uncovered a set of 910 metabolites that were upregulated in alcohol-induced injury rats but subsequently downregulated by FC treatment. In addition, 621 of FC-responsive metabolites were involved in a robust interaction network and 96 of them were identified as hub metabolites that were involved in amino acids-related metabolism. These results suggested that FC can alleviate alcohol-induced liver injury and the protective effect might be partly driven by restitution of metabolic homeostasis.

It is well known that TG, AST, ALT, and AST are credible markers of liver diseases and alcohol-induced liver damages. Here, we found that TG, AST, ALT, and AST were increased in the alcohol-treated rats, indicating that the alcohol-induced acute liver injury model was successfully established. FC is known for its multifarious therapeutic and preventive effects against diverse human diseases [11, 12]. However, the effect of FC on the alcohol-induced acute liver injury has not been systematically demonstrated before. Here, we found that FC could improve the liver function by downregulating TG, AST, ALT, and ROS in the alcoholic acute liver injury model, suggesting that FC exerts therapeutic and preventive effects against alcohol-induced liver injury.

Alcohol-induced liver injury is generally followed by metabolic disorders due to the shift in the metabolite profile

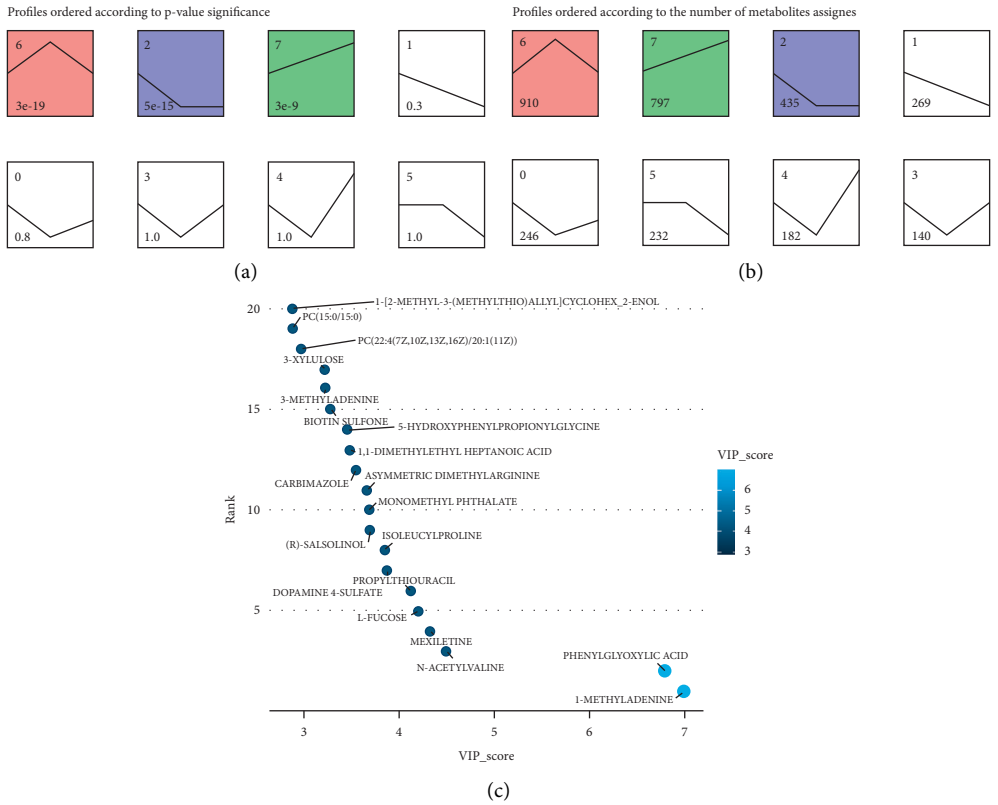

FIGURE 6: Time series clustering for the identification of FC-responsive metabolites in alcoholic liver injury. (a) Profiles ordered by p values. (b) Profiles ordered by number of metabolites assigned. (c) Bubble chart indicating the top 20 metabolites in profile 6 containing FC-responsive metabolites based on their VIP scores as obtained from the PLS-DA.

[26, 27]. Several metabolomics studies have indicated a drastic change in the liver and blood metabolite profiles in alcohol-induced liver injury [28–30]. Here, we found that alcohol induced significant changes in the metabolite profiles of rat serum. These metabolites can serve as metabolic biomarkers for alcohol-induced acute liver injury. The metabolites deregulated by alcohol treatment were those significantly related to amino acid metabolism, lipid metabolism, and terpenoid metabolism. Our study corroborated with previous studies indicating that amino acid metabolism is subjected to disturbances in liver injury [31–33]. Other studies indicated that the regulation of amino acids plays a significant role in the attenuation of deleterious features in the injured liver [34]. Studies have also indicated that lipid metabolism is significantly shifted in the acute liver injury [35–37]. As antioxidant compounds, terpenoids play a significant role in the homeostasis of human tissue. The disturbance of terpenoid metabolism in the present study may be one of the causes of deleterious phenotypes observed in the present study. More importantly, we found that most of the metabolites upregulated in the liver injury model were downregulated by FC treatment, indicating that FC may exert its protective effect via modulation of the metabolite profile. A significant cluster of 96 hub metabolites was identified, which also regulated the metabolism of amino acids. This further confirmed that FC was able to correct the metabolic disorders induced by alcohol treatment.

Up to date, the metabolic pathways involved in the pathogenesis of the alcoholic liver injury are not well elucidated. In the present study, we identified the pathways associated with the metabolites upregulated in alcoholic acute liver injury and that could be reversed by FC. As a result, we found that these pathways were involved in multiple metabolic pathways with lactose degradation as the most enriched. Though the involvement of lactose degradation pathway has not been reported in acute liver injury as demonstrated in the present study, previous studies have indicated that the lactose degradation pathway, as well as other carbohydrates-related pathways, is induced in the plasma and tissues and may be a target for the protective effect of the traditional Chinese medicine *Achyranthes bidentata* Blume in ovariectomia rats [38]. Another important pathway that was found upregulated was the "de novo triacylglycerol biosynthesis." Previous studies have indicated that the upregulation of de novo triacylglycerol biosynthesis is conductive to increased oxidative stress in the liver cells, which causes liver damage [39, 40]. Thus, our results suggested that alcoholic injury of the liver was followed by increased oxidative stress, which could be reversed by the treatment with FC. This observation was also in corroboration with our results of increased ROS production in the MG and its reversal by FC treatment. Previous studies have indicated that de novo lipogenesis is involved in the multiple

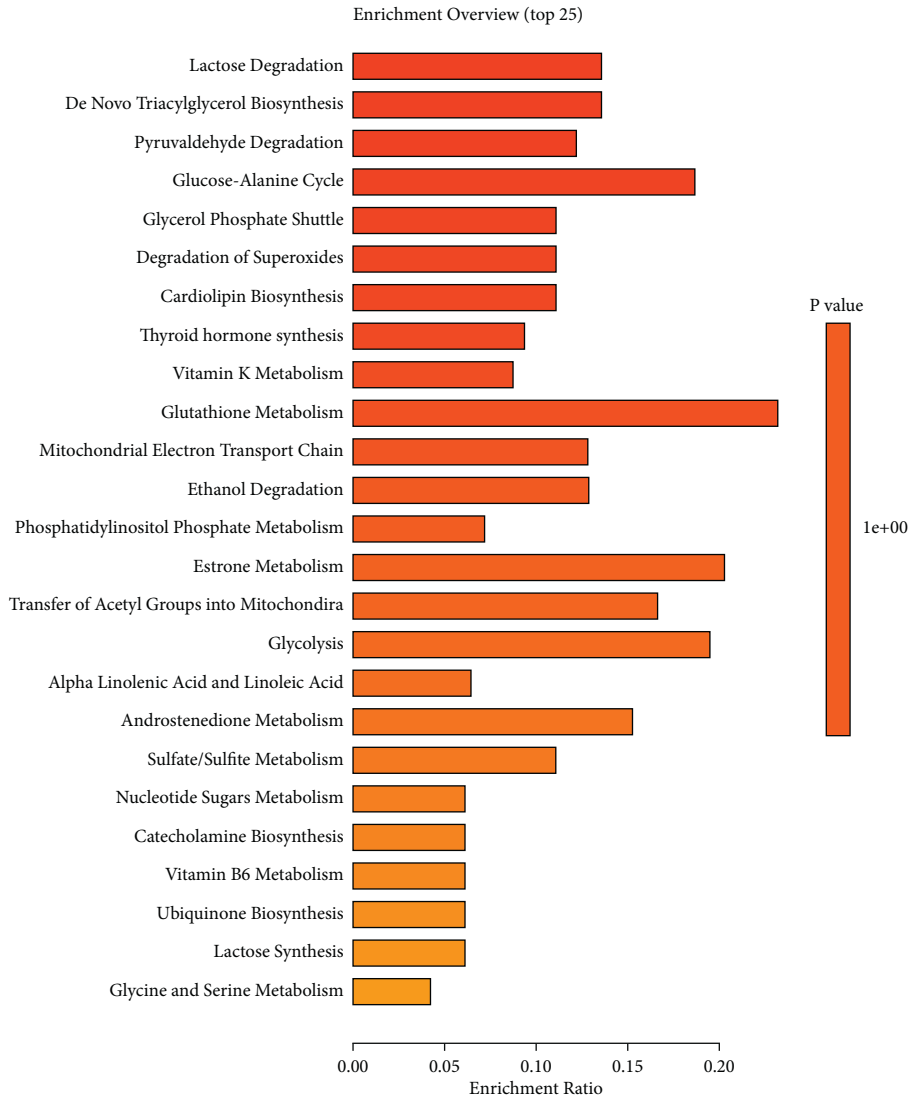

Figure 7: Enrichment analysis of metabolites in profile 6 containing FC-responsive metabolites.

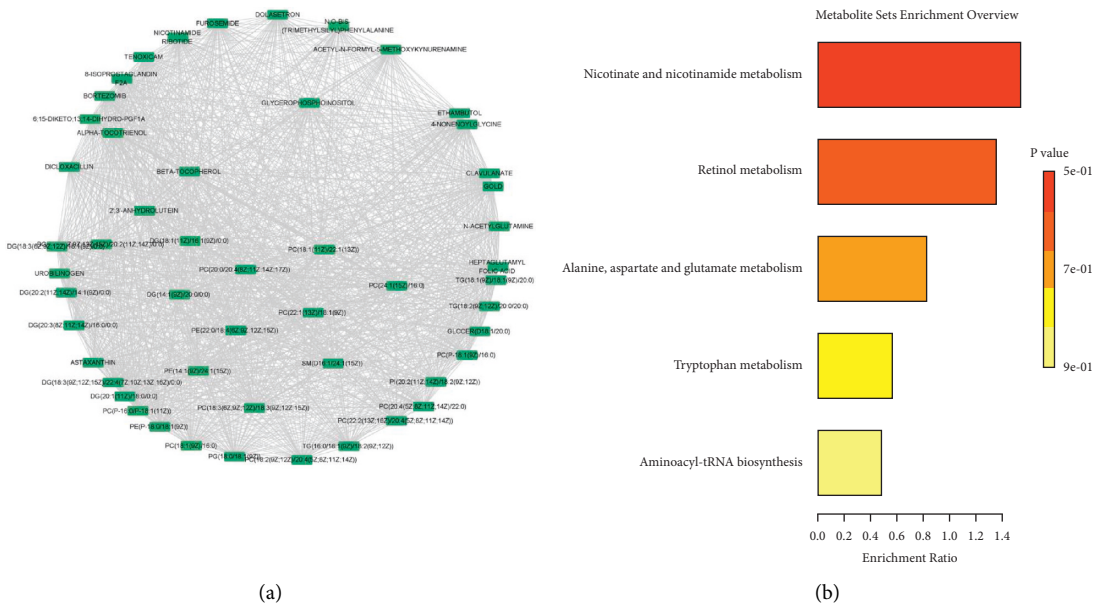

Figure 8: Identification of the hub metabolites and metabolites network in profile 6 containing FC-responsive metabolites. (a) Hub metabolite network containing metabolites with node degree equal or higher than 100. (b) Enrichment of hub metabolites.

conditions associated with the liver, for example, fatty liver disease [41]. The pyruvaldehyde degradation pathway is the main pathway involved in the degradation of pyruvaldehyde, a toxic metabolite that interacts with proteins and nucleic acids [42]. Here, we found that the pyruvaldehyde degradation metabolic pathway was dysregulated in the alcoholic liver injury and was reversed by the FC treatment. This is the first study to report the effect of FC on this pathway in alcoholic liver injury. The glucose-alanine cycle metabolic pathway was also found to be regulated by FC in the treatment of alcoholic liver injury animals. In a previous study, it was found that the dysregulation of the glucose-alanine cycle may be responsible for the increased levels of glucose and lactate in the blood in hepatotoxicity conditions [43]. This observation was also in corroboration with the dysregulation of lactose degradation stated above. Glycerol phosphate shuttle is involved in the transfer of reducing equivalents from the cytoplasm to the mitochondria. This pathway was impaired in the alcoholic liver injury and could be targeted by FC treatment. The impairment of the glycerol phosphate shuttle was involved in the impairment of oxidative stress in the experimental model of diabetes [44]. The enrichment analysis of the hub metabolites indicated their involvement in nicotinate and nicotinamide metabolism, retinol metabolism, "alanine, aspartate, and glutamate metabolism," and tryptophan metabolism. A previous study found that nicotinate and nicotinamide metabolism was impaired in acute liver failure and could be reversed by mahuang decoction [45], which similarly corroborates with our present findings. Altered retinol metabolism has been incriminated in diverse liver conditions such as hepatic fibrosis and nonalcoholic fatty liver disease [46]; here, we also found similar results. Our findings of altered "alanine, aspartate, and glutamate metabolism" pathway were also in corroboration with previous studies indicating that "alanine, aspartate, and glutamate metabolism" is impaired in acute liver injury [47] and nonalcoholic fatty liver [48]. Numerous studies have also indicated the dysregulation of tryptophan metabolism in liver injury [49, 50], which was in conformity with our findings. Thus, our study indicated the involvement of numerous pathways in alcohol-induced liver injury and these changes could be reversed by the treatment of FC.

5. Conclusions

The present study identified a cluster of metabolites that are activated in alcohol-induced liver injury. In addition, FC was proven efficient to correct these metabolic disturbances. The obtained results potentiate FC as a candidate therapeutic for preventing or treating alcohol-induced acute liver injury. The results are to be considered with reservation because of a number of shortcomings: (1) although the experimental conditions and instrument stability were good, the number of samples remains small, which impinges on the relevance of the results obtained; and (2) the identification of metabolites in this study requires additional metabolite validation work.

Data Availability

The experimental data used to support the findings of this study are available from the corresponding author upon request.

Conflicts of Interest

The authors declare that there are no conflicts of interest regarding the publication of this paper.

Acknowledgments

This work was supported by the National Natural Science Foundation of China (62162049), Mongolian Medicine Safety Evaluation and Innovation Team Project (MY20190003), Science and Technology Projects of Inner Mongolia Autonomous Region (2020GG0190), Natural Science Foundation of Inner Mongolia Autonomous Region of China (2021LHMS06007, 2019MS08036), Research Program of Science and Technology at Universities of Inner Mongolia Autonomous Region (NJZY20112), Program for Young Talents of Science and Technology in Universities of Inner Mongolia Autonomous Region (NJYT-19-B18), and Grassland Talents-Mongolian Medicine Data Mining Key Technology Research Innovative Talent Team, Inner Mongolia University for Nationalities doctoral research start fund project (BS543).

Supplementary Materials

Additional Figure S1. Enrichment analysis of metabolites differentially expressed between the CG and MG. Additional Figure S2. Enrichment analysis of metabolites differentially expressed between the FC and MG. Additional Figure S3. Metabolite interaction network of FC-responsive metabolites in alcoholic liver injury. Additional File S1. List of ingredients in FC as reported in TCMSP. Additional File S2. List of metabolites differentially expressed between the CG and MG. Additional File S3. List of metabolites differentially expressed between the FC and MG. Additional File S4. List of FC-responsive metabolites in alcoholic liver injury. Additional File S5. Pearson correlation of FC-responsive metabolites in alcoholic liver injury. (*Supplementary Materials*)

References

[1] W. Bernal, G. Auzinger, A. Dhawan, and J. Wendon, "Acute liver failure," *The Lancet*, vol. 376, no. 9736, pp. 190–201, 2010.

[2] V. Dong, R. Nanchal, and C. J. Karvellas, "Pathophysiology of acute liver failure," *Nutrition in Clinical Practice*, vol. 35, no. 1, pp. 24–29, 2020.

[3] A. Grek and L. Arasi, "Acute liver failure," *AACN Advanced Critical Care*, vol. 27, no. 4, pp. 420–429, 2016.

[4] B. Gao and R. Bataller, "Alcoholic liver disease: pathogenesis and new therapeutic targets," *Gastroenterology*, vol. 141, no. 5, pp. 1572–1585, 2011.

[5] C. A. Marroni, A. D. M. Fleck Jr., S. A. Fernandes et al., "Liver transplantation and alcoholic liver disease: history, controversies, and considerations," *World Journal of Gastroenterology*, vol. 24, no. 26, pp. 2785–2805, 2018.

[6] C. Torruellas, S. W. French, and V. Medici, "Diagnosis of alcoholic liver disease," *World Journal of Gastroenterology*, vol. 20, no. 33, pp. 11684–11699, 2014.

[7] R. Khan and S. Koppe, "Modern management of acute liver failure," *Gastroenterology Clinics of North America*, vol. 47, no. 2, pp. 313–326, 2018.

[8] F. M. Trovato, L. Rabinowich, and M. J. W. McPhail, "Update on the management of acute liver failure," *Current Opinion in Critical Care*, vol. 25, no. 2, pp. 157–164, 2019.

[9] J. Fu, X. Li, H. Lu, and Y. Liang, "Analysis of volatile components in herbal pair semen persicae-flos carthami by GC-MS and chemometric resolution," *Journal of Separation Science*, vol. 35, no. 21, pp. 2940–2948, 2012.

[10] N. D. Hostert, C. L. Blomquist, S. L. Thomas, D. G. Fogle, and R. M. Davis, "First report of ramularia carthami, causal agent of ramularia leaf spot of safflower, in California," *Plant Disease*, vol. 90, no. 9, p. 1260, 2006.

[11] H. Liao, L. Banbury, H. Liang et al., "Effect of Honghua (flos carthami) on nitric oxide production in RAW 264.7 cells and α-glucosidase activity," *Journal of Traditional Chinese Medicine*, vol. 34, no. 3, pp. 362–368, 2014.

[12] J. Y. Wu, Z. L. Yu, W. F. Fong, and Y. Q. Shi, "Chemotherapeutic activities of carthami flos and its reversal effect on multidrug resistance in cancer cells," *African Journal of Traditional, Complementary and Alternative Medicines*, vol. 10, no. 4, pp. 36–40, 2013.

[13] H.-P. Mao, X.-Y. Wang, Y. H. Gao et al., "Danhong injection attenuates isoproterenol-induced cardiac hypertrophy by regulating p38 and NF-κb pathway," *Journal of Ethnopharmacology*, vol. 186, pp. 20–29, 2016.

[14] M. Sun, J.-J. Zhang, J.-Z. Shan et al., "Clinical observation of Danhong injection (herbal TCM product from radix *Salviae miltiorrhizae* and flos carthami tinctorii) in the treatment of traumatic intracranial hematoma," *Phytomedicine*, vol. 16, no. 8, pp. 683–689, 2009.

[15] H. Ao, W. Feng, and C. Peng, "Hydroxysafflor yellow A: a promising therapeutic agent for a broad spectrum of diseases," *Evidence-based Complementary and Alternative Medicine*, vol. 2018, 17 pages, Article ID 8259280, 2018.

[16] R. Bujak, W. Struck-Lewicka, M. J. Markuszewski, and R. Kaliszan, "Metabolomics for laboratory diagnostics," *Journal of Pharmaceutical and Biomedical Analysis*, vol. 113, pp. 108–120, 2015.

[17] K. Kusonmano, W. Vongsangnak, and P. Chumnanpuen, "Informatics for metabolomics," *Advances in Experimental Medicine and Biology*, vol. 939, pp. 91–115, 2016.

[18] I. Laíns, M. Gantner, S. Murinello et al., "Metabolomics in the study of retinal health and disease," *Progress in Retinal and Eye Research*, vol. 69, pp. 57–79, 2019.

[19] L. D. Roberts, A. L. Souza, R. E. Gerszten, and C. B. Clish, "Targeted metabolomics," *Current Protocols in Molecular Biology*, John Wiley & Sons, vol. 30, Hoboken, NJ, USA, 2012.

[20] S. C. Kalhan, L. Guo, J. Edmison et al., "Plasma metabolomic profile in nonalcoholic fatty liver disease," *Metabolism*, vol. 60, no. 3, pp. 404–413, 2011.

[21] S. Sookoian and C. J. Pirola, "Liver enzymes, metabolomics and genome-wide association studies: from systems biology to the personalized medicine," *World Journal of Gastroenterology*, vol. 21, no. 3, pp. 711–725, 2015.

[22] L. N. Tu, M. R. Showalter, T. Cajka et al., "Metabolomic characteristics of cholesterol-induced non-obese nonalcoholic fatty liver disease in mice," *Scientific Reports*, vol. 7, no. 1, p. 6120, 2017.

[23] Y. Xu, J. Han, J. Dong et al., "Metabolomics characterizes the effects and mechanisms of quercetin in nonalcoholic fatty liver disease development," *International Journal of Molecular Sciences*, vol. 20, no. 5, 2019.

[24] B. Chen, M. Ning, and G. Yang, "Effect of paeonol on antioxidant and immune regulatory activity in hepatocellular carcinoma rats," *Molecules*, vol. 17, no. 4, pp. 4672–4683, 2012.

[25] H. Li, P. Qiu, J. Wang, C. Niu, and S. Pan, "Effects of compound Ginkgo biloba on intestinal permeability in rats with alcohol-induced liver injury," *Food and Function*, vol. 6, no. 2, pp. 470–478, 2015.

[26] L. Kaphalia and W. J. Calhoun, "Alcoholic lung injury: metabolic, biochemical and immunological aspects," *Toxicology Letters*, vol. 222, no. 2, pp. 171–179, 2013.

[27] P. E. Molina, C. McClain, D. Valla et al., "Molecular pathology and clinical aspects of alcohol-induced tissue injury," *Alcoholism: Clinical and Experimental Research*, vol. 26, no. 1, pp. 120–128, 2002.

[28] P. Deng, J. Barney, M. C. Petriello, A. J. Morris, B. Wahlang, and B. Hennig, "Hepatic metabolomics reveals that liver injury increases PCB 126-induced oxidative stress and metabolic dysfunction," *Chemosphere*, vol. 217, pp. 140–149, 2019.

[29] T. Ramirez, A. Strigun, A. Verlohner et al., "Prediction of liver toxicity and mode of action using metabolomics in vitro in HepG2 cells," *Archives of Toxicology*, vol. 92, no. 2, pp. 893–906, 2018.

[30] H. Ziarrusta, L. Mijangos, S. Picart-Armada et al., "Non-targeted metabolomics reveals alterations in liver and plasma of gilt-head bream exposed to oxybenzone," *Chemosphere*, vol. 211, pp. 624–631, 2018.

[31] J. Gomes, A. H. Dawodu, O. Lloyd, D. M. Revitt, and S. V. Anilal, "Hepatic injury and disturbed amino acid metabolism in mice following prolonged exposure to organophosphorus pesticides," *Human and Experimental Toxicology*, vol. 18, no. 1, pp. 33–37, 1999.

[32] Y.-S. Jung, "Metabolism of sulfur-containing amino acids in the liver: a link between hepatic injury and recovery," *Biological and Pharmaceutical Bulletin*, vol. 38, no. 7, pp. 971–974, 2015.

[33] V. R. Pannala, S. K. Estes, M. Rahim et al., "Toxicant-induced metabolic alterations in lipid and amino acid pathways are predictive of acute liver toxicity in rats," *International Journal of Molecular Sciences*, vol. 21, no. 21, 2020.

[34] Y. S. Jung, S. J. Kim, D. Y. Kwon et al., "Alleviation of alcoholic liver injury by betaine involves an enhancement of antioxidant defense via regulation of sulfur amino acid metabolism," *Food and Chemical Toxicology*, vol. 62, pp. 292–298, 2013.

[35] L. P. Bechmann, R. A. Hannivoort, G. Gerken, G. S. Hotamisligil, M. Trauner, and A. Canbay, "The interaction of hepatic lipid and glucose metabolism in liver diseases," *Journal of Hepatology*, vol. 56, no. 4, pp. 952–964, 2012.

[36] B. Bhushan and G. K. Michalopoulos, "Role of epidermal growth factor receptor in liver injury and lipid metabolism: emerging new roles for an old receptor," *Chemico-Biological Interactions*, vol. 324, Article ID 109090, 2020.

[37] Y. Lai, C. Zhou, P. Huang et al., "Polydatin alleviated alcoholic liver injury in zebrafish larvae through ameliorating lipid metabolism and oxidative stress," *Journal of Pharmacological Sciences*, vol. 138, no. 1, pp. 46–53, 2018.

[38] Y. Tao, S. Huang, J. Yan, W. Li, and B. Cai, "Integrated metallomic and metabolomic profiling of plasma and tissues provides deep insights into the protective effect of raw and salt-processed achyranthes bidentata blume extract in

ovariectomia rats," *Journal of Ethnopharmacology*, vol. 234, pp. 85–95, 2019.

[39] F. Yang, S. Yan, Y. He et al., "Expression of hepatitis B virus proteins in transgenic mice alters lipid metabolism and induces oxidative stress in the liver," *Journal of Hepatology*, vol. 48, no. 1, pp. 12–19, 2008.

[40] S.-J. Kim, M. Khan, J. Quan, A. Till, S. Subramani, and A. Siddiqui, "Hepatitis B virus disrupts mitochondrial dynamics: induces fission and mitophagy to attenuate apoptosis," *PLoS Pathogens*, vol. 9, no. 12, Article ID e1003722, 2013.

[41] C. C. Cohen, K. W. Li, A. L. Alazraki et al., "Dietary sugar restriction reduces hepatic de novo lipogenesis in adolescent boys with fatty liver disease," *Journal of Clinical Investigation*, vol. 131, no. 24, 2021.

[42] M. P. Kalapos, "Methylglyoxal in living organisms," *Toxicology Letters*, vol. 110, no. 3, pp. 145–175, 1999.

[43] M. Sun, J. Zhang, S. Liang et al., "Metabolomic characteristics of hepatotoxicity in rats induced by silica nanoparticles," *Ecotoxicology and Environmental Safety*, vol. 208, Article ID 111496, 2021.

[44] M. H. Giroix, J. Rasschaert, D. Bailbe et al., "Impairment of glycerol phosphate shuttle in islets from rats with diabetes induced by neonatal streptozocin," *Diabetes*, vol. 40, no. 2, pp. 227–232, 1991.

[45] W. Liao, Q. Jin, J. Liu et al., "Mahuang decoction antagonizes acute liver failure via modulating tricarboxylic acid cycle and amino acids metabolism," *Frontiers in Pharmacology*, vol. 12, Article ID 599180, 2021.

[46] P. Pettinelli, B. M. Arendt, A. Teterina et al., "Altered hepatic genes related to retinol metabolism and plasma retinol in patients with non-alcoholic fatty liver disease," *PLoS One*, vol. 13, no. 10, Article ID e0205747, 2018.

[47] M. Dai, F. Wang, Z. Zou, G. Xiao, H. Chen, and H. Yang, "Metabolic regulations of a decoction of hedyotis diffusa in acute liver injury of mouse models," *Chinese Medicine*, vol. 12, no. 1, p. 35, 2017.

[48] E. Lee, Y. Lim, S. W. Kwon, and O. Kwon, "Pinitol consumption improves liver health status by reducing oxidative stress and fatty acid accumulation in subjects with non-alcoholic fatty liver disease: a randomized, double-blind, placebo-controlled trial," *The Journal of Nutritional Biochemistry*, vol. 68, pp. 33–41, 2019.

[49] L. Wrzosek, D. Ciocan, C. Hugot et al., "Microbiota tryptophan metabolism induces aryl hydrocarbon receptor activation and improves alcohol-induced liver injury," *Gut*, vol. 70, no. 7, pp. 1299–1308, 2021.

[50] Y. Egashira, T. Komine, T. Ohta, K. Shibata, and H. Sanada, "Change of tryptophan-niacin metabolism in D-galactosamine induced liver injury in rat," *Journal of Nutritional Science and Vitaminology*, vol. 43, no. 2, pp. 233–239, 1997.

Hindawi
Evidence-Based Complementary and Alternative Medicine
Volume 2022, Article ID 4604601, 15 pages
https://doi.org/10.1155/2022/4604601

Research Article

Comparative Pharmacokinetics of Seven Major Compounds in Normal and Atherosclerosis Mice after Oral Administration of Simiao Yong'an Decoction

Ke-han Sun,[1,2] Man-fang Yang,[1,2] Xin-rui Xu,[1] Yang Li,[1,2] Zhao Gao,[1] Qing-yue Zhang,[1] Hui Li,[2] Shu-qi Wang,[3] Li-xia Lou,[1] Ai-ming Wu,[1] Qiu-shuo Jin,[1] Sheng-xian Wu,[1] and Bo Nie[1]

[1]*Key Laboratory of Chinese Internal Medicine of Ministry of Education and Beijing, Dongzhimen Hospital, Beijing University of Chinese Medicine, Beijing 100700, China*
[2]*School of Chinese Materia Medica, Beijing University of Chinese Medicine, Beijing 100029, China*
[3]*Zibo Hospital of Traditional Chinese Medicine, Zibo 255399, Shandong, China*

Correspondence should be addressed to Sheng-xian Wu; wushx@sina.com and Bo Nie; nieboww_1977@163.com

Received 31 December 2021; Revised 31 March 2022; Accepted 11 April 2022; Published 28 April 2022

Academic Editor: Li-Ping Kang

Simiao Yong'an decoction (SMYAD), a classic traditional Chinese medicine formula, has been used to treat atherosclerosis (AS) in clinical in China, but its therapeutic mechanism and pharmacodynamic material basis are not clear. In this study, the AS model was caused by a high-fat diet and perivascular carotid collar placement (PCCP), and SMYAD was orally administered to the model and normal mice. A rapid, sensitive, selective, and reliable method using ultrahigh-performance liquid chromatography (UHPLC) system combined with a Q Exactive HF-X mass spectrometer (UHPLC-Q Exactive HF-X MS) was established and validated for the simultaneous determination of seven compounds, including harpagide, chlorogenic acid, swertiamarin, sweroside, angoroside C, liquiritin, and isoliquiritigenin in the plasma of normal and AS mice. The specificity, linearity, precision, accuracy, recovery, and stability of the method were all within the acceptable criteria. The results showed that some pharmacokinetic behaviors of harpagide, chlorogenic acid, and isoliquiritigenin were significantly different among the two groups of mice. The specific parameter changes were harpagide (AUC_{0-t} and $AUC_{0-\infty}$ were 11075.09 ± 2132.38 and 16221.95 ± 5622.42 ng·mL^{-1}·h, respectively; CLz/F was 2.45 ± 0.87 L/h/mg), chlorogenic acid ($t_{1/2}$ was 21.59 ± 9.16 h; $AUC_{0-\infty}$ was 2637.51 ± 322.54 ng·mL^{-1}·h; CLz/F was 13.49 ± 1.81 L/h/mg) and isoliquiritigenin (AUC_{0-t} and $AUC_{0-\infty}$ were 502.25 ± 165.65 and 653.68 ± 251.34 ng·mL^{-1}·h, respectively; CLz/F was 62.16 ± 23.35 L/h/mg) were altered under the pathological status of AS. These differences might be partly ascribed to the changes in gastrointestinal microbiota, nonspecific drug transporters, and cytochrome P450 activity under the AS state, providing research ideas and experimental basis for pharmacological effects and pharmacodynamic material basis.

1. Introduction

Atherosclerosis (AS) is the significant pathological basis of cardiovascular and cerebrovascular diseases, which may cause stroke, coronary atherosclerotic heart disease, and myocardial infarction [1]. The pathogenesis of AS is complex and involves various factors, such as endothelial dysfunction, lipid deposition, smooth muscle cell proliferation, oxidative stress, cell apoptosis, and systemic and local inflammation [2]. According to the guideline, lipid-lowering drugs are the first-line drugs for the secondary prevention of coronary heart disease, and statins are the most widely used lipid-lowering drugs in clinical practice [3]. Statins have a significant effect on reducing blood lipid, but there are also adverse reactions, such as muscle symptoms and diabetes in long-term use [4]. Traditional Chinese medicine (TCM) contains a variety of active ingredients, which has good effects on the treatment and prevention of AS in clinical in China [5].

Simiao Yong'an decoction (SMYAD) is a traditional Chinese medicine formula, which consists of *Lonicera japonica* Thunb. (JYH), *Scrophularia ningpoensis* Hems. (XS), *Angelica sinensis* (Oliv.) Diels (DG), and *Glycyrrhiza uralensis* Fisch. (GC). SMYAD was used to treat gangrene in ancient times according to the traditional Chinese medicine classics. In recent years, this prescription has had a remarkable clinical effect in the treatment of atherosclerosis. It has been confirmed by pharmacological research that SMYAD can affect the migration of smooth muscle cells, inhibit the angiogenesis in plaques, and inhibit the release of inflammatory factors, antioxidative stress, but its pharmacodynamic material basis is indistinct [6, 7]. Previous studies [8, 9] have shown that SMYAD contains many kinds of compounds, such as iridoids, flavonoids, organic acids, and phenylpropanoids. Some of these components have anti-AS-related activities. Harpagide has an effect on facilitating cell migration into the inflamed tissue and promoting the anti-inflammatory activity of the resident macrophages [10]. Chlorogenic acid could protect the ApoE$^{-/-}$ mice against AS through accelerating the cholesterol efflux from macrophages [11]. Swertiamarin has been reported to have high antiatherogenic and cholesterol-lowering potential and can inhibit HMG-Co-A reductase [12]. Sweroside, angoroside C, and liquiritin can take many pharmacological roles, including anti-inflammatory, antioxidation, and cardiovascular protection [13–15]. Isoliquiritigenin could attenuate AS in ApoE$^{-/-}$ mice and inhibit the proliferation of human arterial smooth muscle cell [16, 17]. Since plasma component concentrations and exposure times could well reflect the close relationship between the drug and its pharmacokinetic effect, it is important to interpret the blood components and pharmacokinetic changes for explaining prescription pharmacodynamic substances. Liu et al. investigated the pharmacokinetic characteristics following oral administration of extracts of SMYAD and its single and combined TCMs to rats [18]. However, the data on the pharmacokinetics of SMYAD are limited to normal physiological conditions, and its multicomponent pharmacokinetic investigation in disease conditions has been rarely conducted.

The ultrahigh-performance liquid chromatography (UHPLC) system combined with a Q Exactive HF-X mass spectrometer can provide high resolution in a short analysis time, allowing the simultaneous detection and quantification of a large number of compounds [19]. Therefore, we developed an analysis method for the simultaneous determination of harpagide, chlorogenic acid, swertiamarin, sweroside, angoroside C, liquiritin, and isoliquiritigenin in normal mice and ApoE$^{-/-}$ mice with a high-fat diet and perivascular carotid collar placement (PCCP)-induced AS using UHPLC-Q Exactive HF-X MS and conducted pharmacokinetic studies in normal and disease conditions. The results will discover the material basis of SMYAD for treating AS to support further drug development, and the pharmacokinetic differences between normal and model mice could provide a reference for the pharmacological mechanism.

2. Materials and Methods

2.1. Reagents, Chemicals, and Materials. Linarin (internal standard, IS), harpagide, chlorogenic acid, swertiamarin, sweroside, angoroside C, liquiritin, and isoliquiritigenin (purity ≥98%) were purchased from Shanghai Yuanye Bio-Technology Co., Ltd. (Shanghai, China). Methanol (HPLC grade) was purchased from Fisher Scientific (USA). Formic acid (MS grade) was purchased from ANPEL Laboratory Technologies Co., Ltd. (Shanghai, China). The distilled water was purchased from A.S. Watson Group Ltd. (Beijing, China).

Lonicera japonica Thunb. (JYH), *Scrophularia ningpoensis* Hems. (XS), *Angelica sinensis* (Oliv.) Diels (DG), and *Glycyrrhiza uralensis* Fisch. (GC) were purchased from the pharmacy of Dongzhimen Hospital of Beijing University of Traditional Chinese Medicine (Beijing, China).

2.2. Preparation of SMYAD. Pieces of JYH, XS, DG, and GC were weighed according to the proportion of 3 : 3 : 2 : 1 with appropriate amounts. The mixed pieces were crushed and decocted two times (60 mins first time and 30 mins second time) with water (1 : 10 w/v first time and 1 : 8 w/v second time) after being soaked. The decoctions were then combined and condensed to a concentration of 2 g/mL.

2.3. Animal Experiment. Male C57BL/6J mice and ApoE$^{-/-}$ mice on a C57BL/6 background (7 weeks old, 18–22 g) were purchased from Beijing Vital River Laboratory Animal Technology Co., Ltd. (Beijing, China, Certificate No.: SCXK (Jing) 2016-0006). All the mice were kept in an SPF animal house (Dongzhimen Hospital Affiliated to Beijing University of Chinese Medicine, Certificate No.: SYXK (Jing) 2015-0001) with food and water freely available, 12 h light/dark, and environmental conditions of 22°C–24°C, 50% relative humidity. All protocols of animal experiments were performed in accordance with the National Guidelines for Laboratory Animal Welfare and were approved by the Animal Ethics Committee of Beijing University of Chinese Medicine (NO. BUCM-4-2015071701-3001). High-fat feeding (containing 15% fat and 0.25% cholesterol) was provided by Beijing HFK bioscience CO., LTD. (Beijing, China, Certificate No.: SCXK (Jing) 2014-0018).

The AS model was established by a high-fat diet and perivascular carotid collar placement (PCCP) surgery in the ApoE$^{-/-}$ mice. After a 7-day adaptive feeding, the mice were given a high-fat diet for 2 weeks; before anesthesia, all ApoE$^{-/-}$ mice were fasted for 12 hours. During the surgery, the right common carotid artery was exposed, and a silicone cannula (length: 2.5 mm, inner diameter: 0.3 mm) was fixed around the carotid artery (external diameter: about 0.5 mm). Penicillin was injected intraperitoneally for 3 days after surgery to prevent infection. High-fat diet continued for 8 weeks after surgery to establish AS model. Biochemical assays and hematoxylin and eosin (HE) staining were used to evaluate whether AS model was successfully established.

The serum concentrations of total cholesterol (TC), triacylglycerols (TG), low-density lipoprotein

cholesterol (LDL-C), and high-density lipoprotein cholesterol (HDL-C) were determined by the automatic biochemical analyzer (AU5800, Beckman Coulter Co., Ltd.). The right carotid arteries of the mice were obtained under stereoscopic observation and fixed by 4% paraformaldehyde, and every consecutive section (3 μm thick) throughout the right carotid artery of the mice was stained with HE.

2.4. Pharmacokinetic Study. Normal control (NC) and AS mice (30 per group) were employed to investigate the pharmacokinetic properties of harpagide, chlorogenic acid, swertiamarin, sweroside, angoroside C, liquiritin, and isoliquiritigenin after the oral administration of SMYAD. After successful induction of AS model, SMYAD was administered to NC and AS mice by intragastric gavage at the crude drug dose of 35 g/kg/d for seven days. Blood samples were collected from each mouse in heparinized tubes via the postorbital venous plexus veins at 0, 0.25, 0.5, 1, 2, 4, 6, 8, 10, 12, 18, and 24 h after seven days of drug administration. Then blood samples were immediately centrifuged at 3500 rpm at 4°C for 10 min and the plasma was stored at −80°C until use.

2.5. Preparation of Stocks Calibration Standard and Quality Control (QC) Samples. Stock solutions of linarin (internal standard, IS), harpagide, chlorogenic acid, swertiamarin, sweroside, angoroside C, liquiritin, and isoliquiritigenin were dissolved in methanol at the concentration of 100 μg/mL, respectively. Then the mixed stock solution was obtained by 6 μg/mL of harpagide, 8 μg/mL of chlorogenic acid, 48 μg/mL of swertiamarin, 10 μg/mL of sweroside, 2 μg/mL of angoroside C, liquiritin, and isoliquiritigenin. The IS working solution was diluted with the methanol to a final concentration of 400 ng/mL.

Standard calibration curves were constructed by spiking 100 μL of blank mouse plasma with 25 μL of the standard working solutions and 25 μL of the IS working solution, yielding final plasma concentrations in the range of 2–1500 ng/mL for harpagide, 1–2000 ng/mL for chlorogenic acid, 5–12000 ng/mL for swertiamarin, 5–2500 ng/mL for sweroside, 5–500 ng/mL for angoroside C and liquiritin, and 2–500 ng/mL for isoliquiritigenin.

Quality control (QC) samples at three concentration levels (38.4, 240, and 600 ng/mL for harpagide; 51.2, 320, and 800 ng/mL for chlorogenic acid; 307.2, 1920, and 4800 ng/mL for swertiamarin; 64, 400, and 1000 ng/mL for sweroside; 12.8, 80, and 200 ng/mL for angoroside C, liquiritin, and isoliquiritigenin) were prepared by the same operation described above. All solutions were stored at 4°C.

2.6. Preparation of Plasma Samples. Each plasma sample (100 μL) was mixed with a threefold volume of methanol and 25 μL IS in a 1.5 mL EP tube. Then the mixture was vortexed for 100 seconds and centrifuged at 12,000 rpm for 10 min at 4°C. The supernatant was transferred to another EP tube and evaporated to dryness under a nitrogen vacuum. The residue was reconstituted with 100 μL of 50% methanol and centrifuged at 15,000 rpm for 15 min. Then the supernatant was transferred to sample vials for the LC-MS analysis.

2.7. Instruments and Experimental Conditions. A Vanquish UHPLC™ system (Thermo Fisher Scientific Inc., USA) was used for the analysis. Samples were separated on an Atlantis T3 column (4.6 mm × 150 mm, 3 μm; Waters, USA). The column temperature was 40°C. The mobile phase, at 0.4 mL/min, consisted of water containing 0.1% formic acid (v/v, A) and methanol (B). The quantitative analysis gradient program was as follows: 0-1 min, 0 B; 1–6 min, 0–100% B; 6–12 min, 100% B; 12–12.1 min, 100%-0 B; 12.1–15 min, 0 B. The injection volume was 5 μL.

The mass spectrometer Q Exactive HF-X (Thermo Fisher Scientific Inc., USA) system was connected to the UHPLC system via heated electrospray ionization (HESI) and controlled by Xcalibur 4.2 software (Thermo Fisher) that was used for data collection and analysis. The mass spectrometer was operated in a negative ionization mode. The MS parameters were set as follows: probe heater temperature, 350°C; capillary temperature: 320°C; sheath gas (N2) flow rate: 30 arbs; auxiliary gas (N2) flow rate: 10 arbs; spray voltage: 3.2 kV (negative); S-Lens RF level: 55 V; scan mode: full MS (resolution 12000); scan range: m/z 150–1500. The most abundant ions in the spectra were selected for sensitive quantitation ($[M\text{-}H]^-$of chlorogenic acid, angoroside C, liquiritin, isoliquiritigenin, and IS, $[M + COOH]^-$ of harpagide, swertiamarin, and sweroside). The m/z of harpagide was 409.13405, chlorogenic acid was 353.08671, swertiamarin was 419.11840, sweroside was 403.12349, angoroside C was 783.27061, liquiritin was 417.11801, isoliquiritigenin was 255.06519, and IS was 591.17083. The structures and mass spectrum of seven analytes and IS are shown in Figure 1.

2.8. Data Analysis. The pharmacokinetic parameters, including maximum plasma concentration (C_{max}), time corresponding to C_{max} (T_{max}), terminal elimination half-life ($T_{1/2}$), area under plasma concentration-time curve (AUC_{0-t}) and area under the plasma concentration-time curve from 0 to infinity time ($AUC_{0-\infty}$), apparent volume of distribution (Vz/F) and clearance (CLz/F), were calculated using the noncompartment model in DAS 2.0 software package (Shanghai, China). GraphPad prism 6.02 (GraphPad Software, USA) was used in the statistical analysis. All values are expressed as mean ± standard error. For the pharmacokinetic parameter values of the NC and AS groups, Student's *t*-test was employed for data comparisons. *P* values <0.05 were considered statistically significant.

3. Results and Discussion

3.1. ApoE$^{-/-}$ Mice as Model Were Successfully Established. Serum biochemical parameters of mice including TC, TG, LDL-C, and HDL-C were determined (see Table 1). Compared to the normal group, TC and LDL-C levels were significantly increased in the AS model group ($P < 0.01$), and

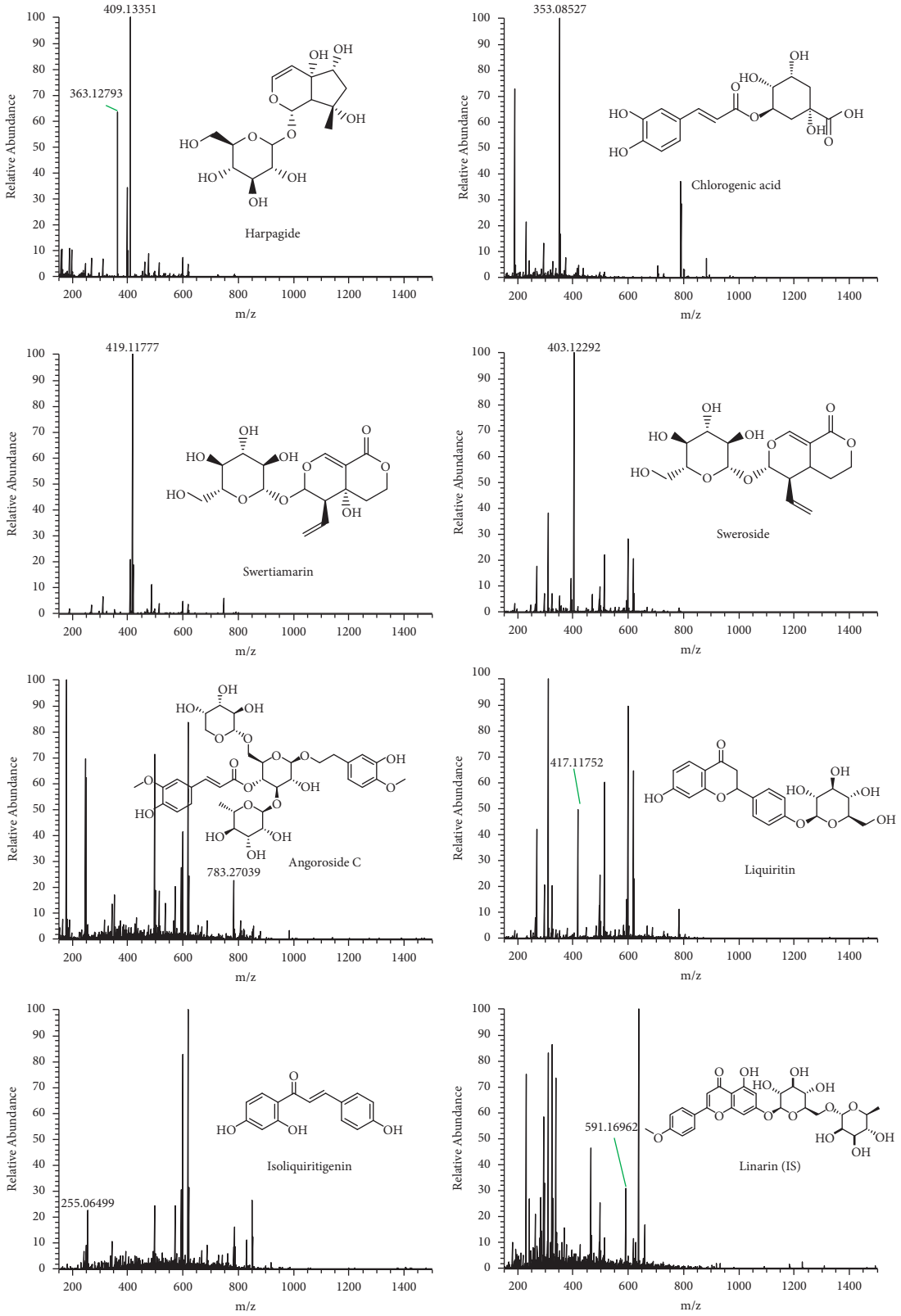

Figure 1: Chemical structures and mass spectrum of the seven compounds and IS.

Table 1: Comparison of blood lipids in the normal group and model group (mean ± SD, $n = 6$, mmol/L).

Group	TC	TG	HDL-C	LDL-C
NC	2.42 ± 0.28	1.64 ± 0.33	1.35 ± 0.18	0.35 ± 0.06
AS	29.15 ± 0.78**	1.35 ± 0.26	1.16 ± 0.10	7.39 ± 0.69**

Compared with the NC group, $^{*}P < 0.05$, $^{**}P < 0.01$.

there were no significant differences in TG and HDL-C levels between the two groups.

HE staining (see Figure 2) showed that the NC group had intact carotid artery structure and no obvious AS plaque formation. Compared with the NC group, the AS group showed AS plaque protruding to the lumen, the vascular lumen was significantly narrowed, foam cells were piled up in the intima, the smooth muscle was disordered and migrated to the intima, and AS plaque was obviously formed. The above results indicated that the AS model was successfully established.

3.2. Method Validation

3.2.1. Specificity. The selectivity was evaluated by comparing the typical chromatograms of blank plasma (in Figure 3(a)), the blank plasma spiked with the seven target analytes and IS (in Figure 3(b)), and the plasma after oral administration of SMYAD (in Figure 3(c)). There was no endogenous interference in the full scan mode for each of the analytes in all samples, indicating the good specificity of the analysis method.

3.2.2. Linearity and Lower Limit of Quantification (LLOQ). The calibration curves for the seven components were established by plotting the peak area ratios of each analyte to the IS against plasma concentrations using the least-square linear regression with a weighted ($1/x$) factor. The limit of detection (LOD) was determined for a signal-to-noise(S/N) ratio of more than 3. The lower limit of quantification (LLOQ) was determined as the lowest concentration on the calibration curve (S/N > 10). As shown in Table 2, the standard curves of the seven target analytes had good linearity with correlation coefficients more than 0.9969. The lowest LLOQ was 1.0 ng/mL.

3.2.3. Recovery and Matrix Effect. The extraction recoveries and matrix effects of the seven compounds were evaluated by determining the QC samples at three concentration levels with five replicates. The recovery of six analytes was measured by comparing the peak areas obtained from the extracted QC samples with those obtained from mixed standards spiked into postextracted blank plasma. The matrix effect was expressed as comparing the peak response of the analytes in plasma samples with those of the pure standards prepared in methanol. The extraction recoveries were in the acceptable range from 90.17% to 111.33%. Regarding the matrix effects, all ratios were between 89.23% and 112.72%, suggesting that there were no endogenous substances and interference for the ionization of the analytes in the coeluting matrix (see Table 3).

3.2.4. Precision and Accuracy. Precision and accuracy were evaluated as five replicate QC samples at LLOQ, low, middle, and high four concentration levels. Intraday precision and accuracy were analyzed during the same day while interday precision and accuracy were investigated on three successive days. Precision (relative standard deviation, RSD) and accuracy (RE) for intra- and interday values were below 15% and within ±15% for the seven compounds (see Table 4), respectively. The results indicated that the intra- and interday precision (RSD%) of these analytes were in the range of 9.39% to 10.5%, respectively, while the corresponding REs ranged from −9.73% to 13.69%, respectively. These results suggested that this method had an acceptable precision and accuracy.

3.2.5. Stability. Stability was evaluated as five replicate QC samples at two concentration levels (see Table 5). The extracted samples were stable under the testing conditions including autosampler temperature (4°C) for 24 h, room temperature (20°C) for 24 h, three freeze-thaw cycles, and long-term cold storage (−20°C for 30 days) with RE% values of −13.11% to 11.89%, indicating that all active ingredients were stable during the analysis.

3.3. Pharmacokinetic Study. The validated method was successfully utilized to examine the concentrations of harpagide, chlorogenic acid, swertiamarin, sweroside, angoroside C, liquiritin, and isoliquiritigenin in NC and AS mice plasma. The mean blood concentration-time curves of seven active components after oral administration of SMYAD (35 g/kg/day) in NC and AS mice are illustrated in Figure 4, and the main pharmacokinetic parameters are listed in Table 6.

The results suggested that active components harpagide, chlorogenic acid, swertiamarin, sweroside, angoroside C, liquiritin, and isoliquiritigenin were quickly absorbed in NC and AS mice after oral administration of SMYAD showing good pharmacokinetic parameters, which was consistent with previous reports [14, 15, 20–24].

Compared with the normal mice, the trends of plasma concentration-time curves of the seven ingredients were changed in AS mice. In terms of pharmacokinetic parameters, the absorption of some active ingredients in AS mice was altered. Specifically, the AUC_{0-t} of harpagide (11075.09 ± 2132.38 ng·mL^{-1}·h, $P < 0.01$), the $AUC_{0-\infty}$ of hapagide (16221.95 ± 5622.42 ng·mL^{-1}·h, $P < 0.05$), and the chlorogenic acid (2637.51 ± 322.54 ng·mL^{-1}·h, $P < 0.01$) in

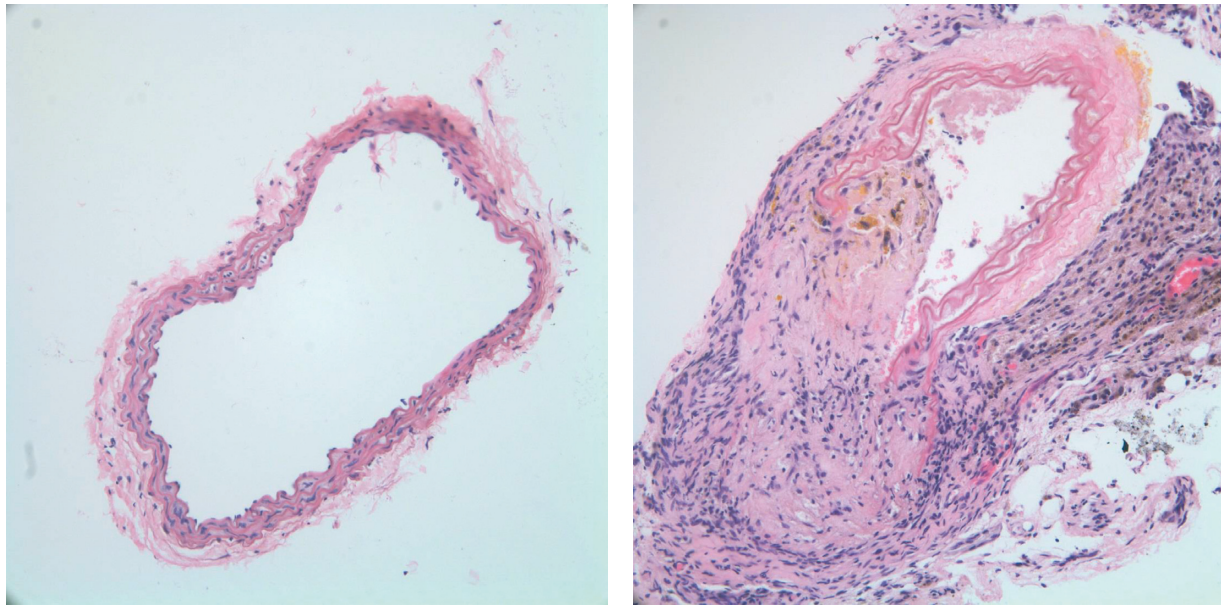

(a) (b)

Figure 2: HE-stained carotid artery sections from NC and AS model. (a) NC group; (b) AS group (magnification, ×20).

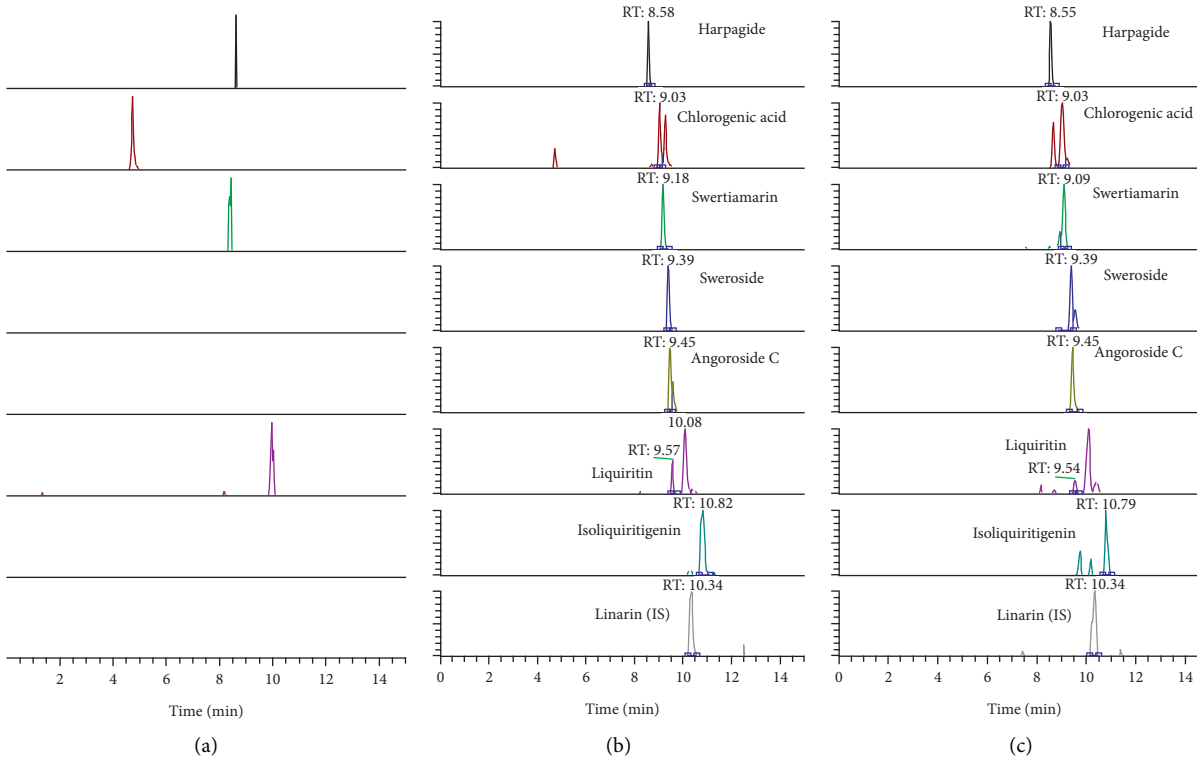

(a) (b) (c)

Figure 3: Extracted-ion chromatograms of harpagide, chlorogenic acid, swertiamarin, sweroside, angoroside C liquiritin, isoliquiritigenin, and IS. (a) Blank plasma; (b) blank plasma spiked with the seven target analytes and IS; (c) drug-containing plasma after administration of SMYAD.

Table 2: Liner range, regression equation, and correlation coefficient for seven compounds.

Compounds	Liner range (ng/ml)	Regression equation	Correlation coefficient (r^2)	LOD (ng/mL)	LLOQ (ng/mL)
Harpagide	2~1500	$y = 0.0021x - 0.0015$	0.9982	1	2
Chlorogenic acid	1~2000	$y = 0.0020x + 0.0131$	0.9978	0.5	1
Swertiamarin	5~12000	$y = 0.0040x - 0.0118$	0.9980	2.5	5
Sweroside	5~2500	$y = 0.0056x + 0.0241$	0.9969	2.5	5
Angoroside C	5~500	$y = 0.0027x - 0.0053$	0.9981	2.5	5
Liquiritin	5~500	$y = 0.0150x + 0.0040$	0.9998	2.5	5
Isoliquiritigenin	2~500	$y = 0.0297x - 0.0562$	0.9968	1	2

Table 3: Recovery and the matrix effect of seven target analytes in QC plasma samples ($n = 5$).

Compounds	QC conc. (ng/mL)	Recovery (%)		Matrix effect (%)	
		Mean (%)	RSD (%)	Mean (%)	RSD (%)
Harpagide	600	101.14	6.37	95.40	3.74
	240	110.32	13.18	91.60	11.41
	38.4	96.61	7.33	96.65	3.13
Chlorogenic acid	800	104.87	5.66	112.72	10.05
	320	107.35	13.24	105.99	6.96
	51.2	100.99	5.50	95.46	4.97
Swertiamarin	4800	99.16	2.23	98.75	3.36
	1920	111.33	1.76	92.09	3.75
	307.2	92.68	9.61	92.37	6.59
Sweroside	1000	102.26	4.23	97.44	3.29
	400	109.48	6.11	89.23	2.33
	64	103.26	7.61	94.33	6.33
Angoroside C	200	98.04	4.06	106.36	6.23
	80	108.81	11.18	103.66	4.81
	12.8	90.17	12.76	109.11	11.46
Liquiritin	200	109.31	6.04	102.86	3.65
	80	106.23	6.80	100.54	3.08
	12.8	103.04	13.81	92.59	5.93
Isoliquiritigenin	200	92.80	8.01	108.26	2.50
	80	106.81	10.11	112.06	6.92
	12.8	94.89	7.79	110.64	11.11

Table 4: Precision and accuracy of seven target analytes in QC plasma samples (mean ± SD, $n = 15$).

Compounds	QC conc. (ng/ml)	Intraday			Inter-day		
		Calc. conc. (ng/ml)	Precision RSD (%)	Accuracy RE (%)	Calc. conc. (ng/ml)	Precision RSD (%)	Accuracy RE (%)
Harpagide	600	621.92 ± 33.83	5.44	3.65	625.92 ± 44.85	7.17	4.32
	240	216.64 ± 10.24	4.73	−9.73	230.99 ± 18.93	8.19	−3.75
	38.4	40.84 ± 3.07	7.51	6.36	39.58 ± 3.30	8.33	3.07
	2	1.74 ± 0.07	3.75	−13.21	1.88 ± 0.23	11.98	−6.03
Chlorogenic acid	800	816.65 ± 48.51	5.94	2.08	827.94 ± 49.36	5.96	3.49
	320	352.34 ± 12.96	3.68	10.11	337.79 ± 24.01	7.11	5.56
	51.2	53.83 ± 5.05	9.39	5.14	53.31 ± 4.59	8.62	4.12
	1	0.97 ± 0.09	9.20	−3.36	0.97 ± 0.08	8.02	−3.35
Swertiamarin	4800	5457.20 ± 189.52	3.47	13.69	5238.94 ± 266.24	5.08	9.14
	1920	1980.91 ± 65.11	3.29	3.17	2056.51 ± 84.80	4.12	7.11
	307.2	297.15 ± 6.53	2.20	−3.27	304.89 ± 18.84	6.18	−0.75
	5	4.37 ± 0.31	7.09	−12.54	5.30 ± 0.70	13.30	5.96
Sweroside	1000	1084.72 ± 35.82	3.30	8.47	1071.96 ± 52.80	4.93	7.20
	400	396.99 ± 14.08	3.55	−0.75	418.16 ± 24.41	5.84	4.54
	64	63.54 ± 4.14	6.52	−0.73	64.87 ± 5.66	8.73	1.36
	5	5.09 ± 0.43	8.51	1.84	4.77 ± 0.41	8.57	−4.70
Angoroside C	200	190.43 ± 10.30	5.41	−4.79	198.76 ± 15.54	7.82	−0.62
	80	81.37 ± 4.63	5.70	1.71	79.58 ± 8.35	10.50	−0.53
	12.8	12.19 ± 0.81	6.63	−4.80	12.62 ± 1.08	8.59	−1.43
	5	4.51 ± 0.29	6.47	−9.86	4.41 ± 0.36	8.17	−11.80
Liquiritin	200	204.79 ± 5.51	2.69	2.39	190.27 ± 12.20	6.41	−4.86
	80	77.78 ± 1.25	1.60	−2.78	75.51 ± 3.80	5.03	−5.61
	12.8	13.15 ± 0.79	5.99	2.76	13.11 ± 0.96	7.30	2.42
	5	4.89 ± 0.47	9.54	−2.14	4.51 ± 0.44	9.86	−9.85
Isoliquiritigenin	200	218.31 ± 6.58	3.01	9.16	216.37 ± 7.84	3.62	8.19
	80	79.91 ± 3.17	3.97	−0.11	78.55 ± 3.72	4.73	−1.81
	12.8	13.68 ± 0.41	3.02	6.85	13.16 ± 1.01	7.70	2.80
	2	1.97 ± 0.21	10.68	−1.41	1.95 ± 0.25	12.92	−2.64

Table 5: Stability of seven target analytes in QC plasma samples (mean ± SD, $n = 5$).

Compounds	QC (ng/ml)	Postpreparative stability 24 h in the autosampler (4°C)		Short-term stability 24 h in room temperature (20°C)		Freeze-thaw stability 3 freeze-thaw cycles		Long-term stability −20°C for 30 d	
		Calc. conc. (ng/ml)	Accuracy RE (%)	Calc. conc. (ng/ml)	Accuracy RE (%)	Calc. conc. (ng/ml)	Accuracy RE (%)	Calc. conc. (ng/ml)	Accuracy RE (%)
Harpagide	600	575.51 ± 22.16	−4.08	654.47 ± 22.87	9.08	587.47 ± 36.62	−2.09	612.90 ± 22.28	2.15
	38.4	38.35 ± 3.75	−0.13	39.34 ± 1.92	2.45	38.05 ± 4.19	−0.92	40.68 ± 3.21	5.94
Chlorogenic acid	800	833.85 ± 63.43	4.23	816.58 ± 29.60	2.07	863.78 ± 21.49	7.97	847.20 ± 32.63	5.90
	51.2	53.43 ± 3.66	4.35	49.06 ± 4.43	−4.19	56.51 ± 2.77	10.38	51.69 ± 5.02	0.96
Swertiamarin	4800	4968.64 ± 208.19	3.51	5274.04 ± 147.92	9.88	5153.93 ± 132.15	7.37	4835.93 ± 153.29	0.75
	307.2	292.85 ± 19.45	−4.67	279.92 ± 15.61	−8.88	289.21 ± 13.27	−5.86	311.53 ± 14.38	1.41
Sweroside	1000	1035.71 ± 53.35	3.57	1113.06 ± 32.37	11.31	1079.40 ± 37.61	7.94	973.49 ± 29.27	−2.65
	64	60.97 ± 4.81	−4.74	66.44 ± 4.64	3.81	63.90 ± 2.67	−0.16	63.40 ± 2.49	−0.94
Angoroside C	200	185.46 ± 9.39	−7.27	203.84 ± 4.39	1.92	196.52 ± 13.15	−1.74	178.97 ± 6.04	−10.51
	12.8	13.02 ± 1.05	1.70	13.32 ± 1.09	4.09	13.53 ± 0.98	5.68	13.02 ± 1.17	1.73
Liquiritin	200	173.78 ± 5.96	−13.11	189.11 ± 4.81	−5.45	180.23 ± 4.39	−9.88	184.99 ± 6.52	−7.50
	12.8	13.43 ± 0.75	4.90	12.47 ± 0.97	−2.58	12.41 ± 0.76	−3.04	13.40 ± 0.70	4.70
Isoliquiritigenin	200	220.77 ± 9.12	10.39	192.67 ± 7.93	−3.66	223.78 ± 4.10	11.89	177.89 ± 4.50	−11.06
	12.8	13.27 ± 0.64	3.66	13.72 ± 0.54	7.15	13.83 ± 1.09	8.02	13.81 ± 0.76	7.87

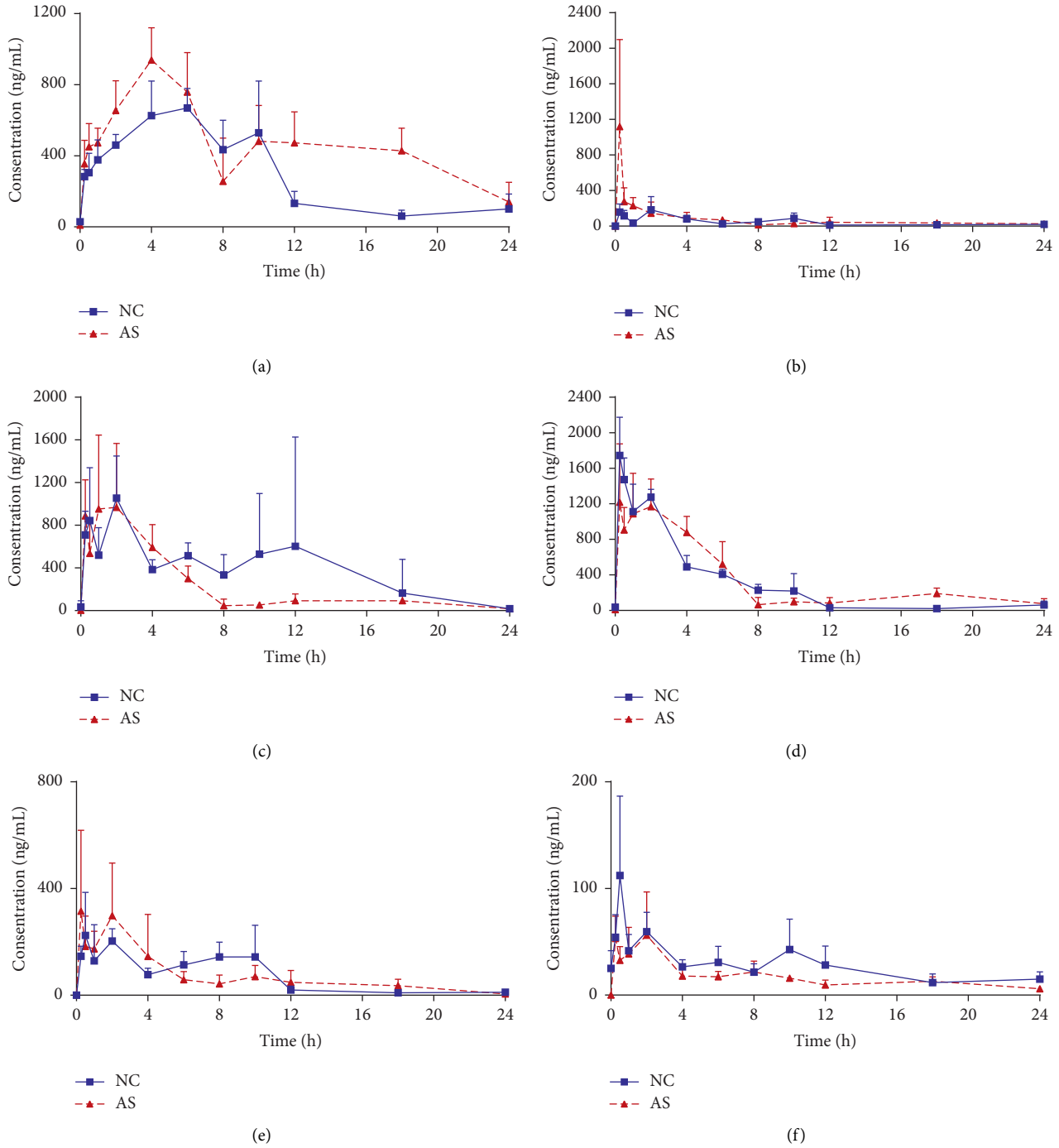

Figure 4: Continued.

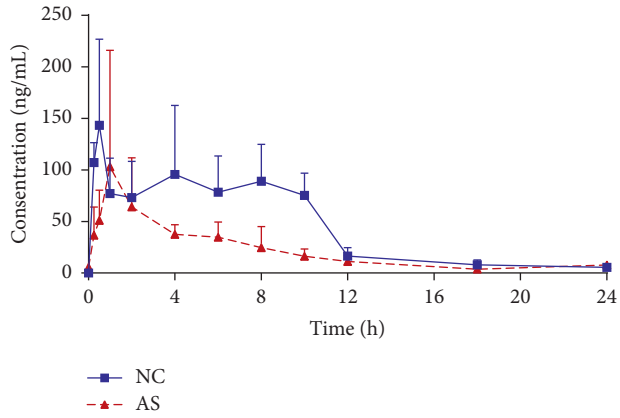

(g)

Figure 4: Mean concentration-time curves of seven compounds in NC and ASmouse plasma after oral administration of SMYAD (mean ± SD, $n = 5$). (a) Harpagide; (b) chlorogenic acid; (c) swertiamarin; (d) sweroside; (e) angoroside C; (f) liquiritin; (g) isoliquiritigenin.

the AS group significantly increased compared with the normal group, indicating that harpagide and chlorogenic acid exhibited high absorption in AS status. For swertiamarin, sweroside, and angoroside C, the increased tendencies of AUC_{0-t} and $AUC_{0-\infty}$ value were also observed, but no significant difference was discovered. However, significant reduction of AUC_{0-t} ($502.25 \pm 165.65\ ng{\cdot}mL^{-1}{\cdot}h$, $P < 0.01$) and the $AUC_{0-\infty}$ ($653.68 \pm 251.34\ ng{\cdot}mL^{-1}{\cdot}h$, $P < 0.05$) for isoliquiritigenin in the AS group were discovered, indicating that the bioavailability of isoliquiritigenin was remarkably reduced in the AS group. For liquiritin, the decreased tendencies of AUC_{0-t} and $AUC_{0-\infty}$ were also observed, but no significant difference was discovered. Furthermore, a longer $T_{1/2}$ for chlorogenic acid (21.59 ± 9.16 h, $P < 0.05$) wase observed in the AS group compared with the NC group, whereas no significant change in $T_{1/2}$ was observed for other compounds between the two groups. And the obvious lower CLz/F ($P < 0.01$) of harpagide and chlorogenic acid compared with NC group were observed, which means the metabolic rate of the two compounds slow down under pathological conditions. However, a significant increase in CLz/F ($P < 0.05$) of isoliquiritigenin was observed in the AS group. The results indicated that the oral administration of SMYAD could lead to slower elimination of chlorogenic acid and harpagide, but the elimination of isoglycyrrhizin was accelerated in AS mice. In addition, The Vz/F value of these compounds in both normal and model was large, indicating that the active compounds in SMYAD were possibly bound to tissue proteins, mainly distributed in tissue and intracellular fluids.

The pathogenesis of AS is complex, and inflammatory reaction runs through the whole process of plaque rupture and thrombosis, especially unstable plaque rupture [25]. AS is often accompanied by a number of metabolic syndromes such as glycometabolism dysfunction and lipid-metabolism dysfunction. Under the pathological conditions of AS, the absorption, distribution, metabolism, and excretion of the main bioactive components of SMYAD may be affected by complex factors. The possible reasons for pharmacokinetic differences between normal and AS model mice may be addressed by the following explanations. It was reported that the abundance and composition of the gut microbiota were altered in AS patients [26]. The gut microbiota has the genetic mechanisms necessary to produce enzymes that metabolize oral drugs, focusing on two main types of reactions: hydrolysis and reduction. Microbial metabolism converts hydrophilic drugs into hydrophobic compounds, thereby enhancing their absorption in the gut, and the hydrolytic enzyme activities of intestinal flora may decrease in the atherosclerotic disease state [27], while the level of related proinflammatory factors (NF-κB, TNF-α, IL-1β, and IL-6) increases in AS [28]. Study [29] has shown that the increase of inflammatory factors will further reduce the expression of some enzymes, and these may be the cause of the slow metabolism of harpagide and chlorogenic acid, the increased absorption for harpagide and chlorogenic acid, and the decreased absorption for isoliquiritigenin in AS model mice. The cause of their absorption changes may also be relative to nonspecific drug transporters, such as P-glycoprotein. Changes in normal and AS status drug transporters can be further studied. Research [30] suggested that marked inhibition of hepatic cytochrome P450 activity in cholesterol-induced atherosclerosis in rabbits and decreased metabolism of harpagide and chlorogenic acid in AS mice may be related to the decrease in CYP450 activity in the disease state. All the above considerations suggested that the anti-AS mechanisms of SMYAD should be based on gut microbiota, drug transporters, and CYP450 activity.

Harpagide, chlorogenic acid, and isoliquiritigenin have anti-inflammatory, inhibition of oxidative stress, lowering blood lipids, and other pharmacological activities to ameliorate AS. Therefore, it is speculated that these components may be the key active constituents of SMYAD in the treatment of AS. In addition, there was a large difference in mean blood concentration at some time points, and some pharmacokinetic parameters showed the trend of difference between normal and model, but it was not statistically significant, which may be the reason for the small sample size.

Table 6: Main pharmacokinetic parameters of the seven compounds in mouse plasma after oral administration of SMYAD (mean ± SD, $n = 5$).

Compounds	Group	Parameters						
		$t_{1/2}$/h	t_{max}/h	C_{max}/ng·mL^{-1}	AUC$_{0-t}$/ng·mL^{-1}·h	AUC$_{0-\infty}$/ng·mL^{-1}·h	Vz/F (L/mg)	CLz/F (L/h/mg)
Harpagide	NC	8.40 ± 1.80	6.00 ± 2.19	838.40 ± 126.54	6936.17 ± 533.23	7194.33 ± 588.34	32.74 ± 7.64	4.90 ± 0.40
	AS	8.55 ± 3.97	4.00 ± 0.00	939.74 ± 180.83	11075.09 ± 2132.38**	16221.95 ± 5622.42*	24.34 ± 16.57	2.45 ± 0.87**
Chlorogenic acid	NC	4.51 ± 1.10	1.13 ± 0.88	266.84 ± 72.39	1109.84 ± 418.97	1257.70 ± 424.87	247.01 ± 150.71	30.37 ± 7.58
	AS	21.59 ± 9.16*	0.25 ± 0.00	1128.91 ± 969.58	1560.11 ± 476.37	2637.51 ± 322.54**	302.49 ± 211.89	13.49 ± 1.81**
Swertiamarin	NC	4.43 ± 2.06	5.00 ± 4.97	1431.10 ± 636.23	5349.68 ± 1183.98	5401.77 ± 1243.88	20.82 ± 11.26	5.82 ± 2.64
	AS	5.74 ± 1.90	0.90 ± 0.64	1335.08 ± 603.03	5542.40 ± 2011.02	7243.79 ± 3391.00	55.16 ± 45.04	5.70 ± 1.93
Sweroside	NC	3.81 ± 0.56	0.40 ± 0.30	1793.48 ± 368.69	6983.11 ± 381.87	7083.75 ± 389.99	16.99 ± 3.78	4.96 ± 0.28
	AS	6.56 ± 2.75	0.90 ± 0.64	1588.23 ± 496.61	7501.27 ± 1799.94	8926.84 ± 2117.67	29.99 ± 14.26	4.29 ± 1.55
Angoroside C	NC	7.40 ± 4.76	0.85 ± 0.62	288.62 ± 123.79	1732.42 ± 882.96	1865.70 ± 1053.21	148.22 ± 76.23	29.75 ± 24.10
	AS	7.33 ± 4.68	2.05 ± 1.19	491.04 ± 238.94	1838.19 ± 298.23	1891.33 ± 226.37	126.00 ± 102.72	18.79 ± 2.39
Liquiritin	NC	16.98 ± 3.43	0.75 ± 0.63	132.03 ± 57.09	606.62 ± 229.46	760.40 ± 333.88	565.81 ± 116.60	58.74 ± 30.94
	AS	13.54 ± 3.57	0.75 ± 0.69	67.62 ± 33.62	407.58 ± 115.29	481.57 ± 137.03	887.57 ± 397.82	67.62 ± 33.62
Isoliquiritigenin	NC	6.65 ± 1.31	1.90 ± 2.13	175.33 ± 49.02	1036.28 ± 144.06	1063.27 ± 144.39	198.37 ± 58.53	33.51 ± 4.41
	AS	6.01 ± 2.32	0.95 ± 0.60	134.59 ± 101.80	502.25 ± 165.65**	653.68 ± 251.34*	658.87 ± 555.51	62.16 ± 23.35*

Compared with the NC group, $^{*}P < 0.05$, $^{**}P < 0.01$.

4. Conclusions

A sensitive, rapid, and reliable UHPLC-Q Exactive HF-X MS analytical method was established and validated for the simultaneous determination and quantification of harpagide, chlorogenic acid, swertiamarin, sweroside, angoroside C, liquiritin, and isoliquiritigenin in the plasma of normal and AS mice. It is the first comparative study of the pharmacokinetics of seven active components of SMYAD in normal and AS mice. The results demonstrated that AUC of harpagide and chlorogenic acid was significantly increased and CLz/F was decreased, meanwhile $t_{1/2}$ of chlorogenic acid was prolonged, while the AUC of isoliquiritigenin was decreased and its CLz/F was increased. Pharmacokinetic behaviors of swertiamarin, sweroside, angoroside C, and liquiritin were not changed obviously after oral administration of SMYAD in normal and AS model. This study laid the experimental foundation for further elucidating the pharmacodynamic substances of SMYAD against AS, and the difference in pharmacokinetic parameters provided a scientific reference for clarifying the targets of SMYAD *in vivo*.

Data Availability

The data used to support the findings of this study are included within the article.

Conflicts of Interest

The authors declare no conflicts of interest.

Authors' Contributions

Ke-han Sun and Man-fang Yang contributed equally to this work.

Acknowledgments

This work was supported by National Science and Technology Major Project of the Ministry of Science and Technology of China (no.2017ZX09304019) and National Natural Science Foundation of China (no.81874446)

References

[1] E. Falk, "Pathogenesis of atherosclerosis," *Journal of the American College of Cardiology*, vol. 47, no. 8, pp. C7–C12, 2006.

[2] Z. Gao, X. Xu, Y. Li et al., "Mechanistic insight into PPARγ and tregs in atherosclerotic immune inflammation," *Frontiers in Pharmacology*, vol. 12, Article ID 750078, 2021.

[3] D. K. Arnett, R. S. Blumenthal, M. A. Albert et al., "2019 ACC/AHA guideline on the primary prevention of cardiovascular disease: executive summary: a report of the American college of cardiology/American heart association task force on clinical practice guidelines," *Journal of the American College of Cardiology*, vol. 74, no. 10, pp. 1376–1414, 2019.

[4] R. Collins, C. Reith, J. Emberson et al., "Interpretation of the evidence for the efficacy and safety of statin therapy," *Lancet*, vol. 388, no. 10059, pp. 2532–2561, 2016.

[5] T.-T. Li, Z.-B. Wang, Y. Li, F. Cao, B.-Y. Yang, and H.-X. Kuang, "The mechanisms of traditional Chinese medicine underlying the prevention and treatment of atherosclerosis," *Chinese Journal of Natural Medicines*, vol. 17, no. 6, pp. 401–412, 2019.

[6] C. Su, Q. Wang, H. Zhang et al., "Si-Miao-Yong-An decoction protects against cardiac hypertrophy and dysfunction by inhibiting platelet aggregation and activation," *Frontiers in Pharmacology*, vol. 10, p. 990, 2019.

[7] Z. Qi, M. Li, K. Zhu, and J. Zhang, "Si-Miao-Yong-An on promoting the maturation of Vasa Vasorum and stabilizing atherosclerotic plaque in ApoE(−/−) mice an experimental study," *Biomedicine & Pharmacotherapy*, vol. 114, Article ID 108785, 2019.

[8] Y. Ren, X. Chen, P. Li et al., "Si-Miao-Yong-An decoction ameliorates cardiac function through restoring the equilibrium of SOD and NOX2 in heart failure mice," *Pharmacological Research*, vol. 146, Article ID 104318, 2019.

[9] X. Y. Chen, X. H. Chen, L. Li et al., "Deciphering the effective combinatorial components from Si-Miao-Yong-An decoction regarding the intervention on myocardial hypertrophy," *Journal of Ethnopharmacology*, vol. 271, Article ID 113833, 2021.

[10] P. Schopohl, P. Gruneberg, and M. F. Melzig, "The influence of harpagoside and harpagide on TNFα-secretion and cell adhesion molecule mRNA-expression in IFNγ/LPS-stimulated THP-1 cells," *Fitoterapia*, vol. 110, pp. 157–165, 2016.

[11] C. Wu, H. Luan, X. Zhang, S. Wang, X. Sun, and P. Guo, "Chlorogenic acid protects against atherosclerosis in ApoE−/− mice and promotes cholesterol efflux from RAW264.7 macrophages," *PLoS One*, vol. 9, no. 9, Article ID e95452, 2014.

[12] X. Y. Leong, P. V. Thanikachalam, M. Pandey, and S. Ramamurthy, "A systematic review of the protective role of swertiamarin in cardiac and metabolic diseases," *Biomedicine & Pharmacotherapy*, vol. 84, pp. 1051–1060, 2016.

[13] J. Wang, X. Cai, R. Ma, D. Lei, X. Pan, and F. Wang, "Anti-inflammatory effects of sweroside on LPS-induced ALI in mice via activating SIRT1," *Inflammation*, vol. 44, no. 5, pp. 1961–1968, 2021.

[14] C. Zhang, W. Ma, Y. Zhang et al., "Pharmacokinetics, bioavailability, and tissue distribution study of angoroside C and its metabolite ferulic acid in rat using UPLC-MS/MS," *Frontiers in Pharmacology*, vol. 9, p. 1186, 2018.

[15] D. Gong, M. Zhai, F. Yang, G. Sun, and H. Zhang, "Rapid determination of twelve bioactive components in rat plasma by UHPLC-MS/MS and its application to pharmacokinetic and in vitro-in vivo correlation study of compound liquorice tablets," *Microchemical Journal*, vol. 170, Article ID 106649, 2021.

[16] T. Chen, S. Deng, and R. Lin, "The inhibitory effect of Isoliquiritigenin on the proliferation of human arterial smooth muscle cell," *BMC Pharmacol Toxicol*, vol. 18, no. 1, p. 57, 2017.

[17] F. Du, Q. Gesang, J. Cao et al., "Isoliquiritigenin attenuates atherogenesis in apolipoprotein E-deficient mice," *International Journal of Molecular Sciences*, vol. 17, no. 11, p. 1932, 2016.

[18] Y. Liu, S. Chi, W. Wang, L. Su, and B. Liu, "Simultaneous determination of seven components in rat plasma by the UPLC-MS/MS method and application of pharmacokinetic

studies to SimiaoYong'an decoction," *Molecules*, vol. 22, no. 11, p. 1937, 2017.

[19] J. X. Gao, L. Qin, S. Y. Wen et al., "Simultaneous determination of acrylamide, 5-hydroxymethylfurfural, and heterocyclic aromatic amines in thermally processed foods by ultrahigh-performance liquid chromatography coupled with a Q exactive HF-X mass spectrometer," *Journal of Agricultural and Food Chemistry*, vol. 69, no. 7, pp. 2325–2336, 2021.

[20] B. Wen, R. He, P. Li et al., "Pharmacokinetics of 8-O-acetylharpagide and harpagide after oral administration of Ajuga decumbens Thunb extract in rats," *Journal of Ethnopharmacology*, vol. 147, no. 2, pp. 503–508, 2013.

[21] M. Shi, K. Xiong, T. Zhang, and H. Han, "Pharmacokinetics and metabolic profiles of swertiamarin in rats by liquid chromatography combined with electrospray ionization tandem mass spectrometry," *Journal of Pharmaceutical and Biomedical Analysis*, vol. 179, p. 112997, 2020.

[22] N. Sheng, L. Yuan, X. Zhi et al., "Application of a liquid chromatography-tandem mass spectrometry method to the pharmacokinetics, tissue distribution and excretion studies of sweroside in rats," *Journal of Chromatography B*, vol. 969, pp. 1–11, 2014.

[23] Y. H. Choi, Y. J. Kim, H. S. Chae, and Y. W. Chin, "In vivo gastroprotective effect along with pharmacokinetics, tissue distribution and metabolism of isoliquiritigenin in mice," *Planta Medica*, vol. 81, no. 07, pp. 586–593, 2015.

[24] J. An, F. Hu, C. Wang, Z. Zhang, L. Yang, and Z. Wang, "Pharmacokinetics and tissue distribution of five active ingredients of Eucommiae cortex in normal and ovariectomized mice by UHPLC-MS/MS," *Xenobiotica*, vol. 46, no. 9, pp. 793–804, 2016.

[25] N. Ruparelia and R. Choudhury, "Inflammation and atherosclerosis: what is on the horizon?" *Heart*, vol. 106, no. 1, pp. 80–85, 2020.

[26] B. J. H. Verhaar, A. Prodan, M. Nieuwdorp, and M. Muller, "Gut microbiota in hypertension and atherosclerosis: a review," *Nutrients*, vol. 12, no. 10, p. 2982, 2020.

[27] S. Tuteja and J. F. Ferguson, "Gut microbiome and response to cardiovascular drugs," *Circulation: Genomic and Precision Medicine*, vol. 12, no. 9, pp. 421–429, 2019.

[28] D. Wolf and K. Ley, "Immunity and inflammation in atherosclerosis," *Circulation Research*, vol. 124, no. 2, pp. 315–327, 2019.

[29] Z. Zidek, P. Anzenbacher, and E. Kmonickova, "Current status and challenges of cytokine pharmacology," *British Journal of Pharmacology*, vol. 157, no. 3, pp. 342–361, 2009.

[30] A. Irizar and C. Ioannides, "Marked inhibition of hepatic cytochrome P450 activity in cholesterol-induced atherosclerosis in rabbits," *Toxicology*, vol. 126, no. 3, pp. 179–193, 1998.

Hindawi
Evidence-Based Complementary and Alternative Medicine
Volume 2022, Article ID 5325431, 12 pages
https://doi.org/10.1155/2022/5325431

Review Article

Pathogenesis of Liver Fibrosis and Its TCM Therapeutic Perspectives

Yang Nan,[1] **HongChan Su**,[1] **XiaoMei Lian**,[1] **Juan Wu**,[2] **SuJie Liu**,[2] **PingPing Chen**,[2] **and ShuMin Liu**[2]

[1]*Heilongjiang University of Chinese Medicine, College of Pharmacy, Heilongjiang, Haerbin 150040, China*
[2]*Heilongjiang University of Chinese Medicine, Chinese Medicine Research Institute, Heilongjiang, Haerbin 150040, China*

Correspondence should be addressed to ShuMin Liu; keji-liu@163.com

Received 30 December 2021; Accepted 15 March 2022; Published 28 April 2022

Academic Editor: Lifeng Han

Liver fibrosis is a pathological process of abnormal tissue proliferation in the liver caused by various pathogenic factors, which will further develop into cirrhosis or even hepatocellular carcinoma if liver injury is not intervened in time. As a diffuse progressive liver disease, its clinical manifestations are mostly excessive deposition of collagen-rich extracellular matrix resulting in scar formation due to liver injury. Hepatic fibrosis can be caused by hepatitis B and C, fatty liver, alcohol, and rare diseases such as hemochromatosis. As the metabolic center of the body, the liver regulates various vital activities. During the development of fibrosis, it is influenced by many other factors in addition to the central event of hepatic stellate cell activation. Currently, with the increasing understanding of TCM, the advantages of TCM with multiple components, pathways, and targets have been demonstrated. In this review, we will describe the factors influencing liver fibrosis, focusing on the effects of cells, intestinal flora, iron death, signaling pathways, autophagy and angiogenesis on liver fibrosis, and the therapeutic effects of herbal medicine on liver fibrosis.

1. Introduction

Liver fibrosis is a wound-healing response when the liver is injured, showing a dynamic process, which can be caused by nonalcoholic steatohepatitis (NASH), nonalcoholic fatty liver disease (NAFLD), and cholestatic liver disease [1]. In addition, liver fibrosis is a determinant of mortality in NASH [2]. Advanced liver fibrosis creates the risk of cirrhosis and hepatocellular carcinoma, which kills approximately 1 million people worldwide each year as a complication of cirrhosis, while hepatocellular carcinoma ranks as the 16th most common cause of death, making the early diagnosis of liver fibrosis crucial [3]. Fibrosis is characterized by the production of myofibroblasts (MFB) that promote scar formation by activated Hepatic stellate cells (HSC), and the synthesis of extracellular matrix (ECM) by both MFB and HSC, and the balance of ECM is regulated by both matrix metalloproteinases (MMP) and tissue inhibitor of metalloproteinases (TIMP) that ultimately target HSC to form fibrosis, so it can be said that the dynamics of ECM regulation process is the process of liver fibrosis formation. In addition, nonparenchymal cells such as macrophages (MAC) and liver sinusoidal endothelial cells (LSEC) are also involved [4]. In addition, various signaling pathways, including transforming growth factor (TGF-β), platelet-derived growth factor (PDGF), and nuclear factor-κB (NF-κB), are also key pathways affecting liver fibrosis. Currently, there are still no specific and effective drugs to treat liver fibrosis, but there is increasing evidence that Chinese medicine and natural products provide effective help in the prevention and treatment of liver fibrosis [5, 6]. Therefore, in this paper, a large number of collections were carried out in the PUBMED database to fully understand the main events of liver fibrosis, which provided the possibility for targeted liver fibrosis therapy, as shown in Figure 1.

2. Cellular Factors

HSC, MAC, and LSEC all have a dual role in the formation of liver fibrosis. During liver injury, the activation and

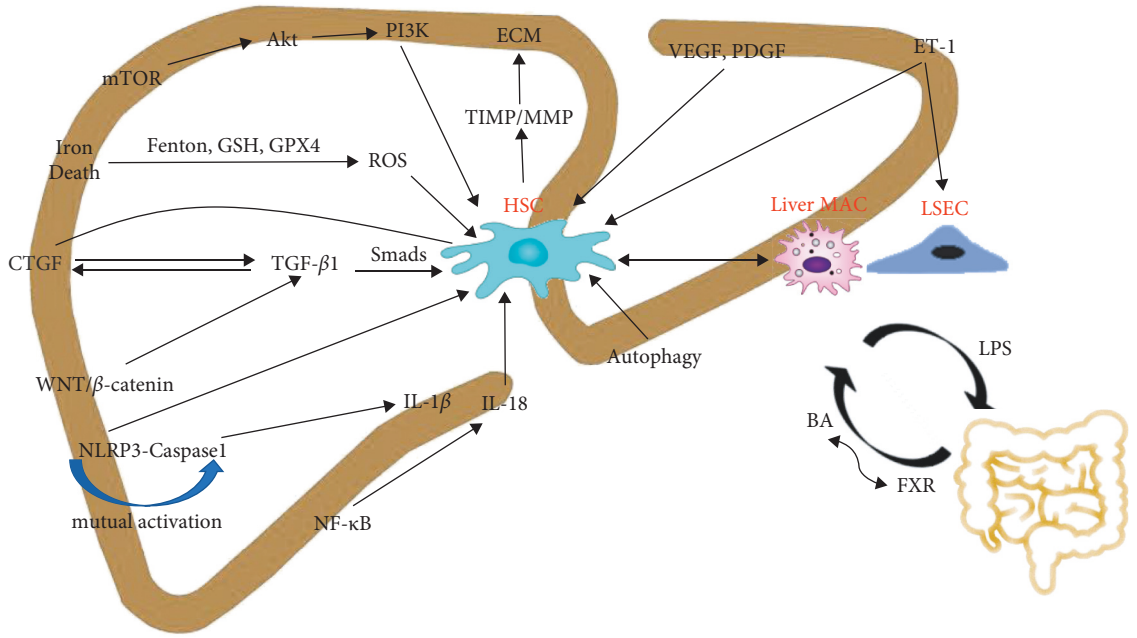

Figure 1: Diagram of pathogenesis associated with liver fibrosis. Intestinal-liver interactions; lipopolysaccharide (LPS); bile acids (BA); nuclear transcription factor receptor (FXR); hepatic stellate cells (HSC); liver macrophages (Liver MAC); liver sinusoidal endothelial cells (LSEC); transforming growth factor (TGF); connective tissue growth factor (CTGF); WNT/β-linked protein (WNT/β-catenin); NOD-like receptor protein 3 (NLRP3); cysteine aspartate-specific proteinase 1 (caspase-1); nuclear factor-κB (NF-κB); interleukins (IL); glutathione (GSH); glutathione peroxidase 4 (GPX4); reactive oxygen species (ROS); mammalian target of rapamycin (mTOR); protein kinase B (Akt); phosphatidylinositol 3-kinase (PI3K); endothelin-1 (ET-1); vascular endothelial growth factor (VEGF); platelet-derived growth factor (PDGF); TIMP/MMP (tissue inhibitor of metalloproteinases/matrix metalloproteinases); ECM (extracellular matrix).

proliferation of hepatic stellate cells, the increase of Ly6C^{hi} in macrophages, the capillarization of hepatic sinusoidal endothelial cells, and the concomitant secretion of various inflammatory factors all contribute to the formation of fibrosis. The apoptosis of hepatic stellate cells, the increase of Ly6C^{lo} in macrophages, and the normal differentiation of hepatic sinusoidal endothelial cells can make the activated hepatic stellate cells quiescent and even degrade the excess extracellular matrix, which can effectively prevent the development of liver fibrosis. This article will explain how cellular factors are actively activated to cause liver fibrosis.

2.1. Hepatic Stellate Cells. Hepatic stellate cells (HSC) are a class of nonparenchymal cells located in the endothelial cells of the hepatic sinusoids and the sinusoidal spaces surrounding the hepatocytes, also known as hepatic lipid storage cells. Under pathological conditions, HSC is converted to an activated state by stimulation of various environmental factors, which is a critical step in the development of liver fibrosis [7, 8]. Chronic liver injury leads to multiple damage-associated molecular patterns (DAMPS) producing a series of cytokines including insulin growth factor (IGF-1) and ET-1 that activate the secretion of HSC. At the same time, long-term stimulation that triggers an inflammatory response combined with LSEC [9] and KC [10] also releases damage factors like IL-6, TNF-α, and TGF-β to further promote the initiation of HSC activation [11]. Activated HSC themselves also secrete fibrogenic factors such as CTGF and leptin, which in turn enhance the ability to induce proliferation of HSC. In addition, α-SMA-containing myofibroblasts (MFB) contribute to the formation of fibrotic scar and synthesize I and III collagen-based ECM [12, 13], and excessive accumulation of ECM activates HSC, creating a positive feedback loop leading to fibrosis formation. In particular, PDGF and VEGF released from platelets are mitogenic mediators of HSC and bind to ECM to enable the already activated HSC to undergo the next step of proliferation [14]. Chemokine-chemokine receptors play a key role in liver fibrosis, especially the C-C motif chemokine receptor 2 (CCR2) activates HSC [15]. The process by which epithelial cells gradually lose their phenotypic characteristics while acquiring mesenchymal cell characteristics is called epithelial-mesenchymal transition (EMT), and the involvement of EMT also mediates the transdifferentiation and fibrosis of HSC [16]. When the Hh signaling pathway derepresses Smo and activates the Gli transcription factor, Gli contains a predicted paired frame 6 (PAX6) binding site in its transcriptional region, which promotes both HSC activation and proliferation [17].

2.2. Macrophages. Macrophages are derived from precursor cells in the bone marrow, which are immune cells [18]. Those active in the liver are called liver macrophages (Liver MAC) and mainly include kwashiorkor cells (KCs) and monocyte-derived macrophages (MoMF) [19].

Under pathological conditions, there is a large amount of Ly6C^{hi} from MoMF, which has a proinflammatory properties and can overexpress CCR1 and CCR2 [20], and Ly6C^{hi}

can not only release a large number of cellular, inflammatory, and chemokines such as TGF-β, PDGF, TNF-α, IL-1β, and CCL2 [21–24] but can also depend on chemokine aggregation to the site of liver injury. The precursor cells of $Ly6C^{lo}$ are $Ly6C^{hi}$ monocytes, but $Ly6C^{lo}$ has the opposite effect to $Ly6C^{hi}$, where $Ly6C^{lo}$ can downregulate inflammatory factors and increase MMP, promoting the degradation of ECM. Through the study, when the CCR2 gene was knocked down in mice, $Ly6C^{hi}$ was reduced and $Ly6C^{lo}$ quantity was increased in the liver, corresponding to the reduction of HSC activation and some relief of liver fibrosis, indicating that $Ly6C^{hi}$ has proinflammatory and profibrotic properties, while $Ly6C^{lo}$ has anti-inflammatory and antifibrotic properties.

KCs are located in macrophages within the hepatic sinusoids, also known as resident cells [25]. When a liver injury occurs, KCs are activated by DAMPs and pathogen-associated molecular patterns (PAMPs) interacting with Toll-like receptors (TLRs). Activated KC generates various types of mediators of liver fibrosis progression (e.g., TGF-β, PDGF, IL-1β, MMPs, CCL2, cysteine-3, etc.) and also accelerates the progression of liver fibrosis by activating HSC to produce large amounts of collagen, allowing ECM to settle and aggregate [26].

2.3. Liver Sinusoidal Endothelial Cells. Liver sinusoidal endothelial cells (LSEC) are highly specialized endothelial cells with pores on the cell surface and open windows, whose vascular secretory signals regulate liver function and have an important role in maintaining the homeostasis of the hepatic endotrophic environment, which, in turn, is a key factor in the activation of HSC [27, 28]. Differentiated LSEC can maintain HSC in a quiescent form, which can accelerate the regression of liver fibrosis and stop its progression, but the opposite is true for capillary LSEC [29]. When LSEC forms an organized basement membrane and lacks open windows, it is capillary vascularization of LSEC, which then eventually leads to the activation of HSC through the synthesis of factors like TGF-β to form fibrosis, fibrosis aggravates LSEC, and LSEC promotes fibrosis, leading to a vicious cycle. The vascular endothelial factor VGEF pathway was found to protect LSEC from opening windows and prevent fibrosis [30]. Capillarization is induced in LSEC if the Gata4 gene is absent, inducing the expression of profibrotic vascular secretory factors, which in turn leads to the possibility of perisinusoidal capillarization or fibrosis and liver lesions [31]. It has been claimed that the addition of bone morphogenetic protein (BMP9) to LSEC in primary culture, as a regulator of the intrahepatic environment, not only prevents the loss of window pores but also integrates the Gata4 gene and restores LSEC differentiation [32]. Furthermore, autophagy affects liver fibrosis by affecting LSEC [33], when the liver is mildly injured, autophagy of LESC enhances sinusoidal endothelial dysfunction (ED) and activates HSC, but, if the liver is too long or more severely injured, autophagy decreases, and ED fails to proceed. Autophagy of LSEC also enables chemokines, inflammatory factors such as C-C chemokine ligand 2 (CCL2), C-C chemokine ligand 2 (CCL5), and interleukin-6 (IL-6) are enhanced, promoting the hepatic inflammatory response and thus liver fibrosis [34].

3. Signaling Pathways

3.1. TGF-β1/Smads Signaling Pathway. Transforming growth factor β1 (TGF-β1) is the most prominent way to promote fibrosis formation [35], which is through the intracellular Smads signaling pathway [36]. The Smads pathway promotes HSC activation, and inactivated HSC and activated Smad2 and Smad3 induce type I and type III collagen production [37], promote MFB cell proliferation, and increase ECM deposition in the liver [38]. Smad4 inhibits the binding activity of Smad3 to collagen and the aggregation and degradation of ECM in vitro and in vivo. In acute liver injury, Smad7 can compete with receptor-activated Smad2 and Smad3 to bind TGF-β1 receptors and reduce ECM production, or Smad7 can interrupt TGF-β1 signaling by enhancing the degradation of TGF-β receptors. However, after HSC transdifferentiation to MFB, the ability of TGF-β1 to induce Smad7 expression decreases, Smad2 and Smad3 are phosphorylated, the TGF-β1/Smads signaling pathway is activated, and ECM is secreted in large amounts, accelerating liver fibrosis [39–41]. TGF-β1 can also promote liver fibrosis by activating non-Smads pathways, such as MAPK, NF-κB, and PI3K [42]. TGF-β1 can induce TIMP-1 expression after signaling to Smad3, while inhibiting MMP-1 expression, making the ratio of TIMP-1 to MMP-1 increase, and promoting liver fibrosis. Smad2 can induce MMP-2 expression, and by knocking down the Smad2 gene, we obtained that TGF-β1 through the Smad3 pathway upregulated the expression of TIMP-1 and inhibited the expression of MMP-2, which in turn inhibited the degradation of ECM [43].

3.2. WNT/β-Catenin Signaling Pathway. Wnt acts as a signaling cascade that transfers signals through cell surface receptors to protein components in the cell. There are two types of this signaling pathway, the nonclassical planar cell polarization pathway that regulates the cytoskeleton and thus cell shape, and Wnt/Ca^{2+} that regulates intracellular Ca^{2+} concentration, and the classical signaling pathway that regulates specific gene transcription, which is dependent on β-catenin for further action on downstream factors and ultimately translocates to the nucleus where it binds to the intranuclear transcription factor Tcf/Lef, thereby activating expression of the relevant target gene [44]. The main difference between the two pathways is that the nonclassical pathway operates independently of it, and the classical pathway involves the involvement of β-catenin. It is believed that the Wnt/β-catenin pathway is now considered to be the main influential pathway involved in the development of liver fibrosis, and β-catenin has an important role as a key signaling molecule in this pathway [45]. When Wnt is activated and β-catenin is phosphorylated, ECM accumulation leads to HSC activation [46]. The deletion of β-catenin leads to TGF-β upregulation and oxidative stress [47]. In addition

to the apoptotic effects of HSC that can be produced by the inhibition of Wnt and β-catenin [48], many substances can influence the homeostasis of the intestinal flora, the progression of cirrhosis, and the activation of inflammatory factors by participating in the WNT/β-catenin signaling pathway, which affects the process of fibrosis [49]. This justifies the reliability of using the Wnt/β-catenin signaling pathway as an entry point for the treatment of fibrosis. Silencing or inhibition of β-catenin, in the Wnt/β-catenin signaling pathway, promotes improvement of liver fibrosis or cirrhosis by limiting the contractility of HSC and portal hypertension [50].

3.3. Inflammasome (NLRP3) Caspase-1 Signaling Pathway. Inflammasome (NLRP3) is a part of the natural immune system, and it has been shown that all components of NLRP3 are present in the HSC, that multiple functions of the HSC are regulated by NLRP3, and that NLRP3 recognizes the release of damage patterns such as DAMPs and PAMPs caused by liver injury, by recruiting and activating proinflammatory cysteine-containing aspartate proteolytic enzyme 1 caspase-1, so that activated caspase-1 activates the proinflammatory cytokines IL-1β and IL-18, leading to the activation of HSC and the occurrence of liver fibrosis [51–53]. IL-1β aggregates by recruiting neutrophils, and excess proinflammatory cytokines lead to the activation of reactive oxygen species (ROS), inflammatory cells, and growth factors, which not only further promote activation of inflammatory vesicles but also promote the activation of HSC, leading to liver fibrosis [54]. Signals induced by lipopolysaccharide (LPS) [55] can activate pro-IL-18 and pro-IL-1β to activated IL-18 and IL-1β via NF-κB, which can then activate liver fibrosis via proinflammatory cytokines, or they can act directly on NLRP3 inflammatory vesicles, which in turn activate its downstream signaling pathway caspase-1 via NLRP3 inflammasomes which in turn will promote proinflammatory processes in the maturation and secretion of the precursors pro-IL-1β and pro-IL-18 during the defense process, promoting liver fibrosis formation [42, 56–58]. At the same time, caspase-1 also induces the activation of intracellular NLRP3 inflammatory vesicles, which can lead to a vicious cycle of proinflammatory signaling [59].

3.4. Phosphatidylinositol 3-Kinase (PI3K)-Akt Signaling Pathway. Phosphatidylinositol 3-kinase (PI3K) is a class of inositol lipid substance kinases, the most widely studied class of which is I PI3K, with the regulatory subunit p58 and the catalytic subunit p110 as the main targets [60]. Protein kinase B (Akt) is a downstream target of the PI3K signaling pathway and regulates the cell-initiated kinase cascade reaction that allows AKT to be activated by being readily located on the plasma membrane [61] PI3K and Akt are involved in the regulation of various signaling pathways including liver fibrosis in the liver. Studies have found that the autophagy of BDL and CCL4-induced liver fibrosis can be activated to promote liver injury by activating the TGF-β1/Smads signaling pathway and inhibiting PI3K/Akt signaling pathway and regulating cross-talk between the two pathways [62]. The initiation of phosphorylation of PI3K, AKT, and even mTOR in the PI3K/AKT signaling pathway can trigger the activation and proliferation of HSC and affect the production of liver fibrosis [63]. It is noteworthy that mTOR, as a downstream signaling molecule of AKT, also plays an important role in this pathway [64]. The expression of mTOR acts on the PI3K/Akt signaling pathway, induces HSC proliferation, induces the expression of α-SMA and other fibrogenic factors, and induces ECM synthesis [65].

3.5. Nuclear Factor-κB Signaling Pathway. Nuclear factor-κB (NF-κB) is a transcriptional regulator of greater interest in liver fibrosis and consists of a heterodimer of RelA (p65) and p50 subunits. When a sustained liver injury occurs, it activates HSC and KC, which in turn releases proinflammatory, chemotactic, and cytokines, causing the recruitment of various factors to the damaged sites of liver inflammation and stimulating NF-κB, which in turn stimulates the production of each factor upon NF-κB activation, thus creating a positive feedback between NF-κB and inflammatory factors [66]. Studies have shown that the NF-κB pathway is a key factor in HSC activation and proliferation, and it inhibits apoptosis and promotes HSC activation. When the expression of NF-κB inhibitor protein α (IκBα) increased, the Bax/Bcl-2 ratio rises, the NF-κB signaling pathway is inhibited, and the process of liver fibrosis is slowed down. In contrast, when KC is activated, the expression of NF-κB-p65 is significantly increased, the activity of ATL and AST is also significantly increased, and the progression of fibrosis is significantly accelerated [67, 68]. Through experiments [69], the NF-κB signaling pathway can lead to liver fibrosis through miR-378, as miR-378 leads to the development of NASH and liver fibrosis by promoting the activation of the NFκB-TNFα axis.

3.6. CTGF Signaling. Connective tissue growth factor (CTGF) belongs to a signal in the Hippo signaling pathway and is closely associated with various pathways such as TGF-β, Ras, MEK, ERK, WNT, AKT, and MAPK [70–74]. Through research [75], activated HSC secretes CTGF, which in turn promotes HSC activation and migration and upregulates type I collagen and α-SMA and activated HSC differentiates into MFB, which also secretes a large number of collagen fibers, resulting in a large amount of ECM deposition, and the above process can be analyzed as positive feedback between CTGF and HSC. CTGF may be a downstream response element of the TGF-β1 pathway and mediates some of the active effects of the TGF-β1 pathway, which allows fibrosis to occur, while CTGF has a role in maintaining fibrosis by activating a series of transduction pathways that induce MFB proliferation and ECM synthesis and promote the formation of liver fibrosis [76, 77].

4. Intestinal Flora

4.1. PAMP. In addition to the intestinal flora, which can help the body to digest and absorb and regulate metabolism, its

components and functions and the alteration of the intestinal barrier can directly or indirectly affect the formation of liver disease, and in turn, the occurrence of various liver diseases can affect the stability of the intestinal flora [78, 79]. This is because the liver and the intestine are connected by the portal vein, bile passes through the liver to act on the intestine, nutrients from the intestine flow into the portal circulation to reach the liver, and the two interact to form a feeder loop called the enterohepatic axis [80, 81]. Amid this loop, if there is an imbalance in intestinal homeostasis or translocation between microbial components, etc., called PAMP, hepatocytes such as KC and HSC and immune receptors in the lamina propria of the intestine recognize this pattern, leading to an inflammatory response and thus inducing fibrosis [82]. Thus, it can be said that intestinal flora disorders induce liver fibrosis.

4.2. Lipopolysaccharide. When intestinal permeability is disrupted or the microbial composition of the gut is altered, a series of metabolic toxins are produced, such as LPS, an endotoxin that further affects liver function, mainly by triggering an inflammatory response, via the enterohepatic axis. In binding to Toll4, a Toll-like receptor, or mediated through kupffer cells, inflammatory factors are produced into the portal circulation [83]. Naihua Hu et al. [84] demonstrated that different concentrations of LPS had an inducing effect in a model of inflammation and fibrosis in LX2 cells, resulting in enhanced expression of inflammatory factors such as IL-6, IL-1β, and TNF-α. In addition, LPS was able to regulate the expression of the NF-kB signaling pathway and MAPK proteins, including the JNK and p38 pathways associated with the activation of inflammatory mediators, with the consequent production of inflammatory factors that induce liver fibrosis formation [85].

4.3. FXR. Nuclear transcription factor receptor (FXR) and bile acids (BA) also interfere with fibrogenesis in terms of intestinal flora; BA is synthesized by the liver and acts in the intestine to produce secondary bile acids that inhibit FXR, which together with BA regulate the homeostasis of intestinal flora. When elevated concentrations of BA induce physiological activation and proliferation of HSC leading to pathological lesions of liver fibrosis, FXR can reverse this phenomenon by maintaining low concentrations of bile in hepatocytes. In addition, it prevents liver injury, which triggers liver fibrosis when FXR is inhibited [86, 87]. In addition, FXR can regulate the inflammatory response activated by BA in concert with LPS, mainly because FXR interconnects with NLRP3 or caspase-1 to produce nonpositive regulation of NLRP3 action [88].

5. Autophagy

When HSC is normal, its cytoplasm contains a large number of lipid droplets [89]. When the liver is damaged and the HSC is activated, the lipid droplet content in the cytoplasm decreases, and as the HSC is converted to MFB, the autophagic flux increases, and when inhibited by the autophagy inhibitor bafilomycin A1, the lipid droplet content normalizes and the HSC returns to normal; i.e., the increased autophagic content is associated with HSC activation [90, 91]. Because autophagy lysosomes degrade abnormal proteins, etc., eliminating intracellular metabolic wastes and improving HSC survival and the substances recovered by autophagy provide energy and nutrients to HSC [92]. Studies have shown that autophagy is dependent on ROS, mTOR, and IL-7, and another factor in the process of liver fibrosis [93, 94]. When damage occurs in hepatocytes, it stimulates the production of large amounts of ROS in the liver, and the accumulation of excessive ROS can exceed the normal range of the antioxidant system in the body, allowing the occurrence of oxidative stress that causes abnormal fibrosis in the liver, while the activation of mTOR accelerates liver fibrosis when the organism is in a state of nutritional deficiency [95]. Autophagy can also protect the liver by degrading abnormal metabolites to prevent cellular damage or generate excessive autophagy leading to cellular scorching and the inability of HSC to survive [96, 97].

6. Iron Death

Iron death can occur through the Fenton reaction that generates a large amount of ROS that accumulate in the body and cannot be metabolized in time, leading to excessive oxidative stress, promoting lipid peroxidation and oxidative damage to the cell membrane, which in turn leads to cell death [98–100]. When the body lacks glutathione (GSH) also causes excessive accumulation of ROS and iron death, and when glutathione peroxidase 4 (GPX4) activity decreases, polyunsaturated fatty acids are produced in the body to undergo lipid peroxidation and cannot be metabolized by GPX4, resulting in cell death by intracellular hoarding [101, 102].

In the liver, HSC contains iron ions, and the development of liver fibrosis is closely related to iron ions and lipid peroxidation in HSC, and the progression of liver fibrosis can be regulated by iron death. When hepatic iron concentration (HIC) exceeds the normal level, HSC function is abnormal, and in more severe cases, it progresses to cirrhosis. Iron death in HSC leads to an increase in α-SMA and type I collagen, allowing ECM deposition, or increased production of proinflammatory factors through TGF-β and NF-κB signaling pathways, resulting in liver fibrosis. Liver fibrosis due to iron death also occurs mostly in hepatocytes and macrophages, which can likewise lead to an inflammatory response through the overproduction of HIC and inflammatory cells, activating HSC and producing liver fibrosis [103]. Through studies [104], the therapeutic effect of MgIG on liver fibrosis is produced by promoting the accumulation of iron and lipid peroxides, and the complete disappearance of the antifibrosis effect of MgIG when the inhibitor Fer-1 inhibits iron death in liver fibrosis also confirms the strong association between iron death and liver fibrosis.

7. Angiogenesis

Angiogenesis is an important factor contributing to liver fibrosis and is essential for the repair of liver injury [105].

LSEC and HSC express a range of proangiogenic cytokines, including vascular endothelial growth factor (VEGF), endothelin-1 (ET-1), and platelet-derived growth factor (PDGF), with downregulation of VEGF expression and upregulation of ET-1 expression indicating that LSEC undergoes capillarization [33].

7.1. VEGF. HSC can promote the expression of VEGF and even the receptor of VEGF, resulting in angiogenesis-induced fibrosis, and VEGF has a better ability to regulate angiogenesis than other cytokines, and, in terms of intestinal inflammation and monocyte infiltration, VEGF also produces effects leading to fibrosis [105]. It was shown that, after histochemical scoring, VEGF can be used as a predictor for the study of fibrosis progression [106]. In addition, VEGF is known to have the ability to alleviate liver fibrosis in bone marrow mesenchymal stem cells (BMSC), and it has been reported that VEGF can increase the permeability of sinusoidal endothelial cells and can affect changes in tissue collagen, a pathway in which BMSC can be better expressed [107].

7.2. ET-1. ET-1 is caused by the massive accumulation of extracellular matrix ECM activated by HSC and also stimulates proliferation and collagen synthesis by inducing contraction of activated HSC, which can act on LSEC in addition to HSC [108], and ET-1 can reduce the size and number of window pores in LSEC [30], which in turn can affect liver microcirculation. In CCL4-induced liver fibrosis, ET-1 expression was increased, suggesting that ET-1 could be a promising marker [109]. Not only that, ET-1 acts as a mitogen of smooth muscle vessels with its receptors ET_AR and ET_BR to regulate vasoconstriction and diastole. When ET-1 is upregulated in the expression of HSC, ETR is also elevated, leading to increased hepatic sinusoidal resistance and producing portal hypertension, which suggests an exacerbation of fibrosis [110].

7.3. PDGF. PDGFs have five isoforms and two receptors, PDGFR-α and PDGFR-β. PDGFR-α has more affinity than PDGFR-β and binds more easily to other signaling molecules, such as Ras, MEK, and the extracellular signal-regulated kinase ERK, which are involved in the regulation of fibrogenesis [111, 112]. PDGFR-β expression shows an upregulation trend with HSC activation and PDGFR-β acts as the most promising proliferation mediator for HSC, inducing further HSC proliferation [113]. Liver sinusoidal endothelial cell vascularization increases liver permeability due to loss of PDGFR-β activity [30], and most liver samples from patients with liver fibrosis show increased levels of PDGFR-β expression, while PDGFR-β is a key pathway to induce HSC activation and proliferation [114].

8. TCM Therapeutic Perspectives

So far, the treatment effect of liver fibrosis in Western medicine has progressed slowly, except for surgical treatments such as liver resection; there is no specific curative medicine that can have a good treatment effect on liver fibrosis without complications and adverse reactions. Although the term "liver fibrosis" does not exist in traditional Chinese medicine, it has a long history and profound sources, and the concept of "ruffian, lumps, and accumulation" has been used for a long time, and the modern concept of liver fibrosis belongs to this concept [115]. Moreover, many TCM have the advantages of multicomponent, multipathway, and multitarget, with antioxidant, anti-inflammatory, anticancer, and hepatoprotective effects, and this feature can be fully reflected in liver fibrosis.

Through studies [116–119], tetramethylpyrazine can increase the MMP/TIMP-1 ratio and accelerate the degradation of ECM with antifibrotic effects, block the pathway of TGF-β1 and Nrf2/β-linked protein, inhibit the activation and migration of HSC, increase the storage of lipid droplets within HSC, or exert antifibrotic effects through cellular autophagy, with anti-inflammatory and antioxidant effects, etc., or inhibit hepatic fibrosis by reducing oxidative stress. *Chrysanthemum* [120, 121] can reverse liver fibrosis, mainly by inhibiting the TGF-β1 signaling pathway and thus reducing the value-added activation of HSC. Evodiamine [122] was able to reduce IL-6, TNF-α, and types I and III collagen expression, inhibit the TGF-β1/Smads signaling pathway, and attenuate liver fibrosis. Breviscapin [123] reduces inflammatory factors by killing TLR4/NF-κB signaling pathway, which can reduce liver fibrosis by decreasing apoptotic response, blocking oxidative stress, and inhibiting inflammation. Curcumin, a major component of turmeric, activates PPAR-α signaling, inhibits PI3K/Akt signaling, enhances cellular autophagy, and thus inhibits ECM production [89, 124] and also reduces lipid peroxidation to prevent liver fibrosis. α-SMA, a marker of HSC activation, was significantly reduced in expression after treatment with the flavonoid baicalin and reversed the effect of PDGF-BB on promoting the ability of HSC-T6 cells to promote activation [125, 126]. In contrast, *Scutellaria baicalensis* decoction has a preventive effect on liver injury, which may be related to the involvement in the metabolism of some tryptophan to reduce oxidative stress and inhibit collagen regeneration [127]. Emodin extracted from various anthraquinones further affects the fibrotic process by inhibiting epithelial-mesenchymal transition (EMT), reducing $Ly6C^{hi}$ macrophage infiltration $Ly6C^{hi}$ [128], mediating the p53 signaling pathway to induce HSC apoptosis and the TLR4 pathway to slow down inflammation production and lipid deposition in NAFLD models [129, 130]. Moreover, all three can mediate the NF-kB pathway, inhibit the TGF-β and the levels of inflammatory factors such as TNF-α, and antagonize the profibrotic effects of the inflammatory response [129–135]. Studies have shown that ursolic acid (UA) can regulate EMT or MFB via Rho [136, 137], improve the integrity of the intestinal barrier, reduce intestinal flora disorders [138, 139], and modulate the NOX4/NLRP3 inflammatory vesicle signaling pathway to attenuate liver fibrosis [140].

Yinchenhao decoction [115], whose main components are *Artemisia capillaris* Thunb., *Gardenia jasminoides*, and rhubarb, is one of the classical herbal formulas that can

effectively repair liver tissues and cure hepatic fibrosis. Studies have shown [141, 142] that the protective effect of Yinchenhao decoction on liver fibrosis is closely related to PI3K-Akt, TNF, and MAPK signaling pathways and the components of the decoction such as aloe vera emodin, rheinic acid, kaempferol, and quercetin are important components for liver protection, and they not only have therapeutic effects on liver injury caused by CCL4 but also improve fatty liver and inhibit cirrhosis, as well as improving liver fibrosis by inhibiting HSC proliferation and activation. In addition, gardenia glycosides [143], the main component of Yinchenhao decoction, can inhibit TGF-β/Smad and ERK-MAPK pathways to inhibit TGF-β1-induced EMT and also inhibit type I collagen-induced by the TGF-β1 pathway to protect the liver and inhibit the development of liver fibrosis. Fuzheng Huayu capsule (FZHYC), as a Chinese medicine preparation approved by the State Food and Drug Administration (SPDA) of China and the Food and Drug Administration (FDA) of the United States [144], is effective in improving fibrosis or cirrhosis including hepatitis B with liver and kidney deficiency and blood stasis blockage [145]. The expression of HBV liver fibrosis was adjusted by inhibiting HSC activation by altering the number or function of CD4T cells in T lymphocytes [146]. Another study noted that *a*-SMA was significantly inhibited in HSC regulated by the FZHYC action JNK pathway [144]. In addition to this, inhibition of NF-kB signaling pathway, lipid peroxidation, and reduction of HA and collagen content in fibrotic patients help to reach the efficacy of FZHYC in activating blood and removing blood stasis and supporting the deficiency [147–149].

9. Summary

In this paper, we mainly elaborate on liver fibrosis from cytokines and various related signaling pathways and then discuss the relationship with liver fibrosis from important aspects such as intestinal flora, autophagy, iron death, and angiogenesis and elaborate the role and mechanism in the process of liver fibrosis. We found that the influence on the onset and regression of liver fibrosis through various pathways cannot be unilateral; it must be multifactorial, multifaceted, and multiple pathways interacting and cooperating to make changes in liver fibrosis. Finally, the research on the treatment of liver fibrosis from the aspect of Chinese herbal medicine is mainly discussed, and it is found that, in experiments, various types of Chinese herbal medicine and compounding play a good therapeutic effect on the suppression of liver fibrosis with fewer side effects, but still need to be used carefully according to the changes of the disease to avoid aggravating liver fibrosis [150]. Moreover, microRNA, Hedgehog (Hh) signaling pathway, PPAR nuclear receptor signaling pathway, and hepatic lymphocytes also have a certain influence on the formation of liver fibrosis. So far, there are no specific drugs for clinical treatment in either Western or Chinese medicine, and compared to the singularity of research on the development of Western drugs, the treatment of liver fibrosis by Chinese medicine and compound prescriptions is based on a holistic approach, regulating all aspects of the body, providing ideas for the treatment of fibrosis and suggesting the great potential of Chinese medicine [151].

Conflicts of Interest

The authors declare that they have no conflicts of interest.

References

[1] M. M. Akcali and K. C. Akçalı, "Liver fibrosis," *Turkish Journal of Gastroenterology*, vol. 29, no. 1, pp. 14–21, 2018.

[2] V. G. Eduardo, C. B. Luis, W. S. Wong et al., "Fibrosis severity as a determinant of cause-specific mortality in patients with advanced nonalcoholic fatty liver disease," *Gastroenterology*, vol. 155, no. 2, pp. 443–457, 2018.

[3] S. K. Asrani, H. Devarbhavi, J. Eaton, and P. S. Kamath, "Burden of liver diseases in the world," *Journal of Hepatology*, vol. 70, no. 1, pp. 151–171, 2019.

[4] D. Dhar, J. Baglieri, T. Kisseleva, and D. A. Brenner, "Mechanisms of liver fibrosis and its role in liver cancer," *Experimental Biology and Medicine*, vol. 245, no. 2, pp. 96–108, 2020.

[5] P. Manka, A. Zeller, and W.-K. Syn, "Fibrosis in chronic liver disease: an update on diagnostic and treatment modalities," *Drugs*, vol. 79, no. 9, pp. 903–927, 2019.

[6] F.-F. Cai, Y.-Q. Bian, R. Wu et al., "Yinchenhao decoction suppresses rat liver fibrosis involved in an apoptosis regulation mechanism based on network pharmacology and transcriptomic analysis," *Biomedicine & Pharmacotherapy*, vol. 114, Article ID 108863, 2019.

[7] Z. Zhang, M. Guo, Y. Li et al., "RNA-binding protein ZFP36/TTP protects against ferroptosis by regulating autophagy signaling pathway in hepatic stellate cells," *Autophagy*, vol. 16, no. 8, pp. 1482–1505, 2020.

[8] Y. Tao, T. Qiu, X. Yao et al., "Autophagic-CTSB-inflammasome axis modulates hepatic stellate cells activation in arsenic-induced liver fibrosis," *Chemosphere*, vol. 242, Article ID 124959, 2019.

[9] X. Yang, Z. Wang, J. Kai et al., "Curcumol attenuates liver sinusoidal endothelial cell angiogenesis via regulating Gli-PROX1-HIF-1α in liver fibrosis," *Cell Proliferation*, vol. 53, no. 3, Article ID e12762, 2020.

[10] L. Chen, X. Yao, H. Yao, Q. Ji, G. Ding, and X. Liu, "Exosomal miR-103-3p from LPS-activated THP-1 macrophage contributes to the activation of hepatic stellate cells," *The FASEB Journal*, vol. 34, no. 4, pp. 5178–5192, 2020.

[11] H. Liu, F. Dong, G. Li et al., "Liuweiwuling tablets attenuate BDL-induced hepatic fibrosis via modulation of TGF-β/Smad and NF-κB signaling pathways," *Journal of Ethnopharmacology*, vol. 210, pp. 232–241, 2018.

[12] Y. Nakano, A. Kamiya, H. Sumiyoshi, K. Tsuruya, T. Kagawa, and Y. Inagaki, "A deactivation factor of fibrogenic hepatic stellate cells induces regression of liver fibrosis in mice," *Hepatology*, vol. 71, no. 4, pp. 1437–1452, 2020.

[13] B. Khambu, S. Yan, N. Huda, G. Liu, and X.-M. Yin, "Autophagy in non-alcoholic fatty liver disease and alcoholic liver disease," *Liver research*, vol. 2, no. 3, pp. 112–119, 2018.

[14] T. Medeiros, G. N. Saraiva, L. A. Moraes et al., "Liver fibrosis improvement in chronic hepatitis C after direct acting-antivirals is accompanied by reduced profibrogenic biomarkers-a role for MMP-9/TIMP-1," *Digestive and Liver Disease*, vol. 52, no. 10, pp. 1170–1177, 2020.

[15] T. Kisseleva and D. Brenner, "Molecular and cellular mechanisms of liver fibrosis and its regression," *Nature Reviews Gastroenterology & Hepatology*, vol. 18, no. 3, pp. 151–166, 2021.

[16] B. Liu, X. Deng, Q. Jiang et al., "Scoparone alleviates inflammation, apoptosis and fibrosis of non-alcoholic steatohepatitis by suppressing the TLR4/NF-κB signaling pathway in mice," *International Immunopharmacology*, vol. 75, Article ID 105797, 2019.

[17] Y. Zeng, Z. Zhang, W. Wang et al., "Underlying mechanisms of apoptosis in HepG2 cells induced by polyphyllin I through Fas death and mitochondrial pathways," *Toxicology Mechanisms and Methods*, vol. 30, no. 6, pp. 397–406, 2020.

[18] A. Remmerie, L. Martens, T. Castoldi et al., "Osteopontin expression identifies a subset of recruited macrophages distinct from kupffer cells in the fatty liver," *Immunity*, vol. 53, no. 3, pp. 641–657, 2020.

[19] D. Cheng, J. Chai, H. Wang, L. Fu, S. Peng, and X. Ni, "Hepatic macrophages: key players in the development and progression of liver fibrosis," *Liver International*, vol. 41, no. 10, pp. 2279–2294, 2021.

[20] S. She, X. Wu, D. Zheng et al., "PSMP/MSMP promotes hepatic fibrosis through CCR2 and represents a novel therapeutic target," *Journal of Hepatology*, vol. 72, no. 3, pp. 506–518, 2020.

[21] K. Zhang, Z. Shi, M. Zhang et al., "Silencing lncRNA Lfar1 alleviates the classical activation and pyoptosis of macrophage in hepatic fibrosis," *Cell Death & Disease*, vol. 11, no. 2, p. 132, 2020.

[22] J. Leslie, M. G. Macia, S. Luli et al., "c-Rel orchestrates energy-dependent epithelial and macrophage reprogramming in fibrosis," *Nature Metabolism*, vol. 2, no. 11, pp. 1350–1367, 2020.

[23] B. Cai, P. Dongiovanni, K. E. Corey et al., "Macrophage MerTK promotes liver fibrosis in nonalcoholic steatohepatitis," *Cell Metabolism*, vol. 31, no. 2, pp. 406–421, 2020.

[24] Q. Yao, S. Li, X. Li, F. Wang, and C. Tu, "Myricetin modulates macrophage polarization and mitigates liver inflammation and fibrosis in a murine model of nonalcoholic steatohepatitis," *Frontiers of Medicine*, vol. 7, p. 71, 2020.

[25] J. Xue, T. Xiao, S. Wei et al., "miR-21-regulated M2 polarization of macrophage is involved in arsenicosis-induced hepatic fibrosis through the activation of hepatic stellate cells," *Journal of Cellular Physiology*, vol. 236, no. 8, pp. 6025–6041, 2021.

[26] P. An, L.-L. Wei, S. Zhao et al., "Hepatocyte mitochondria-derived danger signals directly activate hepatic stellate cells and drive progression of liver fibrosis," *Nature Communications*, vol. 11, no. 1, p. 2362, 2020.

[27] T. Su, Y. Yang, S. Lai et al., "Single-cell transcriptomics reveals zone-specific alterations of liver sinusoidal endothelial cells in cirrhosis," *Cellular and Molecular Gastroenterology and Hepatology*, vol. 11, no. 4, pp. 1139–1161, 2021.

[28] S. Petrillo, M. Manco, F. Altruda, S. Fagoonee, and E. Tolosano, "Liver sinusoidal endothelial cells at the crossroad of iron overload and liver fibrosis," *Antioxidants & Redox Signaling*, vol. 35, no. 6, pp. 474–486, 2021.

[29] J. Poisson, S. Lemoinne, C. Boulanger et al., "Liver sinusoidal endothelial cells: physiology and role in liver diseases," *Journal of Hepatology*, vol. 66, no. 1, pp. 212–227, 2017.

[30] L. Chen, T. Gu, B. Li et al., "Delta-like ligand 4/DLL4 regulates the capillarization of liver sinusoidal endothelial cell and liver fibrogenesis," *Biochimica et Biophysica Acta (BBA)-Molecular Cell Research*, vol. 1866, no. 10, pp. 1663–1675, 2019.

[31] M. Winkler, T. Staniczek, S. W. Kürschner et al., "Endothelial GATA4 controls liver fibrosis and regeneration by preventing a pathogenic switch in angiocrine signaling," *Journal of Hepatology*, vol. 74, no. 2, pp. 380–393, 2021.

[32] A. Desroches-Castan, E. Tillet, N. Ricard et al., "Bone morphogenetic protein 9 is a paracrine factor controlling liver sinusoidal endothelial cell fenestration and protecting against hepatic fibrosis," *Hepatology*, vol. 70, no. 4, pp. 1392–1408, 2019.

[33] M. Ruart, L. Chavarria, G. Campreciós et al., "Impaired endothelial autophagy promotes liver fibrosis by aggravating the oxidative stress response during acute liver injury," *Journal of Hepatology*, vol. 70, no. 3, pp. 458–469, 2019.

[34] A. Hammoutene, L. Biquard, J. Lasselin et al., "A defect in endothelial autophagy occurs in patients with non-alcoholic steatohepatitis and promotes inflammation and fibrosis," *Journal of Hepatology*, vol. 72, no. 3, pp. 528–538, 2020.

[35] D. Xiang, J. Zou, X. Zhu et al., "Physalin D attenuates hepatic stellate cell activation and liver fibrosis by blocking TGF-β/Smad and YAP signaling," *Phytomedicine*, vol. 78, Article ID 153294, 2020.

[36] Q. Cheng, C. Li, C.-F. Yang et al., "Methyl ferulic acid attenuates liver fibrosis and hepatic stellate cell activation through the TGF-β1/Smad and NOX4/ROS pathways," *Chemico-Biological Interactions*, vol. 299, pp. 131–139, 2019.

[37] Q. Zhang, X. Chang, H. Wang et al., "TGF-β1 mediated Smad signaling pathway and EMT in hepatic fibrosis induced by Nano NiO in vivo and in vitro," *Environmental Toxicology*, vol. 35, no. 4, pp. 419–429, 2020.

[38] N. Liu, J. Feng, X. Lu et al., "Isorhamnetin inhibits liver fibrosis by reducing autophagy and inhibiting extracellular matrix formation via the TGF-beta1/smad3 and TGF-beta1/p38 MAPK pathways," *Mediators of Inflammation*, vol. 2019, Article ID 6175091, 14 pages, 2019.

[39] K. Tzavlaki and A. Moustakas, "TGF-β signaling," *Biomolecules*, vol. 10, no. 3, p. 487, 2020.

[40] M. Mu, S. Zuo, R.-M. Wu et al., "Ferulic acid attenuates liver fibrosis and hepatic stellate cell activation via inhibition of TGF-β/Smad signaling pathway," *Drug Design, Development and Therapy*, vol. 12, pp. 4107–4115, 2018.

[41] X. Zhong, M. Huang, H.-G. Kim et al., "SIRT6 protects against liver fibrosis by deacetylation and suppression of SMAD3 in hepatic stellate cells," *Cellular and Molecular Gastroenterology and Hepatology*, vol. 10, no. 2, pp. 341–364, 2020.

[42] J. Zhao, M. Han, L. Zhou et al., "TAF and TDF attenuate liver fibrosis through NS5ATP9, TGFβ1/Smad3, and NF-κB/NLRP3 inflammasome signaling pathways," *Hepatology International*, vol. 14, no. 1, pp. 145–160, 2020.

[43] H. Xie, D. Su, J. Zhang et al., "Raw and vinegar processed Curcuma wenyujin regulates hepatic fibrosis via bloking TGF-β/Smad signaling pathways and up-regulation of MMP-2/TIMP-1 ratio," *Journal of Ethnopharmacology*, vol. 246, Article ID 111768, 2020.

[44] N. Krishnamurthy and R. Kurzrock, "Targeting the Wnt/beta-catenin pathway in cancer: update on effectors and inhibitors," *Cancer Treatment Reviews*, vol. 62, pp. 50–60, 2018.

[45] Y. S. Jung, S. A. Stratton, S. H. Lee et al., "TMEM9-v-ATPase activates Wnt/β-catenin signaling via APC lysosomal degradation for liver regeneration and tumorigenesis," *Hepatology*, vol. 73, no. 2, pp. 776–794, 2021.

[46] C. Zhang, X.-Q. Liu, H.-N. Sun et al., "Octreotide attenuates hepatic fibrosis and hepatic stellate cells proliferation and activation by inhibiting Wnt/β-catenin signaling pathway, c-Myc and cyclin D1," *International Immunopharmacology*, vol. 63, pp. 183–190, 2018.

[47] N. E. El-Ashmawy, G. M. Al-Ashmawy, H. E. Fakher, and N. F. Khedr, "The role of WNT/β-catenin signaling pathway and glutamine metabolism in the pathogenesis of CCl4-induced liver fibrosis: repositioning of niclosamide and concerns about lithium," *Cytokine*, vol. 136, p. 155250, 2020.

[48] I. H. Lee, E. Im, H. J. Lee et al., "Apoptotic and anti-hepatofibrotic effect of honokiol via activation of GSK3β and suppression of Wnt/β-catenin pathway in hepatic stellate cells," *Phytotherapy Research*, vol. 35, no. 1, pp. 452–462, 2021.

[49] Y. Feng, S. Gao, R. Wei et al., "Effects of probiotics on intestinal flora, inflammation and degree of liver cirrhosis in rats with liver cirrhosis by regulating Wnt/β-catenin signaling pathway," *Journal of Biological Regulators and Homeostatic Agents*, vol. 35, no. 1, pp. 25–33, 2021.

[50] F. Zhang, F. Wang, J. He et al., "Regulation of hepatic stellate cell contraction and cirrhotic portal hypertension by Wnt/β-catenin signalling via interaction with Gli1," *British Journal of Pharmacology*, vol. 178, no. 11, pp. 2246–2265, 2021.

[51] S. Gaul, A. Leszczynska, F. Alegre et al., "Hepatocyte pyroptosis and release of inflammasome particles induce stellate cell activation and liver fibrosis," *Journal of Hepatology*, vol. 74, no. 1, pp. 156–167, 2021.

[52] C. Y. Han, H. S. Rho, A. Kim et al., "FXR inhibits endoplasmic reticulum stress-induced NLRP3 inflammasome in hepatocytes and ameliorates liver injury," *Cell Reports*, vol. 24, no. 11, pp. 2985–2999, 2018.

[53] A. R. Mridha, A. Wree, A. A. B. Robertson et al., "NLRP3 inflammasome blockade reduces liver inflammation and fibrosis in experimental NASH in mice," *Journal of Hepatology*, vol. 66, no. 5, pp. 1037–1046, 2017.

[54] A. Wree, M. D. McGeough, M. E. Inzaugarat et al., "NLRP3 inflammasome driven liver injury and fibrosis: roles of IL-17 and TNF in mice," *Hepatology*, vol. 67, no. 2, pp. 736–749, 2018.

[55] L. Catrysse, M. Farhang Ghahremani, L. Vereecke et al., "A20 prevents chronic liver inflammation and cancer by protecting hepatocytes from death," *Cell Death & Disease*, vol. 7, no. 6, p. e2250, 2016.

[56] H. Hwangbo, M. Y. Kim, S. Y. Ji et al., "Auranofin attenuates non-alcoholic fatty liver disease by suppressing lipid accumulation and NLRP3 inflammasome-mediated hepatic inflammation in vivo and in vitro," *Antioxidants*, vol. 9, no. 11, p. 1040, 2020.

[57] C. Jimenez Calvente, H. Del Pilar, M. Tameda, C. D. Johnson, and A. E. Feldstein, "MicroRNA 223 3p negatively regulates the NLRP3 inflammasome in acute and chronic liver injury," *Molecular Therapy*, vol. 28, no. 2, pp. 653–663, 2020.

[58] Y.-S. Shi, X.-X. Li, H.-T. Li, and Y. Zhang, "Pelargonidin ameliorates CCl4-induced liver fibrosis by suppressing the ROS-NLRP3-IL-1β axis via activating the Nrf2 pathway," *Food & Function*, vol. 11, no. 6, pp. 5156–5165, 2020.

[59] G. Yang, J. H. Jang, S. W. Kim et al., "Sweroside prevents non-alcoholic steatohepatitis by suppressing activation of the NLRP3 inflammasome," *International Journal of Molecular Sciences*, vol. 21, no. 8, p. 2790, 2020.

[60] M. L. Tomasi and K. Ramani, "SUMOylation and phosphorylation cross-talk in hepatocellular carcinoma," *Translational Gastroenterology and Hepatology*, vol. 3, p. 20, 2018.

[61] M. Morales-Ruiz, A. Santel, J. Ribera, and W. Jiménez, "The role of Akt in chronic liver disease and liver regeneration," *Seminars in Liver Disease*, vol. 58, no. 01, pp. 011–016, 2017.

[62] L. Wu, Q. Zhang, W. Mo et al., "Quercetin prevents hepatic fibrosis by inhibiting hepatic stellate cell activation and reducing autophagy via the TGF-β1/Smads and PI3K/Akt pathways," *Scientific Reports*, vol. 7, no. 1, pp. 9289–9313, 2017.

[63] Z. Yu, Y. Jv, L. Cai et al., "Gambogic acid attenuates liver fibrosis by inhibiting the PI3K/AKT and MAPK signaling pathways via inhibiting HSP90," *Toxicology and Applied Pharmacology*, vol. 371, pp. 63–73, 2019.

[64] A.-Y. Xiu, Q. Ding, Z. Li, and C.-Q. Zhang, "Doxazosin attenuates liver fibrosis by inhibiting autophagy in hepatic stellate cells via activation of the PI3K/Akt/mTOR signaling pathway," *Drug Design, Development and Therapy*, vol. 15, pp. 3643–3659, 2021.

[65] R. Wang, F. Song, S. Li, B. Wu, Y. Gu, and Y. Yuan, "Salvianolic acid A attenuates CCl4-induced liver fibrosis by regulating the PI3K/AKT/mTOR, Bcl-2/Bax and caspase-3/cleaved caspase-3 signaling pathways," *Drug Design, Development and Therapy*, vol. 13, pp. 1889–1900, 2019.

[66] J. Feng, K. Chen, Y. Xia et al., "Salidroside ameliorates autophagy and activation of hepatic stellate cells in mice via NF-& kappa; B and TGF-& beta; 1/Smad3 pathways," *Drug Design, Development and Therapy*, vol. 12, pp. 1837–1853, 2018.

[67] Q. Yu, P. Cheng, J. Wu, and C. Guo, "PPARγ/NF-κB and TGF-β1/Smad pathway are involved in the anti-fibrotic effects of levo-tetrahydropalmatine on liver fibrosis," *Journal of Cellular and Molecular Medicine*, vol. 25, no. 3, pp. 1645–1660, 2021.

[68] C. Wan, F. Jin, Y. Du et al., "Genistein improves schistosomiasis liver granuloma and fibrosis via dampening NF-kB signaling in mice," *Parasitology Research*, vol. 116, no. 4, pp. 1165–1174, 2017.

[69] T. Zhang, J. Hu, X. Wang et al., "MicroRNA-378 promotes hepatic inflammation and fibrosis via modulation of the NF-κB-TNFα pathway," *Journal of Hepatology*, vol. 70, no. 1, pp. 87–96, 2019.

[70] A. Mohammadalipour, M. Hashemnia, F. Goudarzi, and A. P. Ravan, "Increasing the effectiveness of tyrosine kinase inhibitor (TKI) in combination with a statin in reducing liver fibrosis," *Clinical and Experimental Pharmacology and Physiology*, vol. 46, no. 12, pp. 1183–1193, 2019.

[71] J. He, J. Gong, Q. Ding et al., "Suppressive effect of SATB1 on hepatic stellate cell activation and liver fibrosis in rats," *FEBS Letters*, vol. 589, no. 12, pp. 1359–1368, 2015.

[72] Q. Wang, X. Chou, F. Guan et al., "Enhanced Wnt signalling in hepatocytes is associated with schistosoma japonicum infection and contributes to liver fibrosis," *Scientific Reports*, vol. 7, no. 1, p. 230, 2017.

[73] P.-J. Chen, L.-M. Kuo, Y.-H. Wu, Y.-C. Chang, K.-H. Lai, and T.-L. Hwang, "BAY 41-2272 attenuates CTGF expression via sGC/cGMP-Independent pathway in TGFβ1-activated hepatic stellate cells," *Biomedicines*, vol. 8, no. 9, p. 330, 2020.

[74] B. Yu, G.-N. Jin, M. Ma et al., "Taurocholate induces connective tissue growth factor expression in hepatocytes through ERK-YAP signaling," *Cellular Physiology and Biochemistry*, vol. 50, no. 5, pp. 1711–1725, 2018.

[75] F. A. Mendes, J. M. Coelho Aguiar, S. A. Kahn et al., "Connective-tissue growth factor (CTGF/CCN2) induces astrogenesis and fibronectin expression of embryonic neural cells in vitro," *PLoS One*, vol. 10, no. 8, Article ID e0133689, 2015.

[76] Y.-W. Sun, Y.-Y. Zhang, X.-J. Ke, X.-j. Wu, Z.-F. Chen, and P. Chi, "Pirfenidone prevents radiation-induced intestinal fibrosis in rats by inhibiting fibroblast proliferation and differentiation and suppressing the TGF-β1/Smad/CTGF signaling pathway," *European Journal of Pharmacology*, vol. 822, pp. 199–206, 2018.

[77] Y. Cai, G. Huang, L. Ma et al., "Smurf2, an E3 ubiquitin ligase, interacts with PDE4B and attenuates liver fibrosis through miR-132 mediated CTGF inhibition," *Biochimica et Biophysica Acta (BBA) - Molecular Cell Research*, vol. 1865, no. 2, pp. 297–308, 2018.

[78] J. S. Bajaj and A. Khoruts, "Microbiota changes and intestinal microbiota transplantation in liver diseases and cirrhosis," *Journal of Hepatology*, vol. 72, no. 5, pp. 1003–1027, 2020.

[79] R. Wang, R. Tang, B. Li, X. Ma, B. Schnabl, and H. Tilg, "Gut microbiome, liver immunology, and liver diseases," *Cellular & Molecular Immunology*, vol. 18, no. 1, pp. 4–17, 2021.

[80] J. P. Arab, R. M. Martin-Mateos, and V. H. Shah, "Gut-liver axis, cirrhosis and portal hypertension: the chicken and the egg," *Hepatology international*, vol. 12, no. 1, pp. 24–33, 2018.

[81] E. Scorletti, P. R. Afolabi, E. A. Miles et al., "Design and rationale of the INSYTE study: a randomised, placebo controlled study to test the efficacy of a synbiotic on liver fat, disease biomarkers and intestinal microbiota in non-alcoholic fatty liver disease," *Contemporary Clinical Trials*, vol. 71, no. 8, pp. 113–123, 2018.

[82] A. Tripathi, J. Debelius, D. A. Brenner et al., "The gut-liver axis and the intersection with the microbiome," *Nature Reviews Gastroenterology & Hepatology*, vol. 15, no. 7, pp. 397–411, 2018.

[83] K. M. Schneider, C. Elfers, A. Ghallab et al., "Intestinal dysbiosis amplifies acetaminophen-induced acute liver injury," *Cellular and Molecular Gastroenterology and Hepatology*, vol. 11, no. 4, pp. 909–933, 2021.

[84] N. Hu, C. Wang, X. Dai et al., "Phillygenin inhibits LPS-induced activation and inflammation of LX2 cells by TLR4/MyD88/NF-κB signaling pathway," *Journal of Ethnopharmacology*, vol. 248, Article ID 112361, 2020.

[85] C. Xie, X. Li, J. Zhu, J. Wu, S. Geng, and C. Zhong, "Magnesium isoglycyrrhizinate suppresses LPS-induced inflammation and oxidative stress through inhibiting NF-κB and MAPK pathways in RAW264.7 cells," *Bioorganic & Medicinal Chemistry*, vol. 27, no. 3, pp. 516–524, 2019.

[86] M. Camilleri, S. L. Nord, D. Burton et al., "Randomised clinical trial: significant biochemical and colonic transit effects of the farnesoid X receptor agonist tropifexor in patients with primary bile acid diarrhoea," *Alimentary Pharmacology & Therapeutics*, vol. 52, no. 5, pp. 808–820, 2020.

[87] J. Zhou, N. Huang, Y. Guo et al., "Combined obeticholic acid and apoptosis inhibitor treatment alleviates liver fibrosis," *Acta Pharmaceutica Sinica B*, vol. 9, no. 3, pp. 526–536, 2019.

[88] H. Hao, L. Cao, C. Jiang et al., "Farnesoid X receptor regulation of the NLRP3 inflammasome underlies cholestasis-associated sepsis," *Cell Metabolism*, vol. 25, no. 4, pp. 856–867, 2017.

[89] D. Kong, Z. Zhang, L. Chen et al., "Curcumin blunts epithelial-mesenchymal transition of hepatocytes to alleviate hepatic fibrosis through regulating oxidative stress and autophagy," *Redox Biology*, vol. 36, Article ID 101600, 2020.

[90] J. Gao, B. Wei, T. M. de Assuncao et al., "Hepatic stellate cell autophagy inhibits extracellular vesicle release to attenuate liver fibrosis," *Journal of Hepatology*, vol. 73, no. 5, pp. 1144–1154, 2020.

[91] X.-W. Zhang, J.-C. Zhou, D. Peng et al., "Disrupting the TRIB3-SQSTM1 interaction reduces liver fibrosis by restoring autophagy and suppressing exosome-mediated HSC activation," *Autophagy*, vol. 16, no. 5, pp. 782–796, 2020.

[92] D. Meng, Z. Li, G. Wang, L. Ling, Y. Wu, and C. Zhang, "Carvedilol attenuates liver fibrosis by suppressing autophagy and promoting apoptosis in hepatic stellate cells," *Biomedicine & Pharmacotherapy*, vol. 108, pp. 1617–1627, 2018.

[93] M. Bernard, B. Yang, F. Migneault et al., "Autophagy drives fibroblast senescence through MTORC2 regulation," *Autophagy*, vol. 16, no. 11, pp. 2004–2016, 2020.

[94] J. Zhu, W. Zhang, L. Zhang et al., "IL-7 suppresses macrophage autophagy and promotes liver pathology in Schistosoma japonicum -infected mice," *Journal of Cellular and Molecular Medicine*, vol. 22, no. 7, pp. 3353–3363, 2018.

[95] M. Shen, M. Guo, Z. Wang et al., "ROS-dependent inhibition of the PI3K/Akt/mTOR signaling is required for Oroxylin A to exert anti-inflammatory activity in liver fibrosis," *International Immunopharmacology*, vol. 85, Article ID 106637, 2020.

[96] Q. He, L. Wang, R. Zhao et al., "Mesenchymal stem cell-derived exosomes exert ameliorative effects in type 2 diabetes by improving hepatic glucose and lipid metabolism via enhancing autophagy," *Stem Cell Research & Therapy*, vol. 11, no. 1, p. 223, 2020.

[97] W. Chen, Z. Zhang, Z. Yao et al., "Activation of autophagy is required for Oroxylin A to alleviate carbon tetrachloride-induced liver fibrosis and hepatic stellate cell activation," *International Immunopharmacology*, vol. 56, pp. 148–155, 2018.

[98] L. Wang, Z. Zhang, M. Li et al., "P53-dependent induction of ferroptosis is required for artemether to alleviate carbon tetrachloride-induced liver fibrosis and hepatic stellate cell activation," *IUBMB Life*, vol. 71, no. 1, pp. 45–56, 2019.

[99] C. Li, Y. Liu, Z. Dong et al., "TCDD promotes liver fibrosis through disordering systemic and hepatic iron homeostasis," *Journal of Hazardous Materials*, vol. 395, Article ID 122588, 2020.

[100] Y. Li, C. Jin, M. Shen et al., "Iron regulatory protein 2 is required for artemether -mediated anti-hepatic fibrosis through ferroptosis pathway," *Free Radical Biology and Medicine*, vol. 160, pp. 845–859, 2020.

[101] Z. Kong, R. Liu, and Y. Cheng, "Artesunate alleviates liver fibrosis by regulating ferroptosis signaling pathway," *Biomedicine & Pharmacotherapy*, vol. 109, pp. 2043–2053, 2019.

[102] Z. Zhang, M. Guo, M. Shen et al., "The BRD7-P53-SLC25A28 axis regulates ferroptosis in hepatic stellate cells," *Redox Biology*, vol. 36, Article ID 101619, 2020.

[103] K. J. Mehta, S. J. Farnaud, and P. A. Sharp, "Iron and liver fibrosis: mechanistic and clinical aspects," *World Journal of Gastroenterology*, vol. 25, no. 5, pp. 521–538, 2019.

[104] M. Sui, X. Jiang, J. Chen, H. Yang, and Y. Zhu, "Magnesium isoglycyrrhizinate ameliorates liver fibrosis and hepatic stellate cell activation by regulating ferroptosis signaling pathway," *Biomedicine & Pharmacotherapy*, vol. 106, pp. 125–133, 2018.

[105] Z. Wang, J. a. Li, W. a. Xiao, J. Long, and H. Zhang, "The STAT3 inhibitor S3I-201 suppresses fibrogenesis and angiogenesis in liver fibrosis," *Laboratory Investigation*, vol. 98, no. 12, pp. 1600–1613, 2018.

[106] S. Elzamly, H. A. Agina, A. E.-L. Elbalshy, M. Abuhashim, E. Saad, and Z. Y. Abd Elmageed, "Integration of VEGF and α-SMA expression improves the prediction accuracy of fibrosis in chronic hepatitis C liver biopsy," *Applied Immunohistochemistry & Molecular Morphology*, vol. 25, no. 4, pp. 261–270, 2017.

[107] K. Yuan, C. Lai, L. Wei et al., "The effect of vascular endothelial growth factor on bone marrow mesenchymal stem cell engraftment in rat fibrotic liver upon transplantation," *Stem Cells International*, vol. 2019, Article ID 5310202, 13 pages, 2019.

[108] D. Ezhilarasan, "Endothelin-1 in portal hypertension: the intricate role of hepatic stellate cells," *Experimental Biology and Medicine*, vol. 245, no. 16, pp. 1504–1512, 2020.

[109] G. Li, Y. Peng, T. Zhao et al., "Plumbagin alleviates capillarization of hepatic sinusoids in vitro by downregulating ET-1, VEGF, LN, and type IV collagen," *BioMed Research International*, vol. 2017, Article ID 5603216, 12 pages, 2017.

[110] H. Kong, J. He, S. Guo et al., "Endothelin receptors promote schistosomiasis-induced hepatic fibrosis via splenic B cells," *PLoS Pathogens*, vol. 16, no. 10, Article ID e1008947, 2020.

[111] H.-Z. Ying, Q. Chen, W.-Y. Zhang et al., "PDGF signaling pathway in hepatic fibrosis pathogenesis and therapeutics," *Molecular Medicine Reports*, vol. 16, no. 6, pp. 7879–7889, 2017.

[112] N. Roehlen, E. Crouchet, and T. F. Baumert, "Liver fibrosis: mechanistic concepts and therapeutic perspectives," *Cells*, vol. 9, no. 4, p. 875, 2020.

[113] C. Chen, X. Li, and L. Wang, "Thymosinβ4 alleviates cholestatic liver fibrosis in mice through down regulating PDGF/PDGFR and TGFβ/Smad pathways," *Digestive and Liver Disease*, vol. 52, no. 3, pp. 324–330, 2020.

[114] X. Wang, Y. Gao, Y. Li et al., "Roseotoxin B alleviates cholestatic liver fibrosis through inhibiting PDGF-B/PDGFR-β pathway in hepatic stellate cells," *Cell Death & Disease*, vol. 11, no. 6, p. 458, 2020.

[115] H. Li, "Advances in anti hepatic fibrotic therapy with Traditional Chinese Medicine herbal formula," *Journal of Ethnopharmacology*, vol. 251, Article ID 112442, 2020.

[116] C. Lu, W. Xu, F. Zhang, J. Shao, and S. Zheng, "Nrf2 knockdown attenuates the ameliorative effects of ligustrazine on hepatic fibrosis by targeting hepatic stellate cell transdifferentiation," *Toxicology*, vol. 365, pp. 35–47, 2016.

[117] Z. Hu, H. Su, Y. Zeng et al., "Tetramethylpyrazine ameliorates hepatic fibrosis through autophagy-mediated inflammation," *Biochemistry and Cell Biology*, vol. 98, no. 3, pp. 327–337, 2020.

[118] X. Ma, Q. Ruan, X. Ji, J. Yang, and H. Peng, "Ligustrazine alleviates cyclophosphamide-induced hepatotoxicity via the inhibition of Txnip/Trx/NF-κB pathway," *Life Sciences*, vol. 274, Article ID 119331, 2021.

[119] F. Zhang, C. Ni, D. Kong et al., "Ligustrazine attenuates oxidative stress-induced activation of hepatic stellate cells by interrupting platelet-derived growth factor-β receptor-mediated ERK and p38 pathways," *Toxicology and Applied Pharmacology*, vol. 265, no. 1, pp. 51–60, 2012.

[120] C. Balta, H. Herman, O. M. Boldura et al., "Chrysin attenuates liver fibrosis and hepatic stellate cell activation through TGF-β/Smad signaling pathway," *Chemico-Biological Interactions*, vol. 240, pp. 94–101, 2015.

[121] Z. Y. Cui, G. Wang, J. Zhang et al., "Parthenolide, bioactive compound of Chrysanthemum parthenium L., ameliorates fibrogenesis and inflammation in hepatic fibrosis via regulating the crosstalk of TLR4 and STAT3 signaling pathway," *Phytotherapy Research*, vol. 35, pp. 1–14, 2021.

[122] D. Yang, L. Li, S. Qian, and L. Liu, "Evodiamine ameliorates liver fibrosis in rats via TGF-β1/Smad signaling pathway," *Journal of Natural Medicines*, vol. 72, no. 1, pp. 145–154, 2018.

[123] Y. Liu, P. H. Wen, X. X. Zhang, Y. Dai, and Q. He, "Breviscapine ameliorates CCl4-induced liver injury in mice through inhibiting inflammatory apoptotic response and ROS generation," *International Journal of Molecular Medicine*, vol. 42, no. 2, pp. 755–768, 2018.

[124] M. Farzaei, M. Zobeiri, F. Parvizi et al., "Curcumin in liver diseases: a systematic review of the cellular mechanisms of oxidative stress and clinical perspective," *Nutrients*, vol. 10, no. 7, p. 855, 2018.

[125] X. Wu, F. Zhi, W. Lun, Q. Deng, and W. Zhang, "Baicalin inhibits PDGF-BB-induced hepatic stellate cell proliferation, apoptosis, invasion, migration and activation via the miR-3595/ACSL4 axis," *International Journal of Molecular Medicine*, vol. 41, no. 4, pp. 1992–2002, 2018.

[126] X. Zhong and H. Liu, "Baicalin attenuates diet induced nonalcoholic steatohepatitis by inhibiting inflammation and oxidative stress via suppressing JNK signaling pathways," *Biomedicine & Pharmacotherapy*, vol. 98, pp. 111–117, 2018.

[127] H. Chang, H. Meng, Y. Wang, Z. Teng, and S.-M. Liu, "Inhibitory effect of Scutellariae Radix on hepatic fibrosis based on urinary metabonomic," *China Journal of Chinese Materia Medica*, vol. 43, no. 10, pp. 2140–2146, 2018.

[128] X.-A. Zhao, G. Chen, Y. Wu et al., "Emodin alleviates liver fibrosis of mice by reducing infiltration of Gr1hi monocytes," *Evidence-based Complementary and Alternative Medicine*, vol. 2018, no. 3, 11 pages, Article ID 5738101, 2018.

[129] B. Liang, L. Gao, F. Wang et al., "The mechanism research on the anti-liver fibrosis of emodin based on network pharmacology," *IUBMB Life*, vol. 73, no. 9, pp. 1166–1179, 2021.

[130] X. Xue, Y. Quan, L. Gong, X. Gong, and Y. Li, "A review of the processed Polygonum multiflorum (Thunb.) for hepatoprotection: clinical use, pharmacology and toxicology," *Journal of Ethnopharmacology*, vol. 261, Article ID 113121, 2020.

[131] S. Saadati, B. Hatami, Z. Yari et al., "The effects of curcumin supplementation on liver enzymes, lipid profile, glucose homeostasis, and hepatic steatosis and fibrosis in patients with non-alcoholic fatty liver disease," *European Journal of Clinical Nutrition*, vol. 73, no. 3, pp. 441–449, 2019.

[132] S. Saadati, A. Sadeghi, A. Mansour et al., "Curcumin and inflammation in non-alcoholic fatty liver disease: a randomized, placebo controlled clinical trial," *BMC Gastroenterology*, vol. 19, no. 1, pp. 133–136, 2019.

[133] E. Nozari, A. Moradi, and M. Samadi, "Effect of Atorvastatin, Curcumin, and Quercetin on miR-21 and miR-122 and their correlation with TGFβ1 expression in experimental liver fibrosis," *Life Sciences*, vol. 259, Article ID 118293, 2020.

[134] J. Yang, D. Xiang, D. Xiang et al., "Baicalin protects against 17α-ethinylestradiol-induced cholestasis via the sirtuin 1/hepatic nuclear receptor-1α/farnesoid X receptor pathway," *Frontiers in Pharmacology*, vol. 10, p. 1685, 2020.

[135] R. Xie, M. Liu, and S. Li, "Emodin weakens liver inflammatory injury triggered by lipopolysaccharide through elevating microRNA-145 in vitro and in vivo," *Artificial Cells,*

Nanomedicine, and Biotechnology, vol. 47, no. 1, pp. 1877–1887, 2019.

[136] C. Huang, D. Gan, F. Luo et al., "Interaction mechanisms between the NOX4/ROS and RhoA/ROCK1 signaling pathways as new anti- fibrosis targets of ursolic acid in hepatic stellate cells," *Frontiers in Pharmacology*, vol. 10, p. 431, 2019.

[137] E. Nomikou, M. Livitsanou, C. Stournaras, and D. Kardassis, "Transcriptional and post-transcriptional regulation of the genes encoding the small GTPases RhoA, RhoB, and RhoC: implications for the pathogenesis of human diseases," *Cellular and Molecular Life Sciences*, vol. 75, no. 12, pp. 2111–2124, 2018.

[138] S.-Z. Wan, C. Liu, C.-K. Huang, F.-Y. Luo, and X. Zhu, "Ursolic acid improves intestinal damage and bacterial dysbiosis in liver fibrosis mice," *Frontiers in Pharmacology*, vol. 10, p. 1321, 2019.

[139] W. Zhang, D. Gan, J. Jian et al., "Protective effect of ursolic acid on the intestinal mucosal barrier in a rat model of liver fibrosis," *Frontiers in Physiology*, vol. 10, p. 956, 2019.

[140] Q. Liu, Y. Nie, W. Zhang, Y. Wan, C. Huang, and X. Zhu, "Ursolic acid reverses liver fibrosis by inhibiting NOX4/NLRP3 inflammasome pathways and bacterial dysbiosis," *Gut Microbes*, vol. 13, no. 1, Article ID 1972746, 2021.

[141] F.-F. Cai, R. Wu, Y.-N. Song et al., "Yinchenhao decoction alleviates liver fibrosis by regulating bile acid metabolism and TGF-β/smad/ERK signalling pathway," *Scientific Reports*, vol. 8, no. 1, Article ID 15367, 2018.

[142] J. Zhang, X. Liu, J. Wu et al., "A bioinformatics investigation into the pharmacological mechanisms of the effect of the Yinchenhao decoction on hepatitis C based on network pharmacology," *BMC Complementary Medicine and Therapies*, vol. 20, no. 1, p. 50, 2020.

[143] J.-H. Park, J. Yoon, K. Y. Lee, and B. Park, "Effects of geniposide on hepatocytes undergoing epithelial-mesenchymal transition in hepatic fibrosis by targeting TGFβ/Smad and ERK-MAPK signaling pathways," *Biochimie*, vol. 113, pp. 26–34, 2015.

[144] W. Wu, H. Piao, F. Wu et al., "Yu Jin Pulvis inhibits carbon tetrachloride-induced liver fibrosis by blocking the MAPK and PI3K/Akt signaling pathways," *American Journal of Tourism Research*, vol. 11, no. 9, pp. 5998–6006, 2019.

[145] X. J. Ge, C. Q. Zhao, and L. M. Xu, "Effect of Fuzheng Huayu capsules on survival rate of patients with liver cirrhosis," *Chinese Journal of Hepatology*, vol. 25, no. 11, pp. 834–840, 2017.

[146] M. Wu, Y. Zhou, S.-L. Qin et al., "Fuzheng huayu capsule attenuates hepatic fibrosis by inhibiting activation of hepatic stellate cells," *Evidence-based Complementary And Alternative Medicine*, vol. 2020, Article ID 3468791, 14 pages, 2020.

[147] T. Wang, X. Zhou, H. Liu et al., "Fuzheng Huayu capsule as an adjuvant treatment for HBV-related cirrhosis: a systematic review and meta-analysis," *Phytotherapy Research*, vol. 32, no. 5, pp. 757–768, 2018.

[148] W. Liu, Z. Li, Z. Sun et al., "The components data of fuzheng huayu extracts, cordyceps sinensis mycelia polysaccharide, gypenosides and amygdalin," *Data in Brief*, vol. 25, Article ID 104087, 2019.

[149] H. Tian, L. Liu, Z. Li et al., "Chinese medicine CGA formula ameliorates liver fibrosis induced by carbon tetrachloride involving inhibition of hepatic apoptosis in rats," *Journal of Ethnopharmacology*, vol. 232, pp. 227–235, 2019.

[150] L.-M. Xu and P. Liu, "Guidelines for diagnosis and treatment of hepatic fibrosis with integrated traditional Chinese and Western medicine (2019 edition)," *Journal of Integrative Medicine*, vol. 18, no. 3, pp. 203–213, 2020.

[151] L. Shan, Z. Liu, L. Ci, C. Shuai, X. Lv, and J. Li, "Research progress on the anti-hepatic fibrosis action and mechanism of natural products," *International Immunopharmacology*, vol. 75, Article ID 105765, 2019.

Hindawi
Evidence-Based Complementary and Alternative Medicine
Volume 2022, Article ID 5092742, 12 pages
https://doi.org/10.1155/2022/5092742

Research Article

The Inhibitory Effect and Mechanism of *Ferula akitschkensis* Volatile Oil on Gastric Cancer

Rong Han,[1,2] **Yun Sun**,[3] **Ruoting Ma**,[4] **Dexi Wang**,[4] **Jianan Sun**,[4,5] **Shengjun Zhao**,[1,2] **and Haiying Zhang**[1,2]

[1]*Department of Pharmacy, Affiliated Hospital of Traditional Chinese Medicine of Xinjiang Medical University, Urumqi 830000, Xinjiang, China*
[2]*Xinjiang Key Laboratory of Processing and Research of Traditional Chinese Medicine, Urumqi 830000, Xinjiang, China*
[3]*Department of Traditional Chinese Medicine, The Traditional Chinese Medicine College of Xinjiang Medical University, Urumqi 83000, Xinjiang, China*
[4]*Graduate School, The Fourth Clinical College of Xinjiang Medical University, Urumqi 83000, Xinjiang, China*
[5]*State Key Laboratory of Pathogenesis, Prevention and Treatment of High Incidence Diseases in Central Asia, Xinjiang Medical University, Urumqi 830000, Xinjiang, China*

Correspondence should be addressed to Shengjun Zhao; 1519531677@qq.com and Haiying Zhang; zzhhyy2583@126.com

Received 14 October 2021; Revised 4 March 2022; Accepted 15 March 2022; Published 29 March 2022

Academic Editor: Lifeng Han

Ferula akitschkensis volatile oil (FAVO) has a good inhibitory activity on gastric cancer cell proliferation, but the mechanism of action is not yet clear. In this study, we tested the antigastric cancer efficacy and mechanism of FAVO using both *in vivo* and *in vitro* models. The results showed that FAVO effectively inhibited the proliferation, migration, and invasion of human gastric cancer SGC-7901 cells, the formation of small tubules of human umbilical vein endothelial cells as well as zebrafish intersegmental vessel and intestinal vein angiogenesis. *In vivo* experiments showed that FAVO significantly delayed the growth of SGC-7901 tumor-bearing nude mice and induced higher serum IL-2 and IFN-γ and reduced serum IL-6. Western blot results showed that FAVO reduced the expression of HIF-2α, VEGF, VEGFR2, P-VEGFR2, Akt, and P-Akt in SGC-7901 cells with $CoCl_2$ induced hypoxia. We further clarified the main chemical components of FAVO through GC-MS analysis. In summary, FAVO may inhibit tumor growth and angiogenesis via inhibiting the HIF-2α/VEGF signaling pathway.

1. Introduction

Ferula belongs to Peucedaneae Drude of Apiaceae and is mainly distributed in Central Asia, including Iran, Pakistan, and Turkey. There are 31 species distributed in China [1]. *Ferula* has many biological activities such as anti-inflammation, anticancer, and antiangiogenesis [2–5]. For example, it has been reported that *Ferula* inhibited the proliferation and metastasis of human colon cancer HCT116 cells, human glioma U87 cells, Raji lymphoma cells, cervical adenocarcinoma HeLa cells, and breast cancer MCF-7 cells and induced apoptosis as well as cell cycle arrest [4, 6–8]. Our previous results also showed the ethyl acetate extract of *Ferula* sinkiangensis had an inhibitory effect on colon cancer, gastric cancer, and cervical cancer [9–11].

The medicinal part of *Ferula akitschkensis* is root and oleoresin, which have been used to treat headaches, colds, stomach diseases, and other diseases [12–14]. *Ferula akitschkensis* can regulate estrogen activity and neutrophils and inhibit methicillin-resistant *Staphylococcus aureus*. *Ferula* plants are rich in volatile components, which are mostly extracted by steam distillation and solvent methods. *Ferula akitschkensis* volatile oil (FAVO) is the characteristic active component of *Ferula akitschkensis* and has antitumor, antibacterial, anti-inflammatory, antioxidative, and anti-parasitic effects. For example, Sheng et al. [15] reported that

FAVO prepared by steam distillation and microwave extraction had a strong inhibitory effect on gastric cancer cell SGC-7901. Hosseinzadeh et al. [16] found that FAVO had cytotoxicity on colon cancer CT26 cells and could induce apoptosis. Daneshkazemi et al. [17] showed that FAVO had antibacterial activity against 4 kinds of oral bacteria (*Streptococcus mutans*, *Streptococcus sanguis*, *Streptococcus salivarius*, and *Lactobacillus rhamnosus*). Youssef et al. [18] reported that FAVO had strong antioxidant activity. The composition of FAVO varies greatly among different species of *Ferula akitschkensis*. The main components of FAVO are mainly terpenes and alkenes, and some FAVO also has polysulfides. However, the studies about FAVO on gastric cancer are less reported. Additionally, the mechanism and effective chemical components of FAVO in inhibiting human gastric cancer are still unclear, which all further limits its clinical application.

The rapid proliferation of tumor cells causes the tissue within the tumor to be under hypoxia due to lack of blood supply. Hypoxia not only induces the differentiation and proliferation of vascular endothelial cells but also promotes tumor angiogenesis [19, 20]. Hypoxia inducible factor (HIF), including HIF-1α and HIF-2α, produced by tumor cells is involved in the signal transduction between cells. HIF-2α has 48% sequence homology with HIF-1α. HIF-1α is activated during short-term hypoxia, which will gradually decrease or even disappear under continuous hypoxia. The current research mainly focuses on HIF-2α. HIF-2α continues to increase during hypoxia and regulates the expression of hypoxia response genes under continuous hypoxia, such as VEGF [21–23]. VEGF, also known as vascular permeability factor, plays a vital role in the occurrence, development, invasion, and metastasis of tumors [24–27]. VEGF binds to receptors on the cell membrane, promotes the proliferation, differentiation, and migration of vascular endothelial cells, and promotes the permeability of vascular endothelial cells [28–30]. VEGFR2 (vascular endothelial growth factor receptor 2), the main receptor of VEGF, is mainly distributed on the surface of vascular endothelial cells, lymphatic endothelial cells, megakaryocytes, and hematopoietic stem cells and is the most important factor for VEGF to regulate angiogenesis [31, 32].

In this study, we investigated the effects and mechanisms of FAVO on the proliferation, migration, and invasion of human gastric cancer SGC-7901 cells. The chemical components of FAVO were primarily determined by GC-MS. Both in vitro and in vivo experiments were performed. Our results confirm that FAVO could affect the proliferation, migration, and invasion of human gastric cancer cells via the HIF-2α/VEGF pathway. Our results demonstrate that *Ferula akitschkensis* may serve as a potential antitumor drug and provide a new option for combination therapy or supportive treatment of gastric cancer.

2. Materials and Methods

2.1. Extraction of FAVO. The root of *Ferula akitschkensis*, which was collected from Jimunai County, Altay Region, Xinjiang, China in June 2019 and was identified by Yonghe Li, the Chief Pharmacist of traditional Chinese medicine from the Chinese Medicine Hospital Affiliated to Xinjiang Medical University, was chopped into small pieces. After that, 10 times the amount of water were added, and the samples were placed in an electric heating mantle connected with the volatile oil tester and the reflux condenser. The samples were slowly heated to boiling and kept boiling for 5 h. After drying with anhydrous sodium sulfate, an oily liquid with a special fragrance was obtained.

2.2. GC-MS Analysis. GC-MS analysis was performed on 5977A MSD-7890B GC/MS (Agilent, USA). Briefly, for gas chromatographic analysis, a chromatographic column HP-5MS capillary column (30 m × 0.25 mm × 0.25 μm) (Agilent, USA) was used. The injection volume was 0.05 μL, and the split ratio was 60 : 1. The program was as follows: starting temperature 60°C, 2 min; heating up to 80°C at a rate of 4°C/min, 5 min; heating up to 180°C at 2°C/min, 5 min; heating up to 200°C at 10°C/min, 2 min. Mass spectrometry conditions are as follows: ionization method, EI; ionization energy, 70 eV; ion source generator temperature, 230°C; and mass scanning range, 30–350°amu.

2.3. MTT Assay. Human gastric cancer SGC-7901 cells, from the Institute of Cell Research, Chinese Academy of Sciences (Shanghai, China), were inoculated into 96-well plates, and FAVO of different concentrations (300 μg mL^{-1}, 150 μg mL^{-1}, 75 μg mL^{-1}, 37.5 μg mL^{-1}, 18.75 μg mL^{-1}, and 9.375 μg mL^{-1}) was added for treatment for 24 h. After that, MTT (Sigma) was added and incubated for 3 to 4 h. Finally, 150 μL DMSO was added for development. The absorbance (490 nm) was detected with a microplate reader (Thermo, USA). The proliferation inhibition rate (%)°=°(OD (control group)−OD (volatile oil group))/(OD (control group)−OD (blank group)) × 100%.

2.4. Transwell Assay. Gastric cancer SGC-7901 cells were seeded in a 6-well plate, and FAVO (37.5 μg mL^{-1}, 18.75 μg mL^{-1}, and 9.375 μg mL^{-1}) and cisplatin (30 μg mL^{-1}, Jiangsu Hansoh Pharmaceutical Group Co., Ltd., China) were added. After treatment for 48 h, SGC-7901 cells were collected, resuspended in serum-free cell culture medium, and added to the upper chamber of the Transwell chamber (Corning, USA). The chamber precoated with Matrigel (Corning) was used for the invasion assay and that without Matrigel was used for the migration assay. Cell culture medium containing 10% fetal bovine serum was added to the lower chamber. After culturing for 48 h, the cells in the lower Transwell chamber were fixed with paraformaldehyde (4%) for 30 min and stained for 30 min. Finally, the number of migrated and invaded cells in each group was counted under the microscope.

2.5. Zebrafish Intersegmental Vessel Angiogenesis. The vascular fluorescence transgenic zebrafish (VEGFR2 : GFP) was provided by the Scientific Research Laboratory of Longhua Hospital (Shanghai). The 1 μg mL^{-1} Pronase E (SOLARBIO)

was used to remove the egg membrane when the fertilized egg developed for 24 h. The zebrafish embryos were selected and transferred to a 24-well plate. FAVO was prepared with dimethyl sulfoxide (DMSO) to final concentrations of 37.5, 18.75, and 9.375 μg mL^{-1}. The normal control group was treated with culture medium containing 0.1% DMSO. After FAVO treatment, the sample was placed in a light incubator at 28°C for 14 h, and then, the number of zebrafish intersegmental vessels was observed and calculated by a fluorescence microscope (IX71-12FL/PH; Olympus).

2.6. Angiogenesis of the Inferior Intestinal Vein of SGC-7901-Transplanted Zebrafish. The newborn zebrafish embryos were lightly anesthetized with 1% tricaine. Then, the human gastric cancer SGC-7901 cells adjusted to 2×106 mL^{-1} (about 0.1 μL, about 200 cancer cells) were injected under the yolk of the embryo with a microinjector. Afterwards, the zebrafish was treated with FAVO (37.5, 18.75, and 9.375 μg mL^{-1}) and cultured at 28°C for 48 h. After that, the anesthetized embryos were placed under a confocal microscope (FV-1000, Olympus) to analyze the effects of FAVO on the subintestinal veins (SIVs) of zebrafish.

2.7. Endothelial Cell Tube Formation Assay. Human umbilical vein endothelial cells (HUVECs), from the Institute of Cell Research, Chinese Academy of Sciences (Shanghai, China), were placed on a 96-well plate precoated with Matrigel. Then, HUVECs were suspended in 50 μL basal F-12K medium (2.5×105 cells/mL) that also contained VEGF (50 ng/mL) and treated with or without various concentrations of FAVO (37.5, 18.75, and 9.375 μg mL^{-1}) for 8 hours. Through the length of tubules and the number of branch points per unit area, the effect of FAVO on the ability of HUVECs to form tubules was evaluated.

2.8. Animals. The BALB/c nude mice (weighing 18–22 g) were obtained from Vital River Laboratory Animal Technology Co., Ltd. (Beijing, China). They were kept in standard conditions. All animal experimental procedures were approved by the Ethics Review Board of The First Affiliated Hospital of Xinjiang Medical University.

2.9. Tumor Bearing Model Establishment and Treatment and Grouping of Animals. Nude mice model bearing gastric cancer SGC-7901 transplanted tumor was established by inoculating of 0.2 mL of 1×107 cells mL^{-1} SGC-7901 under the axilla of the left forelimb. On the next day, mice (10 mice in each group) were randomly divided into control group, tumor-bearing model group, cisplatin group, and FAVO (low, medium, and high dose) groups. The FAVO was given by gavage for 2 weeks. The low, medium, and high doses of FAVO were 0.75 g kg^{-1}, 1.5 g kg^{-1}, and 3.0 g kg^{-1}, respectively. The dosage of cisplatin was 5 mg·kg^{-1}, which was given intraperitoneally once every 3 days for two weeks.

2.10. Data Collection and Sampling. From the 7th day of administration, the length, width, and thickness of the transplanted tumor were measured, and the tumor volume was calculated as $\pi \times a \times b \times c/6$ (a: tumor length, b: tumor width, c: tumor thickness). One hour after the last administration, mice were sacrificed after anesthesia. Blood samples were collected. The tumors were isolated and weighted. Tumor inhibition rate was calculated as

$$\frac{\text{Average tumor weight of type group} - \text{average tumor weight of drug} - \text{administered group}}{\text{Average tumor weight in model group}} \times 100\%. \quad (1)$$

2.11. HE Staining. After 24 hours of fixation, the tumor tissues were dehydrated by ethanol and transparent with xylene before embedding in paraffin. After that, the samples were cut into sections and stained with hematoxylin and eosin. After mounting, the samples were observed under an optical microscope.

2.12. ELISA. The serum levels of IL-2, IFN-γ, and IL-6 in each group were detected by IL-2/IFN-γ/IL-6 ELISA kits (ExCell bio, Shanghai, China), respectively. The absorbance was analyzed with a microplate reader (xMarkTM, Bio-Rad). Finally, the serum levels of IL-2, IFN-γ, and IL-6 were calculated according to the standard curves.

2.13. Western Blot. According to different treatments, the human gastric cancer SGC-7901 cells were divided into normoxia group, hypoxia group, hypoxia + FAVO high/medium/low dose groups, and hypoxia + HIF-2α inhibitor PT2385 group. Cells in the normoxia group were cultured under normoxia. Hypoxia was induced with 200 μmol L^{-1} $CoCl_2$ (Sigma, USA) for 24 h. Then, for cells in hypoxia + FAVO high-/medium-/low-dose groups, FAVO (37.5, 18.75, and 9.375 μg mL^{-1}) were added for incubation of 24 h. For cells in the hypoxia + HIF-2α inhibitor PT2385 group, 5 μmol·L^{-1} of HIF-2α inhibitor PT2385 (Selleck, USA) was added for incubation of 24 h. After treatment, the total protein of cells was extracted, and the protein concentration was determined by the BCA method. After SDS-PAGE electrophoresis, proteins were transferred to membrane and then subjected to labeling with primary and secondary antibodies. The primary antibodies from Cell Signaling Technology (Beverly, MA, USA) included anti-HIF-2α (#7096); anti-VEGF (#2463S); anti-VEGFR2 (#9698S); anti-P-VEGFR2 (#2478S); anti-AKT (#9272S); and anti-P-AKT (#4060S). The anti-β-actin primary antibody was purchased from Abcam (ab8226, USA). The secondary antibodies (#31430, Pierce Goat Anti-Mouse IgG (H + L), Peroxidase

Conjugated, Thermo Scientific; #31460, Pierce Goat Anti-Rabbit IgG (H + L), Peroxidase Conjugated, Thermo Scientific) were used. After color development, ChemiScope mini chemiluminescence imaging system (Chemiscope 3000, Clinx Science Instruments Co., Ltd, Shanghai, China) was used to detect protein bands.

2.14. Statistical Analysis. The SPSS17.0 statistical software was used, and the data are expressed as mean ± standard deviation (SD). One-way ANOVA was used for multiple comparisons followed by pairwise comparison with the LSD method. A P value < 0.05 indicates that the difference is statistically significant.

3. Results

3.1. GC-MS Analysis of FAVO Components. By referring to the standard database (NIST 98 Mass Spectral Library), the standard spectrum, and GC-MS analysis, we determined the components of FAVO by the peak area normalization method (Figure 1 and Table 1). The results showed that the volatile oil of *Ferula akitschkensis* was mainly composed of tricyclo [4.4.0.0(2,7)] dec-3-ene-3-methanol, 1-methyl-8-(1-methylethyl) (24.56%), and adamantane, 2-hydroperoxy-2-(2-oxiranyl) (13.86%).

3.2. FAVO Inhibits the Proliferation of Human Gastric Cancer SGC-7901 Cells. The MTT assay was performed to analyze cell proliferation. As shown in Figure 2(a), with the increase of the concentration, the growth of SGC-7901 cells was inhibited. The cell morphology changed from spindle to oval, and some cells were not attached to the culture plate and became suspended cells. The proliferation inhibition rate of cells treated with 75 μg mL^{-1} and 150 μg mL^{-1} FAVO was 99.17% and 95.89%, respectively, significantly lower than that of the normal group. According to the proliferation inhibition rate of each concentration, the IC50 of FAVO was determined at 20.33 μg mL^{-1}. The above results indicate that FAVO could inhibit the proliferation of human gastric cancer cells.

3.3. FAVO Inhibits Migration and Invasion of Human Gastric Cancer SGC-7901 Cells. Transwell assay tested the effects of different concentrations of FAVO on the migration and invasion of human gastric cancer SGC-7901 cells. The results showed that after 48 h of treatment with FAVO, the numbers of migrated (Figure 2(b)) and invaded (Figure 2(c)) cells were significantly decreased compared with the normal control group ($P < 0.05$). These results indicate that FAVO effectively inhibits tumor cell migration and invasion.

3.4. FAVO Inhibits Intersegmental Vessel Angiogenesis in Zebrafish. The effect of FAVO on angiogenesis of the inferior intestinal vein was performed in SGC-7901 transplanted zebrafish. As shown in Figure 3(a), in the control group, the intersegmental vessels grew well and were evenly arranged. After treatment with FAVO, the fluorescence intensity of GFP was reduced. The vessels became thinner and partially missing. Statistically, the number of intersegmental vessels in zebrafish treated with FAVO was significantly reduced ($P < 0.05$). Thus, FAVO could inhibit intersegmental vessel angiogenesis in zebrafish.

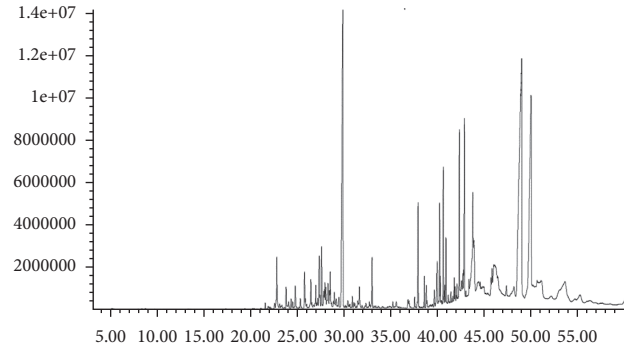

Figure 1: GC-MS fingerprint of the volatile oil of *Ferula akitschkensis*.

3.5. FAVO Inhibits Angiogenesis in the Inferior Intestinal Vein of SGC-7901 Transplanted Zebrafish. Confocal microscopy showed that in the normal control group, the zebrafish embryonic SIVs were half-moon-shaped, fence-like, and showing continuous branches without collateral branches and budding (Figure 3(b)). After treatment with FAVO, the number of intestinal venous plexus, budding and collateral branches decreased dose-dependently. The OD value after FAVO treatment was significantly reduced ($P < 0.05$). The above results indicate that FAVO inhibits angiogenesis in the subintestinal vessels of the zebrafish intestine.

3.6. FAVO Inhibits the Tubule Formation Ability of HUVECs. Tube formation assay was performed with HUVECs. Compared with the normal control group, the length of the tubule per unit area and the number of branch points of HUVECs after FAVO treatment were significantly reduced (Figure 3(c)). The above results indicate that FAVO inhibits the tubule formation ability of HUVECs.

3.7. FAVO Inhibits Tumor Growth In Vivo. The effects of FAVO on tumor growth were further evaluated using nude mice bearing gastric cancer SGC-7901 transplanted tumor. Compared with the control group, the tumor growth of the nude mice treated with FAVO slowed down, with significantly decreased tumor volume (Figure 4(a)) and significantly lower tumor weight (Figure 4(b)). Thus, FAVO could inhibit tumor growth in vivo.

We further tested the levels of cytokines in the serum of tumor-bearing mice and found that FAVO increased the serum levels of IL-2 and IFN-γ but reduced the serum level of IL-6 (Figure 4(a)).

The pathological changes of tumors by HE staining showed that the tumor cells in the control group were densely arranged, with more cells in mitotic phases. In addition, there was avascular necrosis in some areas (Figure 4(c)). However, in the cisplatin treatment group, the pathological mitosis of the cells

Table 1: Component analysis of volatile oil from *Ferula akitschkensis*.

No.	Retention time (min)	Compound	Area (Ab*s)	Relative content (%)
1	22.751	(E)-β-Famesene	126051757	1.46
2	23.743	β-Vatirenene	43229897	0.50
3	24.729	(+)-δ-Cadinene	53738054	0.62
4	25.709	Froggatt ether	62168666	0.72
5	26.394	3,4-Pyridinediamine	61588463	0.71
6	26.925	Guaiol	46440842	0.54
7	27.285	Aristolene epoxide	122320760	1.41
8	27.539	Epi-7-γ-eudesmol	111028260	1.28
9	27.775	Ylangenol	39974833	0.46
10	27.887	β-Funebrene	54293770	0.63
11	27.987	Valencene	36060516	0.42
12	28.229	α-Muurolene	78498374	0.91
13	28.383	α-Gurjunene	27837705	0.32
14	28.466	β-Gurjunene	77109208	0.89
15	28.908	(8S, 14)-Cedran-diol	34477440	0.40
16	29.812	2-Hydroxy-2,4,4-trimethyl-3-(3-methylbuta-1,3-dienyl) cyclohexanone	1102247854	12.75
17	31.589	Isoshyobunone	47731042	0.55
18	32.946	Elemol	97480526	1.13
19	37.870	7-Cyclohexyl-2,3-dihydro-2-methyl-benzofuran	174053067	2.01
20	38.537	Ledene oxide-(II)	45863546	0.53
21	38.737	2-(4a,8-Dimethyl-2,3,4,4a,5,6-hexahydro-naphthalen-2-yl)-prop-2-en-1-ol	32056412	0.37
22	39.895	5-Methoxypsoralen	93722677	1.08
23	40.172	Linoleic acid ethyl ester	133054039	1.54
24	40.243	Ethyl Oleate	35037797	0.41
25	40.562	3b,4,5,6,7,7a,9,10,11,12-Decahydrobenzo[b]fluoranthene	176473713	2.04
26	40.845	[4ar-(4aα,6α,8aβ)]-4a,5,6,7,8,8a-Hexahydro-6-[1-(hydroxymethyl) ethenyl]-4,8a-dimethyl-2(1H)-naphthalenone	80451285	0.93
27	41.730	3-Hydroxy-2,5,5,8a-tetramethyl-3,4,4a,5,6,7,8,8a-octahydronaphthalene-1-carboxylic acid, methyl ester	28793536	0.33
28	42.279	2-(3,7-Dimethylocta-2,6-dienyl)-Phenol	226236742	2.62
29	42.516	5-(7a-Isopropenyl-4,5-dimethyl-octahydroinden-4-yl)-3-methyl-penta-2,4-dien-1-ol	65737854	0.76
30	42.657	Murolan-3,9(11)-diene-10-peroxy	38467970	0.44
31	42.823	4a,7,7,10a-Tetramethyldodecahydrobenzo[f]chromen-3-ol	277813865	3.21
32	43.319	4,4-Dimethyl-(5α,17β)-androstan-17-ol	27798844	0.32
33	43.738	[3as-(3aα,6β,6aα,9aβ,9bα)]-9a-[(acetyloxy)methyl] decahydro-6-methyl-3-methylene-azuleno [4,5-b] furan-2,9-dione	389145276	4.50
34	43.85	1-(9-Borabicyclo [3.3.1] non-9-yl)-3,5-bis(1,1-dimethylethyl)-4-ethyl-1H-pyrazole	198076654	2.29
35	44.334	3-Methyl-4-nitrobenzyl alcohol, n-butyl ether	67183486	0.78
36	45.774	o-Menth-8-ene	42185291	0.49
37	46.069	3′,4′-Dihydro-cholest-1-eno [2,1-a] naphthalene	194464417	2.25
38	48.124	2-(1H-Imidazo [4,5-b] pyridin-2-yl)-1-(4-morpholyl)-ethenone	75754222	0.88
39	48.944	1-Methyl-8-(1-methylethyl)-tricyclo [4.4.0.0(2,7)] dec-3-ene-3-methanol	2123603896	24.56
40	49.954	2-Hydroperoxy-2-(2-oxiranyl)-adamantane	1198660970	13.86
41	53.596	Betulinaldehyde	402406008	4.65

was reduced, but the infiltrating lymphocytes and macrophages increased. Correspondingly, after FAVO treatment, the number and mitosis of tumor cells decreased compared with the control group, but the infiltration of lymphocytes and macrophages increased. These results indicate that high-dose *Ferula akitschkensis* inhibited the tumor growth of SGC-7901 transplanted tumor nude mice.

3.8. Effect of FAVO on HIF-2α/VEGF Pathway. Western blot analysis showed that under $CoCl_2$-induced hypoxia, the expression levels of HIF-2α and downstream proteins including VEGF, VEGFR2, P-VEGFR2, P-Akt, and Akt were all significantly upregulated. However, after treatment with the HIF-2α inhibitor PT2385 and FAVO, their levels were all significantly reduced (Figure 5). Therefore, FAVO might inhibit the activation of the HIF-2α/VEGF pathway.

4. Discussion

Among *Ferula* plants, *Ferula akitschkensis* can be distinguished by smell [33]. The main components of the volatile oil of *Ferula akitschkensis* from Xinjiang and Fukang are sulfides and terpenes, which makes it to have a garlic-like odor [34]. Our analysis showed that components in FAVO contained no sulfides. The main components were tricyclo

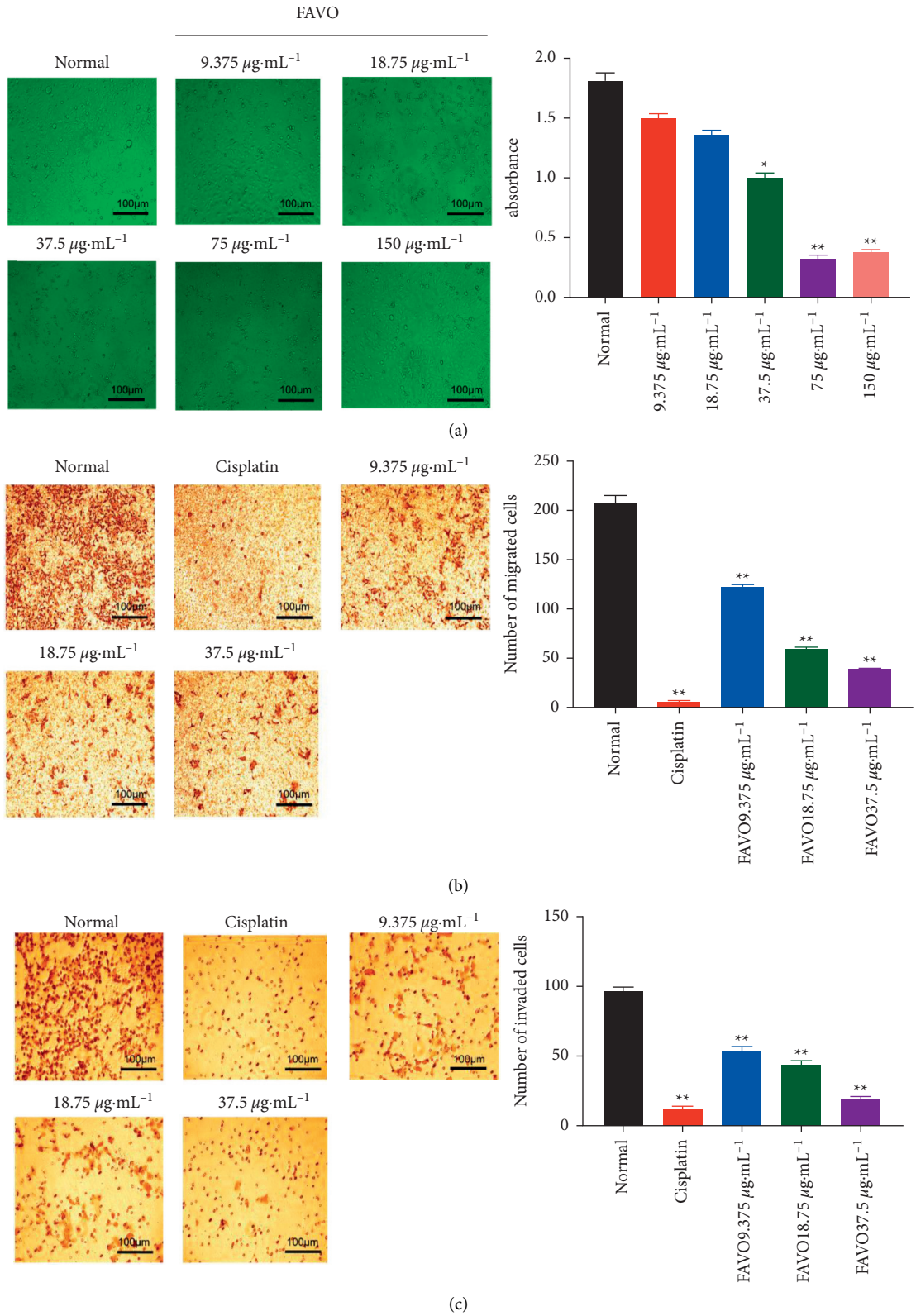

Figure 2: FAVO inhibits the proliferation, migration, and invasion of human gastric cancer SGC-7901 cells. SGC-7901 cells were treated with different concentrations of FAVO for 24 h. (a) The cell growth morphology of SGC-7901 cells were observed. Cell viability was detected by the MTT assay. The migration (b) and invasion (c) ability of the cells was tested by the Transwell assay. $^{**}P < 0.01$, compared with normal control.

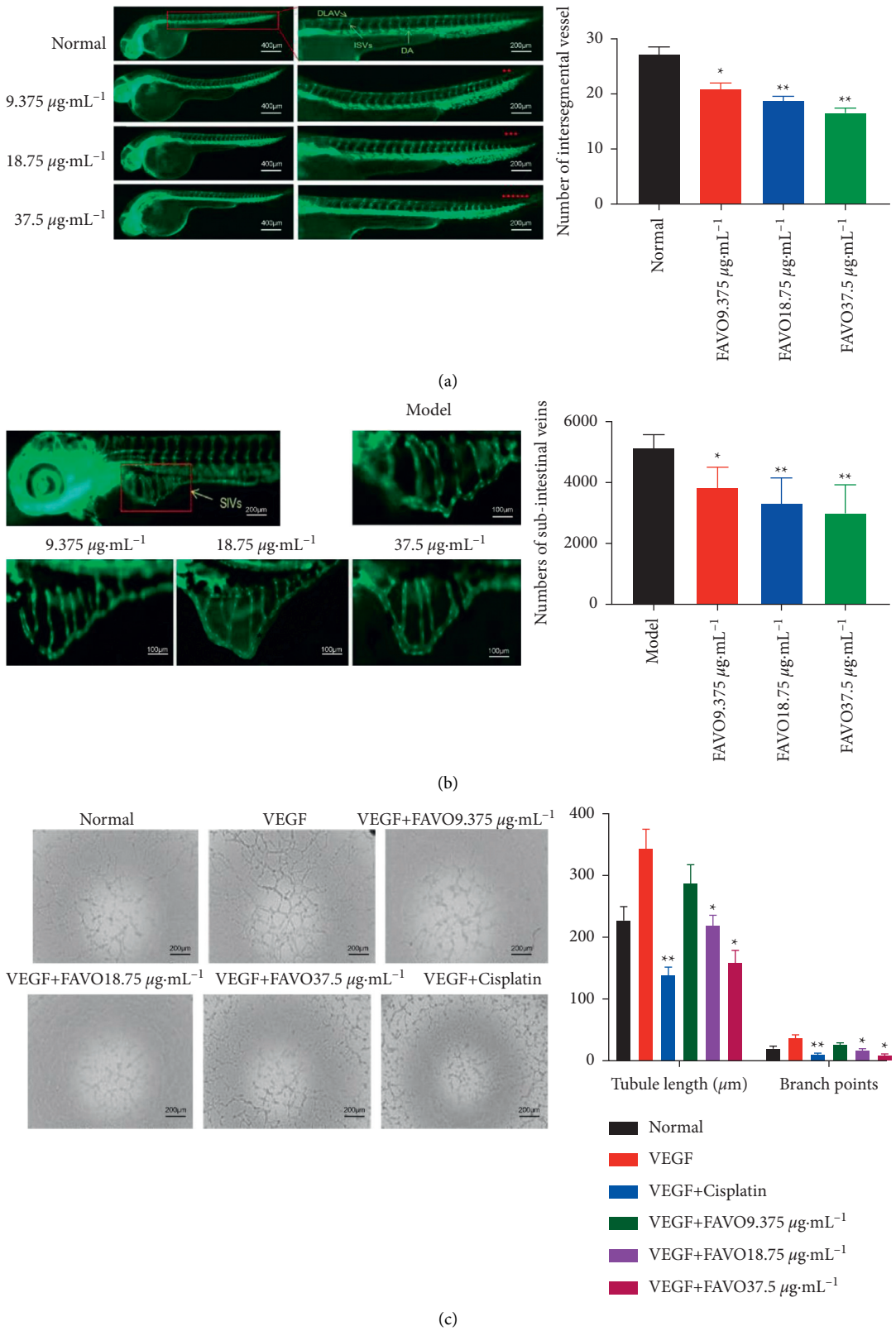

Figure 3: FAVO inhibits angiogenesis in zebrafish and human umbilical vein endothelial cells. (a) The effect of different concentrations of FAVO on the number of intersegmental vessels in zebrafish. (b) Human gastric cancer SGC-7901 cells were injected under the yolk of wild zebrafish embryos, and after treatment with different concentrations of FAVO for 48 h, the OD of the intestinal vein was analyzed by laser confocal microscopy. (c) After treating human umbilical vein endothelial cells with FAVO for 24 h, the cell growth morphology was observed. The length of the tubule per unit area and the number of branch points were measured. $^{*}P < 0.05$, $^{**}P < 0.01$, compared with the normal control.

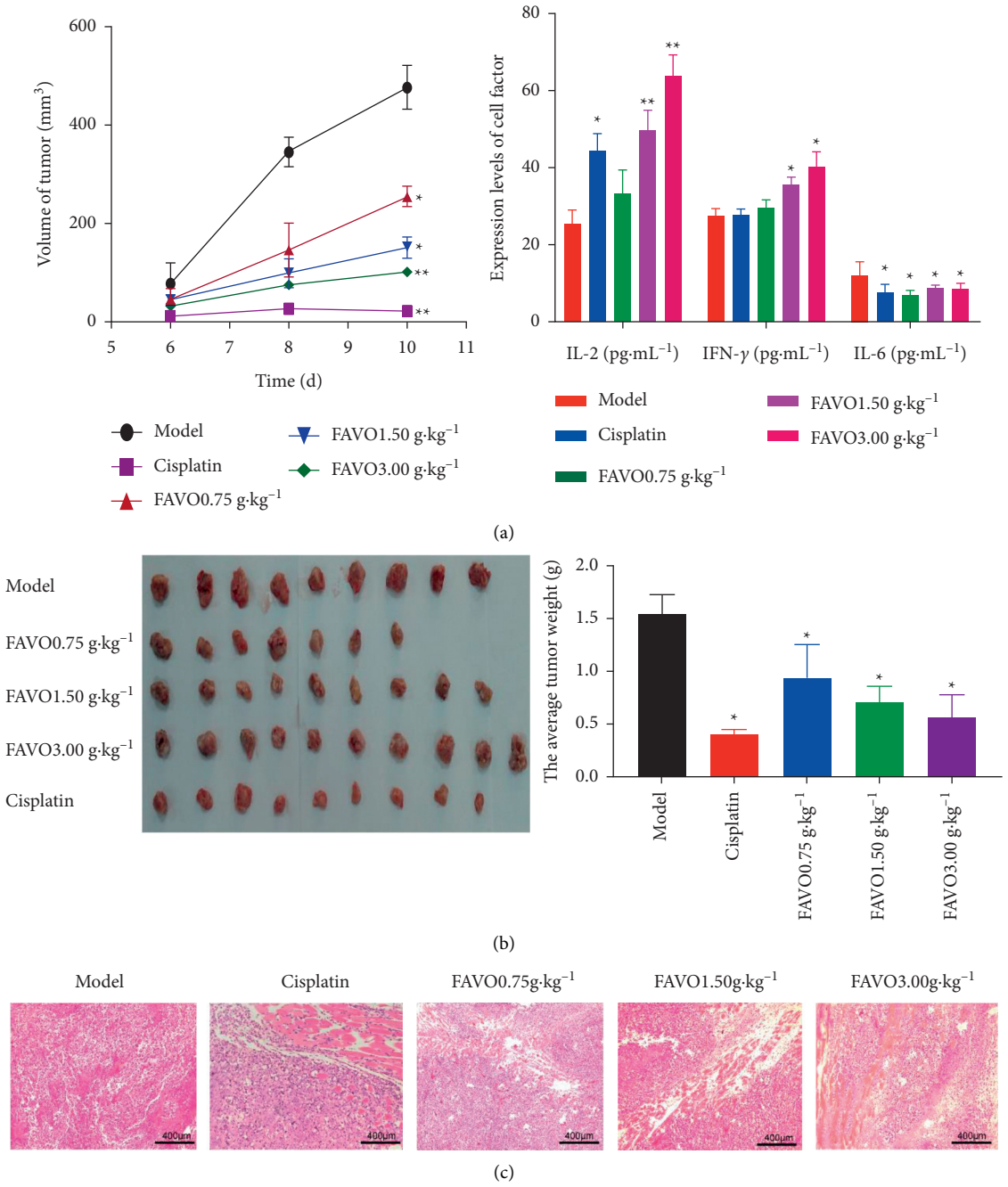

Figure 4: FAVO inhibits the growth of human gastric cancer SGC-7901 tumor in nude mice. After inoculation with human gastric cancer SGC-7901 cells, nude mice were given continuous gastric administration of FAVO (0.75 g kg^{-1}, 1.5 g kg^{-1}, and 3.0 g kg^{-1}) for 2 weeks. (a) Tumor volume (right panel). After treatment for 2 weeks, the levels of IL-2, IFN-γ, and IL-6 in serum were detected by ELISA (left panel). (b) Tumor gross morphology and tumor weight after 2 weeks of intragastric administration. (c) HE staining of tumor. $^{*}P < 0.05$, $^{**}P < 0.01$, compared with the control group.

[4.4.0.0(2,7)] dec-3-ene-3-methanol, 1-methyl-8-(1-methylethyl) (24.56%), and adamantane, 2-hydroperoxy-2-(2-oxiranyl). However, further studies are needed to clarify the main effective components in FAVO.

Metastasis is a manifestation of malignant proliferation and development of tumors. Thus, we further determined the ability of FAVO in inhibiting the proliferation and migration of human gastric cancer SGC-7901 cells. The Transwell results showed that FAVO significantly inhibited the migration and invasion of human gastric cancer SGC-7901 cells. According to the "Guiding Principles of Pharmacodynamics of Anti-tumor Drugs," the antitumor natural drugs should have a tumor-inhibiting rate greater than 40%. The SGC-7901 nude mouse model showed that the tumor inhibition rates of *Ferula akitschkensis* at low, medium, and high doses were 50.43%, 58.86%, and 63.20%, respectively, suggesting that *Ferula akitschkensis* is a potential anticancer drug. In addition, HE staining showed that the tumor cells in

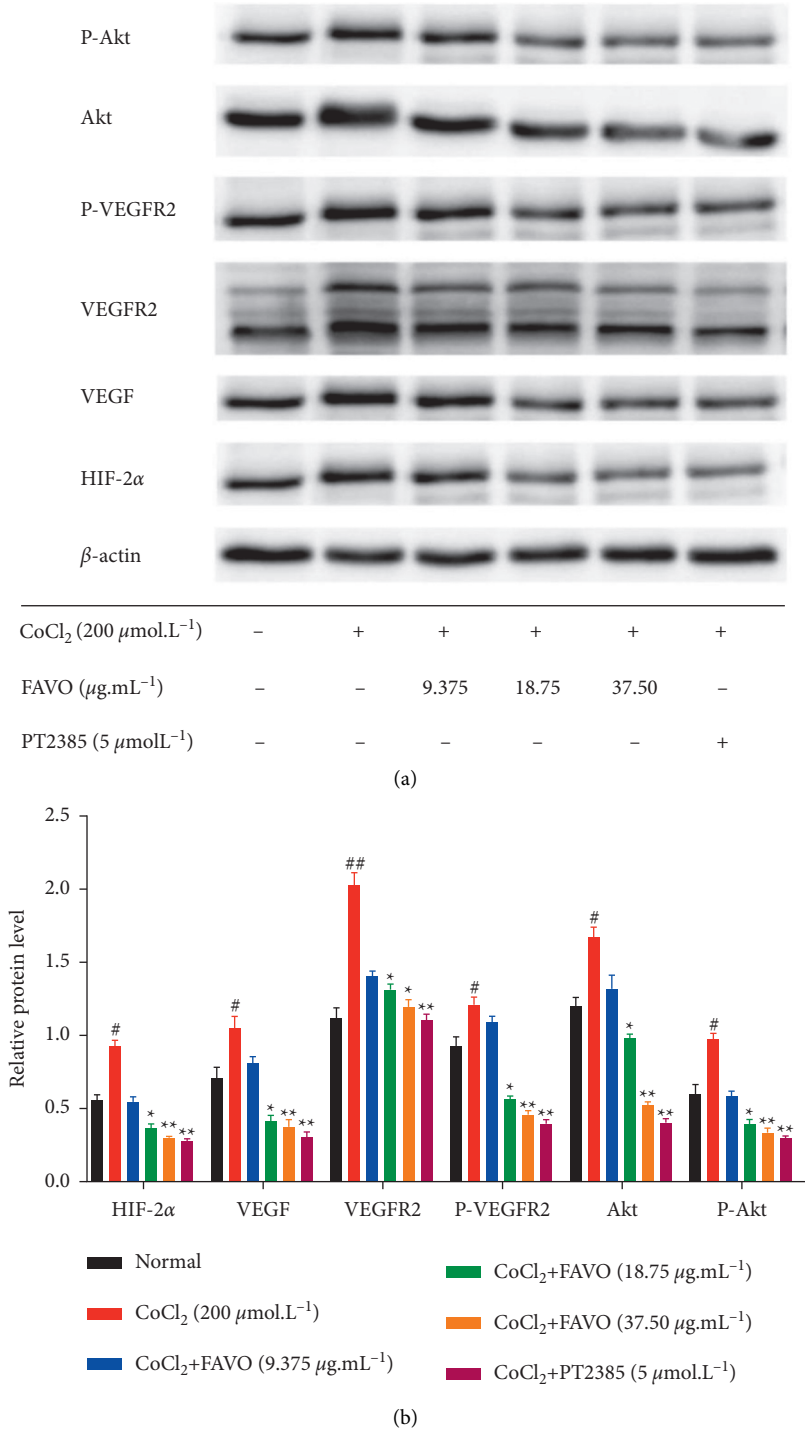

Figure 5: The effect of FAVO on the HIF-2α/VEGF pathway in gastric cancer SGC-7901 cells. The levels of HIF-2α, VEGF, VEGFR2, P-VEGFR2, P-Akt, and Akt in gastric cancer SGC-7901 cells after FAVO treatment detected by Western blot. (a) Representative western blot results. (b) Quantitative western blot results. $^{\#}P < 0.05$ $^{\#}P < 0.05$, $^{\#\#}P < 0.01$, compared with the model control group; $^{*}P < 0.05$, $^{**}P < 0.01$, compared with the $CoCl_2$ group.

the tumor tissues of the *Ferula akitschkensis* high-dose group were loosely arranged and had more lymphocyte and macrophage infiltration. All these indicate the inhibitory effect of *Ferula akitschkensis* on SGC-7901 tumor cells.

Zebrafish is widely used in the screening of angiogenesis inhibitors, and in this study, we used zebrafish labeled with GFP-VEGFR2 [35, 36] for angiogenesis study. Due to the transparent characteristics of zebrafish embryos and specific expression of green fluorescent protein during the formation of blood vessels, the development of blood vessels can be observed more intuitively and finely. We found that FAVO significantly inhibited the formation of zebrafish

intersegmental blood vessels. Moreover, it significantly inhibited tumor-induced intestinal vein angiogenesis in zebrafish transplanted with SGC-7901 cells. These suggest that FAVO may have antitumor effects by inhibiting tumor angiogenesis. The migration and fusion of endothelial cells and the formation of tubular structures are important links in the process of blood vessel formation, which may be blocked to inhibit tumor blood vessel formation [37]. Further results of this study showed that FAVO reduced the tubule length per unit area and the number of branch points, indicating that it inhibits the tubule-forming ability of HUVECs and has the effect of inhibiting tumor angiogenesis.

IL-2 is mainly produced by activated $CD4^+$ T cells and $CD8^+$ T cells, which can promote the survival of T cells and activate the growth of B cells. Studies have shown that IL-2 has a significant antitumor effect [38, 39]. IFN-γ has powerful immunomodulatory effect, which can extensively promote T and B cell differentiation and CTL maturation and stimulate B cells to secrete antibodies [40, 41]. IL-6 can be produced by T cells, macrophages, B cells and other cells. In the process of tumor development, IL-6, as a proinflammatory factor, has antiapoptosis effects, promotes cell proliferation, and blood vessel formation [42, 43]. IL-6 overexpression in cancer tissues promotes the growth and development of tumors by increasing the inflammatory response around the tissues in the tumors [44, 45]. In this study, we found that FAVO significantly promoted the expression of tumor IL-2 and IFN-γ, and inhibited the level of IL-6, which may be the mechanisms underlying the antitumor effects of FAVO. However, further studies are needed.

HIF-2α promotes angiogenesis during tumor growth, increases the stability of VEGF, and promotes the transcription and expression of VEGF-encoding genes [46]. VEGF is one of the most important factors to promote the proliferation and angiogenesis of vascular endothelial cells, and it plays a very important role in the process of angiogenesis [47]. VEGFR2 is a receptor tyrosine kinase that regulates the survival and proliferation of endothelial cells by activating PI3K/AKT signals [48–50]. The activation of AKT can further promote the survival of endothelial cells, induce angiogenesis, and promote tumor growth [51, 52]. In this study, we established a hypoxia model in vitro by $CoCl_2$ treatment. The results showed that $CoCl_2$ induced a significant increase in HIF-2α and its downstream proteins of VEGF, VEGFR2, P-VEGFR2, P-Akt, and Akt. The compound PT2385 binds to the PAS-B domain of HIF-2α subunit and affects the polymerization of HIF-2α subunit and β-subunit ARNT, thereby inhibiting the action of HIF-2α [53]. However, it has no effect on HIF-1. PT2385 reduced circulating VEGF-A levels and exhibited antitumor effects in a xenograft model [54]. PT2385 showed good efficacy in a phase I clinical trial (NCT02293980) in the treatment of advanced clear cell carcinoma of the kidney [55, 56]. Herein, after intervention with HIF-2α inhibitor PT2385, the levels of HIF-2α and downstream proteins were significantly reduced. Interestingly, similar results were obtained with FAVO. Therefore, we speculate that FAVO may abrogate the HIF-2α-VEGF-Akt signaling pathway, thereby inhibiting the proliferation and angiogenesis of human gastric cancer SGC-7901 cells.

5. Conclusions

In summary, FAVO weakened the proliferation, migration, and invasion of human gastric cancer SGC-7901 cells, inhibited vessel formation of zebrafish, impaired the tubule formation ability of HUVECs, suppressed tumor growth in vivo, increased the serum levels of IL-2 and IFN-γ in tumor-bearing nude mice, and inhibited HIF-2α-VEGF signaling. Thus, our results indicate that *Ferula akitschkensis* may become a potential antitumor drug, providing a new option for combination therapy or supportive treatment of gastric cancer.

Data Availability

The data used to support the findings of this study are included within the article.

Conflicts of Interest

The authors declare that there are no conflicts of interest regarding the publication of this paper.

Acknowledgments

This work was supported by the National Natural Science Foundation of China (82060734) and State Key Laboratory of Pathogenesis, Prevention and Treatment of High Incidence Diseases in Central Asia Fund (SKL-HIDCA-2020-ZY8).

References

[1] N. P. Commission, *The Pharmacopoeia of the People's Republic of China: One, Ferula akitschkensis*, China Medical Science and Technology Press, Beijing, China, 2015.

[2] V. R. Askari, V. Baradaran Rahimi, A. Assaran, M. Iranshahi, and M. H. Boskabady, "Evaluation of the anti-oxidant and anti-inflammatory effects of the methanolic extract of Ferula szowitsiana root on PHA-induced inflammation in human lymphocytes," *Drug and Chemical Toxicology*, vol. 43, no. 4, pp. 353–360, 2020.

[3] N. Hosseinzadeh, T. Shomali, S. Hosseinzadeh, F. Raouf Fard, J. Jalaei, and M. Fazeli, "Cytotoxic activity of Ferula persica gum essential oil on murine colon carcinoma (CT26) and Vero cell lines," *Journal of Essential Oil Research*, vol. 32, no. 2, pp. 169–177, 2020.

[4] H. Bamehr, M. Saidijam, D. Dastan, R. Amini, M. Pourjafar, and R. Najafi, "Ferula pseudalliacea induces apoptosis in human colorectal cancer HCT-116 cells via mitochondria-dependent pathway," *Archives of Physiology and Biochemistry*, vol. 125, no. 3, pp. 284–291, 2019.

[5] S. Mirzaaghaei, H. Akrami, M. H. Asadi, and H. Mahdiuni, "Ferula gummosa Boiss flower and leaf extracts inhibit angiogenesis in vitro," *Indian Journal of Cancer*, vol. 51, no. 4, pp. 615–620, 2014.

[6] M. Jalili-Nik, H. Sabri, E. Zamiri et al., "Cytotoxic effects of Ferula latisecta on human glioma U87 cells," *Drug Research*, vol. 69, no. 12, pp. 665–670, 2019.

[7] N. Abutaha, F. A. Nasr, M. Al-Zharani et al., "Effects of hexane root extract of Ferula hermonis boiss. On human breast and colon cancer cells: an in vitro and in vivo study," *BioMed Research International*, vol. 2019, Article ID 3079895, 12 pages, 2019.

[8] Y. Asemani, A. Azadmehr, R. Hajiaghaee, and Z. Amirghofran, "Anticancer potential of Ferula hezarla-lehzarica Y. Ajani fraction in Raji lymphoma cell line: induction of apoptosis, cell cycle arrest, and changes in mitochondrial membrane potential," *Daru Journal of Pharmaceutical Sciences*, vol. 26, no. 2, pp. 143–154, 2018.

[9] P. Guo, W. Li, and H. Zhang, "Anti-tumor effects of ethyl acetate extract in Ferula sinkiangensis on CT-26.WT orthotopic transplantation tumor model mice and its mechanism study," *China Pharmacy*, vol. 29, no. 23, pp. 3221–3226, 2018.

[10] L. Yan, W. Li, S. Zhao, and H. Zhang, "Study on GC-MS fingerprint of volatile oil from Ferula Soongarica and its anti-gastric cancer effect," *Journal of Xinjiang Medical University*, vol. 43, no. 7, pp. 957–961, 2020.

[11] H. Zhang, J. Lu, L. Zhou, L. Jiang, and M. Zhou, "Antioxidant and antitumor effects of ferula sinkiangensis K. M. Shen," *International Journal of Clinical and Experimental Medicine*, vol. 8, no. 11, pp. 20845–20852, 2015.

[12] S. S. Nazrullaev, A. I. Saidkhodzhaev, K. S. Akhmedkhodzhaeva, V. N. Syrov, B. F. Rasulev, and Z. A. Khushbaktova, "Estrogen activity of terpenoids from plants of the genus Ferula," *Chemistry of Natural Compounds*, vol. 44, no. 5, pp. 572–577, 2008.

[13] I. A. Schepetkin, S. V. Kushnarenko, G. Özek et al., "Modulation of human neutrophil responses by the essential oils from *Ferula akitschkensis* and their constituents," *Journal of Agricultural and Food Chemistry*, vol. 64, no. 38, pp. 7156–7170, 2016.

[14] G. A. Utegenova, K. B. Pallister, S. V. Kushnarenko et al., "Chemical composition and antibacterial activity of essential oils from *Ferula L.* Species against methicillin-resistant *Staphylococcus aureus*," *Molecules*, vol. 23, no. 7, 2018.

[15] P. Sheng, S. Wang, and L. Miao, "Comparison of chemical constituents and in vitro anti-gastric cancer activity of volatile oil extracted by different methods," *Chinese Patent Medicine*, vol. 35, no. 11, pp. 2442–2448, 2013.

[16] N. Hosseinzadeh, T. Shomali, and S. Hosseinzadeh, "Cytotoxic activity of Ferula persica gum essential oil on murine colon carcinoma (CT26) and Vero cell lines," *Journal of Essential Oil Research*, vol. 32, no. 2, pp. 1–9, 2020.

[17] A. Daneshkazemi, H. Zandi, A. Davari et al., "Antimicrobial activity of the essential oil obtained from the seed and oleo-gum-resin of Ferula assa-foetida against oral pathogens," *Frontiers in dentistry*, vol. 16, no. 2, pp. 113–120, 2019.

[18] F. S. Youssef, M. A. Mamatkhanova, N. Z. Mamadalieva et al., "Chemical profiling and discrimination of essential oils from six *Ferula* species using GC analyses coupled with chemometrics and evaluation of their antioxidant and enzyme inhibitory potential," *Antibiotics*, vol. 9, no. 8, 2020.

[19] X. Y. Lian, H. Zhang, Q. Liu et al., "Ovarian cancer-excreted exosomal miR-199a-5p suppresses tumor metastasis by targeting hypoxia-inducible factor-2α in hypoxia microenvironment," *Cancer Communications*, vol. 40, no. 8, pp. 380–385, 2020.

[20] X. J. Huang, Y. Yang, Z. M. Deng et al., "Clostridium novyi exhibits antitumor effect in mice transplanted with H22 hepatocarcinoma by down-regulation of hypoxia-inducible factor-1alpha," *Journal of Biological Regulators & Homeostatic Agents*, vol. 34, no. 6, pp. 2159–2164, 2020.

[21] E. J. Jarman, C. Ward, A. K. Turnbull et al., "HER2 regulates HIF-2α and drives an increased hypoxic response in breast cancer," *Breast Cancer Research*, vol. 21, no. 1, p. 10, 2019.

[22] E. Moreno Roig, A. J. Groot, and A. Yaromina, "HIF-1α and HIF-2α differently regulate the radiation sensitivity of NSCLC cells," *Cells*, vol. 8, no. 1, 2019.

[23] S. J. Cowman, D. G. Fuja, X.-D. Liu et al., "Macrophage HIF-1α is an independent prognostic indicator in kidney cancer," *Clinical Cancer Research*, vol. 26, no. 18, pp. 4970–4982, 2020.

[24] R.-T. Wang, R.-C. Miao, X. Zhang et al., "Fork head box M1 regulates vascular endothelial growth factor-A expression to promote the angiogenesis and tumor cell growth of gallbladder cancer," *World Journal of Gastroenterology*, vol. 27, no. 8, pp. 692–707, 2021.

[25] Y. Ma, W. Wang, L. Liu, Y. Liu, and W. Bi, "Co-expression of VEGF-B and FLT-1 correlates with malignancy and prognosis of gastric cancer," *Biomarkers in Medicine*, vol. 15, no. 7, pp. 481–488, 2021.

[26] C. Huang, J. Huang, and G. Yu, "Co-suppression of VEGF-A and VEGF-C inhibits development of experimental hemangioma," *American Journal of Tourism Research*, vol. 10, no. 9, pp. 2911–2919, 2018.

[27] A. Goulart, C. Ferreira, A. Rodrigues, B. Coimbra, N. Sousa, and P. Leão, "The correlation between serum vascular endothelial growth factor (VEGF) and tumor VEGF receptor 3 in colorectal cancer," *Annals of Surgical Treatment and Research*, vol. 97, no. 1, pp. 15–20, 2019.

[28] S. Marcella, A. Petraroli, M. Braile et al., "Vascular endothelial growth factors and angiopoietins as new players in mastocytosis," *Clinical and Experimental Medicine*, vol. 21, no. 3, pp. 415–427, 2021.

[29] C. Ríos-Navarro, L. Hueso, A. Díaz et al., "Role of anti-angiogenic VEGF-A(165)b in angiogenesis and systolic function after reperfused myocardial infarction," *Revista Espanola de Cardiologia*, vol. 74, no. 2, pp. 131–139, 2021.

[30] E. Reina-Torres, J. C. Wen, K. C. Liu et al., "VEGF as a paracrine regulator of conventional outflow facility," *Investigative Opthalmology & Visual Science*, vol. 58, no. 3, pp. 1899–1908, 2017.

[31] R. Tamma, T. Annese, S. Ruggieri, A. Marzullo, B. Nico, and D. Ribatti, "VEGFA and VEGFR2 RNAscope determination in gastric cancer," *Journal of Molecular Histology*, vol. 49, no. 4, pp. 429–435, 2018.

[32] J. Yang, J. Yan, J. Shao et al., "Immune-Mediated antitumor effect by VEGFR2 selective inhibitor for gastric cancer," *OncoTargets and Therapy*, vol. 12, pp. 9757–9765, 2019.

[33] L. Wang, R. Sun, and M. Xu, "Research progress in the chemical constituents, pharmacological effects and toxicology of *Ferula akitschkensis*," *World Traditional Chinese Medicine*, vol. 15, no. 24, 2020.

[34] M. Yang, J. Luo, M. Qiao, M. Yang, and P. Sheng, "GC-MS analysis of volatile oil from Ferula Ferulaeoides and anti-gastric cancer activity of D-limonene in vitro," *Chinese Journal of Modern Applied Pharmacy*, vol. 37, no. 07, pp. 806–813, 2020.

[35] M. Fazio, J. Ablain, Y. Chuan, D. M. Langenau, and L. I. Zon, "Zebrafish patient avatars in cancer biology and precision cancer therapy," *Nature Reviews Cancer*, vol. 20, no. 5, pp. 263–273, 2020.

[36] K. R. Astell and D. Sieger, "Zebrafish in vivo models of cancer and metastasis," *Cold Spring Harbor perspectives in medicine*, vol. 10, no. 8, 2020.

[37] M. Xie, T. Yu, X. Jing et al., "Exosomal circSHKBP1 promotes gastric cancer progression via regulating the miR-582-3p/HUR/VEGF axis and suppressing HSP90 degradation," *Molecular Cancer*, vol. 19, no. 1, p. 112, 2020.

[38] J. E. Lopes, J. L. Fisher, H. L. Flick et al., "Alks 4230: a novel engineered IL-2 fusion protein with an improved cellular selectivity profile for cancer immunotherapy," *Journal for immunotherapy of cancer*, vol. 8, no. 1, 2020.

[39] L. Shi, J. Sheng, G. Chen et al., "Combining IL-2-based immunotherapy with commensal probiotics produces enhanced antitumor immune response and tumor clearance," *Journal for immunotherapy of cancer*, vol. 8, no. 2, 2020.

[40] D. Jorgovanovic, M. Song, L. Wang, and Y. Zhang, "Roles of IFN-γ in tumor progression and regression: a review," *Biomarker Research*, vol. 8, no. 1, p. 49, 2020.

[41] N. M. Clark, L. M. Martinez, S. Murdock et al., "Regulatory T cells support breast cancer progression by opposing IFN-γ-Dependent functional reprogramming of myeloid cells," *Cell Reports*, vol. 33, no. 10, Article ID 108482, 2020.

[42] M. Turano, F. Cammarota, F. Duraturo, P. Izzo, and M. De Rosa, "A potential role of IL-6/IL-6R in the development and management of colon cancer," *Membranes*, vol. 11, no. 5, 2021.

[43] L. López-Ferreras, F. Longo, J. E. Richard et al., "Key role for hypothalamic interleukin-6 in food-motivated behavior and body weight regulation," *Psychoneuroendocrinology*, vol. 131, Article ID 105284, 2021.

[44] Y. Hao, Z. Yan, A. Zhang et al., "IL-6/STAT3 mediates the HPV18 E6/E7 stimulated upregulation of MALAT1 gene in cervical cancer HeLa cells," *Virus Research*, vol. 281, Article ID 197907, 2020.

[45] X. Zhang, J. Chen, H. Jin, W. Zhao, Z. Chang, and H. Wu, "Effect of erlotinib combined with cisplatin on IL-6 and IL-12 in mice with Lewis lung cancer," *Oncology Letters*, vol. 20, no. 1, pp. 902–906, 2020.

[46] L. Lian, X.-L. Li, M.-D. Xu et al., "VEGFR2 promotes tumorigenesis and metastasis in a pro-angiogenic-independent way in gastric cancer," *BMC Cancer*, vol. 19, no. 1, p. 183, 2019.

[47] Y. Jin, X. Che, X. Qu et al., "CircHIPK3 promotes metastasis of gastric cancer via miR-653-5p/miR-338-3p-NRP1 Axis under a long-term hypoxic microenvironment," *Frontiers in Oncology*, vol. 10, p. 1612, 2020.

[48] M. Shen, X. Z. Zhou, L. Ye et al., "Xanthatin inhibits corneal neovascularization by inhibiting the VEGFR2-mediated STAT3/PI3K/Akt signaling pathway," *International Journal of Molecular Medicine*, vol. 42, no. 2, pp. 769–778, 2018.

[49] C. Liu, L. He, J. Wang et al., "Anti-angiogenic effect of Shikonin in rheumatoid arthritis by downregulating PI3K/AKT and MAPKs signaling pathways," *Journal of Ethnopharmacology*, vol. 260, Article ID 113039, 2020.

[50] X. Sun, L. Meng, W. Qiao et al., "Vascular endothelial growth factor A/Vascular endothelial growth factor receptor 2 axis promotes human dental pulp stem cell migration via the FAK/PI3K/Akt and p38 MAPK signalling pathways," *International Endodontic Journal*, vol. 52, no. 12, pp. 1691–1703, 2019.

[51] J. Zhai, J. Shen, G. Xie et al., "Cancer-associated fibroblasts-derived IL-8 mediates resistance to cisplatin in human gastric cancer," *Cancer Letters*, vol. 454, pp. 37–43, 2019.

[52] X. Jia, Z. Wen, Q. Sun et al., "Apatinib suppresses the proliferation and apoptosis of gastric cancer cells via the PI3K/Akt signaling pathway," *Journal of B.U.ON.: Official Journal of the Balkan Union of Oncology*, vol. 24, no. 5, pp. 1985–1991, 2019.

[53] W. Chen, H. Hill, A. Christie et al., "Targeting renal cell carcinoma with a HIF-2 antagonist," *Nature*, vol. 539, no. 7627, pp. 112–117, 2016.

[54] O. Cuvillier, "The therapeutic potential of HIF-2 antagonism in renal cell carcinoma," *Translational Andrology and Urology*, vol. 6, no. 1, pp. 131–133, 2017.

[55] D. Wu, N. Potluri, J. Lu, Y. Kim, and F. Rastinejad, "Structural integration in hypoxia-inducible factors," *Nature*, vol. 524, no. 7565, pp. 303–308, 2015.

[56] H. Cho, X. Du, J. P. Rizzi et al., "On-target efficacy of a HIF-2α antagonist in preclinical kidney cancer models," *Nature*, vol. 539, no. 7627, pp. 107–111, 2016.

Hindawi
Evidence-Based Complementary and Alternative Medicine
Volume 2022, Article ID 1340194, 10 pages
https://doi.org/10.1155/2022/1340194

Research Article

Network Pharmacology Integrated with Transcriptomics Deciphered the Potential Mechanism of *Codonopsis pilosula* against Hepatocellular Carcinoma

Zhili Liu,[1,2] **Yuzhe Sun**,[2,3] **Hefu Zhen**,[2,3] **and Chao Nie**[2,3]

[1]*College of Life Sciences, University of Chinese Academy of Sciences, Beijing 100049, China*
[2]*BGI-Shenzhen, Shenzhen 518083, China*
[3]*China National GeneBank, BGI-Shenzhen, Shenzhen 518120, China*

Correspondence should be addressed to Hefu Zhen; zhenhf@genomics.cn and Chao Nie; niechao@genomics.cn

Received 11 October 2021; Revised 1 March 2022; Accepted 12 March 2022; Published 27 March 2022

Academic Editor: Li-Ping Kang

Hepatocellular carcinoma (HCC) is the fourth main reason of cancer-related death. *Codonopsis pilosula* is a commonly used traditional Chinese medicine (TCM) for patients with HCC. However, its potential mechanism for treatment of HCC remains unclear. Here, we used transcriptomics and network pharmacology to explore the potential molecular mechanisms of *Codonopsis pilosula*. In our study, twelve differentially expressed genes (DEGs) (5 upregulated and 7 downregulated) of *Codonopsis pilosula* treating HepG2 cells (a kind of HCC cell) were identified. Among the 12 DEGs, HMOX1 may play an essential role. *Codonopsis pilosula* mainly affects the mineral absorption pathway in HCC. We acquired 2957, 1877, and 255 targets from TCMID, SymMap, and TCMSP, respectively. *Codonopsis pilosula* could upregulate HMOX1 via luteolin, capsaicin, and sulforaphane. Our study provided new understanding of the potential pharmacological mechanisms of *Codonopsis pilosula* in treating HCC and pointed out a direction for further experimental research.

1. Introduction

There are multiple types of primary liver cancer, of which hepatocellular carcinoma (HCC), the fourth leading cause of cancer-related death overall worldwide, is the most predominant type [1, 2]. During the last few decades, HCC incidence has been increasing at a global level [3, 4], and it is estimated that more than 1 million people will die from HCC in 2030 [5, 6]. In addition to surgical treatments, drugs are the key to HCC therapy [7]. Sorafenib has been the global treatment standard for patients with HCC since 2007 [8], but its efficacy is unsatisfactory [9]. As a widely used alternative therapy, traditional Chinese medicine (TCM) can probably prolong the median survival time and improve the overall survival among patients with HCC [10]. Moreover, some TCMs have been reported to have the ability to assist in elevating the efficacy of sorafenib in the treatment of HCC [11–13].

Codonopsis pilosula, a kind of TCM, has anticancer activity and is widely used in adjuvant anticancer therapy [14]. A lot of evidence has shown that many ingredients of *Codonopsis pilosula*, such as Codonopsis pilosula polysaccharide (CPP) and atractylenolide III (ATL), have anti-HCC effects via different pathways. CPP is one of major active constituents in *Codonopsis pilosula*, and it could inhibit the proliferation and motility of HCC cells through the β-catenin/TCF4 pathway [15]. CPP1a and CPP1c are two water-soluble homogeneous polysaccharides isolated and purified from *Codonopsis pilosula*, and they could induce HepG2 cell apoptosis by upregulating the ratio of Bax/Bcl-2 and activating caspase-3 [16]. ATL, a sesquiterpenoid extracted from *Codonopsis pilosula*, exerts tumor-suppressive functions in liver cancer via the miR-195-5p/FGFR1 signaling axis [17]. However, *Codonopsis pilosula*, as a kind of Chinese herb, is often used as a whole in clinical practice. There are few reports on the mechanisms of *Codonopsis pilosula* in the

treatment of HCC, and its application is greatly limited. The effects of TCM (or herbs of other nations) are not the sum of all active ingredients. In the mixed system of *Codonopsis pilosula*, new effects may emerge that the single active ingredients do not.

In this study, we integrated transcriptomics and network pharmacology to understand the mechanisms of *Codonopsis pilosula* in treating HCC. The differentially expressed genes (DEGs) of *Codonopsis pilosula* were derived from a previous study (GSE115506) [18]. The effective ingredients of *Codonopsis pilosula* and targets were assayed by TCMID, SymMap, and TCMSP [19–21]. The mechanisms of *Codonopsis pilosula* against HCC were assessed by Gene Ontology (GO) and Kyoto Encyclopedia of Genes and Genomes (KEGG) pathway analysis. Furthermore, we found that *Codonopsis pilosula* may regulate mineral absorption through luteolin, capsaicin, and sulforaphane directly targeting HMOX1.

2. Materials and Methods

2.1. Differentially Expressed Genes Screening. We obtained DEGs of *Codonopsis pilosula* from the GEO database (https://www.ncbi.nlm.nih.gov/geo/) (series: GSE115506; samples: GSM3179695, GSM3179696, GSM3179697, GSM3179698, GSM3179699, and GSM3179700). In GSE115506, total RNA was isolated from HepG2 cells 24 hours after 3 mg/mL *Codonopsis pilosula* aqueous extract treatment in vitro. We performed differential analysis by the Limma R packages [22], and the cutoff value for identifying DEG was set to |log2 fold change| >1 and adjusted *p*value <0.05.

2.2. Components and Targets Acquisition. The components and targets of *Codonopsis pilosula* were acquired from TCMID (http://www.megabionet.org/tcmid/) [20], SymMap (http://www.symmap.org/) [21], and TCMSP (https://tcmsp-e.com/) databases [19]. They are all integrative databases of traditional Chinese medicine.

2.3. Network Building. We performed the protein-protein interaction (PPI) network analysis using STRING (https://string-db.org/) [23]. The *Codonopsis pilosula*-gene network, protein-protein interaction (PPI) network, and *Codonopsis pilosula*-component-target network were visualized by Cytoscape software [24].

2.4. Functional Enrichment Analysis. We conducted Kyoto Encyclopedia of Genes and Genomes (KEGG) pathway analysis and biological process (BP) of Gene Ontology (GO) analysis by R package clusterProfiler [25].

2.5. Expression Analysis of HMOX1. The expression of HMOX1 in HCC was obtained through UALCAN, which is a comprehensive and interactive web resource for analyzing cancer OMICS data [26].The expression of HMOX1 after apigenin, luteolin, capsaicin, 4-methylsulfinyl butyl isothiocyanate (sulforaphane), and geniposide treatment was obtained from the GEO database (apigenin series: GSE119552, samples: GSM3377483, GSM3377484, GSM3377485, GSM3377486, GSM3377495, GSM3377496, GSM3377497, and GSM3377498; luteolin series: GSE18740, samples: GSM465440, GSM465441, GSM465442, GSM465443, GSM465444, and GSM465445; capsaicin series: GSE59727, samples: GSM1442972, GSM1442973, GSM1442974, GSM1442975, GSM1442976, GSM1442977, GSM1442978, and GSM1442979; sulforaphane series: GSE28813, samples: GSM713517, GSM713518, GSM713519, GSM713520, GSM713521, GSM713522, GSM713523, and GSM713524; and geniposide series: GSE85871, samples: GSM2286350, GSM2286351, GSM2286248, GSM2286249, GSM2286316, GSM2286317, GSM2286398, and GSM2286399). In GSE18740, mouse BV-2 microglia were treated with 50 μM luteolin for 24 hours; in GSE59727, rat TRPV1-positive neurons were treated with 10 μM capsaicin for 30 minutes; in GSE119552, MCF-7 cells were treated with 10 μM apigenin for 24 hours; in GSE28813, MCF10A cells were treated with 15 μM sulforaphane for 24 hours; and in GSE85871, MCF-7 cells were treated with 10 μM geniposide for 12 hours. We extracted the expression level of the HMOX1 gene from these expression matrices and compared its significance with the *t*-test.

2.6. Molecular Docking. The structure of HMOX1 protein was obtained from PDB (https://www.rcsb.org/) [27], and the structures of luteolin, capsaicin, and sulforaphane were acquired from ZINC (https://zinc.docking.org/) [28]. We used AutoDock 4.2 to prepare the PDBQT file and perform molecular docking [29]. Finally, molecular docking maps were visualized through PyMOL.

3. Results

3.1. Codonopsis pilosula-Gene Network and PPI Analysis. We identified 12 DEGs (5 upregulated and 7 downregulated) from the GSE115506 data set (Table S1). A volcano plot (Figure 1(a)) and a heatmap (Figure 1(b)) were established to show the distribution of DEGs in HepG2 cells after treating *Codonopsis pilosula*. The cutoff value for identifying DEG was set to |log2 fold change| >1 and the adjusted *p*value <0.05. Accordingly, we built a *Codonopsis pilosula*-gene network (Figure 1(c)). In order to further explore the potential association among these DEGs, we performed a PPI network analysis for the 12 DEGs by STRING [23]. The final PPI network includes 11 nodes and 13 edges (Figure 1(d)). Furthermore, we identified HMOX1, an upregulated gene, as the hub gene because it has the highest degree.

3.2. GO and KEGG Analysis. Through the clusterProfiler R package for KEGG enrichment analysis, we found that only 1 pathway was significantly affected (*p*adjust <0.05) during *Codonopsis pilosula* treatment of HepG2 cells (Figure 2(a)). HMOX1 (hub gene), MT1F, and MT1G were enriched in mineral absorption. In total, 61 biological processes (GO terms) were notably enriched (*p*adjust <0.05) (Table S2). The top 5 biological processes are shown in Figure 2(b). The highly enriched biological processes include responses to

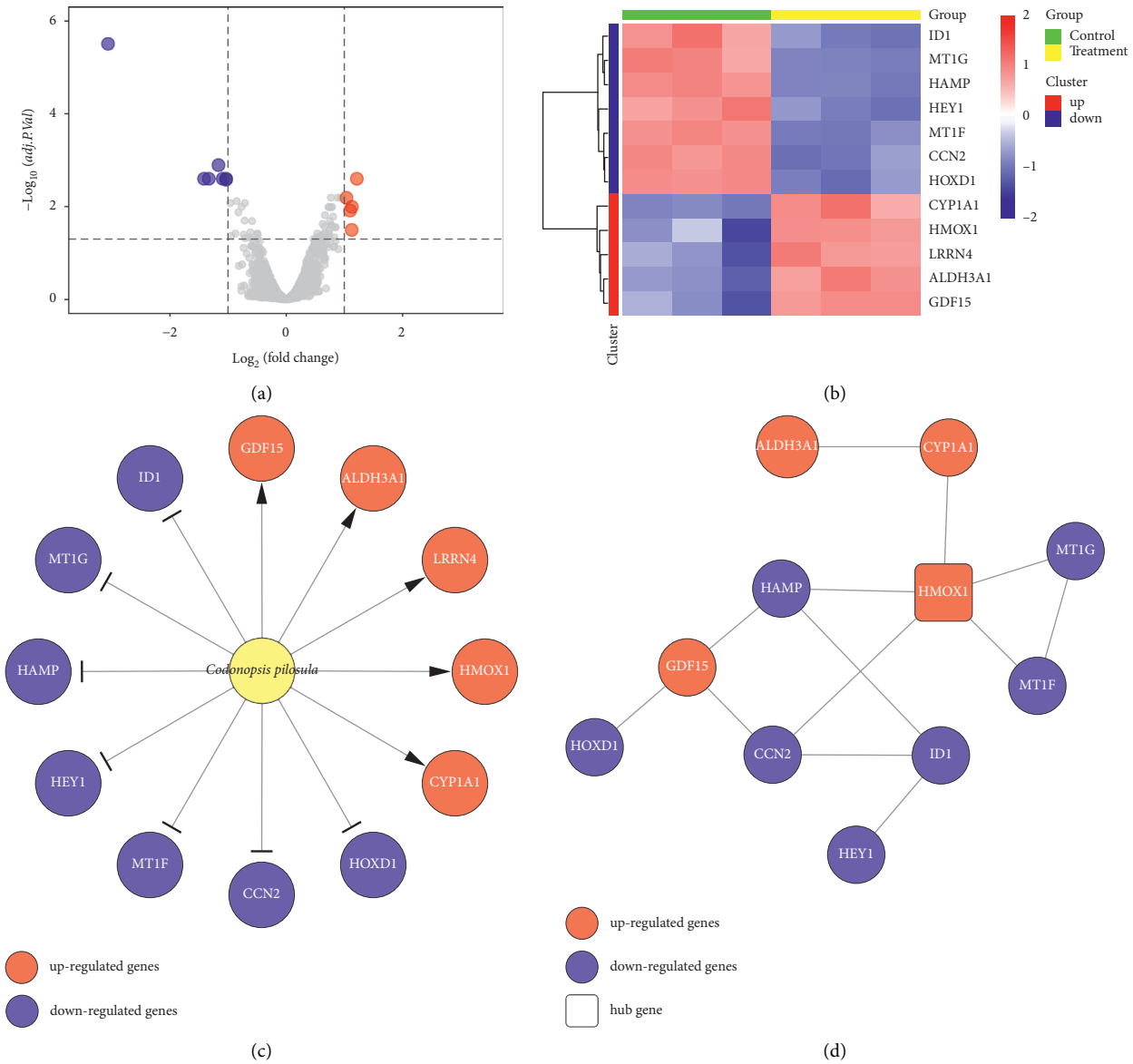

FIGURE 1: *Codonopsis pilosula*-gene network and PPI analysis. (a) Volcano plot and (b) heatmap of DEGs showed that genes with dramatic changes after *Codonopsis pilosula* treatment. (c) *Codonopsis pilosula*-gene network. (d) The PPI analysis of DEGs.

iron ions, cellular responses to copper ions, cellular transition metal ion homeostasis, transition metal ion homeostasis, and response to metal ions. These biological processes and pathways are closely related to the metabolism and homeostasis of metal ions, suggesting that *Codonopsis pilosula* mainly affects the mineral absorption pathway in HCC cells.

3.3. Codonopsis pilosula Reverses HMOX1 Expression in HCC. We acquired 2957 targets from TCMID, 1877 targets from SymMap, and 255 targets from TCMSP (Table S3). According to the intersection of these targets and 12 DEGs, we found that HMOX1 is the direct target of *Codonopsis pilosula* in three databases (Figure 3(a)). Our results showed that the expression of HMOX1 was significantly enhanced (Figure 1). Interestingly, HMOX1 was significantly decreased in HCC patients (Figure 3(b)). The abovementioned results suggest that *Codonopsis pilosula* may resist HCC by reversing HMOX1 expression in HCC patients.

3.4. Codonopsis pilosula Could Upregulate HMOX1 via Luteolin, Capsaicin, and Sulforaphane. To explore how *Codonopsis pilosula* promotes the expression of HMOX1, we established a *Codonopsis pilosula*-component-target network (Figure 4(a)). The result showed that *Codonopsis pilosula* may directly target HMOX1 through apigenin, luteolin, capsaicin, 4-methylsulfinyl butyl isothiocyanate (sulforaphane), and geniposide. In addition, we detected the expression of HMOX1 after treating with these components (Figures 4(b)–4(f)). Figure 4(b) showed that luteolin could upregulate Hmox1 in BV-2 cells, although the p value is 0.081. Figure 4(c) showed that capsaicin could significantly promote the expression of

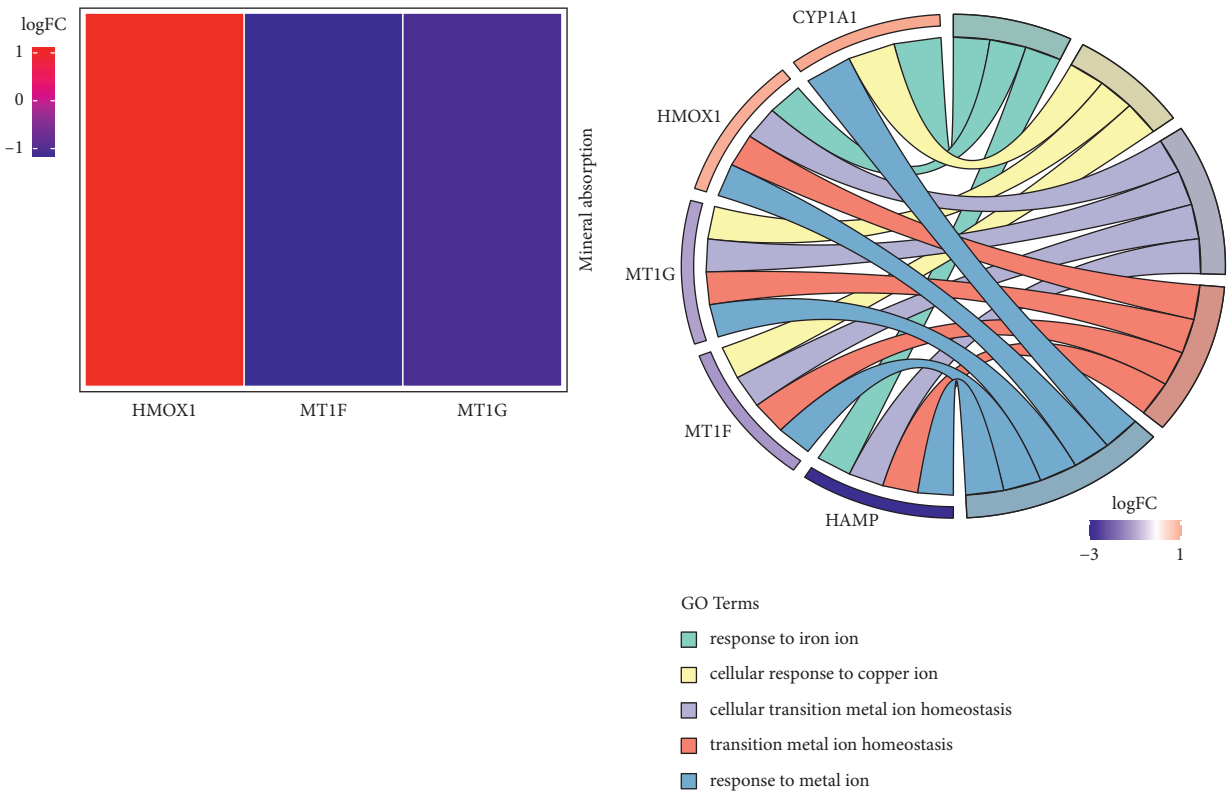

Figure 2: KEGG and GO analysis. (a) KEGG pathway enrichment of *Codonopsis pilosula* treating HepG2 cells. (b) The top 5 biological process in GO terms of *Codonopsis pilosula* treating HepG2 cells.

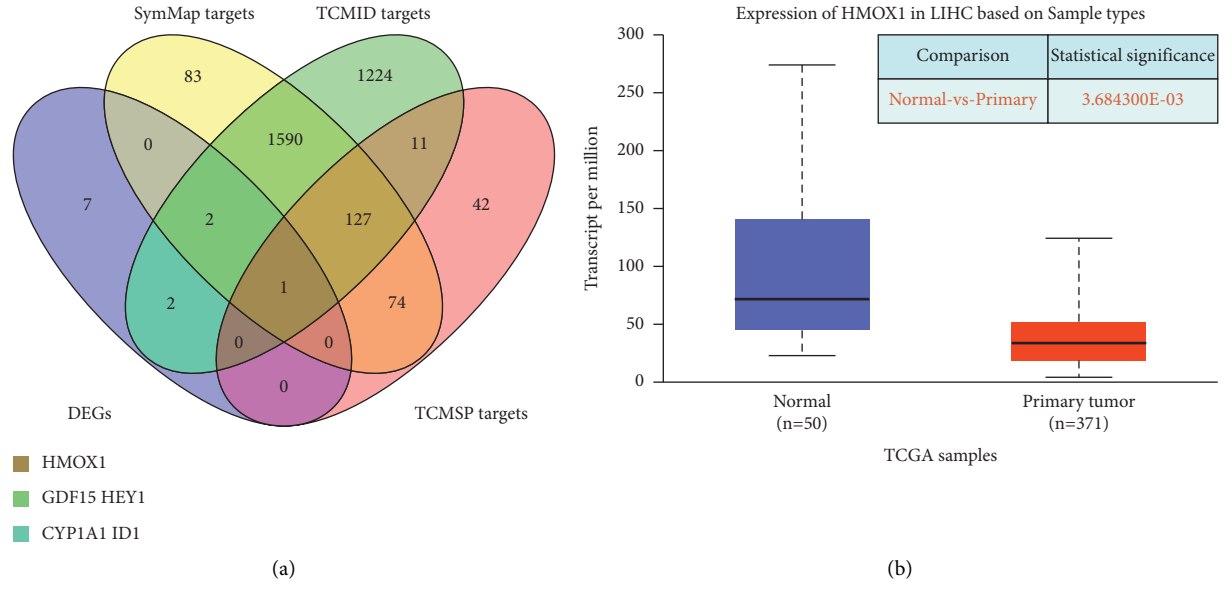

Figure 3: *Codonopsis pilosula* could target HMOX1. (a) Among all targets and 12 DEGs of *Codonopsis pilosula*, HMOX1 is the only common gene. (b) HMOX1 expression is significantly decreased in HCC.

Hmox1 in dorsal root ganglia neurons. Figure 4(d) showed that apigenin could not affect the expression of HMOX1 in MCF-7 cells. Figure 4(e) manifested that sulforaphane could dramatically enhance the expression of HMOX1 in MCF10A cells. Figure 4(f) showed that geniposide could not affect the expression of HMOX1 in MCF-7 cells. These results imply that *Codonopsis pilosula* could upregulate HMOX1 in HCC via luteolin, capsaicin, and sulforaphane.

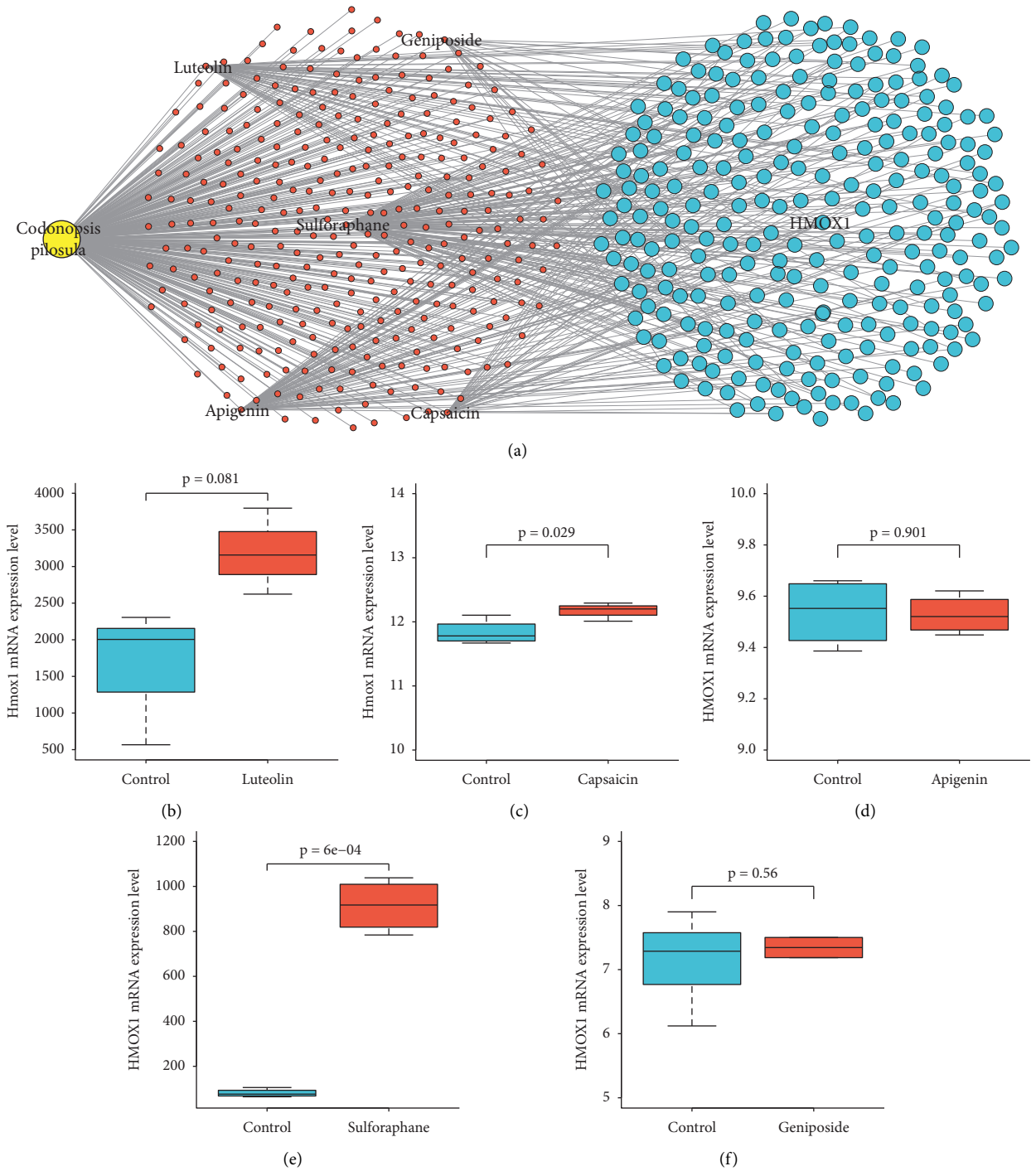

Figure 4: *Codonopsis pilosula* targeted HMOX1 via luteolin, capsaicin, and sulforaphane. (a) *Codonopsis pilosula*-component-target network showed that *Codonopsis pilosula* may target HMOX1 directly through apigenin, luteolin, capsaicin, sulforaphane, and geniposide. (b) Luteolin trends to upregulate Hmox1 in BV-2 cells ($p = 0.081$). (c) Capsaicin could significantly upregulate Hmox1 in dorsal root ganglia neurons ($p = 0.029$). (d) Apigenin could not affect the expression of HMOX1 in MCF-7 cells ($p = 0.901$). (e) Sulforaphane could significantly enhance HMOX1 expression in MCF10A cells ($p = 0.0006$). (f) Geniposide has no effect on the expression of HMOX1 in MCF-7 cells ($p = 0.56$).

3.5. Potential Binding Site between Active Ingredients of Codonopsis pilosula and HMOX1 Protein. For exploring potential interaction between active ingredients of *Codonopsis pilosula* (luteolin, capsaicin, and sulforaphane) and HMOX1 protein, we predicted the potential binding site of them via molecular docking. As shown in Figure 5(a), luteolin may directly bind ASP-140, LEU-141, GLN-145, ALA-173, SER-174, and ALA-175 to promote the expression level of HMOX1. Capsaicin may combine with HMOX1 by ARG-44, LYS-48, and PHE-95, thus enhancing the

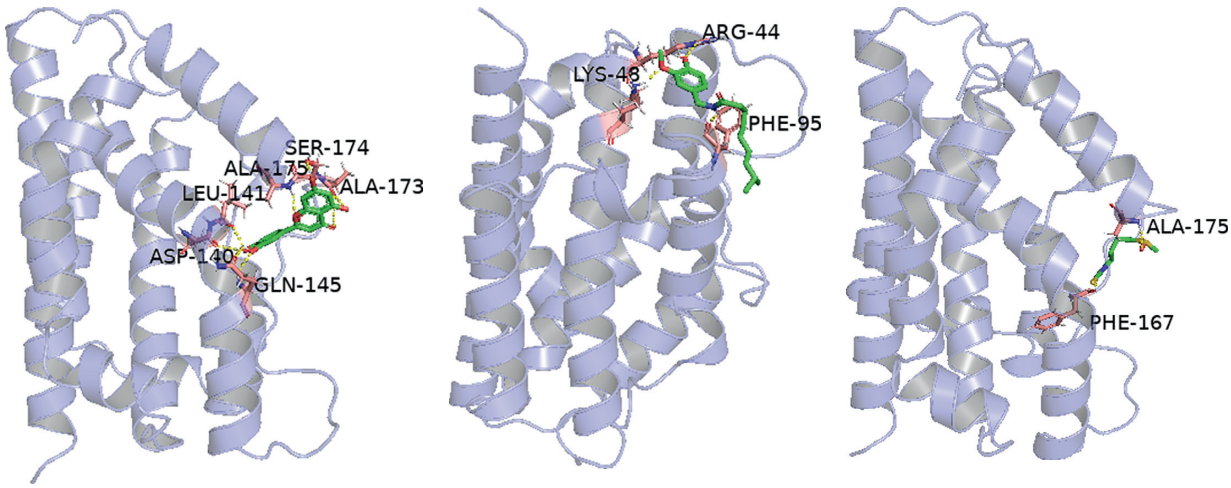

Figure 5: The molecular docking results of luteolin, capsaicin, and sulforaphane. (a) Luteolin may bind to HMOX1 with ASP-140, LEU-141, GLN-145, ALA-173, SER-174, and ALA-175. (b) Capsaicin may combine with HMOX1 by ARG-44, LYS-48, and PHE-95. (c) Sulforaphane may target HMOX1 via PHE-167 and ALA-175.

expression level of HMOX1 (Figure 5(b)). Sulforaphane may target HMOX1 via binding PHE-167 and ALA-175, resulting in increased expression of HMOX1 (Figure 5(c)). These results suggest that luteolin, capsaicin, and sulforaphane may promote HMOX1 expression through direct binding.

4. Discussion

TCMs are widely used during HCC treatment in China [30]. As with traditional medicine in other nations, herbal medicines are the main form of TCM [31]. Unlike small molecule drugs, herbal medicines contain many components and possess complex targets. Besides, some studies have revealed that miRNAs of herbal medicines may be ingested by the body and regulate the process of disease [32–34]. Complex components and targets limit the exploration of mechanisms in herbal medicines. Although multiple active components of *Codonopsis pilosula* were proved to have anti-HCC potential [15–17], the overall mechanism of *Codonopsis pilosula* is unclear.

In the present study, the *Codonopsis pilosula*-gene network was built by 12 striking DEGs (Figure 1(c)), and we identified HMOX1 as the hub gene via the PPI network (Figure 1(d)). HMOX1 was significantly enriched in the mineral absorption pathway, and the biological processes of its enrichment are primarily related to the metabolism of metal ions (Figures 2(a) and 2(b)). A study reported that there is a remarkable correlation between mineral absorption pathways and HCC development [35]. Furthermore, metal ion metabolism plays an essential role in the progression and treatment of HCC [36, 37]. Consequently, *Codonopsis pilosula* is highly likely to treat HCC via targeting HMOX1 to affect the mineral absorption pathway.

HMOX1 (heme oxygenase-1) is a stress-induced enzyme that catalyzes the degradation of heme to carbon monoxide, iron, and biliverdin [38]. The byproducts of HMOX1 enzymatic activity are cytoprotective because of their antioxidant and anti-inflammatory properties, showing that HMOX1 is a potential therapeutic target in many diseases [39]. Our results revealed that HMOX1 was significantly decreased in HCC patients (Figure 3(b)), and *Codonopsis pilosula* could distinctly enhance the expression of HMOX1 in HepG2 cells (Figure 1), suggesting that *Codonopsis pilosula* may reverse the expression pattern of HMOX1 in the HCC environment. Interestingly, HMOX1 overexpression could inhibit the growth, migration, and invasion in vivo, as well as higher HMOX1 expression was also associated with favorable disease-free survival of HBV-HCC patients who underwent hepatectomy [40]. These results indicate that *Codonopsis pilosula* is likely to improve the survival of HCC patients by promoting the expression of HMOX1, and is a potential adjuvant therapy for HCC.

Through the network pharmacology strategies, we built a *Codonopsis pilosula*-component-target network (Figure 4(a)). The network showed that *Codonopsis pilosula* may directly target HMOX1 via apigenin, luteolin, capsaicin, sulforaphane, and geniposide. To verify this result, we examined the effect of luteolin on Hmox1 expression in mouse BV-2 microglia (GSE18740), capsaicin on Hmox1 expression in rat TRPV1-positive neurons (GSE59727), apigenin on HMOX1 expression in human breast cancer cells MCF-7 (GSE119552), sulforaphane on HMOX1 expression in human breast epithelial cells MCF10A (GSE28813), and geniposide on HMOX1 expression in human breast cancer cells MCF-7 (GSE85871) (Figures 4(b)–4(f)). The results indicated that luteolin, capsaicin, and sulforaphane could increase the expression of HMOX1 expression in vitro, although not in HCC cells. Luteolin, a natural flavonoid, plays multiple roles in the anti-HCC process. Growth inhibition of luteolin on HCC cells is induced via multiple signaling pathways of TGF-β1 pathways, p53 pathways, Fas/Fas-ligand pathways [41], ER stress [42], and AKT/OPN pathway [43]. Besides, a recent study reported that luteolin

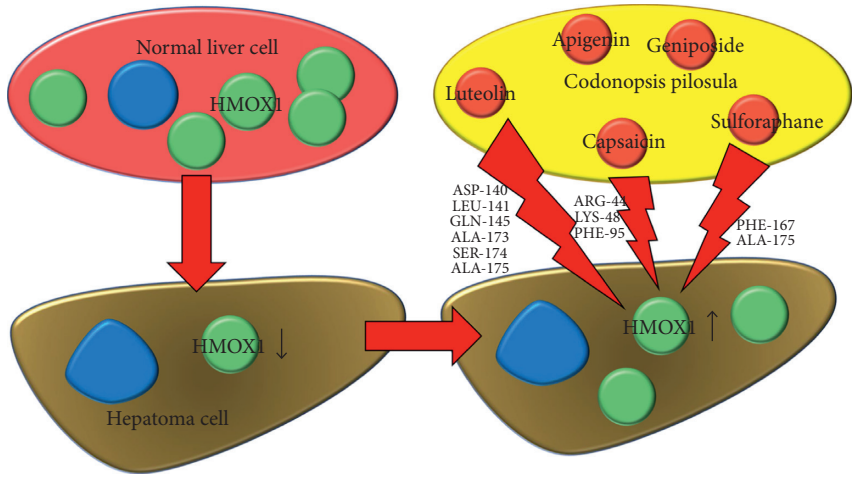

Figure 6: Schematic diagram of *Codonopsis pilosula* for HCC treatment.

could significantly inhibit HCC growth and cause apoptosis and cell cycle arrest in vitro and significantly suppress HCC growth in vivo via upregulating miR-6809-5p [44]. Capsaicin is a natural vanilloid and may inhibit the growth of SK-Hep-1 hepatocellular carcinoma cells by inducing apoptosis via Bcl-2 downregulation and caspase-3 activation [45]. Moreover, capsaicin could induce apoptosis in HepG2 cells by reducing the levels of xIAP and cIAP1 proteins, which are inhibitors of caspase-3 activation [46]. Interestingly, both luteolin and capsaicin are able to assist sorafenib to produce better anti-HCC therapeutic effects [47, 48]. Sulforaphane, a member of the isothiocyanate family, has exhibited promising inhibitory effects on breast cancer, lung cancer, liver cancer, and other malignant tumors [49]. Some studies revealed that sulforaphane could induce apoptosis [50] and enhance the radiation sensitivity [51] in HCC.

Notably, there are about 200 phytometabolites in *Codonopsis pilosula*, and the main bioactive ingredients include polysaccharides, polyyne and polyacetylene glycosides, lignans, penoids, alkaloids, flavonoids, and lactones [52]. Polysaccharides are large-molecule components in *Codonopsis pilosula*, which have a significant inhibitory effect on gastric cancer and lung cancer, in addition to liver cancer [53]. Although luteolin, capsaicin, and sulforaphane are not the most abundant ingredients of *Codonopsis pilosula*, they are essential for understanding the pharmacological effects of *Codonopsis pilosula*. Tang et al. found that *Codonopsis pilosula* may play an antigastric cancer role through luteolin [54], suggesting that luteolin may play an important role in the anticancer effects of *Codonopsis pilosula*. Furthermore, several studies showed that luteolin [55], capsaicin [56], and sulforaphane [57] could target HMOX1 and significantly enhance its expression level. Luteolin, capsaicin, and sulforaphane are components of *Codonopsis pilosula*, but their quantitative studies in *Codonopsis pilosula* are insufficient. It is reported that the content of luteolin in *Codonopsis thalictrifolis* is 0.7% via HPLC [58]. It is important to notice that *Codonopsis thalictrifolis* is not *Codonopsis pilosula*, although they belong to the *Codonopsis* genus, and there may be great differences in chemical composition between them. Nonetheless, as a reference, the data implied that the content of the luteolin in *Codonopsis pilosula* may be less than 0.1% or even 0.01%. The lowest dose of luteolin that has been reported to produce anti-HCC effects in rats is 0.2 mg/kg via intraperitoneal injection [59]. In addition, orally administered luteolin (0.2 mg/kg) could produce anticolon cancer effects in rats [60]. Fuzheng Jiedu Xiaoji formulation (including 15 g of *Codonopsis pilosula*) could inhibit HCC progression in patients [61]. Jian Pi Li Qi Decoction (including 20 g of *Codonopsis pilosula*) could improve the prognosis of patients with HCC [62]. Therefore, it is likely that the effective concentration of luteolin can be reached in the application of *Codonopsis pilosula*. At present, there are no quantitative studies on capsaicin and sulforaphane in *Codonopsis pilosula*. Studies showed that capsaicin (2 mg/kg) [63] and sulforaphane (50 mg/kg) [64] could inhibit the growth of HCC in xenograft mice. Compared with the effective dosage of capsaicin and sulforaphane, the application of *Codonopsis pilosula* (15–20 g) is higher. Consequently, luteolin, capsaicin, and sulforaphane are likely to reach effective concentrations in the clinical application of *Codonopsis pilosula*. These studies suggest that *Codonopsis pilosula* is most likely to exert anti-HCC effects via luteolin, capsaicin, and sulforaphane (Figure 6). In fact, although our study showed that luteolin, capsaicin, and sulforaphane may play roles in the adjuvant treatment of HCC by *Codonopsis pilosula*, they may not be the main active ingredients of *Codonopsis pilosula*. As an herbal medicine, *Codonopsis pilosula* contains a variety of ingredients. An inulin fructan from *Codonopsis pilosula* possessed potential anti-HCC effects (inhibiting proliferation and inducing apoptosis) on Huh-7 and HepG2 cells without side effects on normal cells [65]. In addition, a novel fructose-enriched polysaccharide from *Codonopsis pilosula* inhibited HepG2 cell proliferation and promoted apoptosis [66]. Taken together, apoptosis may be one of the anti-HCC pathways of *Codonopsis pilosula*.

5. Conclusions

The present study explored the effects of *Codonopsis pilosula* in the treatment of HCC via transcriptomics and network pharmacology. We revealed the transcriptome changes of HCC cells induced by *Codonopsis pilosula*. In addition, *Codonopsis pilosula* is likely to upregulate HMOX1 directly through luteolin, capsaicin, and sulforaphane, thus affecting the mineral absorption pathway in HCC cells. This study provides clues to comprehend the potential mechanisms of *Codonopsis pilosula* in treating HCC. Of course, these conclusions require further experimental support.

Data Availability

The data used to support the findings of this study are available from the corresponding author upon request.

Conflicts of Interest

There are no conflicts of interest.

Acknowledgments

The authors thank the Shenzhen Key Lab of Neurogenomics (BGI-Shenzhen) for support in the analysis. The study was supported by the National Key Research and Development Program of China (No. 2020YFC2002902) and the Science, and Technology and Innovation Commission of Shenzhen Municipality under Grant (No. JCYJ20180507183615145).

Supplementary Materials

Tables S1–S3 in the Supplemental files. Table S1: twelve DEGs in HepG2 cells after *Codonopsis pilosula* treatment. Table S2: all significantly enriched biological processes after *Codonopsis pilosula* treatment. Table S3: targets of *Codonopsis pilosula*. (*Supplementary Materials*)

References

[1] A. J. Craig, J. von Felden, T. Garcia-Lezana, S. Sarcognato, and A. Villanueva, "Tumour evolution in hepatocellular carcinoma," *Nature Reviews Gastroenterology & Hepatology*, vol. 17, no. 3, pp. 139–152, 2020.

[2] D. Sia, A. Villanueva, S. L. Friedman, and J. M. Llovet, "Liver cancer cell of origin, molecular class, and effects on patient prognosis," *Gastroenterology*, vol. 152, no. 4, pp. 745–761, 2017.

[3] Z. Liu, Y. Jiang, H. Yuan et al., "The trends in incidence of primary liver cancer caused by specific etiologies: results from the global burden of disease study 2016 and implications for liver cancer prevention," *Journal of Hepatology*, vol. 70, no. 4, pp. 674–683, 2019.

[4] J. Liu, W. Tang, A. Budhu et al., "A viral exposure signature defines early onset of hepatocellular carcinoma," *Cell*, vol. 182, no. 2, pp. 317–328, 2020.

[5] A. Villanueva and H. Carcinoma, "Hepatocellular carcinoma," *New England Journal of Medicine*, vol. 380, no. 15, pp. 1450–1462, 2019.

[6] J. C. Nault and A. Villanueva, "Biomarkers for hepatobiliary cancers," *Hepatology*, vol. 73, no. S1, pp. 115–127, 2021.

[7] F. Foerster and P. R. Galle, "The current landscape of clinical trials for systemic treatment of HCC," *Cancers*, vol. 13, no. 8, 2021.

[8] L. Rimassa, N. Personeni, C. Czauderna, F. Foerster, and P. Galle, "Systemic treatment of HCC in special populations," *Journal of Hepatology*, vol. 74, no. 4, pp. 931–943, 2021.

[9] S. Busche, K. John, F. Wandrer et al., "BH3-only protein expression determines hepatocellular carcinoma response to sorafenib-based treatment," *Cell Death & Disease*, vol. 12, no. 8, p. 736, 2021.

[10] X. Liu, M. Li, X. Wang et al., "Effects of adjuvant traditional Chinese medicine therapy on long-term survival in patients with hepatocellular carcinoma," *Phytomedicine*, vol. 62, Article ID 152930, 2019.

[11] Y. Yang, M. Sun, W. Yao et al., "Compound kushen injection relieves tumor-associated macrophage-mediated immunosuppression through TNFR1 and sensitizes hepatocellular carcinoma to sorafenib," *Journal for immunotherapy of cancer*, vol. 8, no. 1, 2020.

[12] W. Lam, Z. Jiang, F. Guan et al., "PHY906(KD018), an adjuvant based on a 1800-year-old Chinese medicine, enhanced the anti-tumor activity of Sorafenib by changing the tumor microenvironment," *Scientific Reports*, vol. 5, no. 1, p. 9384, 2015.

[13] B. Zhai, F. Hu, H. Yan et al., "Bufalin reverses resistance to sorafenib by inhibiting akt activation in hepatocellular carcinoma: the role of endoplasmic reticulum stress," *PLoS One*, vol. 10, no. 9, Article ID e0138485, 2015.

[14] L. Ye, Y. Jia, K. Ji et al., "Traditional Chinese medicine in the prevention and treatment of cancer and cancer metastasis," *Oncology Letters*, vol. 10, no. 3, pp. 1240–1250, 2015.

[15] Y. Zhang, Y. Zhang, and H. Xu, "Effect of Codonopsis pilosula polysaccharides on the growth and motility of hepatocellular carcinoma HepG2 cells by regulating β-catenin/TCF4 pathway," *International Journal of Polymer Science*, vol. 2019, Article ID 7068437, 7 pages, 2019.

[16] R. Bai, W. Li, Y. Li et al., "Cytotoxicity of two water-soluble polysaccharides from *Codonopsis pilosula* Nannf. var. modesta (Nannf.) L.T.Shen against human hepatocellular carcinoma HepG2 cells and its mechanism," *International Journal of Biological Macromolecules*, vol. 120, pp. 1544–1550, 2018.

[17] L. Sheng, J. Li, N. Li et al., "Atractylenolide III predisposes miR-195-5p/FGFR1 signaling axis to exert tumor-suppressive functions in liver cancer," *Journal of Food Biochemistry*, vol. 45, no. 5, Article ID e13582, 2021.

[18] P.-H. Ko, C.-W. Huang, H.-H. Chang, E. Y. Chuang, M.-H. Tsai, and L.-C. Lai, "Identifying the functions and biomarkers of *Codonopsis pilosula* and Astragalus membranaceus aqueous extracts in hepatic cells," *Chinese Medicine*, vol. 14, no. 1, p. 10, 2019.

[19] J. Ru, P. Li, J. Wang et al., "TCMSP: a database of systems pharmacology for drug discovery from herbal medicines," *Journal of Cheminformatics*, vol. 6, no. 1, p. 13, 2014.

[20] L. Huang, D. Xie, Y. Yu et al., "TCMID 2.0: a comprehensive resource for TCM," *Nucleic Acids Research*, vol. 46, pp. D1117–D1120, 2018.

[21] Y. Wu, F. Zhang, K. Yang et al., "SymMap: an integrative database of traditional Chinese medicine enhanced by symptom mapping," *Nucleic Acids Research*, vol. 47, pp. D1110–D1117, 2019.

[22] M. E. Ritchie, B. Phipson, D. Wu et al., "Limma powers differential expression analyses for RNA-sequencing and microarray studies," *Nucleic Acids Research*, vol. 43, no. 7, p. e47, 2015.

[23] D. Szklarczyk, A. L. Gable, D. Lyon et al., "STRING v11: protein-protein association networks with increased coverage, supporting functional discovery in genome-wide experimental datasets," *Nucleic Acids Research*, vol. 47, pp. D607–D613, 2019.

[24] P. Shannon, A. Markiel, O. Ozier et al., "Cytoscape: a software environment for integrated models of biomolecular interaction networks," *Genome Research*, vol. 13, no. 11, pp. 2498–2504, 2003.

[25] G. Yu, L.-G. Wang, Y. Han, and Q.-Y. He, "clusterProfiler: an R package for comparing biological themes among gene clusters," *OMICS: A Journal of Integrative Biology*, vol. 16, no. 5, pp. 284–287, 2012.

[26] D. S. Chandrashekar, B. Bashel, S. A. H. Balasubramanya et al., "UALCAN: a portal for facilitating tumor subgroup gene expression and survival analyses," *Neoplasia*, vol. 19, no. 8, pp. 649–658, 2017.

[27] H. M. Berman, J. Westbrook, Z. Feng et al., "The protein data bank," *Nucleic Acids Research*, vol. 28, no. 1, pp. 235–242, 2000.

[28] T. Sterling and J. J. Irwin, "Zinc 15—ligand discovery for everyone," *Journal of Chemical Information and Modeling*, vol. 55, no. 11, pp. 2324–2337, 2015.

[29] G. M. Morris, R. Huey, W. Lindstrom et al., "AutoDock4 and AutoDockTools4: automated docking with selective receptor flexibility," *Journal of Computational Chemistry*, vol. 30, no. 16, pp. 2785–2791, 2009.

[30] X. Liao, Y. Bu, and Q. Jia, "Traditional Chinese medicine as supportive care for the management of liver cancer: past, present, and future," *Genes & Diseases*, vol. 7, no. 3, pp. 370–379, 2020.

[31] H. Yuan, Q. Ma, L. Ye, and G. Piao, "The traditional medicine and modern medicine from natural products," *Molecules*, vol. 21, no. 5, 2016.

[32] L.-K. Zhou, Z. Zhou, X.-M. Jiang et al., "Absorbed plant MIR2911 in honeysuckle decoction inhibits SARS-CoV-2 replication and accelerates the negative conversion of infected patients," *Cell Discovery*, vol. 6, no. 1, p. 54, 2020.

[33] C. Xia, H. Zhou, X. Xu et al., "Identification and investigation of miRNAs from gastrodia elata blume and their potential function," *Frontiers in Pharmacology*, vol. 11, no. 1477, 2020.

[34] Z. Zhou, X. Li, J. Liu et al., "Honeysuckle-encoded atypical microRNA2911 directly targets influenza A viruses," *Cell Research*, vol. 25, no. 1, pp. 39–49, 2015.

[35] Y. Li, R. Chen, J. Yang et al., "Integrated bioinformatics analysis reveals key candidate genes and pathways associated with clinical outcome in hepatocellular carcinoma," *Frontiers in Genetics*, vol. 11, p. 814, 2020.

[36] J. Wachsmann and F. Peng, "Molecular imaging and therapy targeting copper metabolism in hepatocellular carcinoma," *World Journal of Gastroenterology*, vol. 22, no. 1, pp. 221–231, 2016.

[37] W. Wang, Q. Xie, X. Zhou et al., "Mitofusin-2 triggers mitochondria Ca^{2+} influx from the endoplasmic reticulum to induce apoptosis in hepatocellular carcinoma cells," *Cancer Letters*, vol. 358, no. 1, pp. 47–58, 2015.

[38] L. L. Dunn, S. M. Y. Kong, S. Tumanov et al., "Hmox1 (heme oxygenase-1) protects against ischemia-mediated injury via stabilization of HIF-1α (Hypoxia-Inducible factor-1α)," *Arteriosclerosis, Thrombosis, and Vascular Biology*, vol. 41, no. 1, pp. 317–330, 2021.

[39] T. D. Hull, A. Agarwal, and J. F. George, "The mononuclear phagocyte system in homeostasis and disease: a role for heme oxygenase-1," *Antioxidants and Redox Signaling*, vol. 20, no. 11, pp. 1770–1788, 2014.

[40] C.-N. Yeh, R.-C. Wu, C.-T. Cheng et al., "HO-1 is a favorable prognostic factor for HBV-HCC patients who underwent hepatectomy," *Cancer Management and Research*, vol. 10, pp. 6049–6059, 2018.

[41] S. B. Yee, H. J. Choi, S. W. Chung et al., "Growth inhibition of luteolin on HepG2 cells is induced via p53 and Fas/Fas-ligand besides the TGF-β pathway," *International Journal of Oncology*, vol. 47, no. 2, pp. 747–754, 2015.

[42] Y. Lee and Y. H. Kwon, "Regulation of apoptosis and autophagy by luteolin in human hepatocellular cancer Hep3B cells," *Biochemical and Biophysical Research Communications*, vol. 517, no. 4, pp. 617–622, 2019.

[43] E. Im, C. Yeo, and E.-O. Lee, "Luteolin induces caspase-dependent apoptosis via inhibiting the AKT/osteopontin pathway in human hepatocellular carcinoma SK-Hep-1 cells," *Life Sciences*, vol. 209, pp. 259–266, 2018.

[44] P.-W. Yang, Z.-Y. Lu, Q. Pan et al., "MicroRNA-6809-5p mediates luteolin-induced anticancer effects against hepatoma by targeting flotillin 1," *Phytomedicine*, vol. 57, pp. 18–29, 2019.

[45] M.-Y. Jung, H.-J. Kang, and A. Moon, "Capsaicin-induced apoptosis in SK-Hep-1 hepatocarcinoma cells involves Bcl-2 downregulation and caspase-3 activation," *Cancer Letters*, vol. 165, no. 2, pp. 139–145, 2001.

[46] S. P. Huang, J. C. Chen, C. C. Wu et al., "Capsaicin-induced apoptosis in human hepatoma HepG2 cells," *Anticancer Research*, vol. 29, no. 1, pp. 165–174, 2009.

[47] N. Dai, R. Ye, Q. He, P. Guo, H. Chen, and Q. Zhang, "Capsaicin and sorafenib combination treatment exerts synergistic anti-hepatocellular carcinoma activity by suppressing EGFR and PI3K/Akt/mTOR signaling," *Oncology Reports*, vol. 40, no. 6, pp. 3235–3248, 2018.

[48] X. Q. Feng, L. W. Rong, R. X. Wang et al., "Luteolin and sorafenib combination kills human hepatocellular carcinoma cells through apoptosis potentiation and JNK activation," *Oncology Letters*, vol. 16, no. 1, pp. 648–653, 2018.

[49] G. Wu, Y. Yan, Y. Zhou et al., "Sulforaphane: expected to become a novel antitumor compound," *Oncology Research Featuring Preclinical and Clinical Cancer Therapeutics*, vol. 28, no. 4, pp. 439–446, 2020.

[50] S. B. Kntayya, M. D. Ibrahim, N. Mohd Ain, R. Iori, C. Ioannides, and A. F. Abdull Razis, "Induction of apoptosis and cytotoxicity by isothiocyanate sulforaphene in human hepatocarcinoma HepG2 cells," *Nutrients*, vol. 10, no. 6, 2018.

[51] K. Ren, Z. Li, Y. Li, W. Zhang, and X. Han, "Sulforaphene enhances radiosensitivity of hepatocellular carcinoma through suppression of the NF-κB pathway," *Journal of Biochemical and Molecular Toxicology*, vol. 31, no. 8, 2017.

[52] X. Zeng, J. Li, X. Lyu, J. Chen, X. Chen, and S. Guo, "Untargeted metabolomics reveals multiple phytometabolites in the agricultural waste materials and medicinal materials of Codonopsis pilosula," *Frontiers of Plant Science*, vol. 12, 2022.

[53] J.-Y. He, N. Ma, S. Zhu, K. Komatsu, Z.-Y. Li, and W.-M. Fu, "The genus Codonopsis (Campanulaceae): a review of phytochemistry, bioactivity and quality control," *Journal of Natural Medicines*, vol. 69, no. 1, pp. 1–21, 2015.

[54] L. Tang, J. Chen, J. Yin, and M. Fang, "Screening of active components and key targets of radix Codonopsis in the treatment of gastric cancer," *Journal of Chemistry*, vol. 2021, Article ID 6056636, 10 pages, 2021.

[55] L. Li, R. Zhou, H. Lv, L. Song, X. Xue, and L. Wu, "Inhibitive effect of luteolin on sevoflurane-induced neurotoxicity through activation of the autophagy pathway by HMOX1,"

ACS Chemical Neuroscience, vol. 12, no. 18, pp. 3314–3322, 2021.

[56] K. Magierowska, D. Wojcik, A. Chmura et al., "Alterations in gastric mucosal expression of calcitonin gene-related peptides, vanilloid receptors, and heme oxygenase-1 mediate gastroprotective action of carbon monoxide against ethanol-induced gastric mucosal lesions," *International Journal of Molecular Sciences*, vol. 19, no. 10, 2018.

[57] W. N. Nowak, H. Taha, J. Markiewicz et al., "Atorvastatin and conditioned media from atorvastatin-treated human hematopoietic stem/progenitor-derived cells show proangiogenic activity in vitro but not in vivo," *Mediators of Inflammation*, vol. 2019, Article ID 1868170, 15 pages, 2019.

[58] X. Liu, J. Liang, S. Peng, L. Ding, and Y. Gu, "Analysis of luteolin from traditional tibetan medicine of *Codonopsis thalictrifolis*," *Chinese Journal of Analysis Laboratory*, vol. 28, pp. 263-264, 2009.

[59] K. Balamurugan and J. Karthikeyan, "Evaluation of luteolin in the prevention of N-nitrosodiethylamine-induced hepatocellular carcinoma using animal model system," *Indian Journal of Clinical Biochemistry*, vol. 27, no. 2, pp. 157–163, 2012.

[60] N. H. A. Osman, U. Z. Said, A. M. El-Waseef, and E. S. A. Ahmed, "Luteolin supplementation adjacent to aspirin treatment reduced dimethylhydrazine-induced experimental colon carcinogenesis in rats," *Tumor Biology*, vol. 36, no. 2, pp. 1179–1190, 2015.

[61] X. Yang, Y. Feng, Y. Liu et al., "Fuzheng Jiedu Xiaoji formulation inhibits hepatocellular carcinoma progression in patients by targeting the AKT/CyclinD1/p21/p27 pathway," *Phytomedicine*, vol. 87, Article ID 153575, 2021.

[62] L. Xu, S. Wang, L. Zhuang et al., "Jian pi Li Qi decoction alleviated postembolization syndrome following transcatheter arterial chemoembolization for hepatocellular carcinoma," *Integrative Cancer Therapies*, vol. 15, no. 3, pp. 349–357, 2016.

[63] C. Xie, G. Liu, M. Li et al., "Targeting TRPV1 on cellular plasticity regulated by Ovol 2 and Zeb 1 in hepatocellular carcinoma," *Biomedicine & Pharmacotherapy*, vol. 118, Article ID 109270, 2019.

[64] J. Wu, J. Han, B. Hou, C. Deng, H. Wu, and L. Shen, "Sulforaphane inhibits TGF-β-induced epithelial-mesenchymal transition of hepatocellular carcinoma cells via the reactive oxygen species-dependent pathway," *Oncology Reports*, vol. 35, no. 5, pp. 2977–2983, 2016.

[65] N. Hu, Z. Gao, P. Cao et al., "Uniform and disperse selenium nanoparticles stabilized by inulin fructans from Codonopsis pilosula and their anti-hepatoma activities," *International Journal of Biological Macromolecules*, vol. 203, pp. 105–115, 2022.

[66] J. Yu, X.-D. Dong, J.-S. Jiao et al., "The inhibitory effects of selenium nanoparticles modified by fructose-enriched polysaccharide from Codonopsis pilosula on HepG2 cells," *Industrial Crops and Products*, vol. 176, Article ID 114335, 2022.

Hindawi
Evidence-Based Complementary and Alternative Medicine
Volume 2022, Article ID 6535977, 18 pages
https://doi.org/10.1155/2022/6535977

Review Article

Treatment of Liver Cancer: Role of the Traditional Mongolian Medicine

Xiaomei Bao,[1,2] Lu Chen,[1] Yiman Liu,[1] Hua Sheng,[2] Kailong Wang,[1] Yanming Luo,[1] Tongling Qin,[3] Ying Liu,[3] and Yuling Qiu[3]

[1]*State Key Laboratory of Component-based Chinese Medicine, Tianjin University of Traditional Chinese Medicine, Tianjin, China*
[2]*School of Pharmacy, Inner Mongolia Medical University, Hohhot, China*
[3]*School of Pharmacy, Tianjin Medical University, Tianjin, China*

Correspondence should be addressed to Yuling Qiu; qiuyuling@tmu.edu.cn

Received 19 November 2021; Accepted 19 January 2022; Published 14 February 2022

Academic Editor: Li-Ping Kang

Liver cancer is an extraordinarily heterogeneous malignancy with relatively high mortality and increasing incidence rate among the so far identified cancers. Improvements in liver cancer therapy have been made in the past decades, but therapeutics against liver cancer are still limited. Traditional Mongolian Medicine, formed and developed by the Mongolian people to maintain health in the medical practice of fighting against diseases, has been recognized as one of the key components of the world healthcare system. Traditional Mongolian Medicine has been used to treat various malignancies, including liver cancer, for a long time in Asia and its advantages have become more and more apparent. Herein, this review made a comprehensive summary of Traditional Mongolian Medicine, including the ideas in the liver cancer treatment, sources of medicines or prescriptions, traditional applications, modern pharmacological research, chemical structure and mechanisms of several monomer compounds isolated from Traditional Mongolian Medicine, with a view to finding promising drugs against liver cancer and expanding the clinical application of Traditional Mongolian Medicine in liver cancer therapy.

1. Introduction

Liver cancer has an insidious onset. Even though many patients have been effectively diagnosed and treated in the early stage of the disease, the recurrence rate is still high [1, 2]. Especially for patients with advanced disease, the prognosis is not optimistic. If cancer spreads to the peripheral lymph nodes, the patient's 5-year survival rate is only 11%. The current treatment methods for liver cancer include surgery, radiotherapy, minimally invasive treatment (radiofrequency ablation, argon helium knife, microwave ablation, interventional therapy), biological immunotherapy, traditional Chinese medicine, and diet therapy. Surgery is the preferred treatment for liver cancer. However, only 20%–30% of patients can get surgical resection because most patients have basic liver disease, or most of them have reached the advanced stage at the time of diagnosis [3, 4]. Although the clinical treatment of liver cancer has been improved in the past years, the overall survival remains unsatisfactory. Especially, patients in the advanced stage still have limited treatment options. Therefore, it is of great significance to further explore the occurrence and development mechanism of liver cancer and find new therapeutics.

Traditional Chinese ethnic medicine is the creation and accumulation of every ethnic minority through their long histories [5]. As an indispensable part of traditional Chinese medicine, Mongolian medicine is an important traditional medicine formed and developed by the Mongolian people in the medical practice of fighting against diseases for a long time and has its own unique diagnostic methods [6]. Mongolian medicine absorbs and digests the theory of Tibetan medicine and other ethnic medicine. It combines its own theories and experience to create the Mongolian

medicine system with characteristics of Mongolian culture and history. Its development has received the attention of the Chinese government and the support of relevant policies [7].

As the only remaining historical documents, Mongolian medical literature has a complete medical theory system and is still used in clinical practice. The classic books of Mongolian medicine include Ren yao bai jing jian, the Four Medical Tantras, and Classic Canon of Mongolian Materia Medica. Ren yao bai jing jian is the foundation of Mongolian medicine, containing 390 kinds of Mongolian medicines [8]. The Four Medical Tantras is a comprehensive work on Tibetan medicine integrating natural sciences, social sciences, and humanities [9, 10]. It summarized the theories, diagnosis, and treatment experience of traditional Tibetan medicine [11–13]. Classic Canon of Mongolian Materia Medica makes a comprehensive summary and some revisions of Mongolian medicine herbal books of the past dynasties [14]. This book records 879 kinds of Mongolian medicinal materials, with 570 medicine illustrations [15]. With the development of Mongolian medicine, the experts of Mongolian medicine actively absorbed the knowledge of plant taxonomy, pharmacognosy, natural pharmaceutical chemistry, pharmacology, and other aspects and compiled a series of teaching materials and authoritative books with the support and organization of the government, such as "Mongolian Pharmacy," "Encyclopedia of Mongolian Medicine," "Prescription of Mongolian Medicine," "Drug standard of the Ministry of health of the people's Republic of China (Mongolian medicine volume)," and "Chinese Materia Medica Mongolian Medicine Volume." These modern Mongolian medicine books and standards have made important contributions to the modernization of Mongolian medicine and will benefit mankind.

Although both Mongolian medicine and traditional Chinese medicine are traditional medicine, there are many differences in their sources and clinical uses [16, 17]. Mongolian medicine covers a wide range of sources, including plants, animals, minerals, and chemicals [7]. There are 511 kinds of medicinal plants in Mongolian medicine, and 23 species-specific for Mongolian medicine are basal plants, such as *Flos Scabiosae, Lomatogonium rotatum, Dracocephalum moldevica*, etc. [18]. Some medicinal plants are unique to Mongolian medicine and are not available in traditional Chinese medicine [16], such as *Punica granatum* L., *Har Gabur*, *Gardenia jasminoides*, *Syringa pinnatifolia*, *Scabiosa comosa* Fisch, *wannianhui (made from calcareous lumps of ancient buildings)*, *Flos of Aconitum kusnezoffii*, *rhaponticum uniflorum*, *Pearl bar*, *Oxytropis Myriophylla*, etc. Modern pharmacological studies show that Mongolian medicine has good antitumor effects. In the process of chemotherapy, Mongolian medicine can protect normal cells from chemotherapeutic/radiotherapeutic injuries, consolidate or enhance the effect of chemotherapy/radiotherapy, and prevent cancer metastasis and recurrence. This review introduces the ideas of Mongolian medicine in the treatment of liver cancer and the research progress of common clinical drugs (Tables 1 and 2.) and their possible mechanisms.

2. Treatment Concept

Every Chinese Minority established their medical system with their own national characteristics based on the living environment, natural resources, national culture, religious beliefs, and so on, which played key roles in preventing disease and maintaining health [28]. Tibetan medicine, Mongolian medicine, Uygur medicine, Zhuang medicine, Hui medicine, Dai medicine, and Miao medicine are important components of traditional Chinese medicine [29]. The holistic view of the basic theory in Mongolian medicine includes two aspects: the unity of man and nature and the unity of the human body itself. The unity of human beings is the most critical factor in maintaining healthy activities in life [30, 31]. Traditional Mongolian medicine not only accepts Chinese ancient native materialism and dialectics thoughts, Wu yuan, Yin and Yang theory, and absorbs the basic theory of traditional Chinese medicine, but also blends the theory of Tibetan medicine and Indian medicine [32]. In the process of development, it has gradually formed a unique Mongolian medicine theory system, based on the philosophy of Yin and Yang, Wu yuan, Han-re theory; meanwhile, San-gen, Qi-su, San-hui, Zang-fu theory, and Liu-yin theory are considered as the main contents. In the theory of Mongolian medicine, the human body can maintain normal physiological activities mainly because the body has three kinds of energy resources and basic substances, namely, He (equivalent to air), Badakan (equivalent to soil and water), and Xiri (equivalent to fire), which are thought to be the origin and foundation of human life and are also called San-gen. The San-gen theory holds that the life phenomenon of the human body is a comprehensive and complex activity process, in which the organic coordination of San-gen makes the whole life in an orderly metabolic state. The organic connection between the internal organs and body surface tissues is the result of the effects of the San-gen. Therefore, San-gen is the material basis on which life depends (Figure 1).

The concept of Mongolian medicine has gained international attention and has been gradually accepted by people in other parts of the world [33]. The Four Medical Tantras [34] details the etiology, symptoms, diagnosis, treatment, and prevention of the tumor. It regards the human body as an organic whole and considers the tumor as a systemic disease whose occurrence, development, recurrence, and metastasis are the local reflection of systemic diseases. According to different patients, different etiology, different time, the syndrome differentiation for treatment has been done [8].

Mongolian physicians think that the incidence of liver cancer is due to long-term emotional depression, mental traumas, improper diet, long-term addiction to tobacco and alcohol, and traumatic injury. The essence of the human body cannot be normally operated and then accumulates in the liver. As a result, "San-gen" is disordered in vivo and the transportation of blood in the liver is abnormal and deposits [35]. Body fluid, blood stasis, and hot evil then coagulate, throw the organism out of balance, and generate heat which can consistently fumigate the condensation. Ultimately, "Pi

Table 1: Prescriptions for the treatment of liver cancer in Mongolian medicine.

Prescription	Components	Treatment concept	Cell model	Animal model	Pharmacologic action	Clinical application	Reference
Qinggan jiuwei powder	Calculus bovis, *Dianthus superbus*, *Trogopterus* dung, *Scabiosa comosa*, *Costus* root, *Herpetospermum* seed, *Angelica sinensis, Aristolochia manshuriensis, Crocus sativus*	Removing heat from the liver; cooling blood	—	CCl_4-induced liver fibrosis in rats	Suppress or alleviate liver fibrosis	Viral hepatitis, cirrhosis, fatty liver, chronic cholecystitis, gastroduodenal ulcer, etc.	[19–21]
Honghua qinggan 13 flavors	Saffron, clove, lotus seeds, radix ophiopogonis, radix aucklandiae, *Melia toosendan, Gardenia, Lignum pterocarri,* musk, pulvis cornus bubali concentratus, calculus bovis, and vermilion	Clearing heat; detoxifying; cooling blood	—	CCl4-induced liver fibrosis in rats	Liver injury and fibrosis	Liver failure, drug-induced hepatitis, alcoholic liver, fatty liver, etc.	[22–24]
Changpu siwei	Galanga rhizome, *Halitum purpureum*, vladimiriae radix, and *Acorus gramineus*	Suppressing "ba dagan and he"; relieving asthma and pain	SMMC-7721 cell	—	Inhibition the proliferation of liver cancer cells	Oppression in chest and dyspnea, indigestion, relieving asthma and pain	[25]
Hepatoprotective Mongolian I	*Terminalia chebula* is the main component	Activating blood circulation, removing blood stasis, and relieving pain	Huh-7 cell	—	Inhibition the proliferation of liver cancer cells, inducing apoptosis	Prevention and treatment of tumors	[26]
Hepatoprotective Mongolian II	*Terminalia chebula* is the main component	Activating blood circulation, removing blood stasis, and relieving pain	Huh-7, HepG2 cell	—	Inducing apoptosis and cell cycle arrest	Prevention and treatment of tumors	[27]

kuai" is gradually formed in the liver and the greater the hot evil, the bigger and harder the block. "Pi kuai" is what we call tumors [36].

3. Prescription

3.1. Qinggan Jiuwei Powder. Qinggan Jiuwei Powder (also named Geiwang-9) is a traditional Mongolian medicine prescription for liver diseases. This prescription was first published in the Four Medical Tantras and then spread to Mongolia and has been used till now. It is recorded in "Encyclopedia of Mongolian Medicine," "Prescription of Mongolian Medicine." "Drug Standards of the Ministry of Health of the People's Republic of China (Mongolian Medicines Volume)" [37] and other classic works. This prescription is composed of *Calculus bovis*, *Dianthus superbus*, *trogopterus dung, Scabiosa comosa*, *costus root*, *herpetospermum seed*, *Angelica sinensis*, *Aristolochia manshuriensis*, and *Crocus sativus* [38]. It has the efficacy of cooling blood and removing heat from the liver. Currently, it has been widely used in the treatment of viral hepatitis, cirrhosis, fatty liver, chronic cholecystitis, gastroduodenal ulcer, and other diseases. The experimental research mainly focuses on quality control, technological research, and pharmacological effect. Early diagnosis and treatment of liver fibrosis can effectively improve the life quality of patients and prevent them from developing cirrhosis and even liver cancer [39]. Hepatic fibrosis is caused by excessive deposition of extracellular matrix (ECM) in the liver, which eventually leads to hepatic fibrosis. In normal liver, ECM synthesis and degradation remain dynamically balanced as a result of precise regulation of matrix metalloproteinases (MMPs) and their specific inhibitor, TIMPs [40]. Previous studies [19] have found that Qinggan Jiuwei powder has a certain effect on serum TIMP-1 level and can effectively reduce the imaging index LSM and values measured by abdominal color Doppler ultrasound in patients with alcoholic liver fibrosis [20]. Meanwhile, Qinggan Jiuwei

Table 2: Monomer compounds against liver cancer in the Mongolian medicine.

	Chemical name	Botanical name	Compound structure	Structure type
1	Pentagalloyl glucose	*Terminalia chebula* retz	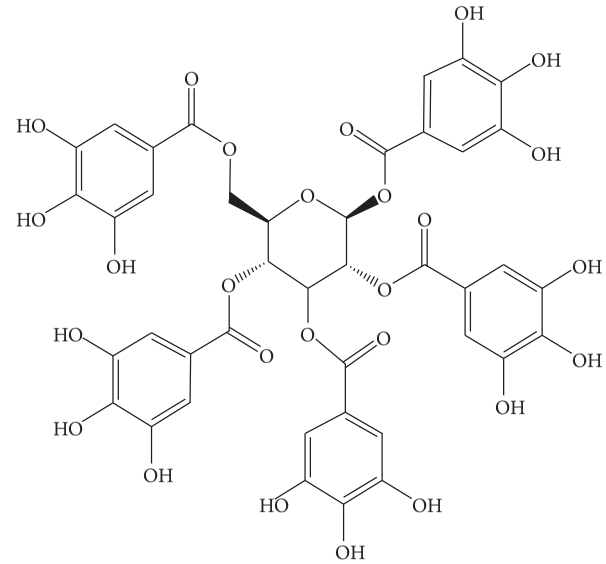	Polyphenols
2	Chebulagic acid	*Terminalia chebula* retz	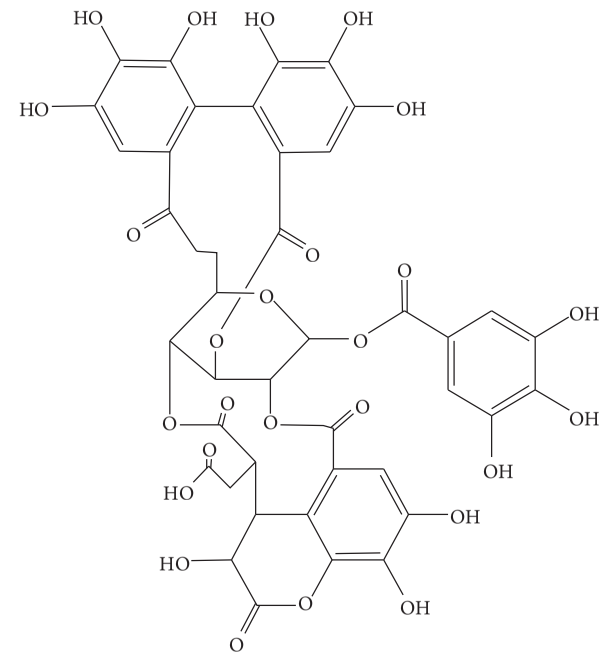	Phenols

Table 2: Continued.

	Chemical name	Botanical name	Compound structure	Structure type
3	Safflower yellow B	*Carthamus tinctorius* L.	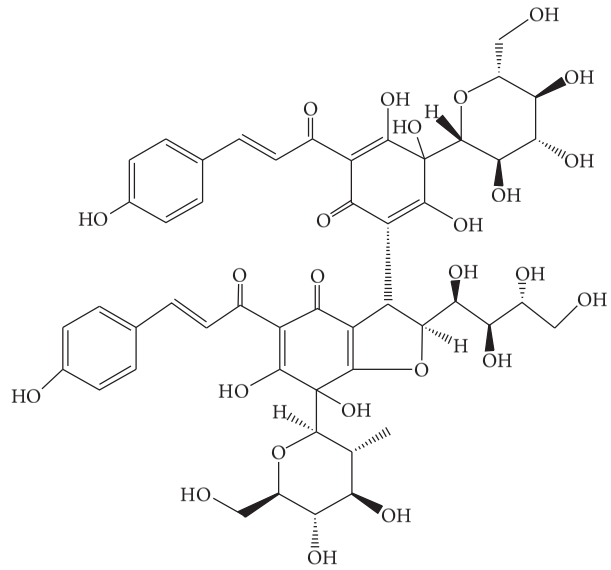	Flavonoid
4	Hydroxysafflor yellow A	*Carthamus tinctorius* L.	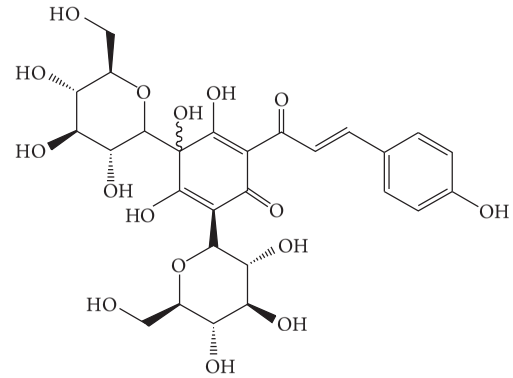	Flavonoid

Table 2: Continued.

	Chemical name	Botanical name	Compound structure	Structure type
5, 6, 7, 8, 9	—	*Xanthoceras sorbifolia* Bunge	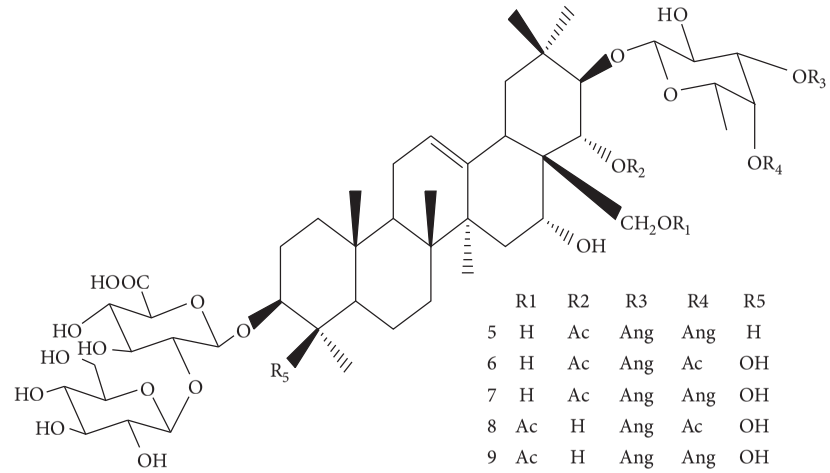	Triterpenoid saponins
10	Quercetin	*Artemisia lavandulaefolia* DC.	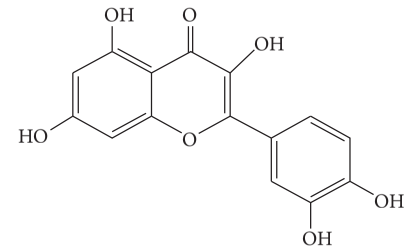	Flavonoid
11	Apigenin	*Artemisia lavandulaefolia* DC.	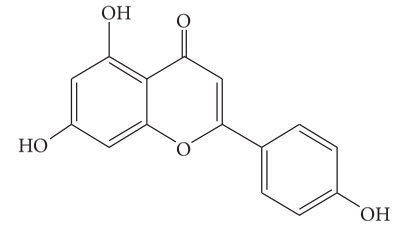	Flavonoid
12	Luteolin	*Artemisia lavandulaefolia* DC.	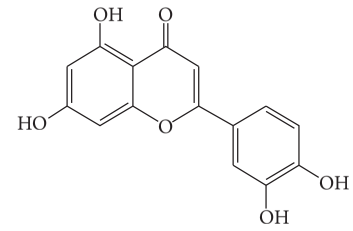	Flavonoid

	R1	R2	R3	R4	R5
5	H	Ac	Ang	Ang	H
6	H	Ac	Ang	Ac	OH
7	H	Ac	Ang	Ang	OH
8	Ac	H	Ang	Ac	OH
9	Ac	H	Ang	Ang	OH

Table 2: Continued.

	Chemical name	Botanical name	Compound structure	Structure type
13	Naringenin	Artemisia lavandulaefolia DC.	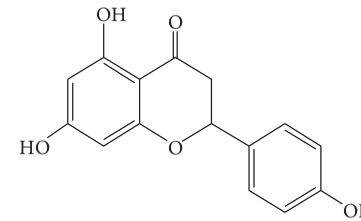	Flavonoid
14	Gitogenin	*Hosta plantaginea*	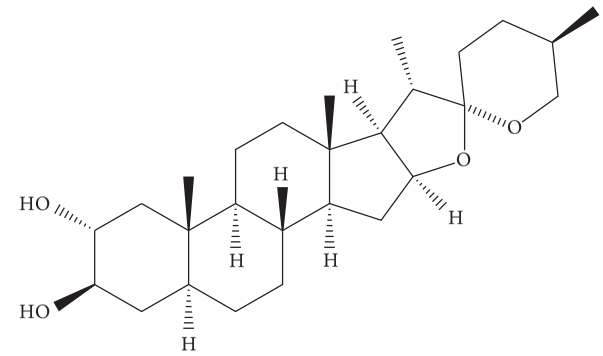	Steroidal saponin
15	Gitogenin3-O-β-dglucopyranosyl (1⟶2)-β-D-glucopyranosyl (1⟶4)-β-D-galactopy ranoside	*Hosta plantaginea*	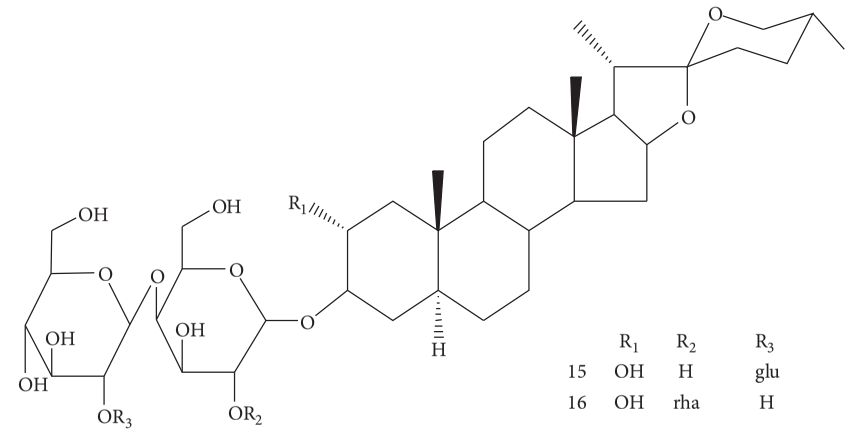	Steroidal saponin
16	Gitogenin3-O-β-D-glucopyranosyl (1⟶4)-O-[α-L-rhamnopyranosyl (1⟶2)]-β-D-galactopyranoside	*Hosta plantaginea*		Steroidal saponin
17	Gitogenin3-O- {β-D-glucopyranosyl (1⟶2)-O-[β-D-xylopyranosyl (1⟶3)]-O-β-D-glucoyranosyl(1⟶4)-β-D-galactopyranoside}	*Hosta plantaginea*		Steroidal saponin
18	Gitogenin3-O- {β-D-glucopyranosyl (1⟶2)-O- [α-L-rhamnopyranosyl (1⟶4)-β-D-xylopyranosyl(1⟶3)]-O-β-D-glucopyranosyl (1⟶4)-β-D-galactop ranoside}	*Hosta plantaginea*		Steroidal saponin

	R_1	R_2	R_3
15	OH	H	glu
16	OH	rha	H

Table 2: Continued.

	Chemical name	Botanical name	Compound structure	Structure type
19	Gitogenin 3-O-{β-D-xylopyranosy l(1⟶4)-β-D-glucopyranosyl (1⟶2)-[β-D-xylopy ranosyl (1⟶3)]-O-β-D-glucopyranosyl(1⟶4)-β-D-galactopyranoside}	*Hosta plantaginea*	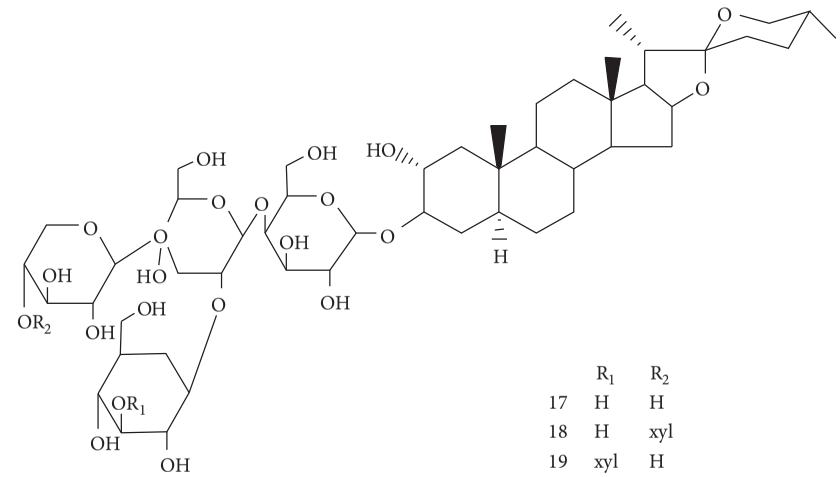	Steroidal saponin
20	—	*Hosta plantaginea*	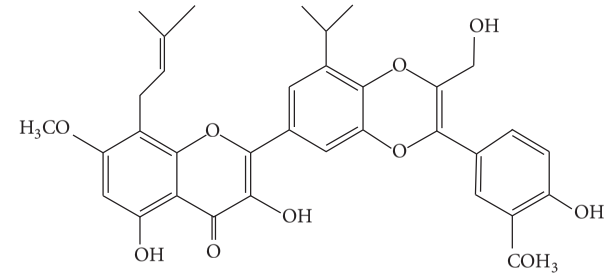	Flavonoid
21	—	*Hosta plantaginea*	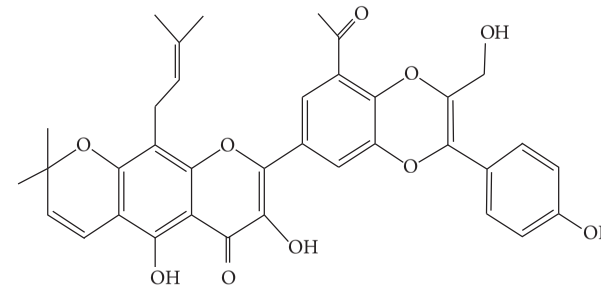	Flavonoid

3

Table 2: Continued.

	Chemical name	Botanical name	Compound structure	Structure type
22	—	*Hosta plantaginea*	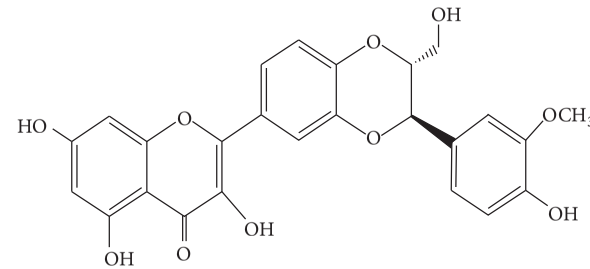	Flavonoid
23	—	*Hosta plantaginea*	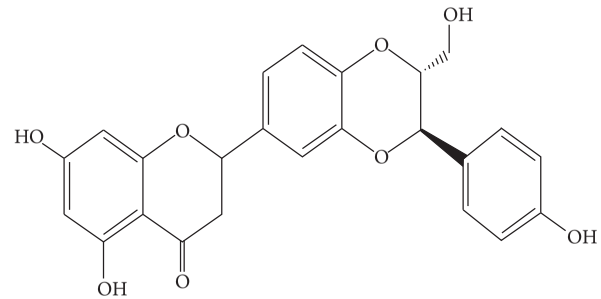	Flavonoid
24	Dehydrocostuslactone	*Artemisia frigida willd*	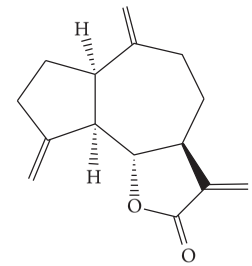	Sesquiterpenoid
25	Dihydrodehydrocostuslactone	*Artemisia frigida willd*	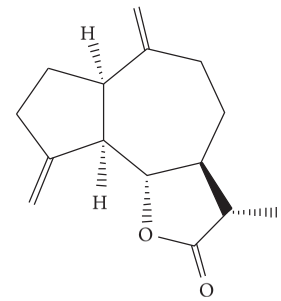	Sesquiterpenoid

Table 2: Continued.

	Chemical name	Botanical name	Compound structure	Structure type
26	Ursolic acid	*Hippophae rhamnoides* L.	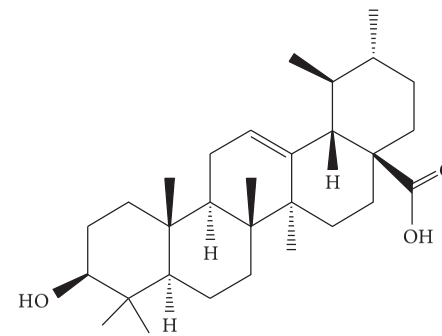	Triterpenoid
27	Isorhamnetin	*Hippophae rhamnoides* L.	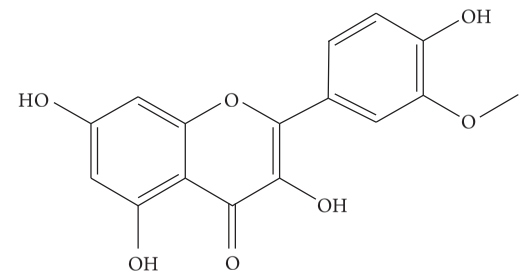	Flavonol aglycone

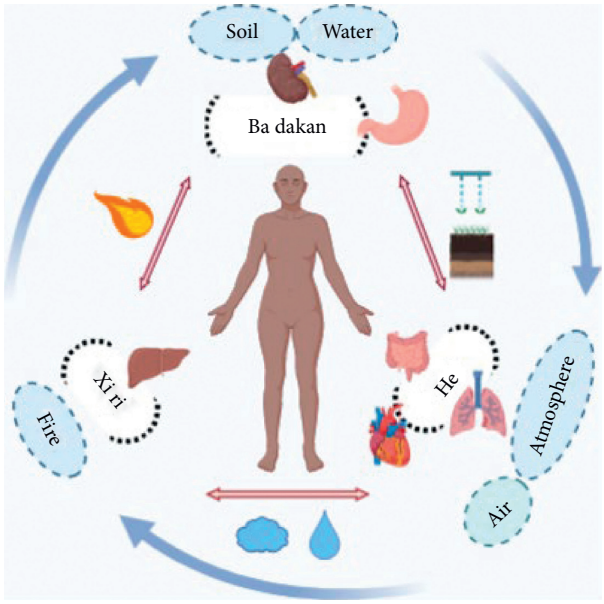

Figure 1: The concept of Mongolian medicine in treating diseases.

powder [21] can alleviate the symptoms of CCl_4-induced liver fibrosis in rats, which may be due to its ability to downregulate the serum transaminase and coordinate the MMPs/TIMPs system.

3.2. Honghua Qinggan 13 Flavors. Honghua Qinggan 13 flavors (HHQG) is from the Four Medical Tantras and is called "gurigumu-13," which is included in the "Pharmaceutical Standards of the Ministry of Health of the People's Republic of China" (Mongolian Medicines Volume) [41]. It is composed of *saffron*, *clove*, *lotus seeds*, *Radix Ophiopogonis*, *Radix aucklandiae*, *Melia toosendan*, *gardenia*, *lignum pterocarri*, *musk*, *pulvis cornus bubali concentratus*, *calculus bovis,* and *vermilion* and has the efficacy of clearing heat, detoxifying and cooling blood. At present, there are many studies on the liver-protecting pharmacological effects of single drugs in the prescription but few studies on the pharmacological effects and mechanism of the prescription. HHQG can be used to treat liver diseases [41, 42], including liver failure, drug-induced hepatitis, alcoholic liver, fatty liver, etc. [43]. HHQG exhibits a certain therapeutic effect on liver injury and fibrosis of rats caused by CCl_4, and the mechanism may be related to the antioxidant effect on regulating the activity of MMP-1 and TIMP-1 [22]. Hepatic fibrosis is the prophase lesion of cirrhosis and the key link in the progression of hepatocellular carcinoma. The anti-inflammation, free radical scavenging, antioxidant, activated HSC apoptosis, immune regulation, antiendotoxin, and other effects of the single drug were analyzed. The main mechanism of its antihepatic fibrosis may be through TGF-1/Smad and NF-κB signal transduction pathways [23]. Ruimin Li [24] discussed the relationship between hepatitis B virus tumor markers and liver cancer. HHQG can significantly decrease four tumor markers, including fetoprotein (AFP), A-L-fucoidase (AFU), R-glutamate transdermal enzyme (R-GT), and carcinoembryonic antigen (CEA) and reduce HBV-DNA, which indicates a lower cancer rate.

3.3. Changpu Siwei. Changpu Siwei is composed of *Galanga Rhizome*, *Halitum Purpureum*, *Vladimiriae Radix,* and *Acorus gramineus*. This prescription has the efficacy of suppressing "Ba dagan and He" and relieving asthma and pain, therefore, being used for oppression in the chest, dyspnea, indigestion, asthma, and pain in clinics [44]. In Mongolia, Changpu Siwei is named Shu da ge-4. It is included in the "Pharmaceutical Standards of the Ministry of Health of China (Mongolian Medicine)" [37]. The Ethanol and petroleum ether extracts of *Changpusiwei* exhibit prominent growth inhibitory effects on SMMC-7721 cells at 12.5~200 g/mL [25].

3.4. Empirical Prescriptions. There are many empirical prescriptions with obvious clinical efficacy [45], such as E ligeng-II, Safflower qinggan 13 flavors, et al. They are effective to treat liver pain and liver enlargement of liver cancer with the function of activating blood circulation, removing blood stasis, and relieving pain [46]. At present, the pharmacological mechanism of most Mongolian prescriptions used in clinics has not been studied. They are used according to pharmacopoeia and physicians' experience. Hepatoprotective Mongolian I and II are two empirical prescriptions commonly used to cure liver cancer.

3.4.1. Hepatoprotective Mongolian I. Hepatoprotective Mongolian I (HM I) is a complex mixture of 18 natural plants in which *Terminalia chebula* is the main ingredient. *Terminalia chebula,* due to its complicated components, has a wide range of pharmacological functions, including prevention and treatment of tumors [47]. Researchers [26] have demonstrated that HM I exhibited significant proliferation inhibition on Huh-7 cells and the mechanism involves cell cycle arrest and cell apoptosis promotion. In addition to the growth inhibition effect, the chemotherapy sensitization effect of HM I was also found. These results have great significance for the popularization and application of HM I against liver cancer in clinics.

3.4.2. Hepatoprotective Mongolian II. Hepatoprotective Mongolian prescription II (MPII) consists of 18 medicinal herbs. It has been reported that MPII [27] significantly inhibited the growth of human liver cancer cells Huh-7 and HepG2. At the molecular level, MPII induced cell apoptosis, arrested G0/G1 cell cycle phase, and promoted expressions of caspase-3, caspase-8, caspase-9, and cytochrome c in Huh-7 and HepG2 cells. *In vivo*, MPII dramatically inhibited human liver cancer growth in a xenograft model in Kunming mice with no apparent cytotoxicity to the hosts. When combined with 5-FU, MPII decreased the toxicity of 5-FU on liver cancer cells. These results have suggested that MPII might have the potential to be a powerful therapy in liver cancer.

4. Monomer Compounds and Extracts

Commonly used medicines for removing stasis and stagnation in Mongolian medicine include *Monetariae concha*, *Concha Mauritiae*, *Clematis aethusifolia Turcz.*, *Clematis intricata Bunge*, *Ranunculus sceleratus L.*, *Parnassia palustris L.*, *GnaphaliumaffineD. Don,* etc. They are used to treat food stagnation, all kinds of "Pi kuai," carbuncle swelling caused by metabolic disorders, and the accumulation of scum and essence [35]. Here, we summarize the common drugs and monomers for the treatment of liver cancer.

4.1. Terminalia chebula (Terminalia chebula Retz). *Terminalia chebula* is the dried ripe fruit of *Terminalia Chebula Retz.* or *Terminalia Chebula Retz. var. tomentella Kurt* which belongs to the family of *Combretaceae R. Br*. It is not only used in Mongolian medicine, Chinese medicine, and Tibetan medicine in China but also used in other countries such as India and Iran. It is included in the "pharmacopoeia of the People's Republic of China," which has the efficacy of restraining "Xiri," astringent trauma, promoting tissue regeneration, and assisting digestion, and detoxication [35]. Mongolian doctors believe that *Terminalia chebula* can cure all kinds of toxicities [48]. Modern pharmacological research has shown that *Terminalia chebula* can be used for asthma, inflammation, neurological disorders, and wound infection and be frequently used as a part of many preparations to treat a variety of diseases; therefore, it is known as "the king of medicine" [49]. Pentagalloyl glucose (PGG, 1) is a natural polyphenol from *Terminalia chebula*. It has been reported that PGG has anticancer activity in ovarian cancer and nasopharyngeal carcinoma [50]. Researchers [51] have suggested that PGG can inhibit the proliferation, migration, and invasion of HepG2 cells and induce cell cycle G1 phase arrest and cell apoptosis. The combination of PGG and 5-FU shows a synergistic effect on the reversal of the aggressive phenotypes of HepG2 cells. PGG has the potential to be used to treat liver cancer in clinics. Chebulagic acid (2) is a benzopyran tannin obtained from *Terminalia chebula*. The combination of Chebulagic acid and doxorubicin shows strong synergism in inhibiting liver cancer cell growth. Furthermore, Chebulagic acid can enhance the sensitivity of HepG2 cells to doxorubicin, thus showing anticancer effects against liver cancer [52]. Chen et al. [53] have found that ethyl acetate extract of *Terminalia chebula* can mediate the gene expression of Fas/FasL family through an exogenous pathway, thus inducing the apoptosis of immortalized rat hepatic stellate cells. Reversing liver fibrosis can effectively prevent the development of liver cancer [54]. The ethyl acetate extract of *Terminalia chebula* can effectively reverse the development of liver fibrosis and, to some extent, prevent liver cancer. The water extract of *Terminalia chebula* can obviously inhibit the proliferation activity of liver cancer cells [55] (Figure 2).

4.2. Safflower (Carthamus tinctorius L.). Safflower is the dry flower of *Compositae Carthamus tinctorius L*. The Mongolian medicine canonical "Classic Canon of Mongolian Materia Medica" [56] has recorded that safflower can remove liver heat, regulate menstruation, detumescence, and stop bleeding. It has long been used in Mongolian medicine and traditional Chinese medicine [57, 58]. This herbal medicine is clinically compatible with other drugs for the treatment of hepatomegaly, liver damage, and irregular menstruation. Safflower yellow B (SYB, 3) is one of the main bioactive constituents of safflower. Sharula et al. [59] have proposed SYB to be a promising therapeutic compound for liver cancer as they found that SYB inhibited cell proliferation and promoted cell apoptosis mainly through miR-34a/P53/caspase-9 axis in HepG2 cells, demonstrating the clinical application value of SYB in liver cancer treatment.

Hydroxysafflor yellow A (HSYA, 4), a water-soluble chalcone from safflower, is frequently studied previously for its neuroprotective effect in cerebrovascular and neurodegenerative diseases. Recently, the positive action of HSYA in the prevention of liver damage caused by chemicals or alcohol and the anticancer effect of HSYA in various types of cancers are also reported. HSYA inhibited proliferation, migration, and induced apoptosis through suppressing p38MAPK signaling in HepG2 cells [60]. Another research has shown that HSYA induced autophagy by promoting the expression of Beclin 1 and inhibited the phosphorylation of ERK in liver cancer cells [58]. These findings provide experimental evidence that HSYA might be a promising anticancer agent for HCC (Figure 3).

4.3. Xanthoceras sorbifolia Bunge. *Xanthoceras sorbifolia* Bunge, which belongs to Sapindaceae, has been used as TCM for curing arterial sclerosis, hyperglycemia, hyperpiesia, chronic hepatitis, rheumatism, and enuresis of children [61, 62]. The chemical constituents and pharmacological activities of its branches, leaves, flowers, stalks, kernels, shells, and wood have been studied by scholars at home and abroad. The wood, branches, and leaves have been used in Mongolian medicine and are thought to have significant effects on drying "Xiri," clearing heat, and relieving swelling and pain. Lili Yu [61] isolated some triterpenoid saponins from the seed oil leavings of *X. sorbifolia* Bunge and found cytotoxicity of these compounds on several human cancer cell lines. Compounds 5 ($IC_{50} = 2.45 \pm 0.58\,\mu M$) and 7 ($IC_{50} = 4.03 \pm 0.75\,\mu M$) show significant activity against $HepG_2$ cell line, while compounds 6 ($IC_{50} = 22.20 \pm 1.92\,\mu M$), 8 ($IC_{50} = 60.83 \pm 0.94\,\mu M$) and 9 ($IC_{50} = 33.11 \pm 2.21\,\mu M$) exhibit moderate activity against HepG2 cell line (Table 2). Extracts from the *X. sorbifolia* Bunge exhibit cytotoxicity toward various human cancer cell lines [63, 64]. Meanwhile, TSXS could lead to apoptosis by stimulating the cells to produce oxidative stress (Figure 3). Total saponins from *X. sorbifolia* Bunge (TSXS) induced apoptosis of HepG2 cells through mitochondria-mediated apoptosis pathway and arrested the cell cycle at the S phase [63]. Polyphenols from the Husks of *X.Sorbifolia* exhibited anticancer and radical-scavenging effects in several cancer cells [64]. The results of these studies provide a theoretical basis for further development of *X. sorbifolia* Bunge.

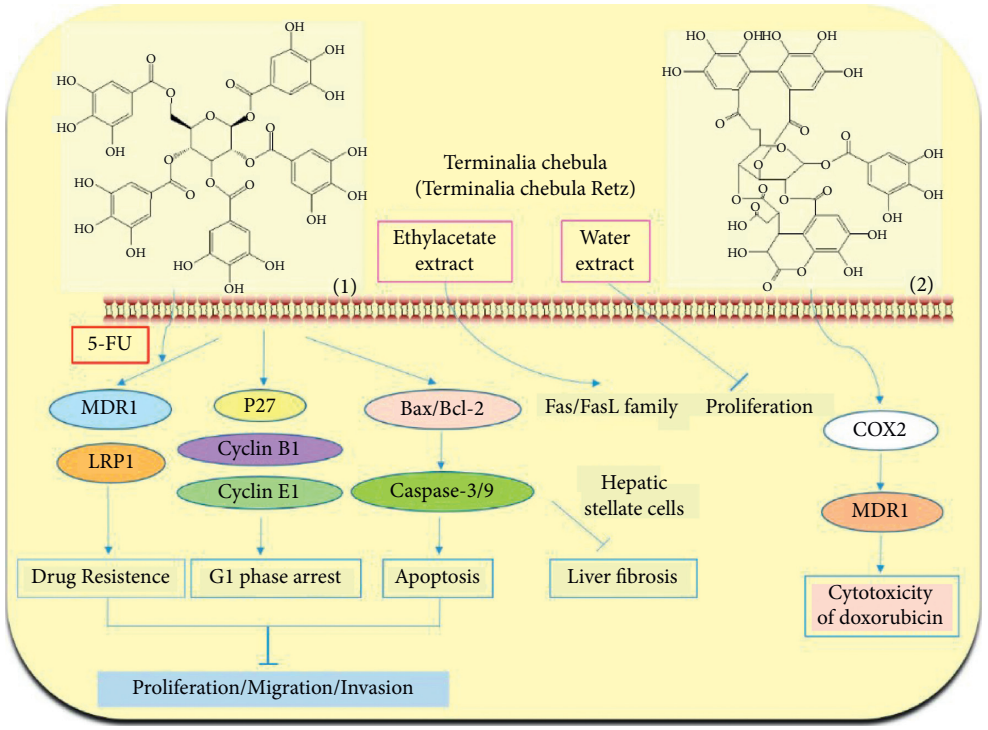

Figure 2: The anticancer mechanism of *Terminalia chebula* in liver cancer.

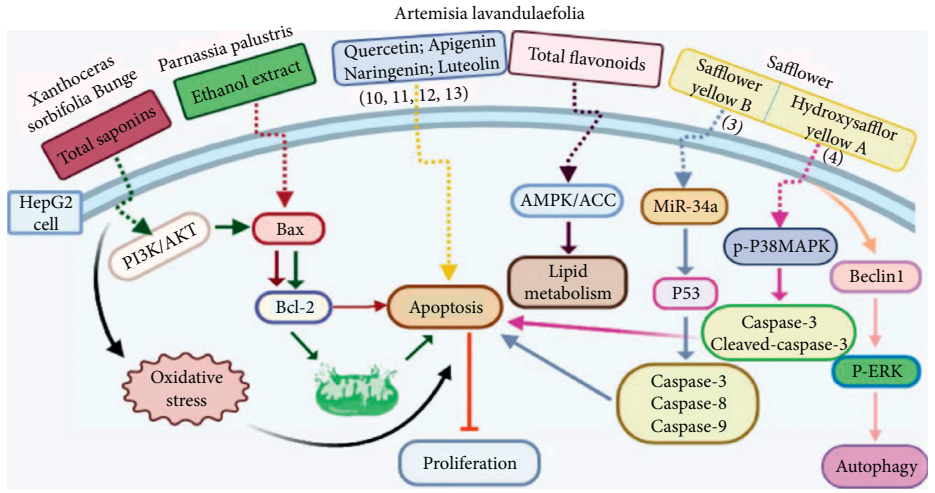

Figure 3: The anticancer mechanism of monomer compounds and extracts in liver cancer.

4.4. Parnassia palustris. Parnassia palustris is the whole herb of *Parnassia palustris* Linn. It is commonly used for clearing heat, detoxifying, reducing swelling and eliminating abscess during the treatment of various diseases, such as Jaundice hepatitis, laryngitis, mumps, vasculitis, tuberculosis, and cancers [65, 66]. It has been demonstrated that the ethanol extract of *Parnassia palustris* significantly inhibited the proliferation of HepG2 cells and, by detecting apoptosis-related proteins, the underlined mechanism might involve apoptosis promotion [67, 68] (Figure 3).

4.5. Artemisia lavandulaefolia DC

Artemisia lavandulaefolia DC. is used in traditional Mongolian medicine as a perennial herb that is widely distributed in Inner Mongolia of China. It is a member of Artemisia compositae, with expelling cold, clearing damp, warming, and activating meridian, halting bleeding, antibacteria, antiallergy, anticancer effects, and it is commonly used in formulae, such as TGLG-1 [69, 70]. Modern pharmacology research has shown that

extracts and compounds from *A. lavandulaefolia* exhibited potential anticancer activities. Quercetin (10) and apigenin (11) which are isolated from *A. lavandulaefolia* [71] displayed apoptosis promotion effect in HepG2 cells. Meanwhile, four kinds of flavonoid glycosides, including luteolin (12), naringenin (13), quercetin, and apigenin, from *A. lavandulaefolia* could inhibit the proliferation of HepG2 cells [72]. The total flavonoids of *A. lavandulaefolia* activated the AMPK-ACC pathway in HepG2 cells, therefore participating in the lipid metabolism of HepG2 cells [73] (Figure 3).

4.6. Flowers of Hosta plantaginea. Hosta is a genus of the Liliaceae family. There are four primitive species in China, *H. plantaginea*, *H. ventricosa*, *H. ensata*, and white *H. albofarinosa* [74]. *H. plantaginea* is a landscaping plant and an annual herb widely distributed in temperate and subtropical Asia, including China, Japan, North Korea, and the far east of Russia, mostly cultivated. The dried flowers of *Hosta plantaginea* as Mongolian medicine were documented in "Chinese Materia Medica Mongolian medicine roll." It possesses diuresis detumescence, heat-clearing, and detoxicating, hemostasis, and anti-inflammatory effects [48]. *H. ventricosa* was also recorded in "Chinese Materia Medica Mongolian medicine roll," with cooling blood and hemostasis and detoxicating effects. The whole plant of *H. ventricosa* is used as medicine [37]. Studies [75] have indicated that the total saponins of *H. ventricosa* (TSHV) could effectively inhibit the proliferation of HepG2 cells *in vitro* with an IC_{50} value as 17.37 μg/L. Pharmacological and chemical studies on *H. plantaginea* have suggested that the alcohol extract and some compounds showed antibacterial [76], ant-fungal [77], anti-inflammatory [78, 79], analgesic [80], and anticancer effects [78], etc. The cytotoxic effect of four monomer compounds isolated from the flowers of *H. plantaginea* has been studied [81]. Among these compounds, compound Gitogenin (14) selectively inhibited the proliferation of cancer cells, including K562, YAC-1 and SMMC-7721 cell lines, and the IC_{50} of compound (14) in SMMC-7721 is 2.84 μg/ml. The steroidal saponins of *H. plantaginea* showed cytotoxicity on various cancer cell lines and these anticancer effects are cell type dependent [82]. Compounds (15), (16), (17), (18), and (19) displayed strong inhibitory effects on human liver cancer cells (HepG2) with IC_{50} values ranging from 0.16 mol/L to 1.16 mol/L, which are equivalent to or stronger than the effect of cisplatin, a positive drug in the experiment. Wei et al. [83] isolated and identified some flavonoids from *H. plantaginea* (Lam.) Aschers. They examined the hepatoprotective activity of these flavonoids on CCl_4-induced injury of human L-O2 cells and found that compounds (20), (21), (22), and (23) exhibited moderate hepatoprotective activities.

4.7. Artemisia frigida Willd. Artemisia frigida belongs to *Artemisia* (Compositae). It has been used for hundreds of years as a Mongolian traditional herbal medicine which is widely distributed in the Inner Mongolia Autonomous Region of China [84]. It is also named Xiaobaihao or Hanhao in Chinese and "Agi" in Mongolian. After flowering, the aboveground part of *A. frigida* is harvested, dried in the shade, and ground into powder. It is used for the treatment of various bleeding, kidney fever, irregular menstruation, sores, and Carbuncle pains [85, 86]. Researchers [87] have found five sesquiterpenoids from *A. frigida* and these compounds exhibited obvious inhibitory effects on human cancer cells. One of the compounds, dehydrocostuslactone (24) exhibited significant inhibition in HLE cells with the IC_{50} of 22.50 μM/L. Dihydrodehydrocostuslactone (25) possessed moderate inhibition in human cancer cells only in high concentration treatment. Unsaturated lactone is the essential functional group of sesquiterpene lactones which inhibited the proliferation of cancer cells.

4.8. Sea Buckthorn (Hippophae rhamnoides L.). Sea buckthorn is the fruit of *Hippophae rhamnoides* L. which is a wild berry plant characterized by multiple economic advantages and versatile properties. *H. rhamnoides* L. is a kind of "medicine and food homologous" plant with high utilization value. Sea buckthorn is commonly used in Mongolian medicine to cure cough, sputum, pulmonary tuberculosis, pulmonary abscess, and lung cancer according to its effects of relieving cough, eliminating phlegm, suppressing "Badakan," and promoting digestion. Sea buckthorn consists of more than 100 kinds of bioactive compounds, including essential amino acids, vitamins, trace elements, tocopherols, carotenoids, polyphenols, flavones, and other active substances [48, 88]. Ursolic acid (26), extracted from *H. rhamnoides* L., has been reported to increase IL-12 and TNF-α [89], activate cell immunity, and further inhibit angiogenesis, finally showing anticancer effect against liver cancer in vivo. Grey et al. [90] have performed a sequential extraction and found that ethanol: water extract of sea buckthorn exerted the strongest proliferation inhibitory effect in HepG2 cells. The 80% ethanol reflux extracts of sea buckthorn fruit, stem, and leaf showed different degrees of anticancer effect on mouse hepatocellular carcinoma H22 tumor strains [91]. Flavonoids from oil-removed seeds of *H. rhamnoides* (FSH) could inhibit cell proliferation and induce cell apoptosis in a dose-dependent manner (200~1200 μg/mL) in BEL-7402 cells [92]. Isorhamnetin (27), a flavonol aglycone, was isolated from *H. rhamnoides* L. and showed cytotoxicity on BEL-7402 cells dose- and time-dependently, with IC_{50} of 74.4 ± 1.13 μg/ml [93]. The mechanism of this cytotoxicity in response to isorhamnetin (50 μg/ml, 48 h) might involve its apoptosis promotion effect (Figure 4).

5. Discussion

Currently, the progress of liver cancer clinical treatment has been few and far between. Due to the rapid development of the disease, most of the patients are in the middle and late stage or even have metastases at the time of clinical diagnosis and could not be treated with radical resection [94].

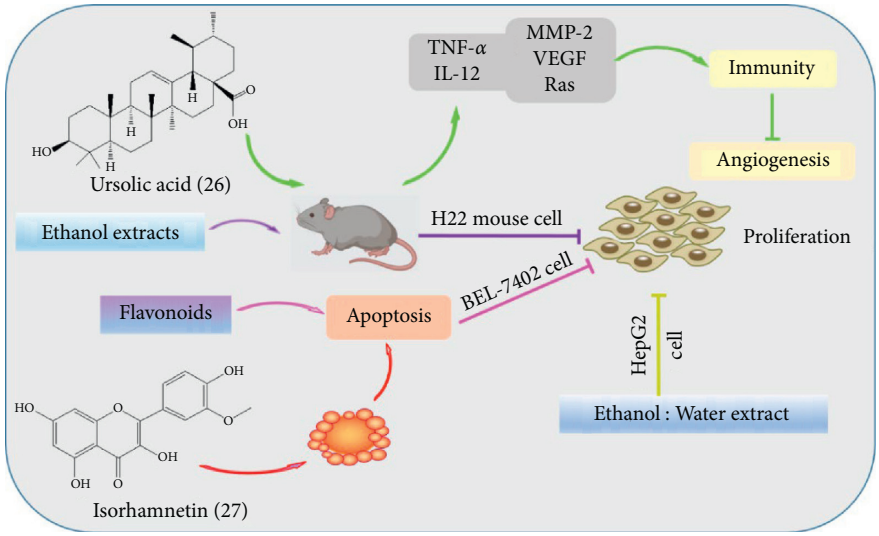

Figure 4: The anticancer mechanism of Sea buckthorn in liver cancer.

Therefore, it is urgent to find more promising treatment strategies.

Mongolian medicine is not only an important part of Chinese traditional medicine but also a treasure of Chinese traditional culture and national intangible cultural heritage. It has important medicinal and academic value. The main drugs (prescriptions) used in the treatment of tumors in Mongolian medicine contain ruyijiedu pill, jisiwunisi-25 pill, hualiu pill, Zhuangxi Power, gamujur, habuder-9 powder, susi-12 powder, etc. Naren mandu la -11 [95, 96] and Aili gen-II are clinical prescriptions commonly used to treat liver cancer and have been proved to be effective in liver cancer therapy. Notably, the research on Mongolian medicine mostly stays at the original treatment level, while the research on the underling mechanism is relatively less. Most of the studies focus on the anticancer activities of monomer compounds obtained from Traditional Mongolian Medicine. However, studies on the activity and mechanism of formulae are few. Furthermore, most experiments evaluating anticancer mechanism of Traditional Mongolian Medicine are just conducted on cancer cell models in vitro. The proofs in vivo are limited [6]. At present, the bottleneck in the development of Mongolian medicine lies in the fact that Mongolian medicine is not well known by the vast majority of people in China so it just plays roles in a relatively small scope. Therefore, further in-depth research of the anticancer mechanism of Mongolian medicine in liver cancer and close combination of the basic research with clinical application is urgently required.

6. Conclusions

Mongolian medicine has been used for a long history to prevent or treat various diseases, including liver cancer. It shows mild and lasting pharmacological effects with multiple advantages: amelioration of sensory symptoms, improvement of the quality of life, prolongation of overall survival and, to some extent, low side effects. This review provides a comprehensive summary of Traditional Mongolian Medicine, with the purpose of finding promising drugs to treat liver cancer and expanding the clinical application of Traditional Mongolian Medicine in liver cancer therapy.

Data Availability

All data used to support the findings of this study are included within the article.

Disclosure

Xiaomei Bao and Lu Chen share first authorship.

Conflicts of Interest

The authors declare no conflicts of interest.

Authors' Contributions

Xiaomei Bao and Lu Chen have contributed equally to this work. YQ contributed to conception and design. XB searched the literature. XB, LC, and YQ wrote the manuscript. YL, HS, KW, YL, TQ, and YL drafted and critically revised the work. All authors read and approved the final manuscript.

Acknowledgments

This work was supported by grants from the National Natural Science Foundation of China (no. 81973570 to Y. Qiu), and the authors thank the same.

References

[1] H.-Y. Lee and I.-S. Hong, "Targeting liver cancer stem cells: an alternative therapeutic approach for liver Cancer," *Cancers*, vol. 12, no. 10, p. 2746, 2020.

[2] S. K. Asrani, J. Mellinger, J. P. Arab, and V. H. Shah, "Reducing the global burden of alcohol-associated liver disease: a blueprint for action," *Hepatology*, vol. 73, no. 5, pp. 2039–2050, 2020.

[3] S. Maruta, S. Ogasawara, Y. Ooka, M. Obu, and N. Kato, "Potential of lenvatinib for an expanded indication from the reflect trial in patients with advanced hepatocellular carcinoma," *Liver Cancer*, vol. 9, no. 4, pp. 1–15, 2020.

[4] T. F. Greten, C. W. Lai, G. Li, and K. F. Staveley-O'Carroll, "Targeted and immune-based therapies for hepatocellular carcinoma," *Gastroenterology*, vol. 156, no. 2, pp. 510–524, 2019.

[5] Z. Zhu, T. Wang, D. Fu, Y. Gui, J. Wang, and T. Cui, "Innovative development path of ethnomedicines: an overview of ethnomedicines in China," *Frontiers of Medicine*, vol. 10, no. 2, pp. 166–177, 2016.

[6] H. S. Peng, L. P. Cha, S. Y. Gui et al., "Current situation and Thinking of basic research and discipline construction of Mongolian medicine," *Bulletin of National Natural Science Foundation of China*, vol. 09, no. 03, pp. 1–8, 2020.

[7] Y. F. Xiao, F. H. Chang, X. Y. Qian, N. Wang, and Y. Q. Han, *Present Situation and Development of Mongolian Medicine*, pp. 93–98, Chinese Society of Toxicology, Hangzhou, China, 2019.

[8] Y. M. Qiao, *A Comparative Study of Chinese and Mongolian Medicine*, Beijing University of Chinese Medicine, Beijing, China, 2013.

[9] H. Y. Tong, X. H. Bai, and X. M. Gao, "Comparative researches on the application of Chinese medicine and Mongolian medicine," *China Journal of Traditional Chinese Medicine and Pharmacology*, vol. 11, pp. 1018–1021, 2008.

[10] C. H. Zhang, D. Man, G. D. Wu et al., "Protection, exploitation and utilization states of specialized Mongolian folk medicine resources and related development strategy," *China Journal of Chinese Materia Medica*, vol. 40, no. 05, pp. 771–777, 2015.

[11] C. X. Liang, "On the compiling and editing features and significance of Tibetan medical classic "the four medical classics"," *Journal of Minzu University of China (Philosophy and Social Sciences Edition)*, vol. 37, no. 02, pp. 108–112, 2010.

[12] W. qimuge and Qiqige, "Brief introduction to the historical origin of Mongolian medicine," *Journal of Medicine & Pharmacy of Chinese Minorities*, vol. 18, no. 12, pp. 60–62, 2012.

[13] C. M. Bai and S. H. Shi, "On the formation, development and prospect of Mongolian medicine," *Journal of Medicine & Mharmacy of Chinese Minorities*, vol. 04, pp. 43-44, 2004.

[14] H. S. Bao, "Jambaldorj and research on herbal medicines in the classic Canon of Mongolian Materia Medica," *Journal of Traditional Chinese Medical Literature*, vol. 28, no. 01, pp. 24–26, 2010.

[15] H. S. Bao, "On contribution of Jambaldorj to the development of Mongolian medicine," *Chinese journal of medical history*, vol. 01, pp. 29–32, 2010.

[16] C. H. Liu, W. Z. Hu, Y. B. He, A. L. Jiang, and G. K. Xu, "Development history and research progress on Mongolian Medicine," *Journal of Anhui Agriculture Science*, vol. 40, no. 22, pp. 11476–11478, 2012.

[17] B. Khandarmaa, *Literature Research on the Influence of Traditional Mongolian Medicine Bloodletting Therapy in the "The Four Medical Tantras"*, Beijing University of Chinese Medicine, Beijing, China, 2020.

[18] Q. Q. Chen, "Research on the medical exchange between han people and Tibetan people in ancient times," *Chinese Medicine and Culture*, vol. 15, no. 04, pp. 61–69, 2020.

[19] H. Y. Ge and J. Hao, "Effect of Qinggan Jiuwei san, a Mongolia herbal medicine,on serum TIMP-1 levels in treatment of patients with alcoholic hepatitis," *Journal Practice Hepatology*, vol. 19, no. 06, pp. 720-721, 2016.

[20] H. Y. Ge, S. H. Zhang, B. S. Zhao, and C. K. Yu, "Clinical effect of Mongolian medicine Qinggan Jiuwei powder in treatment of alcoholic liver fibrosis," *Journal Clinical Hepatology*, vol. 33, no. 12, pp. 2316–2320, 2019.

[21] H. Y. Ge, A. Q. Wang, L. Gao, and Y. X. Li, "Effects and mechanisms of Qinggan jiuwei powder on the liver fibrosis in rats," *Chinese Journal of Clinical Pharmacology*, vol. 35, no. 22, pp. 2859–2862, 2019.

[22] T. Bao, "Research Progress on mechanisms of Honghua Qinggan 13 flavors for primary liver cancer and its metastasis," *Chinese Community Doctors*, vol. 34, no. 36, p. 8+10, 2018.

[23] T. Bao, "Study on the mechanism of Mongolian medicine honghua-13 in treating hepatic fibrosis," *World Latest Medicine Information (Electronic Version)*, vol. 18, no. 80, pp. 239-240, 2018.

[24] R. M. Li and J. B. Liu, "Effect of Honghua Qinggan-13 on tumor markers of liver cancer," *Journal of Medical Forum*, vol. 03, p. 79+81, 2007.

[25] L. L. Bao, Y. X. Wang, J. Q. Bao, X. Jia, and Y. Dong, "Study the effect of Mongolian medicine Changpusiwei on human hepatoma cells in vitro," *Journal of Inner Mongolia Medical University*, vol. 33, no. 06, pp. 495–498, 2011.

[26] A. Nanda, S. Qimuge, J. R. Bao, and X. L. Su, "Study on the role and mechanism of Hepatoprotective Mongolian I on hepatocellular carcinoma Huh-7 cells," *China Medical Herald*, vol. 12, no. 35, pp. 26–30, 2015.

[27] A. Nanda, Q. Suyila, L. Xian, and S. Xiulan, "Hepatoprotective Mongolian prescription II enhances the antitumor effects of chemotherapeutics in hepatocellular carcinoma xenografts," *Pathology, Research & Practice*, vol. 213, no. 5, pp. 531–540, 2017.

[28] L. W. Han, "Characteristics and innovation in projects of ethnomedicine and ethnopharmacology funded by National Natural Science Foundation of China," *China Journal of Chinese Materia Medica*, vol. 40, no. 17, pp. 3379–3384, 2015.

[29] G. B. Zhu, "The practical significance of developing Chinese national medicine," *Shanghai Journal of Traditional Chinese Medicine*, vol. 35, no. 10, pp. 4–6, 2001.

[30] J. Mude, *Basic Theory of Mongolian Medicine"*, Inner Mongolia University Press, Hohhot, China, 3rd edition, 2014.

[31] L. Y. Wu and L. Guo, "Understanding of the holism theory in both of TCM and Mongolian medicine," *Chinese Journal Traditional Chinese Medicine Pharmacology*, vol. 33, no. 12, pp. 5412–5414, 2018.

[32] A. Gl, "Unique Mongolian medicine," *China news of traditional Chinese medicine*, vol. 09, no. 14, 2015.

[33] X. H. Zhu, L. T. Yi, and M. H. Li, "Status analysis and strategic thinking on Mongolian medicine standardization," *China Journal of Chinese Materia Medica*, vol. 33, no. 12, pp. 5412–5414, 2018.

[34] Yu Tuo, Y. Gongbu, *The Four Medical Tantras*, The Tibet People's Publishing House, Lhasa, China, 1982.

[35] S. Zhabu and S. Bilige, *Encyclopedia of Chinese Medicine-Mongolian Medicine*, Science and Technology Press, Shanghai, China, 1992.

[36] A. Gula, *Traditional Therapy and Modern Research of Mongolian Medicine*, Inner Mongolia People's Publishing House, Hohhot, China, 2006.

[37] National Pharmacopoeia Committee of People's Republic of China, *Drug Standard of the Ministry of Health of the People's Republic of China (Mongolian Medicine Volume)*, People's Medical Publishing House, Beijing, China, 1998.

[38] Ba Gena, *Mongolian Medicine Prescription*, Inner Mongolia People's Publishing House, Hohhot, China, 2007.

[39] S. D. Minicis, M. Marzioni, A. Benedetti, and G. Svegliatibaroni, "New insights in hepatocellular carcinoma: from bench to bedside," *Annals of Translational Medicine*, vol. 1, no. 2, 2013.

[40] X. B. Chen, "Changes in expression of MMP-1 and its inhibitor TIMP-1 in rat hepatic fibrosis," *Chinese Journal of Histochemistry and Cytochemistry*, vol. 21, no. 03, pp. 274–278, 2012.

[41] Pharmacopoeia Committee of the Ministry of Public Health, *Pharmaceutical Standards of the Ministry of Health, PRC (Mongolian Medicine)*, People's Medical Publishing House, Beijing, China, 1998.

[42] China Inner Mongolia Autonomous Region Food and Drug Administration (NMFDA), *Drug Instructions of Honghua Qinggan 13 Flavors*, Inner Mongolia, China, 1998.

[43] H. X. Yang, Y. F. Bai, L. Chang et al., "The effect of honghuaqinggan-13 on liver injury fibrosis induced by CCl_4 in rats," *Northwest Pharmaceutical Journal*, vol. 33, no. 03, pp. 349–352, 2018.

[44] X. L. Zhu, F. Bai, B. X. Li, J. Xu, and Y. Dong, "Study on anticancer mechanism of Mongolian medicine Shudage-4 based on network pharmacology," *Chinese Journal of Traditional Chinese Medicine Pharmacology*, vol. 35, no. 07, pp. 3618–3622, 2020.

[45] O. urigi, *Traditional Mongolian Medicine and Prescription*, Inner Mongolia Science and Technology Press, Chi feng, China, 2013.

[46] A. latengtuya and Sa erna, "Clinical observation of Mongolian medicine in the treatment of primary liver cancer," *Chinese Medicine Modern Distance Education of China*, vol. 5, no. 8, pp. 24-25, 2006.

[47] B. Anwesa, S. K. Bhattacharyya, and R. R. Chattopadhyay, "The development of Terminalia chebuLa Retz (Combretacae) in clinical research," *Asian Pacific Journal of Tropical Biomedicine*, vol. 3, no. 3, pp. 244–252, 2013.

[48] National Administration of Traditional Chinese Medicine, *Chinese Materia Medica, Mongolian Medicine*, Shanghai Science and Technology Press, Shanghai, China, 3rd edition, 2009.

[49] U. Pingali, D. Sukumaran, and C. Nutalapati, "Effect of an aqueous extract of Terminalia chebula on endothelial dysfunction, systemic inflammation, and lipid profile in type 2 diabetes mellitus: a randomized double-blind, placebo-controlled clinical study," *Phytotherapy Research*, vol. 34, no. 12, pp. 3226–3235, 2020.

[50] D. Y. Shi, X. B. Jin, H. F. Mei, M. Y. Liu, and J. Y. Zhu, "Effect of pentagalloylglucose on expression of apoptosis regulator genes and caspase-dependent apoptosis pathways in HO-8910 cells," *Chinese Journal of Pharmacology and Toxicology*, vol. 26, no. 04, pp. 534–539, 2018.

[51] X. Q. Ding, S. Zhao, J. Y. Wang, H. C. Zheng, and C. M. Ma, "Inhibitory effects and molecular mechanisms of pentagalloyl glucose in combination with 5-FU on aggressive phenotypes of HepG2 cells," *Natural Product Research*, vol. 10, no. 04, pp. 1–4, 2019.

[52] C. Achari, G. V. Reddy, T. C. M. Reddy, and P. Reddanna, "Chebulagic acid synergizes the cytotoxicity of Doxorubicin in human hepatocellular carcinoma through Cox-2 dependant modulation of MDR-1," *Medicinal Chemistry*, vol. 7, no. 5, pp. 432–442, 2011.

[53] Y.-X. Chen, J. Tong, L.-L. Ge, B.-X. Ma, J.-S. He, and Y.-W. Wang, "Ethyl acetate fraction of Terminalia bellirica fruit inhibits rat hepatic stellate cell proliferation and induces apoptosis," *Industrial Crops and Products*, vol. 76, pp. 364–373, 2015.

[54] Q. Wang, Y. Zhu, F. X. Long et al., "Advances in animal models of precancerous liver cancer," *Hunan Journal of Traditional Chinese Medicine*, vol. 33, no. 8, pp. 212–214, 2017.

[55] Z. Q. Bao, *The Inhibition of Lung Cancer and Liver Cancer Cells and Ascites Tumor Cells by Terminalia Chebula Water Extract*, Inner Mongolia Medical University, Hohhot, China, 2011.

[56] Jambaldorj, *The Mongolian Medicine Canonical*, Inner Mongolia People's Publishing House, Hohhot, China, 2006.

[57] T. Yamazaki, A. Nakamori, E. Sasaki, S. Wada, and O. Ezaki, "Fish oil prevents sucrose-induced fatty liver but exacerbates high-safflower oil-induced fatty liver in ddy mice," *Hepatology*, vol. 46, no. 6, pp. 1779–1790, 2010.

[58] Z. Chen, L. Liu, Y. Liu et al., "Hydroxysafflor yellow A induces autophagy in human liver cancer cells by regulating Beclin 1 and ERK expression," *Experimental and Therapeutic Medicine*, vol. 19, no. 4, pp. 2989–2996, 2020.

[59] S. Sharula and Z. J. Wu, "Regulation of apoptosis by SYB in HepG2 liver cancer cells is mediated by the P53/caspase 9 Axis," *Anti-Cancer Agents in Medicinal Chemistry*, vol. 17, no. 7, pp. 941–947, 2017.

[60] J. Zhang, J. Li, H. Song, Y. Xiong, D. Liu, and X. Bai, "Hydroxysafflor yellow A suppresses angiogenesis of hepatocellular carcinoma through inhibition of p38 MAPK phosphorylation," *Biomedicine & Pharmacotherapy*, vol. 109, pp. 806–814, 2019.

[61] L. Yu, X. Wang, X. Wei et al., "Triterpenoid saponins from Xanthoceras sorbifolia Bunge and their inhibitory activity on human cancer cell lines," *Bioorganic & Medicinal Chemistry Letters*, vol. 22, no. 16, pp. 5232–5238, 2012.

[62] B. Luo, F. Cheng, F. L. Li, and K. Zou, "Studies on the chemical constituents of the spermoderm of Xanthoceras sorbifolia Bunge," *Lishizhen Medicine and Materia Medica Research*, vol. 06, pp. 1329-1330, 2007.

[63] Z. Y. Zhang, *Effect and Molecule Mechanism of Total Saponins from Xanthoceras Sorbifolia Bunge Kernel on Apoptosis in HepG2 Hepatoma Cells*, Shanxi Normal University, Nanchang, China, 2017.

[64] C.-Y. Yang, W. Ha, Y. Lin, K. Jiang, J.-L. Yang, and Y.-P. Shi, "Polyphenols isolated from Xanthoceras sorbifolia Husks and their anti-tumor and radical-scavenging activities," *Molecules*, vol. 21, no. 12, p. 1694, 2016.

[65] B. Luo, *Mongolian Pharmacy*, pp. 459-460, The Ethnic Publishing House, Beijing, China, 1989.

[66] O. urigi and B. Bater, *Traditional Mongolian Medicine and Prescription*, Inner Mongolia Science and Technology Press, Hohhot, China, 2013.

[67] Y. Hong, L. Da, and Y. Xin, "Study on the effect of ethanol extract of Mongolian medicine Parnassia palustris on the proliferation of hepatocellular carcinoma cells," *Journal of Medicine & Pharmacy of Chinese Minorities*, vol. 22, no. 10, pp. 63–65, 2016.

[68] X. Y. Wang, "The study of Proliferation inhibition effects of ethanol extract of Mongolian medicine Parnassia palustris on human liver cancer(HepG2) cells in vitro," *World Latest Medicine Information*, vol. 17, no. 90, p. 48, 2017.

[69] C. J. Zhou, Y. L. He, L. S. Zhou, Z. Y. Zhang, and G. Wu, "Effects of four extracts from Mongolia drug TGLG-1 on expression of low density lipoprotein receptor gene in rat hepatocyte strain BRL," *Chinese Journal of Modern Applied Pharmacy*, vol. 25, no. 3, pp. 186–189, 2008.

[70] G. Wu, D. W. Pang, M. Li Wang et al., "Effect of Mongolia drug TGLG-1 on serum lipids in hyperlipidemic rats," *Chinese Journal of Modern Drug Application*, vol. 23, no. 4, pp. 272–274, 2006.

[71] R. Wen, C. J. Zhou, Y. B. Jia, P. Li, and S. H. Yin, "Effect of quercetin and apigenin on the proliferation and apoptosis of HepG2 cells," *Modern Medicine Journal of China*, vol. 18, no. 01, pp. 5–8, 2016.

[72] R. Wen, C. J. Zhou, Y. B. Jia, and T. Zhong, "Effects of four flavonoid glycosides in Artemisia lavandulaefolia on the expression of AMPK and LPIN1 in HepG2 cells," *Chinese Journal of Pharmaceutical Analysis*, vol. 37, no. 01, pp. 74–82, 2017.

[73] Y. Li and C. J. Zhou, "Effects of total flavonoids from Artemisia lavandulaefolia on AMPK related signal transduction pathway in lipid metabolism of HepG2 cells," *Chinese Journal of Pharmaceutical Analysis*, vol. 39, no. 08, pp. 1396–1403, 2019.

[74] L. G. Fu and T. Q. Chen, *Higher Plants of China.13 Volumes*, pp. 91-92, Qingdao Publishing House, Qingdao, China, 2002.

[75] Z. Y. Qu, X. Li, and X. Zou, "Purification and antitumor activity of total saponins of Hosta ventricosa," *Natural Product Research and Development*, vol. 30, no. 08, pp. 1432–1436, 2018.

[76] Y. Xin and Y. H. Bai, "Study on antibacterial activity of ethanol extract of Mongolian medicine flowers of Hosta plantaginea (Lam.) from outside and inside," *Chinese Traditional Patent Medicine*, vol. 37, no. 3, pp. 653–656, 2015.

[77] W. Y. Li, *Preliminary Study on the Chemical Compositions and Bioactivities of Mongolian Medicine Hosta Plantaginea(Lam,) Ascherson*, Hua zhong University of Science and Technology, Wuhan, China, 2009.

[78] C. Y. Li, P. F. Xue, M. N. Liu, P. P. Wang, and L. Wang, "Study on the anti-inflammatory effects of Hosta plantaginea in Mice," *Lishizhen Medicine and Materia Medica Research*, vol. 26, no. 07, pp. 1559-1560, 2015.

[79] J. W. He, L. Yang, J. X. Zhu, X. M. Wang, Z. R. Zou, and W. W. He, "The comparison of anti-inflammatory effects and HLPC detection on different extracts from the flower of Hosta plantaginea in mice," *Journal of Jiangxi Normal University (Natural Science Edition)*, vol. 40, no. 02, pp. 183–185, 2016.

[80] H. X. Xie, P. F. Xue, J. Zhou, L. Fan, and F. H. Yuan, "The research of analgesic action of H.plantaginea in mice," *Acta Academiae Medicinae Neimongol*, vol. 32, no. 1, pp. 36–38, 2010.

[81] M. M. Wu, X. J. Li, P. F. Xue et al., "Cytotoxic effect of Gitogenin and its three steroidal saponins in Mongolia herbal medicine flos Hostae in vitro," *Research and Pactice on Chinese Medicines*, vol. 32, no. 02, pp. 16–18, 2018.

[82] J. Q. Liu, C. F. Wang, M. H. Qiu, and W. H. Hu, "Steroidal saponins from flowers of Hosta plantaginea and their antitumor activities," *Chinese Traditional and Herbal Drugs*, vol. 41, no. 4, pp. 520–526, 2010.

[83] R. Wei, Q. Ma, G. Zhong, J. He, and Z. Sang, "Isolation and characterization of flavonoid derivatives with anti-prostate cancer and hepatoprotective activities from the flowers of Hosta plantaginea (Lam.) Aschers," *Journal of Ethnopharmacology*, vol. 253, Article ID 112685, 2020.

[84] Y. Q. Ma, *Inner Mongolia Flora*, pp. 604–606, Inner Mongolia People's Press, Huhhot, China, 1992.

[85] O. urigi, R. Bu, and Q. S. Wu, "Ethnobotanical study of Mongolian medicine Agi," *Journal of Chinese Medicinal Materials*, vol. 24, no. 6, p. 394, 2001.

[86] Q. Y. Bai, *Chinese Medicine Encyclopaedia Mongolian Medicine*, pp. 322–324, Inner Mongolia Science & Technology Press, Chi Feng, China, 1986.

[87] J. J. Chen, S. M. Wang, C. F. Li, Q. W. Shi, M. L. Zhang, and M. Dong, "Studies of sesquiterpenoids from Artemisia frigida on the anti-growth activity of human tumor cell lines," *Clinical Journal of Traditional Chinese Medicine*, vol. 27, no. 02, pp. 24–26, 2011.

[88] B. Olas and Beata, "The beneficial health aspects of sea buckthorn (Elaeagnus rhamnoides (L.) A.Nelson) oil," *Journal of Ethnopharmacology*, vol. 213, pp. 183–190, 2018.

[89] N. N. Zhang, R. L. Hou, K. X. Li et al., "Antitumor activity and mechanism of ursolic acid extracted from Hippophae rhamnoides L. On H22 tumor bearing mice," *Food Research and Development*, vol. 40, no. 10, pp. 6–12, 2019.

[90] C. Grey, C. Widén, P. Adlercreutz, K. Rumpunen, and R. D. Duan, "Antiproliferative effects of sea buckthorn (Hippophae rhamnoides L.) extracts on human colon and liver cancer cell lines," *Food Chemistry*, vol. 120, no. 4, pp. 1004–1010, 2009.

[91] J. K. Zhang, M. Z. Lin, and X. M. Zhang, "Pharmacodynamics study on extractives from different seabuckthorn organs to solid tumour mice," *The Global Sea Buckthorn Research and Development*, vol. 10, no. 03, pp. 1–6, 2012.

[92] B. Sun, P. Zhang, W. J. Qu, X. L. Zhang, X. Y. Zhuang, and H. J. Yang, "Study on effect of Flavonoids from oil-removed seeds of Hippophae rhamnoides on inducing apoptosis of human hepatoma cell," *Journal of Chinese Medicinal Materials*, vol. 12, pp. 875–877, 2003.

[93] S. T. Bao, Y. H. Lu, Z. T. Wang, X. Y. Tao, and D. Z. Wei, "In vitro anti-tumor activity of isorhamnetin isolated from Hippophae rhamnoides L. against BEL-7402 cells," *The Pharma Research*, vol. 549, no. 3, pp. 186–194, 2006.

[94] J. M. Llovet, A. Villanueva, A. Lachenmayer, and R. S. Finn, "Advances in targeted therapies for hepatocellular carcinoma in the genomic era," *Nature Reviews Clinical Oncology*, vol. 12, no. 7, pp. 408–424, 2015.

[95] W. Gaowa, S. P. Liu, H. S. Wang, and H. Tao, "A study on Mongolia medicine NaRenManDuLa-11 depressing the proliferation of gastric tumor and its mechanism," *China Practical Medicine*, vol. 3, no. 13, pp. 18-19, 2008.

[96] X. L. Deng, D. Wang, and S. P. Liu, "The study on the induction of gastric cancer cell apoptosis by the Mongolian medicine NaRenManDuLa-11," *The Journal of Practical Medicine*, vol. 28, no. 8, pp. 1350-1351, 2012.

Hindawi
Evidence-Based Complementary and Alternative Medicine
Volume 2021, Article ID 6251559, 8 pages
https://doi.org/10.1155/2021/6251559

Research Article

Quercetin Relieves the Excised Great Saphenous Vein Oxidative Damage and Inflammatory Reaction

Yunpeng Bai,[1,2] Qingliang Chen,[1,2] Xiaolong Zhu,[2] Nan Jiang,[1,2] Ximing Li,[1,2] and Zhigang Guo[1,2]

[1]*Chest Hospital, Tianjin University, Tianjin 300222, China*
[2]*Tianjin Chest Hospital, Tianjin Medical University, Tianjin 300222, China*

Correspondence should be addressed to Ximing Li; jiaohe@tju.edu.cn and Zhigang Guo; tjxkyylxm@sina.com

Received 26 September 2021; Revised 13 November 2021; Accepted 19 November 2021; Published 31 December 2021

Academic Editor: Lifeng Han

Objective. The patency and quality of transplanted great saphenous vein (GSV) can seriously influence the physical state and life quality of patients who accepted the coronary artery bypass grafting (CABG). Quercetin is known for antioxidant, antithrombotic, anti-inflammatory, and antitumor properties. In this study, we examined the protection of quercetin to the great saphenous vein from oxidative and inflammatory damage. *Methods*. The GSVs were collected from 15 patients undergoing CABG and cultured. Treated the veins by H_2O_2 and detected the NO, SOD, and MDA content by the relevant kits to explore the quercetin protection against oxidative damage. Then, for another group of GSVs, sheared them and detected the inflammatory cytokines, such as IL-6, TNF*α*, CCL20, PCNA, and VEGF. Collect the veins for H&E staining and PCNA and VEGF immunofluorescent staining. *Results*. Pretreatment by quercetin reduced the production of NO and MDA induced by H_2O_2, and increased SOD activity. Quercetin also supressed the mRNA expressions of IL-6, TNF*α* after mechanical damage and had no influence on CCL20 and VEGF. Consistent with the lower expression of PCNA treated by quercetin, the vein intima was thinner. *Conclusion*. These results demonstrated that quercetin protects GSVs by reducing the oxidative damage and inflammatory response and also suppresses the abnormal thickening of venous endothelium by inhibiting cell proliferation. It reminded that, to some extent, quercetin has the potential to release the great saphenous vein graft damage.

1. Introduction

Quercetin is a kind of flavonoid, which is widely distributed in a variety of fruits, vegetables, and traditional Chinese medicine, such as apple, onion, mulberry parasitism, chrysanthemum, ginkgo biloba, notoginseng, and so on. Quercetin has many beneficial effects on the human body, including antithrombotic, anti-inflammatory, and antitumor properties [1]. It has been regarded as a good antioxidant that removes reactive oxygen species produced naturally in the body, such as O_2- and ONOO-, and promotes the transfer of zinc into cells as an intracellular antioxidant [2, 3], enhancing antioxidation ability of cells.

The incidence of cardiovascular disease has increased dramatically year by year, becoming a serious health challenges not only in developed countries but also in developing countries, with the improvement and changes of food. Coronary atherosclerosis is a common clinical cardiovascular disease, which is bound up with inflammatory response. Epidemiological research studies have showed that the addition of flavonoids can reduce the risk of cardiovascular disease [4]. Ovsepyan found that macrophages secreted large amounts of C-reactive protein (CRP) and TNF*α*, IL-6, and other proinflammatory factors, promoting the apoptosis of smooth muscle cell and the development of atherosclerosis [5]. Coronary artery bypass surgery (CABG) has become a common cardiac surgery treatment for patients with coronary heart disease (CHD). The migratory vessels are mainly supplied by the patient's own great saphenous vein (GSV), internal mammary artery, or radial artery. The existing clinical studies have showed that patency rate of artery bridge is significantly higher than that of vein bridge after 5 years or 10 years [6]. Gooch believed that the low patency rate of venous bridge is caused by mechanical

damage during operation [7]. Research studies also showed that vascular damage is closely related to oxidative stress [8], especially vascular endothelial damage, which enhances the occurrence and development of arteriosclerosis.

Then, reduced oxidative and mechanical damage are beneficial for the GSV patency. Barros put forward that the preservation methods of GSV can affect the vascular patency rate and failure of venous bridge [9]. After the removal of GSV, the blood supply in vitro was insufficient, and the rapid loss of water caused venous spasm or endothelial injury. Studies revealed that improper preservation of GSV could destroy the membrane integrity in vitro [10]. Therefore, many researchers tried to find a proper preservation solution to reduce the injury and improve the GSV quality. Harscamp proposed that buffer salt solution showed superior benefits on GSV than saline solution and whole blood [11].

Then, can we apply some reagents to better protect the GSV? Above all, we know that the excised GSV injury mainly comes from the intraoperative mechanical damage and oxidative damage caused by hypoperfusion. Quercetin plays a good antioxidant and anti-inflammatory role [12]. In this study, we separately designed the oxidative and mechanical damage models in vitro to explore the protective effect of quercetin on the excised GSV.

2. Materials and Methods

2.1. Patients and GSV Culture. The GSVs were collected from the CABG patients who signed the informed consent. Cleared the perivascular adipose under aseptic conditions, and then, GSV was cut into vascular rings about 3 mm long, divided into 3 groups, and placed in the DMEM medium (Thermo Fisher Scientific, America) containing 20% FBS (Thermo Fisher Scientific, USA) and double antibody (Thermo Fisher Scientific, USA) at 5% CO_2 and 37°C. The excised GSV culture methods referred to Prasongsukarn [13].

This study has been approved by the Institutional Ethical Committee of Tianjin Chest Hospital.

2.2. Oxidative and Mechanical Damage Protocol. The vascular rings were divided into 3 groups: control group, H_2O_2 group cultured in DMEM, and H_2O_2 + quercetin group cultured in DMEM containing 200 umol/L quercetin (Abcam, UK). After 1 hour, the H_2O_2 group and H_2O_2 + quercetin group were treated with 100 umol/L H_2O_2. After 4 hours, the culture supernatant was recovered, and then, the NO content was detected by the nitric oxide (NO) kit (Solarbio, China). Another 3 groups, treated as above, after 24 h, were treated by 100 umol/L H_2O_2. Then, NO, SOD, and MDA contents were detected using the relevant kits (Solarbio, China). In the mechanical damage experiment, shear the veins by scissors to form a 2 mm incised wound. The control group did not do any treatment. The wound group was cultured in DMEM, and the wound + quercetin group was cultured in DMEM containing 200 umol/L quercetin. After 24 hours, the veins were collected, and mRMA levels of IL-6, TNFα, CCL20, PCNA, and VEGF were detected by qRT-PCR. Then, the veins were collected for H&E staining, PCNA, and VEGF immunofluorescent staining.

2.3. H&E and Immunofluorescence Staining. The paraffin sections were heated in an oven. After hydration, they were treated with eosin staining for 1 minute and hematoxylin for 30 seconds. As for immunofluorescence staining, the hydrated sections were first treated by citrate-based antigen unmasking solutions (Vector Laboratory, America). They were incubated with antibodies (1 : 100) against PCNA (Solarbio, China) and VEGF (Solarbio, China), respectively. The sections were then incubated with commercial secondary antibody (1 : 200). The sections were photographed with Nikon microscopy (Nikon, Japan).

2.4. mRNA Analyses. The vein tissues were homogenized with Stat 60 RNA extraction reagent (Tel-Test, TX) with a homogenizer (Kinematica, Switzerland), and then, RNA was extracted and further purified by a RNA easy mini kit (Qiagen, China) for qPCR following the manufacturer's protocol.

The purified RNA was reverse transcribed, and gene expression was evaluated by real-time quantitative PCR. Briefly, cDNA was synthesized, and qPCR was performed using the Power SYBR Green (Applied Biosystems, USA) and 7300 Real-Time PCR system (Applied Biosystems, USA). Reverse transcription was performed following the temperature protocol: 37°C for 1 h and 94°C for 5 min. All primers used are given in Table S1. Subsequently, qPCR was performed using the SYBR Green ER PCR kit (Thermo Fisher Scientific, Inc.). The following cycling conditions were as follows: 95°C for 20 s, followed by 40 cycles of 95°C for 15 sec and 60°C for 1 min. Relative mRNA levels were calculated by comparing with the housekeeping gene GapDH. Quantitative values were calculated using the $2^{-\Delta\Delta Cq}$ method.

3. Results and Discussion

3.1. Results

3.1.1. Short-Time Quercetin Pretreatment Did Not Protect the GSV from H_2O_2-Induced Damage. The GSVs cultured in vitro were induced oxidative damage by 100 umol/L H_2O_2. After treated for about 1 hour, the NO generation was detected using the NO kit. After H_2O_2-induced damage, the generation of NO increased ($P < 0.05$), revealing that H_2O_2 induced oxidative damage. There were no significant statistical differences in NO concentration between H_2O_2 and H_2O_2 + quercetin groups ($P > 0.05$) (Figure 1(a)).

3.1.2. Long-Time Quercetin Pretreatment Protected the GSV from H_2O_2-Induced Damage. We speculated that the protective effect of quercetin might be related to the pretreatment time. Then, we extended the pretreatment to 24 hours and repeated the above experiments; the results revealed the production of oxidative damage decreased. Compared with

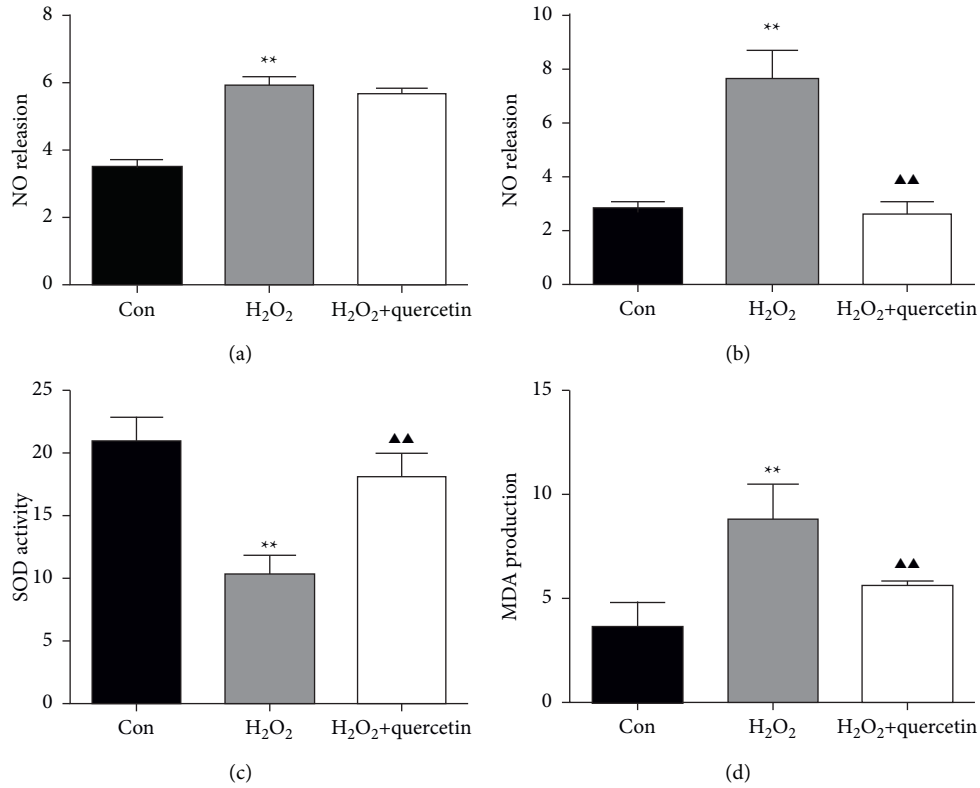

Figure 1: Quercetin pretreatment protects GSV from H_2O_2-induced damage. (a) The NO concentration in the culture supernatant, pretreated by quercetin for 1 h. (b) The NO concentration in the culture supernatant, pretreated by quercetin for 24 h. (c) The MDA concentration in the cultured GSV, pretreated by quercetin for 24 h. (d) The SOD concentration in the cultured GSV, pretreated by quercetin for 24 h. Statistical significance compared with H_2O_2 GSV vs. Con GSV is shown by an asterisk ($^*P < 0.05$, $^{**}P < 0.01$) and with H_2O_2 GSV vs. H_2O_2 + quercetin GSV is shown by a trilateral ($^▲P < 0.05$, $^{▲▲}P < 0.01$). Mean ± SD shown ($n = 6$).

the H_2O_2 group, NO generation was remarkably decreased in the H_2O_2 + quercetin group ($P < 0.01$), even lower than that in the control group (Figure 1(b)). We further tested MDA production and SOD activity (Figures 1(c)-1(d)), and found that MDA content in the H_2O_2 + quercetin group was lower than that in the H_2O_2 group ($P < 0.01$). Furthermore, SOD activity in the H_2O_2 + quercetin group was obviously higher than that in the H_2O_2 group ($P < 0.01$) and lower than the control group ($P < 0.05$).

3.1.3. Quercetin Suppressed the Inflammatory Responses Induced by Mechanical Damage. In order to explore the role of quercetin in the inflammatory response induced by mechanical damage, we established mechanical damage GSV models using a scissor. Then, the mRNA levels of inflammatory cytokines were detected. After quercetin treatment, the transcription levels of IL-6 and TNFα reduced ($P < 0.05$), but still higher than the control group ($P < 0.01$, Figures 2(a)-2(b)). However, the expression of CCL20 showed no significant relation to quercetin ($P > 0.05$, Figure 2(c)).

3.1.4. Quercetin Inhibited the Abnormal GSV Intima Thickening. Mechanical damage often induces an abnormal vascular intima thickening. Therefore, we compared the GSV intima thickness by H&E staining (Figure 3(a)). As shown in figures, the intima of GSV in wound + quercetin in the group was thinner than that in the wound group. To explore the underlying mechanisms, we detected the expression of proliferation markers, PCNA and VEGF (Figures 3(b)-3(c)). The qPCR results revealed the expression of VEGF and PCNA was sharply increased after injury ($P < 0.01$), and quercetin could not influence VEGF transcription ($P > 0.05$), but suppresses the expression of PCNA. These results were consistent with immunofluorescence staining (Figure 4).

3.2. Discussion. Atherosclerosis is characterized by the formation of plaque in medium and large artery vascular wall, leading to tissue damage such as vascular obstruction or myocardial infarction. Endothelial dysfunction or activation is the first step in the pathogenesis of atherosclerosis. Cardiovascular disease risk factors lead to oxidative stress and oxidation of low-density lipoprotein (LDL) cholesterol. The oxidized LDL (oxLDL) attacks the arterial intima, releasing phospholipids to activate endothelial cells, leading to endothelial dysfunction. The oxLDL induced damage by activating the NF-κB pathway with toll-like receptors (TLRs), which promoted expression of vascular cell adhesion factor (VCAM1), intercellular adhesion factor (ICAM-

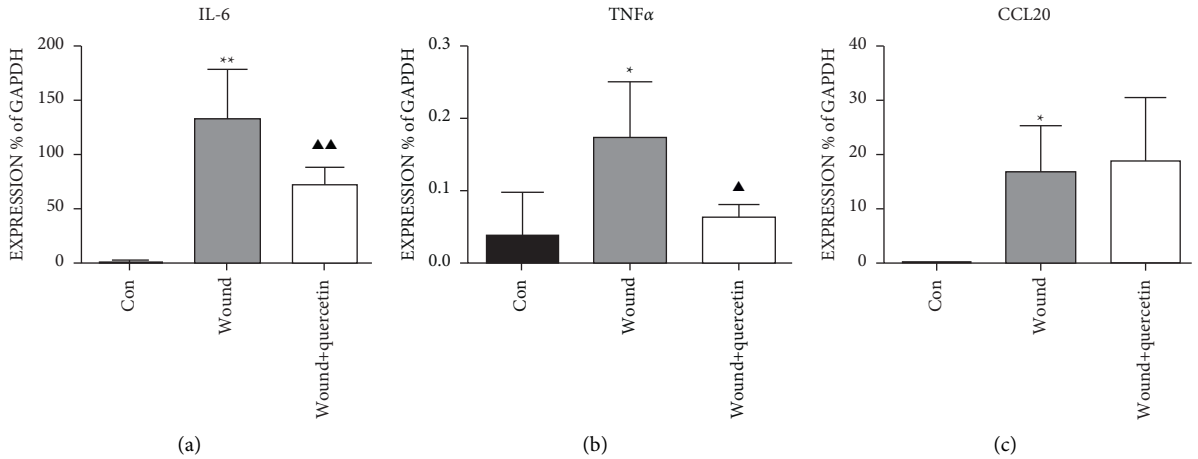

Figure 2: Quercetin pretreatment suppresses the inflammatory responses induced by mechanical damage. (a) The mRNA levels for IL-6 in the 3 groups of cultured GSV, pretreated by quercetin for 24 h. (b) The mRNA levels for TNFα in the 3 groups of cultured GSV, which were pretreated by quercetin for 24 h. (c) The mRNA levels for CCL20 in the 3 groups of cultured GSV, pretreated by quercetin for 24 h. Statistical significance compared with H_2O_2 GSV vs. Con GSV is shown by an asterisk ($^*P < 0.05$, $^{**}P < 0.01$) and with H_2O_2 GSV vs. H_2O_2 + quercetin GSV is shown by a trilateral ($^{\blacktriangle}P < 0.05$, $^{\blacktriangle\blacktriangle}P < 0.01$). Mean ± SD shown ($n = 6$).

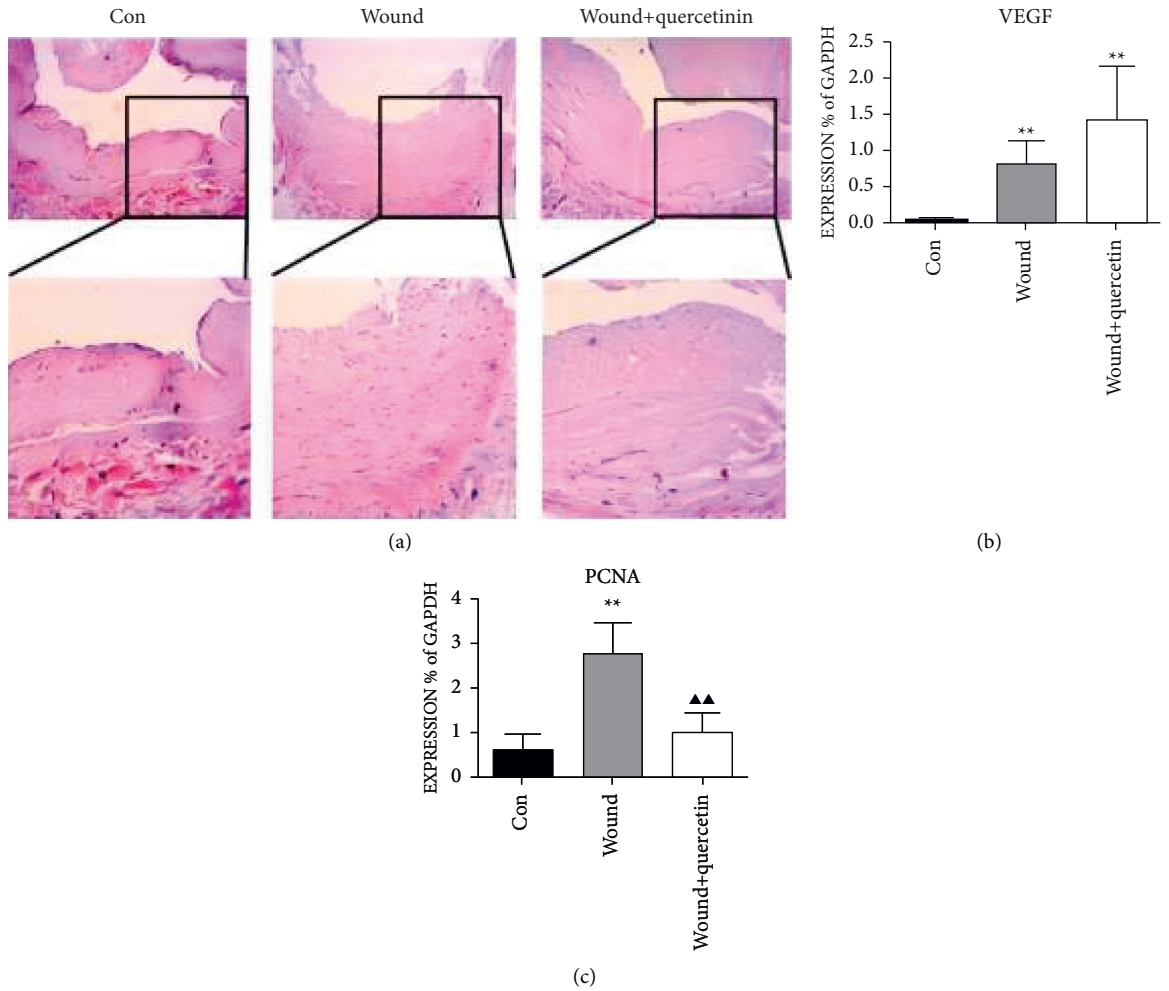

Figure 3: Quercetin inhibits the abnormal GSV intima thickening. (a) H&E staining of GSV showing the intima thickness (×200). The representative images for three groups are shown. The mRNA levels for (b) VEGF and (c) PCNA in the 3 groups of cultured GSV, which were pretreated by quercetin for 24 h. Statistical significance compared with H_2O_2 GSV vs. Con GSV is shown by an asterisk ($^*P < 0.05$, $^{**}P < 0.01$) and with H_2O_2 GSV vs. H_2O_2 + quercetin GSV is shown by a trilateral ($^{\blacktriangle}P < 0.05$, $^{\blacktriangle\blacktriangle}P < 0.01$). Mean ± SD shown ($n = 6$).

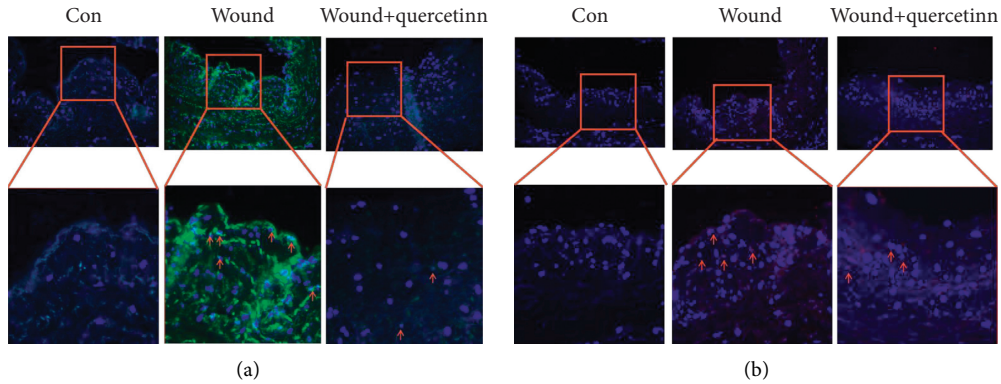

Figure 4: Quercetin inhibits the expression of PCNA and VEGF. (a) PCNA staining and (b) VEGF staining of GSV (×200). The representative images for three groups are shown. The positive cells are shown by arrowhead.

1), proinflammatory factor, and monocyte chemotactic factor (MCP1), raised mononuclear cells and caused endothelial damage, and accelerated atherosclerotic progression. During CABG progress, it is inevitable to cause GSV endothelial injury, which may accelerate the oxLDL accumulation. Many clinical and animal experiments have reported quercetin played good anti-inflammatory and antioxidant function [14, 15]. Reports have pointed out that quercetin itself has biological activities against cardiovascular disease and related risk factors [16]. Clinically, GSV is widely used as bridge graft in CABG surgery to supply blood to the heart. Mechanical damage and oxidation reaction are the key factors influencing the quality of GSV during CABG surgery. In this study, we explored the potential of quercetin in the protection of excised GSVs.

Increasing the intake of quercetin is beneficial for patients with cardiovascular disease. Duarte confirmed that increasing the quercetin-rich diet played an antihypertensive and antioxidant role in a spontaneously hypertensive rats model [17]. In addition to inhibiting thrombosis, quercetin also can serve as a vasodilator factor [18]. Studies about the vascular function have suggested that polyphenols can improve blood vessel function. The polyphenols in red wine can increase the biological activity of NO and improve arterial expansion [19]. Quercetin has a similar effect, improving vasodilatation by increasing the level of intracellular calcium ions [20]. Cogolludo put forward that quercetin improved blood vessel function by activating BKCa (large conductance Ca^{2+}-activated K^+ channels) [21]. These all showed that quercetin can protect blood vessels in vivo.

Current research studies on quercetin mainly focus on the protection of the venous endothelial cells. Although previous studies had showed that quercetin inhibited the generation of NADPH oxidase subunit p47 phox and NO, the concentration of quercetin in the experiments exceeded the physical standard, which led to the differences between the experiments and clinical studies. Angiotensin II induced venous endothelial cell dysfunction by promoting the synthesis of O^{2-} in the cell, reducing the NO production, strengthening the expression of NADPH oxidase subunit, and activating the PKC pathway. Jones used a physiological concentration of quercetin to confirm that quercetin can alleviate Ang II-induced vein endothelial cell damage, which may be related to less p47 phox and O_2 generation [22].

In this experiment, we found that quercetin reduced the generation of NO and weakened injury induced by H_2O_2. But at pretreatment for about 1 h, the effect is not obvious. Considering the short processing time, we prolonged the time and found that quercetin showed good antioxidant ability after 24 h of treatment. Then, we tested the effect of quercetin on SOD activity and MDA production. The SOD and MDA reflect the extent of oxidative stress. We found that quercetin could obviously increase the SOD activity and reduce the generation of the MDA after H_2O_2 stimulation, indicating that quercetin could significantly reduce the oxidative damage to GSV in vitro.

Other researchers proposed that protective role of quercetin is closely related to the migration of smooth muscle cells (SMC). During vascular healing after damage, the migration of SMCs was influenced by MMP2 and MMP9, which could be inhibited by quercetin [23]. Thus, quercetin may play a antioxidant role through various pathways. Our study just reminds that quercetin may reduce the oxidation product by promoting the SOD activity, and further studies are needed for finding out these signal pathways.

Besides the antioxidant effect, quercetin also plays a strong anti-inflammatory role. It can significantly reduce the levels of serum c-reactive protein [24]. Adding it to the diet of mice or plant extracts containing can reduce obesity and insulin resistance induced by the high-fat diet and reduce systemic inflammatory responses. Laura fed mice with 50 μg quercetin or nion extracts containing equal amount of quercetin for nine weeks and found proinflammatory cytokines in the adipose tissue of mice decreased, and chronic inflammatory cytokines, such as Cd11b, Cd68, F4/80, and Mcp1, also decreased, and serum level of IL-6 significantly reduced [25].

Similarly, we found that quercetin can reduce TNFα and IL-6 expression. TNFα is involved in systemic inflammatory response and is mainly generated during the acute inflammatory period, as an early proinflammatory cytokine

that induces the downstream inflammatory responses. In the vein, TNFα can activate multiple signaling pathways, including C-SRC and ICAM-1, to initiate inflammatory response. IL-6 can induce the activation of neutrophils and endothelial cells, which releases inflammatory cytokines that recruit white blood cells. Quercetin can reduce TNFα and IL-6, inhibiting inflammatory response at the beginning, suggesting a good venous protection potential. Our study suggested that quercetin plays the anti-inflammatory effect by blocking TNFα and IL-6-associated signal pathways. It is consistent with Zhang's research [26]. Next, we detected the expression of C-C chemokine CCL20 (chemokine (C-C motif) ligand 20), the another proinflammatory cytokine. The CCL20 is a chemokine expressed mainly in the blood vessels, lymphatic tissue, and lung, produced by cells related with inflammation and autoimmune response such as endothelial cells, neutrophils, natural killer cells, and so on. It is well established that CCL20 contributes to inflammatory cell recruitment [27]. Some researchers believed that CCL20 is a mediator highly sensitive to the inflammatory response, and it could influence the endothelial cell migration [28]. Elnabawi et al. pointed that CCL20 was a potential biomarker of inflammation and impaired vascular health [29]. Regrettably, we found that the expression of CCL20 did not change with or without quercetin, indicating quercetin had no significant effect on CCL20 and lymphocyte chemotaxis.

NF-κB pathways may play a role in the anti-inflammatory function of quercetin. Indra ever pretreated HUVECs with 125 μM quercetin and found that it obviously inhibited leptin-induced ERK1/2 phosphorylation and NF-κB activation, thereby alleviating inflammatory responses [30]. But they did not explore TNFα-related signal pathways due to insufficient RNA samples. Later, other researchers confirmed quercetin could obviously inhibit TNFα-related NF-κB activation [31] and ROS generation [32]. Lu et al. proposed a potential mechanism of quercetin on regulating TNFα, using a atherosclerotic mice model induced by the high-fructose diet [33]. The NF-κB signaling pathway is closely related to transcription of many inflammatory genes, such as IL-1b, IL-18, and TNFα. Studies have shown that activation of PI3K/AKT plays an important role in the inflammatory response balance. It was confirmed the long-term pressure leads to myocardial injury involving NF-κB pathways, which is regulated by PI3K/AKT [34]. Considering that there are some common characters between the vascular inflammation and atherogenesis, Lu believed PI3K/AKT-regulated NF-κB approach may also be involved in the atherosclerotic process induced by the high-fructose diet [33]. These results showed that phosphorylation of IKKa and IkBa activated NF-κB signaling pathways, thus promoting the expression of IL-1β, IL-18, TNFα, and IL-6, and quercetin could inhibit inflammatory response by blocking NF-κB signaling pathways and reduce the expression of proinflammatory cytokines involved in the PI3K/AKT pathway. Our study confirmed the quercetin showed obvious protection for the excised GSVs, just as the protection for the endothelial cells or smooth muscle cells alone in vitro.

Besides the inflammatory reaction, mechanical damage often induces abnormal wound healing and vascular intima thickening, caused by the disordered endothelial cell proliferation. Clinically, GSVs are the widely used bridge vessels in coronary artery bypass graft, and during the operation, GSVs are inevitably mechanical damaged, such as being sheared and sutured; then, the intima thickening and the vascular lumen is gradually narrowed, which influences the quality and blood flow of GSVs. The quality and blood flow of GSVs are essential to the outcomes of surgery and patients. Then, we evaluated the vascular intima thickness with H&E staining and endothelial cells proliferation by detecting PCNA and VEGF. The results showed the quercetin may restrain the abnormal intimal thickening by suppressing the endothelial cells proliferation after the injury and revealed its potential applications in CABG for a superior quality and blood flow of GSVs. Though quercetin shows great potential, it still has a long way to go in clinical application.

Compared to animal and cellular experiments, our study used human GSVs samples to demonstrate the protection of quercetin for oxidation reaction and inflammatory responses. However, application of human tissue can more accurately reflect the existing pathophysiological state of excised GSVs.

4. Conclusion

In summary, we demonstrated that quercetin can inhibit oxidation reaction, reduce inflammatory responses caused by mechanical damage induced, and inhibit the abnormal intimal thickening. The mechanisms involved are those regulated by production of NO, SOD, MDA, and TNFα signaling and endothelial proliferation.

Data Availability

The datasets used and/or analyzed during the current study are available from the corresponding author upon request.

Conflicts of Interest

The authors declare that they have no conflicts of interest.

Authors' Contributions

Yunpeng Bai, Qingliang Chen, and Xiaolong Zhu equally contributed to the work. Ximing Li and Zhigang Guo are corresponding authors.

Acknowledgments

This study was supported by a grant from the Project of Haihe Medical Scholar and Project of Young Medical Talents of Tianjin Health Committee, China. This study was also supported by the Scientific Research Project of Integrated Traditional Chinese and Western Medicine of Tianjin Health Commission (2021204).

Supplementary Materials

Table S1. Primer sequences required for QPCR analysis. (*Supplementary Materials*)

References

[1] C. G. Vazhappilly, S. A. Ansari, R. Al-Jaleeli et al., "Role of flavonoids in thrombotic, cardiovascular, and inflammatory diseases," *Inflammopharmacology*, vol. 27, no. 5, pp. 863–869, 2019.

[2] H. Dabbagh-Bazarbachi, G. Clergeaud, I. M. Quesada, M. Ortiz, C. K. O'Sullivan, and J. B. Fernández-Larrea, "Zinc ionophore activity of quercetin and epigallocatechin-gallate: from hepa 1-6 cells to a liposome model," *Journal of Agricultural and Food Chemistry*, vol. 62, no. 32, pp. 8085–8093, 2014.

[3] J. F. Su, C. J. Guo, J. Y. Wei, J. J Yang, Y. G Jiang, and Y. F Li, "Protection against hepatic ischemia-reperfusion injury in rats by oral pretreatment with quercetin," *Biomedical and Environmental Sciences*, vol. 16, no. 1, pp. 1–8, 2003.

[4] K. Yamagata and Y. Yamori, "Inhibition of endothelial dysfunction by dietary flavonoids and preventive effects against cardiovascular disease," *Journal of Cardiovascular Pharmacology*, vol. 75, no. 1, pp. 1–9, 2020.

[5] V. A. Ovsepyan, A. K. Gabdulkhakova, A. A. Shubenkiva, and E. N. Zotina, "Role of interleukin-10 gene promoter region polymorphism in the development of chronic lymphoid leukemia," *Bulletin of Experimental Biology and Medicine*, vol. 160, no. 2, pp. 275–277, 2015.

[6] M. Gaudino, U. Benedetto, S. Fremes et al., "Radial-artery or saphenous-vein grafts in coronary-artery bypass surgery," *New England Journal of Medicine*, vol. 378, no. 22, pp. 2069–2077, 2018.

[7] K. Gooch, M. Firstenberg, B. Shrefler, and B. W. Scandling, "Biomechanics and mechanobiology of saphenous vein grafts," *Journal of Biomechanical Engineering*, vol. 140, no. 2, pp. 1288–1304, 2017.

[8] E. Gugliandolo, R. Fusco, F. Biundo et al., "Palmitoylethanolamide and Polydatin combination reduces inflammation and oxidative stress in vascular injury," *Pharmacological Research*, vol. 123, pp. 83–92, 2017.

[9] B. C. S. Barros, A. L. D. Araujo, R. L. S. Barros, S. K. A. Fiorelli, and R. F. Gatts, "Efficacy of varicose vein surgery with preservation of the great safenous vein," *Revista do Colégio Brasileiro de Cirurgiões*, vol. 42, no. 2, pp. 111–115, 2015.

[10] B. Winkler, D. Reineke, P. P. Heinisch et al., "Graft preservation solutions in cardiovascular surgery," *Interactive Cardiovascular and Thoracic Surgery*, vol. 23, no. 2, pp. 300–309, 2016.

[11] R. E. Harskamp, J. H. Alexander, P. J. Schulte et al., "Vein graft preservation solutions, patency, and outcomes after coronary artery bypass graft surgery," *JAMA Surgery*, vol. 149, no. 8, pp. 798–805, 2014.

[12] E. Ince, "The protective effect of quercetin in the alcohol-induced liver and lymphoid tissue injuries in newborns," *Molecular Biology Reports*, vol. 47, no. 1, pp. 451–459, 2020.

[13] K. Prasongsukarn, U. Chaisri, P. Chartburus et al., "Phenotypic alterations in human saphenous vein culture induced by tumor necrosis factor-alpha and lipoproteins: a preliminary development of an initial atherosclerotic plaque model," *Lipids in Health and Disease*, vol. 12, no. 1, p. 132, 2013.

[14] X. Cai, L. Bao, Y. Ding, X. Dai, Z. Zhang, and Y. Li, "Quercetin alleviates cell apoptosis and inflammation via the ER stress pathway in vascular endothelial cells cultured in high concentrations of glucosamine," *Molecular Medicine Reports*, vol. 15, no. 2, pp. 825–832, 2017.

[15] M. G. Ortega, A. C. Saragusti, J. L. Cabrera, and G. A. Chiabrando, "Quercetin tetraacetyl derivative inhibits LPS-induced nitric oxide synthase (iNOS) expression in J774A.1 cells," *Archives of Biochemistry and Biophysics*, vol. 498, no. 2, pp. 105–110, 2010.

[16] M. Russo, C. Spagnuolo, I. Tedesco, S. Bilotto, and G. L. Russo, "The flavonoid quercetin in disease prevention and therapy: facts and fancies," *Biochemical Pharmacology*, vol. 83, no. 1, pp. 6–15, 2012.

[17] J. Duarte, M. Galisteo, M. A. Ocete, F. Pérez-Vizcaino, A. Zarzuelo, and J. Tamargo, "Effects of chronic quercetin treatment on hepatic oxidative status of spontaneously hypertensive rats," *Molecular and Cellular Biochemistry*, vol. 221, no. 1/2, pp. 155–160, 2001.

[18] A. Gasparotto Junior, R. Dos Reis Piornedo, J. Assreuy, and J. E. Da Silva-Santos, "Nitric oxide and K ir 6.1 potassium channel mediate isoquercitrin-induced endothelium-dependent and independent vasodilation in the mesenteric arterial bed of rats," *European Journal of Pharmacology*, vol. 788, pp. 328–334, 2016.

[19] W. Zenebe, O. Pechánová, and R. Andriantsitohaina, "Red wine polyphenols induce vasorelaxation by increased nitric oxide bioactivity," *Physiological Research*, vol. 52, pp. 425–432, 2003.

[20] N. K. H. Khoo, C. R. White, L. Pozzo-Miller et al., "Dietary flavonoid quercetin stimulates vasorelaxation in aortic vessels," *Free Radical Biology and Medicine*, vol. 49, no. 3, pp. 339–347, 2010.

[21] A. Cogolludo, G. Frazziano, A. Briones et al., "The dietary flavonoid quercetin activates BKCa currents in coronary arteries via production of H2O2. Role in vasodilatation," *Cardiovascular Research*, vol. 73, no. 2, pp. 424–431, 2007.

[22] H. S. Jones, A. Gordon, S. G. Magwenzi, K. Naseem, S. L. Atkin, and F. L. Courts, "The dietary flavonol quercetin ameliorates angiotensin II-induced redox signaling imbalance in a human umbilical vein endothelial cell model of endothelial dysfunction via ablation of p47phox expression," *Molecular Nutrition & Food Research*, vol. 60, no. 4, pp. 787–797, 2016.

[23] D. E. Lee, M. Y. Chung, T. G. Lim, W. B. Huh, H. J. Lee, and K. W. Lee, "Quercetin suppresses intracellular ROS formation, MMP activation, and cell motility in human fibrosarcoma cells," *Journal of Food Science*, vol. 78, no. 9, pp. 1464–1469, 2013.

[24] B. Shobha, K. S. Kumar, K. Kripa, and A. Antony, "Quercetin alleviates hypercholesterolemic diet induced inflammation during progression and regression of atherosclerosis in rabbits," *Nutrition*, vol. 29, no. 1, pp. 219–229, 2013.

[25] F. Laura, L. Natalie, S. Laura, and T. Henagan, "Dietary quercetin attenuates adipose tissue expansion and inflammation and alters adipocyte morphology in a tissue-specific manner," *International Journal of Molecular Sciences*, vol. 19, no. 3, pp. 895–908, 2018.

[26] M. Zhang, J. M. Lin, X. S. Li, and J. Li, "Quercetin ameliorates LPS-induced inflammation in human peripheral blood mononuclear cells by inhibition of the TLR2-NF-κB pathway," *Genetics and Molecular Research*, vol. 15, no. 2, Article ID 15028297, 2016.

[27] C. Caux, B. Vanbervliet, C. Massacrier et al., "Regulation of dendritic cell recruitment by chemokines," *Transplantation*, vol. 73, no. 1, pp. S7–S11, 2002.

[28] O. Calvayrac, R. Rodríguez-Calvo, J. Alonso et al., "CCL20 is increased in hypercholesterolemic subjects and is upregulated by LDL in vascular smooth muscle cells," *Arteriosclerosis, Thrombosis, and Vascular Biology*, vol. 31, no. 11, pp. 2733–2741, 2011.

[29] Y. A. Elnabawi, M. S. Garshick, B. M. Tawil et al., "CCL20 in psoriasis: a potential biomarker of disease severity,

inflammation, and impaired vascular health-science direct," *Journal of the American Academy of Dermatology*, vol. 84, no. 4, pp. 913–920, 2020.

[30] M. R. Indra, S. Karyono, R. Ratnawati, and S. G. Malik, "Quercetin suppresses inflammation by reducing ERK1/2 phosphorylation and NF kappa B activation in leptin-induced human umbilical vein endothelial cells (HUVECs)," *BMC Research Notes*, vol. 6, no. 1, p. 275, 2013.

[31] W. Zhang, G. Yin, J. Dai et al., "Chemoprevention by quercetin of oral squamous cell carcinoma by suppression of the NF-κB signaling pathway in DMBA-treated hamsters," *Anticancer Research*, vol. 37, no. 8, pp. 4041–4049, 2017.

[32] A. Nakhlband, M. Eskandani, N. Saeedi et al., "Marrubiin-loaded solid lipid nanoparticles' impact on TNF-α treated umbilical vein endothelial cells: a study for cardioprotective effect," *Colloids and Surfaces B: Biointerfaces*, vol. 164, pp. 299–307, 2018.

[33] X.-L. Lu, C.-H. Zhao, X.-L. Yao, and H. Zhang, "Quercetin attenuates high fructose feeding-induced atherosclerosis by suppressing inflammation and apoptosis via ROS-regulated PI3K/AKT signaling pathway," *Biomedicine & Pharmacotherapy*, vol. 85, pp. 658–671, 2017.

[34] Y. Cheng, N. X. Cawley, and Y. P. Loh, "Carboxypeptidase E/NFα1: a new neurotrophic factor against oxidative stress-induced apoptotic cell death mediated by ERK and PI3-K/AKT pathways," *PLoS One*, vol. 8, no. 8, Article ID e71578, 2013.

Hindawi
Evidence-Based Complementary and Alternative Medicine
Volume 2021, Article ID 9255305, 20 pages
https://doi.org/10.1155/2021/9255305

Research Article

Applying Four-Step Characteristic Ion Filtering with HPLC-Q-Exactive MS/MS Spectrometer Approach for Rapid Compound Structures Characterization and Major Representative Components Quantification in Modified Tabusen-2 Decoction

Yu Zhao, Xin Dong, Zhi Wang, Rui Dong, Ren Bu, Qianxi Feng, Peifeng Xue, and Bi Qu

Department of Pharmacy, Inner Mongolia Medical University, Jinshan Development Zone, Hohhot 010110, China

Correspondence should be addressed to Peifeng Xue; xpfdc153@163.com and Bi Qu; yxyqubi@163.com

Received 22 August 2021; Revised 19 November 2021; Accepted 26 November 2021; Published 31 December 2021

Academic Editor: Yingqiu Xie

Modified Tabusen-2 decoction (MTBD) is traditional Chinese Mongolia medicine, mainly used to treat osteoporosis. However, the precise material basis of this prescription is not yet fully elucidated. Herein, we establish an HPLC-Q-Exactive MS/MS spectrometer method with four-step characteristic ion filtering (FSCIF) strategy to quickly and effectively identify the structural features of MTBD and determine the representative compounds content. The FSCIF strategy included database establishment, characteristic ions summarization, neutral loss fragments screening, and secondary mass spectrum fragment matching four steps. By using this strategy, a total of 143 compounds were unambiguously or tentatively annotated, including 5 compounds which were first reported in MTBD. Nineteen representative components were simultaneously quantified with the HPLC-Q-Exactive MS/MS spectrometer, and it is suitable for eight batches of MTBD. Methodology analysis showed that the assay method had good repeatability, accuracy, and stability. The method established above was successfully applied to assess the quality of MTBD extracts. Collectively, our findings enhance our molecular understanding of the MTBD formulation and will allow us to control its quality in a better way. At the same time, this study can promote the development and utilization of ethnic medicine.

1. Introduction

Tabusen-2 decoction (TBD) is composed of *Echinops latifolius* Tausch (ELT) and *Eucommia ulmoides* Oliver (EU) [1]. On this basis, Modified Tabusen-2 decoction (MTBD) adds *Panax notoginseng* (PN) and *Carthamus tinctorius* L. (CT) [2]. Osteoporosis is a common orthopedic disease, especially in the elderly and postmenopausal women in China. TBD is a traditional classic prescription; it has been used to treat osteoporosis for centuries [3]. The literature shows that MTBD has the effect of treating osteoporosis; it can also be used to promote blood circulation, relieve swelling, relieve pain, continue muscles and bones, and treat soft tissue contusions, crush injuries, joint sprains, trauma, and open trauma caused by surgery [4, 5]. The chemical compositions of each herb are various, having different pharmacological effects according to past reports. ELT, a traditional Chinese Mongolia herb, contained isochlorogenic acid A (ICGAA), chlorogenic acid, and other phenylpropanoids [6, 7], which are the main active components in herb. The pharmacological mitigation of ELT on osteoporosis of postmenopausal women was also reported [8]. EU is enriched with lignans and iridoids, including geniposidic acid (GPA) and pinoresinol diglucoside (PDG), having obvious antihypertensive effect [9]. In recent years, EU has attracted considerable attention because of its antiosteoporosis, antisenile dementia, antiaging, anti-inflammatory, antithrombotic, and antitumor activities [10, 11]. The flavonoids are the main active components of CT, with the efficacy of promoting blood circulation,

removing blood stasis, and relieving pain [12]. Varieties of natural pigments isolated from CT, such as yellow pigments and red pigments [13], not only have pharmacological functions but also have some nutritive value. Furthermore, triterpenoid saponins are main active constituents in PN, which are widely used for promoting blood clotting, relieving swelling, and alleviating pain [14].

In accordance with traditional Chinese medicine (TCM), traditional Mongolia medicine (TMM) is characterized with multiple components and multiple targets and plays different roles in clinical therapy. This means that it is a great challenge to explain the main chemical composition of MTBD by traditional analytical methods. In particular, the presence of isomers makes its separation and analysis more difficult. In order to solve this problem, some researchers have used the methods of mass defect, relative mass defect, neutral loss filtering (NLF), mass defect filtering, and precursor ion to characterize the chemical structure in TCM or TMM prescription [15–19]. It has vital-important reference value for our following experiment. With the promotion of high-resolution mass spectrometry [20, 21], we propose an FSCIF strategy for substructure recognition, which can significantly improve the detection effectiveness, accuracy, and sensibility. This analysis program shows obvious efficiency (reduce data processing time) and intelligence (simplify the process of structural identification).

Xie et al. [22] determined hydroxysafflor yellow A, notoginsenoside R_1, ginsenoside Rg_1, and ginsenoside Rb_1 with HPLC, but there are disadvantages of insufficient sensitivity and long running time (40 min). Hua et al. [23] established an HPLC-ELSD method to quantify the content of notoginsenoside R_1, ginsenoside Rg_1, and ginsenoside Re in PN but did not determine the content of the main components of ELT, EU, and CT. Hua et al. [24] conducted three different experiments by using HPLC, Ultraviolet detection, and ELSD methods and finally measured the content of representative components of ELT, EU, PN, and CT. But the shortcomings of this method are cumbersomeness and low responsiveness and they cannot be ignored. On the other hand, the previous literature has qualitatively analyzed the ingredients in a single medicinal material; it is not enough to explain the overall structure of MTBD due to the interaction between temperature and herbs in the process of decoction.

In order to explore the material basis of MTBD, clarify the composition of the compounds, and determine the content of the compounds, this experiment used the HPLC-Q-Exactive MS/MS spectrometer method to conduct a comprehensive material basis determination of MTBD, which provided a foundation for the subsequent quality standard formulation; it also provided guarantee for pharmacodynamic and pharmacokinetic research. Besides, 143 compounds were unambiguously or tentatively annotated with FSCIF strategy, including 5 compounds which were first reported in MTBD. Finally, we evaluated the differences in the content of 19 compounds in samples from different preparation batches, laying a foundation for subsequent quality evaluation.

2. Experimental

2.1. Materials and Reagents. A total of four batches of ELT were collected from various areas of Inner Mongolia (including Hohhot, Ordos, Xilingol, and Ulan Hot) in August 2020 (the GPS coordinates of the plant *Echinops latifolius* Tausch collection site are 41.1206962700 and 111.4084477500). Different batches of EU, CT, and PN herbs were purchased from Bozhou Pharmaceutical Co., Ltd. (Anhui, China) and GuoDa Drugstore (Hohhot, Inner Mongolia). All herbs were authenticated by Professor Bi Qu (Department of Pharmacognosy, Inner Mongolia Medical University). These specimens were preserved in the Department of General Investigation of Traditional Chinese Medicine Resources, Inner Mongolia Medical University.

Isochlorogenic acid A (ICGAA), 1,5-dicaffeoylquinic acid (1,5-DQA), genistein (GE), apigenin (APG), luteolin (LT), kaempferol (KPF), quercetin (QC), apigenin-7-O-glucuronide (A-7-0-G), rutin (RU), hydroxysafflor yellow A (HSYA), notoginsenoside R_1 (NG-R_1), ginsenoside Re (G-Re), ginsenoside Rg_1 (G-Rg_1), ginsenoside Rb_1 (G-Rb_1), caffeic acid (CA), ferulic acid (FA), geniposidic acid (GPA), chlorogenic acid (CGA), pinoresinol diglucoside (PDG), and digoxin (internal standard, IS) were purchased from Cybertech Limited (Beijing, China), with HPLC purity ≥98%. The chemical structures of these 19 compounds are displayed in Figure 1. LC-MS grade methanol, acetonitrile, and formic acid were achieved from Fisher Scientific (Hampton, NH, USA). Deionized water was prepared on a Millipore water purification system (Billerica, MA, USA). The columns used in the experiment were as follows: ACE C18-PFP column (100 × 3.0 mm ID, 3 μm), Grace Alltima C18 column (250 mm × 4.6 nm, 5 μm), HITACHI LaChrom C18 column (250 mm × 4.6 mm ID, 5 μm), and Thermo ODS-2 HYPERSIL column (250 mm × 4.6 mm, 5 μm).

2.2. MTBD Sample and Standard Solutions Preparation. Sample preparation was a critical step for precise and convincing detection by the HPLC-Q-Exactive MS/MS spectrometer method. The MTBD samples were prepared according to our previous extraction process, and the whole operation process was in line with the basic operation safety regulations of the laboratory. EU, ELT, and CT herbal materials were powdered and sieved through 40 meshes for later extraction. A total 3.6 g of MTBD powders was accurately weighed (including 1.6 g of EU, 1.2 g of ELT, and 0.8 g of CT) and placed in a 250 mL round-bottomed flask. These powders were immersed in 50 mL ethanol: water (6 : 4, V/V) mixture and weighed and then reflux extracted twice,

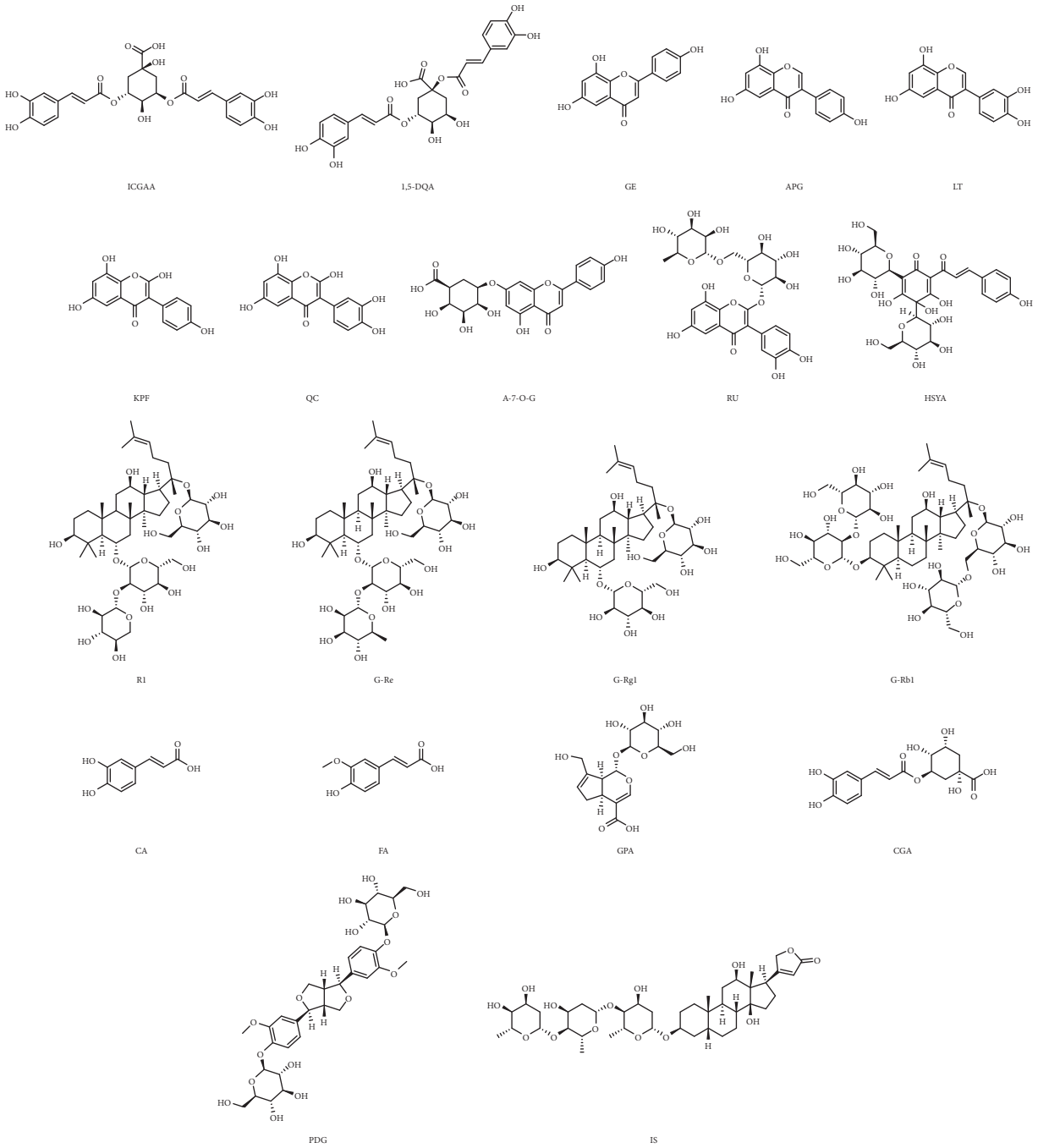

Figure 1: The chemical structures of nineteen analytes: isochlorogenic acid A (ICGAA), 1,5-dicaffeoylquinic acid (1,5-DQA), genistein (GE), apigenin (APG), luteolin (LT), kaempferol (KPF), quercetin (QC), apigenin-7-O-glucuronide (A-7-0-G), rutin (RU), hydroxysafflor yellow A (HSYA), notoginsenoside R_1 (NG-R_1), ginsenoside Re (G-Re), ginsenoside Rg_1 (G-Rg_1), ginsenoside Rb_1 (G-Rb_1), caffeic acid (CA), ferulic acid (FA), geniposidic acid (GPA), chlorogenic acid (CGA), pinoresinol diglucoside (PDG), and digoxin (internal standard, IS).

90 min for each reflux. Taking into account the recovery rate of PN powder, 0.4 g PN was added before the last extraction. After merging and mixing, the solution was filtered through a 0.45 μm microporous membrane. This filtrate was diluted 40 times for HPLC-Q-Exactive MS/MS spectrometer injection.

ICGAA 20.05 mg, 1,5-DQA 11.92 mg, GE 4.03 mg, APG 2.15 mg, LT 4.03 mg, KPF 1.30 mg, QC 2.02 mg, A-7-O-G 3.85 mg, RU 4.23 mg, HSYA 19.80 mg, NG-R_1 10.02 mg, G-Re 19.40 mg, G-Rg_1 10.17 mg, G-Rb_1 20.49 mg, CA 2.07 mg, FA 1.05 mg, GPA 4.05 mg, CGA 18.90 mg, and PDG 23.40 mg were accurately weighted and transferred into 2 mL volumetric flask, respectively. Owing to the solubility of these compounds, methanol was applied to prepare the standard solution. In order to improve the precision and accuracy of the content,

digoxin was selected as the internal standard. These standard solutions were diluted with mobile phase to final concentration (Table S1) before injection into HPLC-Q-Exactive MS/MS spectrometer.

2.3. Chromatography and Mass Spectrometry Conditions. The characterization and quantification of MTBD sample extracts were analyzed using a Thermo HPLC-Q-Exactive MS/MS spectrometer system (HPLC, UltiMate 3000, mass system, Quadrupole Exactive Orbitrap ^{TM}). The qualitative analytical conditions were as follows: HPLC column, COSMOSIL C18 (250 mm × 4.6 mm ID, 5 μm); solvent system, methanol (A), and water containing 0.1% (v/v) formic acid (B); gradient program, 0–5 min, 2%–5%A; 5–10 min, 5%–10%A; 10–15 min, 10%–18%A; 15–25 min, 18%–23%A; 25–35 min, 23%–28%A; 35–55 min, 28%–33%A; 55–60 min, 33%–39%A; 60–70 min, 39%–43%A; 70–75 min, 43%–46%A; 75–85 min, 46%–60%A; 85–100 min, 60%–65%A; 100–105 min, 65%–75%A; 105–110 min, 75%–100%A; 110–130 min, 100%–100%A; flow rate, 0.6 mL/min; column temperature, 30°C; sample injection volume, 10 μL. The quantitative analysis of MTBD sample extracts was separated on an ACE C18-PFP (100 × 3.0 mm ID, 3 μm) column. The mobile phase consisted of methanol (A) and water containing 0.3% (v/v) formic acid (B). A gradient program was used as follows: 0–6 min, 40%–40%A; 6–15 min, 40%–90%A; 15-16 min, 90%–10%A; 16–21 min, 10%-10%A; 21-22 min, 10%–40%A; and 22–25 min, 40%-40%A. The flow rate was set as 0.3 mL/min. The column temperature was kept at 30°C. Sample injection volume was 2 μL.

The qualitative and quantitative mass parameters conditions were set up as follows: auxiliary gas heater temperature, 150°C; capillary temperature, 350°C; spray voltage, 3.5 kv; S-lens RF level, 50; sheath gas flow rate, 40 L; and auxiliary gas flow rate, 2 PSI. AGC was 3×10^6 in MS scan and 1×10^5 in MS/MS scan; IT was 100 ms in MS scan and 50 ms in MS/MS scan; resolution was 70000 in MS scan and 17500 in MS/MS scan; NCE was set as 30 v. Scanning range was 100–1500 *m/z*. Mass spectrometry uses full scan mode for analysis in positive ion mode and negative ion mode.

2.4. Method Validation. The dependent variable was the ratio of the peak area of each analyte to the peak area of the internal standard, while the independent variable was set as the concentration value of each analyte; the least square regression was used to construct the standard curve equation. The intraday and interday precisions and accuracies were assessed by analyzing each concentration level (low, medium, and high) of six repeated QC samples on the same day and three consecutive days, respectively. Sample stability was investigated after the extracts were kept at room temperature for 0 h, 6 h, 12 h, and 24 h. Add the mixed control solution equal to the content of each analyte in the sample to the MTBD sample, repeat the preparation of 6 solutions, and calculate the recovery according to the following formula:

$$\text{recovery}\,(\%) = \frac{(\text{detected amount} - \text{original amount})}{\text{spiked amount}} \times 100\%. \quad (1)$$

3. Results and Discussion

3.1. Construction of the Identification Strategy. Each type of compounds has its similar core and skeleton. On this basis, the characteristic ion will be produced, which provides us with new ideas for identifying these structures. In addition, FSCIF is especially suitable for compounds with the same structural type containing similar fragmentation pathways with some characteristic ions. Correspondingly, an FSCIF-based and substructure scanning strategy will be used for rapid identification of MTBD structures. The analytical strategy is shown in Figure 2. The compounds in MTBD were characterized by HPLC-Q-Exactive MS/MS spectrometer method with FSCIF strategy, including the following steps: (1) established the self-building chemical database of MTBD according to literature and online database; (2) comprehensively summarized characteristic ions for each compound type to conduct global identification of the ingredients in MTBD; (3) rapidly screened relevant structure information by neutral loss fragments (NLF) to conform the sugar type, conjunction position, and other information; (4) concluded the precise compound structure through high-precision MS/MS data. The typical total ion chromatograms (TICs) of MTBD by HPLC-Q-Exactive MS/MS spectrometer system in positive and negative ion modes are shown in Figure 3. 143 compounds were annotated through high-precision MS/MS data, including 51 triterpenoid saponins, 28 flavonoids, 20 phenylpropanoids, 15 iridoids, 12 lignans, 11 polyphenols, and 6 other types (Table 1), in which 5 compounds were first reported in MTBD and 20 compounds were unambiguously identified by comparison with reference standards. These 143 components' structures are shown in Figure S1.

3.2. Qualitative Analysis

3.2.1. Identification of Triterpenoid Saponins. Triterpenoid saponins were typical bioactive components of PN, which were classified into two categories of protopanaxadiol (PPD) triterpenoid saponins and protopanaxatriol (PPT) triterpenoid saponins; the characteristic ions at *m/z* 459.39 $[\text{aglycones-H}]^-$ and at *m/z* 475.38 $[\text{aglycones-H}]^-$ corresponded to the PPD and PPT type ginsenosides [25]. In this study, most triterpenoid saponins (46 compounds) were detected $[M + Na]^+$ in positive ion mode, other triterpenoid saponins (5 compounds) were detected $[M - H]^-$ in negative ion mode, and excimer ion peaks can produce different cleavage modes to provide structural information such as aglycone type, sugar type, and its junction position. Compounds 110 and 123 were filtered by characteristic ion *m/z* 459.39, which tentatively identified PPD type ginsenosides; for compound 110 ($C_{54}H_{92}O_{23}$) $[M - H]^-$ at *m/z* 1107.5956, its molecular ion peak successively lost the four molecules of glucose and obtained *m/z*

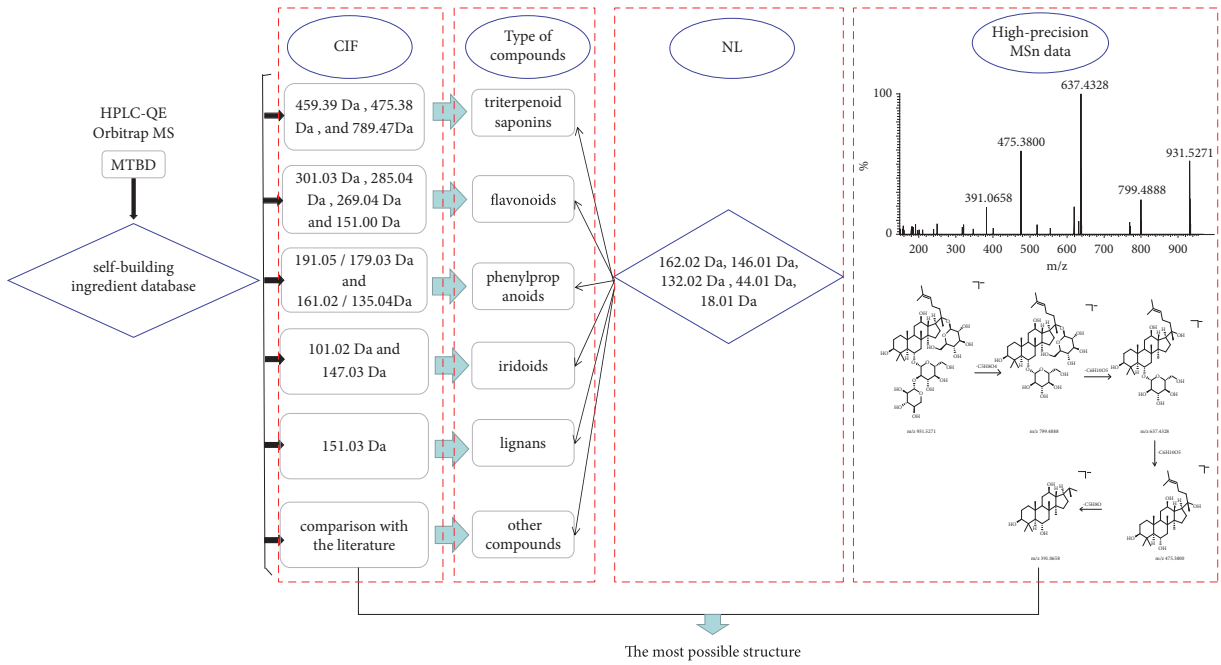

Figure 2: Analysis strategy of qualitative research of MTBD.

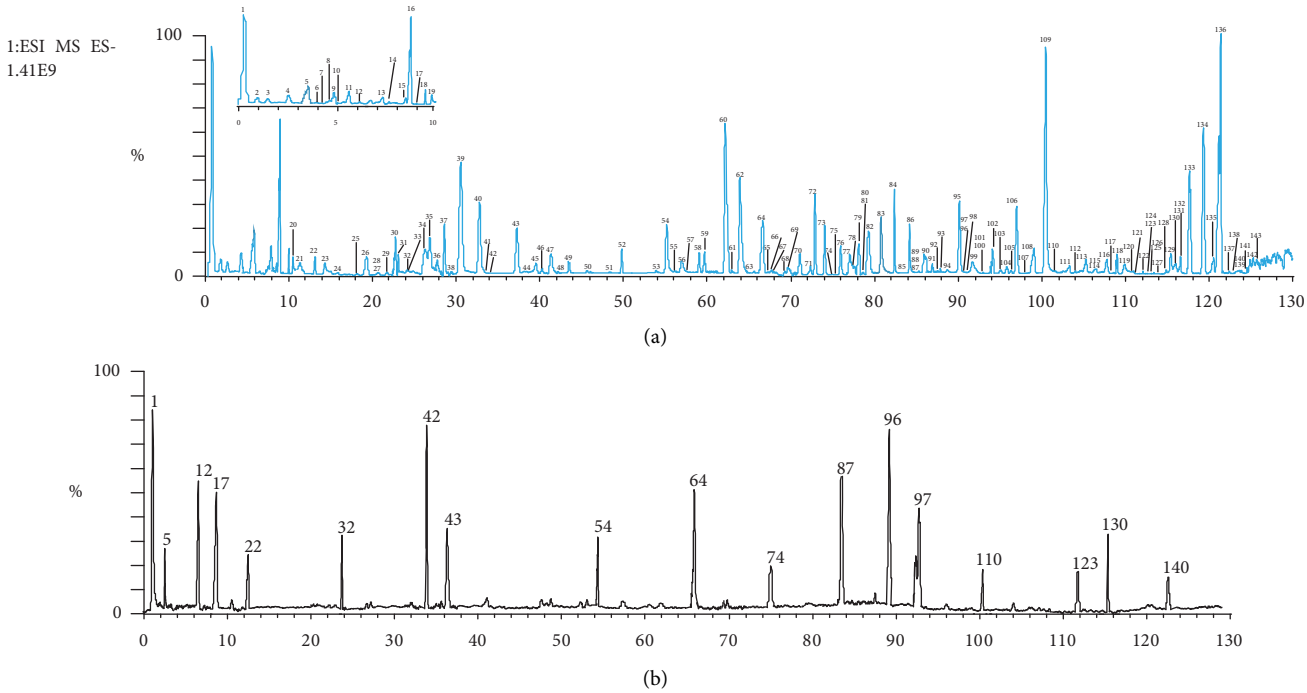

Figure 3: Continued.

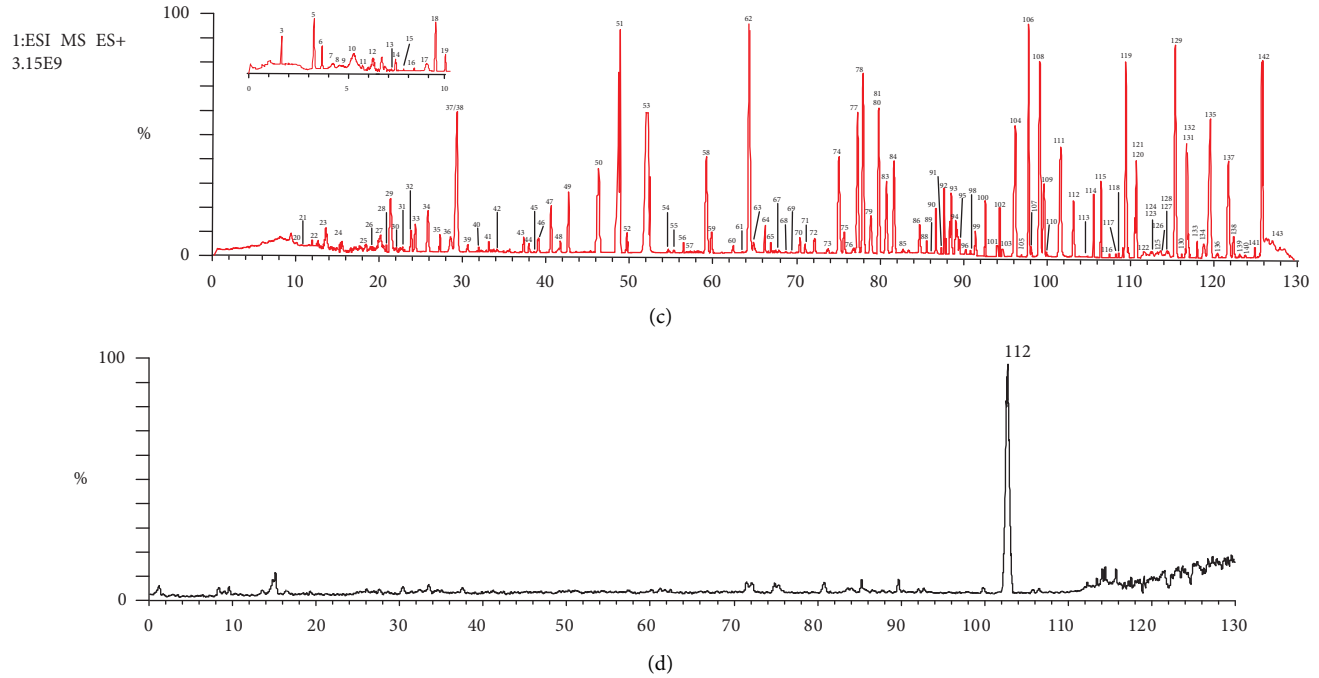

Figure 3: The typical total ion chromatograms (TICs) of MTBD. (a) TIC in negative ion mode. (b) Comparison with standard in negative ion mode. (c) TIC in positive ion mode. (d) Comparison with standard in positive ion mode.

Table 1: Characterization of chemical constituents of MTBD.

No.	tR (min)	Formula	Identification	Precursor ions (m/z)	Diff (ppm)	Fragment (m/z)	Type	Reference standard
1	0.25	$C_{27}H_{30}O_{16}$	Rutin	609.1461 $[M-H]^-$	−3.414	301.0351, 300.0278, 283.0325, 271.0251, 255.0292, 227.0321, 151.0293	F	Yes
2	1.05	$C_{15}H_{10}O_7$	Quercetin	301.0353 $[M-H]^-$	3.724	273.0405, 257.0452, 229.0500, 178.9978, 151.0026, 121.0283, 107.0126	F	
3	1.68	$C_8H_8O_4$	Vanillic acid	167.0349 $[M-H]^-$	0.867	152.0105, 123.0438, 108.0203	PO	
4	2.35	$C_{17}H_{20}O_9$	Methyl chlorogenic acid	367.1034 $[M-H]^-$	5.239	191.0553, 173.0078	P	
5	3.57	$C_{11}H_{14}O_5$	Genipin	225.0768 $[M-H]^-$	2.738	207.0659, 147.0441, 123.0439, 101.0231	I	Yes
6	3.82	$C_6H_6O_3$	Pyrogallic acid	125.0244 $[M-H]^-$	−1.604	107.4741, 97.0282	PO	
7	4.09	$C_{16}H_{22}O_{10}$	Geniposidic acid	373.1140 $[M-H]^-$	−6.227	211.0940, 193.0498, 167.0703, 149.0598, 123.0439	I	

Table 1: Continued.

No.	tR (min)	Formula	Identification	Precursor ions (m/z)	Diff (ppm)	Fragment (m/z)	Type	Reference standard
8	4.47	$C_{16}H_{22}O_{11}$	Deacetyl asperulosidic acid	389.1089 $[M-H]^-$	3.167	227.0550, 209.0356, 191.0553, 183.0655, 165.0541, 147.0285, 139.0389	I	
9	4.85	$C_{10}H_{14}O_{10}$	2-Methylsuccinyl-6′-O-glucoside	293.0514 $[M-H]^-$	6.047	131.0450	PO	
10	4.92	$C_{15}H_{22}O_9$	Aucubin	345.1191 $[M-H]^-$	2.335	183.0660, 165.0543, 139.0391, 121.0285	I	
11	5.37	$C_{17}H_{26}O_{11}$	Harpagide acetate	405.1402 $[M-H]^-$	−1.364	191.0554, 147.0289, 119.0026, 101.0023	I	
12	6.23	$C_{15}H_{10}O_6$	Kaempferol	285.0404 $[M-H]^-$	4.615	257.0453, 243.1601, 239.1650, 229.0322, 199.0395, 185.0420	F	Yes
13	7.41	$C_{23}H_{34}O_{15}$	Genipin gentian diglycoside	549.1824 $[M-H]^-$	5.378	387.2035, 207.1128, 179.0551, 147.0298	I	
14	7.50	$C_{25}H_{24}O_{11}$	3-Caffeoyl-5-coumaroyl-quinic acid	499.12458 $[M-H]^-$	5.81	353.1080, 191.0554	P	
15	8.32	$C_{19}H_{18}O_{11}$	Isomangiferin	421.0776 $[M-H]^-$	−1.966	259.0224	F	
16	8.44	$C_9H_6O_3$	Umbelliferone	161.0244 $[M-H]^-$	−0.249	135.0441, 99.0438, 71.0124	P	
17	8.99	$C_7H_6O_5$	Gallic acid	169.0142 $[M-H]^-$	0.179	125.0232, 141.0914	PO	Yes
18	9.25	$C_6H_6O_4$	2-Hydroxyphenol	141.0193 $[M-H]^-$	3.247	123.0175	PO	
19	9.76	$C_{15}H_{14}O_6$	L-Epicatechin	289.0717 $[M-H]^-$	7.333	271.0235, 245.0411, 205.2713, 179.0110	F	
20	10.56	$C_4H_4O_4$	Maleic acid	115.0036 $[M-H]^-$	−0.479	71.0124	PO	
21	11.43	$C_{15}H_{24}O_{10}$	Harpagide	363.1296 $[M-H]^-$	0.977	183.0652, 89.0228	I	
22	12.53	$C_{16}H_{18}O_9$	Chlorogenic acid	353.0878 $[M-H]^-$	0.854	191.0554, 179.0341, 173.0446, 161.0234, 155.0338, 137.0322, 135.0440, 93.0333	P	Yes
23	14.13	$C_8H_8O_4$	Methyl protocatechuic acid	167.0349 $[M-H]^-$	0.508	152.0106, 123.0439, 108.0203	PO	
24	15.84	$C_8H_8O_4$	Isovanillic acid	167.0349 $[M-H]^-$	−2.536	123.0439	PO	
25	18.23	$C_{13}H_{16}O_9$	Protocatechuic acid-4-glucoside	315.0721 $[M-H]^-$	−1.392	108.0204	PO	

Table 1: Continued.

No.	tR (min)	Formula	Identification	Precursor ions (m/z)	Diff (ppm)	Fragment (m/z)	Type	Reference standard
26	19.56	$C_{14}H_{18}O_9$	4-Glucopyranoxy-3-benzoic acid	329.0878 $[M-H]^-$	4.340	167.0340, 152.0105, 123.0439, 108.0204	O	
27	20.23	$C_9H_{12}O_5$	Rehmaglutin C	199.0611 $[M-H]^-$	3.316	155.0704, 137.0596	I	
28	20.39	$C_{18}H_{24}O_{12}$	Asperulosidic acid	431.1194 $[M-H]^-$	−3.114	269.0198, 251.0098	I	
29	21.77	$C_{16}H_{18}O_9$	Neochlorogenic acid	353.0878 $[M-H]^-$	−0.699	191.0554, 179.0341, 135.0440	P	
30	22.36	$C_{16}H_{18}O_9$	4-Caffeoylquinic acid	353.0878 $[M-H]^-$	3.941	191.0554, 179.0340, 135.1440	P	
31	23.28	$C_{20}H_{24}O_7$	Cycloolivil	375.1449 $[M-H]^-$	−2.075	327.1343, 297.1207, 257.1132, 151.0752	L	
32	24.28	$C_9H_8O_4$	Caffeic acid	179.0349 $[M-H]^-$	0.856	135.0440	P	Yes
33	24.36	$C_9H_{10}O_4$	Dihydrocaffeic acid	181.0506 $[M-H]^-$	1.849	163.0390, 135.0441, 119.0488	P	
34	26.50	$C_7H_6O_4$	Gentianic acid	153.0193 $[M-H]^-$	−0.295	109.0282	PO	
35	27.23	$C_7H_6O_4$	Protocatechuic acid	153.0193 $[M-H]^-$	0.685	109.0283, 91.0175,	PO	
36	28.03	$C_{42}H_{70}O_{12}$	Ginsenoside F_4	789.4759 $[M+Na]^+$	−1.837	707.1499, 643.4222, 349.1090	T	
37	28.55	$C_{20}H_{24}O_7$	Oleoresin	375.1449 $[M-H]^-$	−1.018	179.0341, 161.0233	L	
38	29.40	$C_{16}H_{18}O_9$	Cryptochlorogenic acid	353.0878 $[M-H]^-$	3.516	191.0554, 179.0340, 173.0446, 135.0440	P	
39	30.90	$C_{20}H_{24}0_7$	Olivil	375.1449 $[M-H]^-$	−2.635	327.1360, 195.1251, 179.0341, 161.0220	L	
40	32.26	$C_{17}H_{24}O_{10}$	Geniposide	387.1296 $[M-H]^-$	3.128	207.1025, 123.0444, 101.0232	I	
41	33.49	$C_{33}H_{44}O_{19}$	Naringin dihydrochalcone 4-O-β-D-glucoside	743.2404 $[M-H]^-$	3.128	373.1295, 313.1088, 181.0498, 151.0396	F	
42	34.26	$C_{27}H_{32}O_{16}$	Hydroxysafflor yellow A	611.1617 $[M-H]^-$	2.207	491.1200, 473.1092, 403.1042, 325.0720	F	Yes
43	37.58	$C_{10}H_{10}O_4$	Ferulic acid	193.0506 $[M-H]^-$	2.208	178.0264, 149.0598, 134.0362	P	Yes
44	38.11	$C_{32}H_{42}O_{16}$	Pinoresinol diglucoside	681.2400 $[M-H]^-$	2.039	519.5070, 357.1346, 151.0390, 136.0159	L	
45	39.59	$C_{16}H_{18}O_8$	3-O-p-Coumaroylquinic acid	337.0928 $[M-H]^-$	6.688	191.0553, 173.0448, 163.0390	P	

Table 1: Continued.

No.	tR (min)	Formula	Identification	Precursor ions (m/z)	Diff (ppm)	Fragment (m/z)	Type	Reference standard
46	40.21	$C_{27}H_{36}O_{13}$	Citrusin B	567.2083 $[M-H]^-$	−4.289	341.1384, 329.1394	L	
47	41.77	$C_{27}H_{30}O_{17}$	Quercetin-3, 4′-O-di-β-glucopyranoside	625.1410 $[M-H]^-$	0.831	463.0884, 301.0350, 271.0243	F	
48	42.23	$C_{15}H_{26}O_9$	Eucommioside	349.1504 $[M-H]^-$	−1.102	187.1528, 89.0230	I	
49	43.69	$C_{10}H_{10}O_3$	Coniferyl aldehyde	177.0557 $[M-H]^-$	−0.101	162.0312	P	
50	46.23	$C_{20}H_{22}O_7$	Erythroglycerin-β-terpineol aldehyde ether	373.1292 $[M-H]^-$	4.259	177.0548, 165.0547, 150.0308,	P	
51	48.38	$C_{26}H_{28}O_{16}$	Quercetin 3-O-sambubioside	595.1305 $[M+H]^+$	−0.638	301.0327	F	
52	49.62	$C_{26}H_{32}O_{11}$	Pinoresinol-4′-O-β-D-glucopyranoside	519.1871 $[M-H]^-$	−3.929	357.1345, 151.0390	L	
53	54.63	$C_{26}H_{32}O_{11}$	Pinoresinol-β-D-glucoside	519.1871 $[M-H]^-$	3.334	357.1345, 342.1107, 311.1293, 151.0390, 136.0154	L	
54	55.16	$C_{21}H_{20}O_{12}$	Isoquercitrin	463.0881 $[M-H]^-$	3.623	301.0349, 271.0321, 255.0299	F	Yes
55	56.44	$C_{22}H_{28}O_{14}$	5-(3 ′-o-caffeoylglucosyl) quinine	515.1406 $[M-H]^-$	8.420	191.0555, 161.0234, 135.0440	P	
56	57.45	$C_{22}H_{28}O_{14}$	1-O-(3 ′-o-caffeoylglucosyl) quinine	515.1406 $[M-H]^-$	2.499	179.0341, 173.0446, 161.0233, 135.0440	P	
57*	57.73	$C_{33}H_{40}O_{21}$	Quercetin 3-glucosyl-(1->3)-rhamnosyl-(1->6)-galactoside	771.1989 $[M-H]^-$	2.070	609.1469, 463.0873, 301.0351	F	
58	58.66	$C_{28}H_{36}O_{13}$	Syringaresionl-O-β-D-g1ucopyranoside	579.2083 $[M-H]^-$	3.298	417.1557	P	
59	59.50	$C_{35}H_{60}O_6$	Daucosterol	575.4317 $[M-H]^-$	2.329	397.7564	T	
60	62.59	$C_{25}H_{24}O_{12}$	1,5-Dicaffeoylquinic acid	515.1194 $[M-H]^-$	2.499	353.0881, 191.0554, 135.0440	P	
61	63.34	$C_{25}H_{24}O_{12}$	Isochlorogenic acid A	515.1194 $[M-H]^-$	1.288	353.0881, 191.0554, 179.0341, 173.0446, 135.0440	P	
62	64.00	$C_{42}H_{72}O_{15}$	6-O-β-D-Glucopyranosyl-20-o-β-D-glucopyranosyl-3β,6β,12β,20 (S)7-25-pentaphydroxydammar-23-enedroginsenoside Rg_1	839.4763 $[M+Na]^+$	−2.644	659.4114	T	
63	65.10	$C_{25}H_{24}O_{12}$	Isochlorogenic acid B	515.1194 $[M-H]^-$	1.288	353.0881, 335.0777, 191.0554, 179.0341, 173.0446	P	
64	66.70	$C_9H_{16}O_4$	Eucommitol	187.0975 $[M-H]^-$	1.521	169.0861, 143.1068, 125.0960	I	Yes
65	66.72	$C_6H_4O_4$	Coumalic acid	139.0036 $[M-H]^-$	6.332	119.5097	O	

Table 1: Continued.

No.	tR (min)	Formula	Identification	Precursor ions (m/z)	Diff (ppm)	Fragment (m/z)	Type	Reference standard
66	67.26	$C_{18}H_{16}O_5$	Sideroxylin	311.0924 $[M-H]^-$	2.177	267.0663	F	
67	67.68	$C_{21}H_{20}O_{12}$	Hyperoside	463.0882 $[M-H]^-$	4.206	301.03455, 151.00258	F	
68	68.78	$C_{15}H_{26}O_7$	2-(5-Hydroxyethyl-2,3-dimethyl-2-cyclopenten-1-yl)-glucopyranoside	317.1605 $[M-H]^-$	4.580	243.1238, 225.1132	I	
69	69.40	$C_{21}H_{20}O_{10}$	Apigenin-7-O-glucuronide	431.0983 $[M-H]^-$	3.147	269.0376	F	
70	70.29	$C_9H_{16}O_3$	1-Deoxyeucommitol	171.1026 $[M-H]^-$	0.930	127.1118, 125.0959	I	
71	72.63	$C_{21}H_{20}O_{11}$	Astragalin	447.0933 $[M-H]^-$	2.532	285.0395, 241.0829, 217.0886	F	
72	73.55	$C_{21}H_{18}O_{11}$	Baicalin	445.0776 $[M-H]^-$	4.724	269.0456	F	
73	74.23	$C_{27}H_{30}O_{15}$	Nicotiflorin	593.1511 $[M-H]^-$	3.681	285.0404, 255.0307, 227.0352	F	
74	74.88	$C_{27}H_{30}H_{15}$	Safflor yellow (A)	593.1511 $[M-H]^-$	3.884	285.0404	F	Yes
75	75.61	$C_{18}H_{14}O_6$	Milletenin C	325.0717 $[M-H]^-$	2.650	310.0848	F	
76	76.26	$C_{12}H_{16}O_3$	3-Butyl-4-hydroxy-4,5-dihydro-2-benzofuran-1(3H)-one	207.1026 $[M-H]^-$	0.368	135.0443	O	
77	77.03	$C_{11}H_{12}O_4$	Ethyl caffeate	207.0662 $[M-H]^-$	3.162	179.0341, 161.0234, 135.0440	P	
78	77.96	$C_{48}H_{82}O_{19}$	Notoginsenoside R_6	985.5342 $[M+Na]^+$	−2.049	365.1045, 305.0816	T	
79	78.56	$C_{48}H_{82}O_{19}$	Notoginsenoside R_3	985.5342 $[M+Na]^+$	2.402	645.4159, 365.1044	T	
80*	79.20	$C_{28}H_{32}O_{16}$	6-Methoxykaempferol 3-robinobioside	623.16175 $[M-H]^-$	1.524	315.0509, 301.0320, 300.0276	F	
81*	79.40	$C_{29}H_{36}O_{15}$	3,4,6-Trihydroxy-4,2′-dimethoxychalcone 4′-O-rutinoside	623.19814 $[M-H]^-$	6.18	315.0510, 301.0313, 300.0376	F	
82	79.58	$C_{48}H_{82}O_{19}$	Notoginsenoside M	985.5342 $[M+Na]^+$	−3.227	805.4688, 365.1047	T	
83	81.76	$C_{48}H_{82}O_{19}$	Notoginsenoside N	985.5342 $[M+Na]^+$	−2.983	805.4689	T	
84	82.77	$C_{48}H_{82}O_{19}$	20-O-Glucoginsenoside Rf	985.5342 $[M+Na]^+$	−1.684	805.4689, 365.2320	T	
85*	83.83	$C_{23}H_{22}O_{11}$	Apigenin 7-(2″-acetylglucoside)	473.1089 $[M-H]^-$	1.569	413.0891, 269.0379	F	
86	84.34	$C_{41}H_{68}O_{12}$	Notoginsenoside T_5	775.4602 $[M+Na]^+$	−2.385	692.0035, 643.3312, 463.3556, 335.0930	T	
87	84.47	$C_{47}H_{80}O_{18}$	Notoginsenoside R_1	931.5271 $[M-H]^-$	0.633	799.4888, 637.4328, 475.3800, 391.0658	T	Yes
88	85.37	$C_{15}H_{10}O_6$	Luteolin	285.0404 $[M-H]^-$	4.720	257.0453, 151.0030	F	
89	85.76	$C_{42}H_{72}O_{14}$	Majoroside F_4	823.4814 $[M+Na]^+$	−1.603	643.4166	T	
90	86.17	$C_{42}H_{72}O_{14}$	3-O-β-D-Glucopyranosyl-6-O-β-D-glucopyranosyl-20-(S)-protopanaxatriol	823.4814 $[M+Na]^+$	−3.157	703.0069, 643.4163	T	

Table 1: Continued.

No.	tR (min)	Formula	Identification	Precursor ions (m/z)	Diff (ppm)	Fragment (m/z)	Type	Reference standard
91	87.18	$C_{42}H_{72}O_{14}$	Gynoside B	823.4814 $[M+Na]^+$	−1.603	643.4164	T	
92	87.69	$C_{42}H_{72}O_{14}$	Ginsenoside Rg_1	823.4814 $[M+Na]^+$	−1.603	643.4104	T	
93	88.21	$C_{45}H_{74}O_{17}$	Malonyl ginsenoside Rg_1	909.4818 $[M+Na]^+$	−1.891	865.4895, 729.4166, 685.4270	T	
94	89.59	$C_{48}H_{80}O_{19}$	Notoginsenoside G	983.5186 $[M+Na]^+$	−2.897	803.4535	T	
95*	89.94	$C_{30}H_{28}O_{12}$	4,2′,3′,4′-Tetrahydroxychalcone 4′-O-(2″-O-p-coumaroyl) glucoside	579.1507 $[M-H]^-$	0.622	271.0614, 151.0027, 107.0126	F	
96	90.05	$C_{15}H_{10}O_5$	Genistein	269.0455 $[M-H]^-$	4.572	225.0554, 201.0555, 151.0027, 117.0329, 107.0124	F	Yes
97	90.57	$C_{15}H_{10}O_5$	Apigenin	269.0455 $[M-H]^-$	4.572	225.0555, 201.0553, 151.0025, 117.0328, 107.0124	F	Yes
98	91.24	$C_{41}H_{70}O_{13}$	Pseudoginsenoside RT_3	793.4708 $[M+Na]^+$	3.882	613.4072	T	
99	91.79	$C_{44}H_{74}O_{15}$	Yesanchinoside D	865.4919 $[M+Na]^+$	−4.633	685.4267	T	
100	92.47	$C_{30}H_{26}O_{12}$	Apigenin-7-O-(6″-coumaroyl) glucoside	577.1351 $[M-H]^-$	1.390	431.0988, 269.0457	F	
101	92.96	$C_{20}H_{22}O_6$	Epipinoresinol	357.1343 $[M-H]^-$	1.216	151.1533, 136.0809, 121.0282	L	
102	94.52	$C_{42}H_{72}O_{14}$	Ginsenoside Rf	823.4814 $[M+Na]^+$	−2.113	661.5368, 641.4468, 365.1043	T	
103	95.39	$C_{41}H_{70}O_{13}$	Notoginsenoside R_2	793.4708 $[M+Na]^+$	−2.583	661.4249, 481.3630, 335.0939	T	
104	95.89	$C_{42}H_{72}O_{13}$	Ginsenoside Rg_2	807.4865 $[M+Na]^+$	−1.362	661.4281, 481.3676, 349.1101	T	
105	96.47	$C_{36}H_{62}O_9$	Gypenoside LXXVI	661.4286 $[M+Na]^+$	2.479	601.2890, 481.3620	T	
106	97.28	$C_{36}H_{62}O_9$	Ginsenoside Rh_1	661.4286 $[M+Na]^+$	−1.769	481.3650, 413.2539	T	
107	98.42	$C_{59}H_{100}O_{27}$	Ginsenoside Ra_3	1263.6344 $[M+Na]^+$	−2.327	789.4784, 497.1457, 437.1239	T	
108	99.42	$C_{59}H_{100}O_{27}$	Notoginsenoside Fa	1263.6344 $[M+Na]^+$	−0.688	921.5158	T	
109	100.51	$C_{54}H_{92}O_{22}$	Notoginsenoside I	1115.5972 $[M+Na]^+$	−1.470	773.4795, 365.1046	T	
110	101.91	$C_{54}H_{92}O_{23}$	Ginsenoside Rb_1	1107.5956 $[M-H]^-$	0.589	945.5432, 783.4906, 621.4368, 459.3851	T	Yes
111	102.94	$C_{42}H_{72}O_{13}$	Ginsenoside Rg_3	807.4865 $[M+Na]^+$	−0.904	365.1046	T	
112	103.85	$C_{48}H_{82}O_{18}$	Ginsenoside Re	969.5393 $[M+Na]^+$	−1.908	789.4742	T	Yes
113	105.07	$C_{54}H_{92}O_{23}$	Yesanchinoside E	1131.5921 $[M+Na]^+$	−5.768	789.4737, 365.1045	T	

Table 1: Continued.

No.	tR (min)	Formula	Identification	Precursor ions (m/z)	Diff (ppm)	Fragment (m/z)	Type	Reference standard
114	106.08	$C_{38}H_{64}O_{10}$	6′-O-Acetylginsenoside F_1	703.4391 $[M+Na]^+$	0.071	481.3647	T	
115	106.58	$C_{56}H_{94}O_{24}$	Quinquenoside R_1	1173.6027 $[M+Na]^+$	−2.548	831.4845, 365.1044	T	
116	107.65	$C_{56}H_{94}O_{24}$	6‴-O-Acetylginsenoside Rb_1	1173.6027 $[M+Na]^+$	−2.326	831.4845, 789.4744, 407.1151, 347.0945	T	
117	108.75	$C_{53}H_{90}O_{22}$	Ginsenoside Rb_2	1101.5815 $[M+Na]^+$	−1.479	789.4740, 335.0939	T	
118	109.76	$C_{53}H_{90}O_{22}$	Notoginsenoside L	1101.5815 $[M+Na]^+$	−1.479	789.4740	T	
119	110.33	$C_{57}H_{94}O_{26}$	Malonyl ginsenoside Rb_1	1217.5925 $[M+Na]^+$	−2.727	1173.5993, 875.4738, 831.4844, 789.4738	T	
120	111.31	$C_{48}H_{82}O_{17}$	Vina-ginsenoside R_3	953.5444 $[M+Na]^+$	−2.349	773.4788	T	
121	111.47	$C_{48}H_{82}O_{18}$	Gypenoside XVII	969.5393 $[M+Na]^+$	−0.908	365.1048	T	
122	112.04	$C_{57}H_{94}O_{26}$	3-(β-D-Glucopyranosyl-β-D-glucopyranosyl)-20-O-(6-O-malonyl-β-D-glucopyranosyl-β-D-glucopyranosyl)-3β,12β,20(S)-trihydroxydammar-24-ene	1217.5925 $[M+Na]^+$	−1.07	1173.6008, 1131.5912, 875.4739, 831.4839, 789.4733, 451.1044, 407.1150	T	
123	112.53	$C_{48}H_{82}O_{18}$	Ginsenoside Rd	945.5428 $[M-H]^-$	0.857	783.4907, 621.4375, 459.3848, 375.3146	T	Yes
124	112.57	$C_{36}H_{62}O_8$	Notoginsenoside R_7	645.4336 $[M+Na]^+$	−3.249	627.3813, 465.3691	T	
125	113.48	$C_{36}H_{60}O_8$ $C_{36}H_{60}O_7$	Ginsenoside Rh_3	643.4180 $[M+Na]^+$	−3.232	583.3644, 463.3514	T	
126	113.89	$C_{51}H_{84}O_{21}$	Malonyl ginsenoside Rd	1055.5397 $[M+Na]^+$	3.598	875.4738, 789.4740	T	
127	114.07	$C_{48}H_{82}O_{18}$	Gypenoside LXXII	969.5393 $[M+Na]^+$	−1.691	789.4739	T	
128	114.88	$C_{36}H_{62}O_{11}$	Notoginsenoside T_4	693.4184 $[M+Na]^+$	−3.763	633.3707	T	
129	115.36	$C_{47}H_{80}O_{17}$	3-O-[β-D-Glucopyranosyl(1–2)-β-D-glucopyranosyl]-20-O-β-D-xylopyranosyl-3β,12β,20(s)-trihydroxydammar-24-ene	939.5287 $[M+Na]^+$	−0.872	789.4735	T	
130	116.22	$C_{15}H_{10}O_5$	Baicalein	269.0455 $[M-H]^-$	4.238	197.1905	F	Yes
131	117.02	$C_{47}H_{80}O_{18}$	6-O-[Xylopyranosyl-β-D-glucopyranosyl]-3β,6β,12β,20(s),25-pentahydroxydammar	811.4814 $[M+Na]^+$	1.208	793.3365, 751.2600, 679.2239, 499.1350, 412.1227, 335.0018	T	
132	117.70	$C_{20}H_{22}O_6$	Pinoresinol	357.1343 $[M-H]^-$	1.340	313.1811, 151.1520, 136.0819	L	
133	118.87	$C_{42}H_{72}O_{13}$	Ginsenoside F_2	807.4865 $[M+Na]^+$	0.458	627.4217	T	
134	120.08	$C_{42}H_{72}O_{13}$	Gypenoside LXXV	807.4865 $[M+Na]^+$	7.789	365.1045	T	

Table 1: Continued.

No.	tR (min)	Formula	Identification	Precursor ions (*m/z*)	Diff (ppm)	Fragment (*m/z*)	Type	Reference standard
135	121.53	$C_{29}H_{42}O_5$	Ulmoidol	469.2959 $[M-H]^-$	3.715	423.2238	T	
136	121.65	$C_{28}H_{34}O_4$	Unknown	433.2384 $[M-H]^-$	−0.685	433.2577	O	
137	122.04	$C_{36}H_{60}O_9$	Ginsenoside Rh_7	659.4129 $[M+Na]^+$	−0.349	599.3925	T	
138	122.50	$C_{32}H_{42}O_{17}$	1-Hydroxypinoresinol-4,4″-di-O-*β*-D-glucopyranoside	697.2349 $[M-H]^-$	0.112	535.1532, 373.0323	L	
139	122.99	$C_{20}H_{24}O_8$	Threo-dihydroxydehy-drodiconiferyl alcohol	391.1398 $[M-H]^-$	−3.313	313.1747, 295.0882	L	
140	123.91	$C_{16}H_{32}O_2$	Palmitic acid	255.2329 $[M-H]^-$	1.978	241.3251	O	Yes
141	124.01	$C_{20}H_{24}O_8$	Erytho-dihydroxydehydrodiconiferyl alcohol	391.1398 $[M-H]^-$	−2.359	341.1587, 313.0930, 207.0832	L	
142	125.83	$C_{18}H_{36}O_2$	Palmitic acid ethyl ester	283.2642 $[M-H]^-$	3.859	89.0229	O	
143	127.10	$C_9H_{12}O_4$	Eucommidiol	183.0662 $[M-H]^-$	0.268	139.1124, 93.7235	I	

945.5432, *m/z* 783.4906, *m/z* 621.4368, and *m/z* 459.3851. Compared with the standard, compound 110 was identified as ginsenoside Rb_1; the possible cleavage pathways of ginsenoside Rb_1 are shown in Figure S2-A. Similarly, $[M-H]^-$ at *m/z* 945.5428 (compound 123) was tentatively identified ginsenoside Rd; the main fragment ions were [M-H-glc]$^-$ *m/z* 783.4907, [M-H-glc-glc]$^-$ *m/z* 621.4375, and [M-H-glc-glc-glc]$^-$ *m/z* 459.3848 [26]. Compound 87 was filtered by characteristic ion *m/z* 475.38, which tentatively identified PPT type ginsenoside. In the secondary mass spectrum, fragment ions *m/z* 799.4888, *m/z* 637.4328, *m/z* 475.3800, and *m/z* 391.0658 were [M-H-xyl]$^-$, [M-H-xyl-glc]$^-$, [M-H-xyl-glc-glc]$^-$, and aglycon; the possible cleavage pathways of $[M-H]^-$ are shown in Figure S2-B.

By using the FSCIF strategy, a total of eleven compounds (107, 112, 113, 116, 117, 118, 119, 122, 126, 127, and 129) were detected by characteristic ion of 789.47 Da ([M + Na-glcglc^{6}malonyl]$^+$). The retention time of compound 122 was 112.04 min; the fragment ions *m/z* 451.1044 and *m/z* 789.4733 were a pair of complementary ions [glcglc^{6}malonyl + Na]$^+$ and [M + Na-gicglc^{6}malonyl]$^+$. In addition, the fragment ions were observed in *m/z* 1173.6008, 113l.5912, 875.4739, 83l.4839, and 407.1150, which were assigned to [M + Na-CO_2]$^+$, [M + Na-malonyl]$^+$, [M + Na-glcglc]$^+$, [M + Na-(glcglc + CO_2)$^+$], and [glcglc^{6}malonyl + Na-CO_2]$^+$ fragment ions. The possible cleavage pathways of compound 122 are shown in Figure S2-C.

Additionally, the sugar type and its junction position were concluded with the application of NLF strategy. The position of sugar fragments on the aglycon was relatively fixed (C3, C6, and C12), and the main types of sugars were glc (162.02 Da), rha (146.01 Da), and xyl (132.02 Da); the linkage between sugars is mainly l–2 and 1–6. In this experiment, nineteen compounds (62, 82, 83, 84, 89, 90, 91, 92, 93, 94, 98, 99, 102, 105, 106, 120, 124, 125, and 133) were detected by NLF with 162.02 Da. Compounds 36, 86, 103, and 104 filtered by 146.01 Da or 132.02 Da were obtained. Compound 103 ($C_{42}H_{72}O_{13}$) $[M+Na]^+$ at *m/z* 793.4708 tentatively annotated notoginsenoside R_2; the main fragment ions were [M-H-xyl]$^-$ *m/z* 661.4249, [M-H-xyl-glc]$^-$ *m/z* 481.3630, and [M-H-xyl-glc-rha]$^-$ *m/z* 335.0939. Compound 104 ($C_{42}H_{72}O_{13}$) $[M+Na]^+$ at *m/z* 807.4865 tentatively annotated ginsenoside Rg_2. First, the ion at *m/z* 661.4281 was formed by the neutral loss of a rhamnose unit of the ion at *m/z* 807.4865. Second, the ion at *m/z* 481.3676 was formed by the neutral loss of a glucose unit of the ion at *m/z* 661.4281. Finally, ion at *m/z* 349.1101 was formed by the neutral loss of a xylose unit of the ion at *m/z* 481.3676.

3.2.2. Identification of Flavonoids. Most flavonoid aglycones were derivatives of quercetin, kaempferol, and apigenin, so we set 301.03 Da, 285.04 Da, and 269.04 Da as characteristic ions templates for these components annotation, which contributes to the rapid annotate flavonoids. A total of nine compounds (1, 2, 47, 51, 54, 57, 67, 80, and 81) screened with 301.03 Da were found; compound 1 showed $[M-H]^-$ at *m/z* 609.1461, which was tentatively identified as rutin; its important fragment ion was 301.03 Da in secondary mass spectra, indicating the neutral loss of 308.11 Da ($C_{12}H_{20}O_9$). In addition, the occurrences of *m/z* 283.0325, *m/z* 255.0292, and *m/z* 227.0321 were a better proof of [M-H-$C_{12}H_{20}O_9$-H_2O]$^-$, [M-H-$C_{12}H_{20}O_9$-H_2O-CO]$^-$, and [M-H-$C_{12}H_{20}O_9$-H_2O-2CO]$^-$, which were the main peak, appearing in second mass spectra (Figure S3-A). Moreover, compounds 57, 80, and 81 were annotated for the first time in MTBD. Compound 57 showed $[M-H]^-$ at *m/z* 771.1989; the ion at *m/z* 609.1469 was formed by the neutral loss of a glucose unit of the ion at *m/z* 771.1989. Besides, the ion at *m/z* 463.0873 was formed by the neutral loss of an xylose unit of the ion at *m/z* 609.1469. Finally, ion at *m/z* 301.0351 was formed by the

neutral loss of a glucose unit of the ion at *m/z* 463.0873. Hence, compound 57 was tentatively annotated Quercetin 3-glucosyl-(1->3)-rhamnosyl-(1->6)-galactoside.

A total of five compounds (12, 71, 73, 74, and 88) acquired with 285.04 Da were found. Compound 12 showed $[M-H]^-$ at *m/z* 285.0404, *m/z* 257.0453, *m/z* 239.1650, *m/z* 229.0322, and *m/z* 185.0420, corresponding to $[M\text{-}H\text{-}CO]^-$, $[M\text{-}H\text{-}CO\text{-}H_2O]^-$, $[M\text{-}H\text{-}2CO]^-$, and $[M\text{-}H\text{-}2CO\text{-}CO_2)^-$, which contributed to the crack of C2-C3 and C4–C10. In addition, the fracture of C4–C10 bond can also lead to the removal of C_2H_2O (42.02 Da), which corresponded to *m/z* 243.1601. Next, the removal of CO_2 (44.01 Da) results in the generation of *m/z* 199.0395. By using the FSCIF strategy, seven compounds (69, 72, 85, 96, 97, 100, and 130) screened with 269.04 Da were found. Compound 97 was tentatively identified as apigenin; a high abundance secondary mass spectrometer fragment ion *m/z* 225.0555 was formed after CO_2 (44.01 Da) loss, indicating that apigenin derivatives were easier to lose CO_2. In addition, *m/z* 269.0455 lost one molecule, C_3O_2 (68.02 Da), resulting in *m/z* 201.0553. Apigenin, which is a flavonoid with double bond on the six-membered ring, can also undergo ring opening reaction of C ring, resulting in fragment ions such as *m/z* 151.0025, *m/z* 117.0328, and *m/z* 107.0124. These structural changes were also reflected at a retro-Diels-Alder (RDA) reaction [27]. Hence, the characteristic ion of RDA was set by 151.00 Da; compounds 1, 2, 41, 67, 88, 95, 96, and 97 screened with 151.00 Da were found. Compound 95 was annotated as 4,2′,3′,4′-tetrahydroxychalcone 4′-O-(2″-O-p-coumaroyl) glucoside (*m/z* 579.1507), which was being reported from MTBD for the first time. Its molecular ion peak *m/z* 269.0455 at $[M-H]^-$ was observed; the fragment ions *m/z* 271.0614, *m/z* 151.0027, and *m/z* 107.0126 proved $[M-H\text{-}C_{15}H_{16}O_7]^-$, $[M\text{-}H\text{-}C_{15}H_{16}O_7\text{-}C_8H_8O]^-$, and $[M\text{-}H\text{-}C_{15}H_{16}O_7\text{-}C_8H_8O\text{-}C_9H_9O_2]^-$.

3.2.3. Identification of Phenylpropanoids. Phenylpropanoids and their derivatives, including monocaffeoylquinic acids, biscaffeoylquinic acids, and caffeoylquinic acid derivatives, were main components widely present in MTBD. Some papers [28] have previously shown that phenylpropanoids have multifaceted effects which include anti-inflammatory, antioxidant, antimicrobial, and antidiabetic activities and exhibit renoprotective, hepatoprotective, and cardioprotective effects. By using the FSCIF strategy, twenty phenylpropanoids were found; the ions at *m/z* 191.05 Da and 179.03 Da represented the base peaks of quinic acid, whereas ions at *m/z* 161.02 Da and 135.04 Da represented the base peaks of caffeic acid. Chlorogenic acid is an ester of caffeic acid and quinic acid, which indicates that chlorogenic acid contains the feature ions of both caffeic acid and quinic acid. A total of twelve compounds (4, 14, 22, 29, 30, 38, 45, 55, 56, 60, 61, and 63) were detected by *m/z* 191.05 Da and 179.03 Da. Compound 22 was tentatively identified as chlorogenic acid, producing *m/z* 191.0554, *m/z* 179.0341 (compound 32), *m/z* 173.0446, *m/z* 161.0234, *m/z* 155.0338, *m/z* 137.0322, *m/z* 135.0440, and *m/z* 93.0333, which were corresponding to $[M\text{-}H\text{-}C_9H_6O_3]^-$, $[M\text{-}H\text{-}C_7H_{10}O_5]^-$, $[M\text{-}H\text{-}C_9H_6O_3\text{-}H_2O]^-$, $[M\text{-}H\text{-}C_7H_{10}O_5\text{-}H_2O]^-$, $[M\text{-}H\text{-}C_9H_6O_3\text{-}2H_2O]^-$, $[M\text{-}H\text{-}C_9H_6O_3\text{-}3H_2O]^-$, $[M\text{-}H\text{-}C_7H_{10}O_5\text{-}CO_2]^-$, and $[M\text{-}H\text{-}C_9H_6O_3\text{-}3H_2O\text{-}CO_2]^-$. Figure S3-B shows the main cracking pathways of chlorogenic acid. Compounds 16, 32, 33, and 77 were filtered by *m/z* 161.02 Da and 135.04 Da, which were indicative of caffeic acid derivatives. Take compound 77 ($C_{11}H_{12}O_4$) as an example; $[M-H]^-$ at *m/z* 207.0662 and the secondary mass spectrometry were detected at *m/z* 179.0341 $[M\text{-}H\text{-}CO]^-$, *m/z* 161.0234 $[M\text{-}H\text{-}CO\text{-}H_2O]^-$, and *m/z* 135.0440 $[M\text{-}H\text{-}CO\text{-}CO_2]^-$, which were tentatively identified as ethyl caffeate. Compounds 32 and 33 also have similar pyrolysis laws.

3.2.4. Identification of Iridoids. The most basic core of iridoids is iridoid alcohol, containing cyclic ethers and alcoholic hydroxyl groups, which imply that the basic skeleton of iridoid glycosides contains a characteristic dihydropyran ring which is cis-connected to a cyclopentane unit structure. A total of 15 iridoids were detected $[M-H]^-$ in negative ion mode. In the ESI^- mode, the fragment ion $^{2,7}F0^-$ ion at *m/z* 101.02 was obtained by the fragmentation of the aglycon part of the excimer ion, which was a characteristic ion to annotate the structure of the excimer ion [29, 30]. According to the literature [11], the ion at *m/z* 147.03 was the prominent ion of iridoids. Compounds 5, 8, 11, 13, and 40 were detected by characteristic ions 147.03 Da or 101.02 Da. Taking the derivation process of compound 8 as an example, the quasi-molecular ion peak of compound 8 was *m/z* 389.1089 $[M-H]^-$, yielding a formula of $C_{16}H_{22}O_{11}$. The $[M-H]^-$ ion of *m/z* 227.0550 was the absence of glucose neutral fragment from *m/z* 389.1089. The fragment ions *m/z* of 209.0356 and 183.0655 were losing one molecule of H_2O and one molecule of CO_2 from $[M-H]^-$ ion of *m/z* 227.0550. Then, the ion of m/z 183.0655 losses two molecules of H_2O, convert to the fragment ions of *m/z* 165.0543 and *m/z* 147.0285. Consistently, the dehydration of fragment ion *m/z* 209.0356 leads to the production of *m/z* 191.0553; and the fragment ion *m/z* 147.0285 was decarboxylation of *m/z* 191.0553. The cleavage detail of each ion is displayed in Figure S3-C.

In addition, iridoid glycosides are usually connected to a glucose at the C1 position, so they are easy to lose neutral fragments such as 162.02 Da (glc), 44.01 Da (CO_2), and 18.01 Da (H_2O) [31]. A total of five compounds (7, 10, 21, 28, and 48) were filtered by 162.02 Da. Compound 7 ($C_{16}H_{22}O_{10}$) showed $[M-H]^-$ at *m/z* 373.1140; the fragment ions determined from MS/MS spectra were *m/z* 211.0606 $[M\text{-}H\text{-}glc]^-$, *m/z* 193.0498 $[M\text{-}H\text{-}glc\text{-}H_2O]^-$, *m/z* 167.0703 $[M\text{-}H\text{-}glc\text{-}CO_2]$, and *m/z* 149.0598 $[M\text{-}H\text{-}glc\text{-}CO_2\text{-}H_2O]$; *m/z* 211.0940 (373.1140 Da-162.02 Da) were characteristic fragments of compound 7, which was tentatively annotated as geniposidic acid. To sum up, the iridoids were easier to lose the glucose neutral fragment ion 162.02 Da and obtain aglycon fragment ions and then the aglycon ions decarboxylated or dehydrated to become a series of fragments.

3.2.5. Identification of Lignans. A large number of the bisepoxylignans and monoepoxylignans combine with glucose to form monoglycoside or diglycoside. Therefore, the majority of them could lose glycosyl and methyl neutral

fragments first and then lose one or two molecular of CH_2O and finally formed 151.03 Da. Therefore, characteristic ion fragment 151.03 Da was used to annotate lignans. Compounds 31, 44, 52, 53, 101, and 132 were detected by FSCIF with 151.03 Da. Compound 44 showed $[M-H]^-$ at *m/z* 681.2400; the fragment ions *m/z* 519.5070, *m/z* 357.1346, and *m/z* 151.0390 were corresponding to [M-H-glc]$^-$, [M-H-glc-glc]$^-$, and [M-H-glc-glc-$C_{12}H_{14}O_3$]$^-$. Subsequently, compounds 37, 39, 138, and 139 were filtered by NLF with ions of 162.02 Da, 44.01 Da, or 18.01 Da.

3.2.6. Other Compounds. A total of 11 polyphenols (3, 6, 9, 17, 18, 20, 23, 24, 25, 34, and 35) were recognized by FSNLF analysis. Because of the presence of hydroxyl and carboxyl groups, these compounds were filtered by 18.01 Da (H_2O) and 44.01 Da (CO_2). In addition, six other compounds were identified by comparison with the literature.

3.3. Quantification of 19 Major Compounds in MTBD. The 19 compounds quantified were the screening of osteoporosis targets by network pharmacology in the early stage of our laboratory, and then the representative and top ranked compounds were selected. Methodology analysis showed that the assay method of 19 compounds (including three pairs of isomers) had good repeatability and stability.

3.3.1. Specificity. The extracted ion chromatograms (EICs) of blank sample, standard mixture sample, and MTBD extracts sample are presented in Figure 4. Nineteen compounds in MTBD extracts were separated within 25 minutes, where baseline separation of each compound was achieved and no obvious signal noises occurred around determinate peak. Additionally, no interferences were detected between the three isomers.

3.3.2. Linearity and Lower Limit of Quantification. Three batches of standard curve solutions with six different concentrations were prepared. The typical standard curves were assessed by using DAS 2.0 software with the quadratic weight ($W = 1/C^2$). The dependent variable was the ratio of the peak area of each analyte to the peak area of the internal standard, while the independent variable was set as the concentration value of each analyte; the least square regression was used to construct the standard curve equation. The standard curves and correlation coefficients are listed in Table 2, proving the calibration curves of the components with a good linearity over the studied concentration range.

The lower limit of quantification (LLOQ) for each analyte was all with signal-to-noise ratio higher than 10, which was sufficient to perform quantitative studies of MTBD extracts.

3.3.3. Precision and Accuracy. Three batches of quality control samples were prepared according to three concentration levels. Each concentration was analyzed with 6 duplications. The intraday precision values were between 1.13% and 6.66%, and the interday ones were between 2.42% and 10.62% and accuracy ranged from 86.11% to 114.27%. The above results demonstrated the acceptable precision and accuracy of the present method.

3.3.4. Repeatability and Stability. Six MTBD sample extracts were prepared on the same day according to Section 2.2. The repeatability of 19 components was within 6.26% relative standard deviation (*RSD*).

Sample stability was investigated after the extracts were kept at room temperature for 0 h, 6 h, 12 h, and 24 h. The stability results of 19 compounds are summarized in Table 3; the acceptability of the data was within 3.92% deviation from the 0 h sample values, which indicated that a large number of samples could be stable in each analytical run.

3.4. Application to Samples Modified Tabusen-2 Decoction (MTBD). The method established above was successfully utilized for quantitative studies of MTBD extracts, as shown in Table S2. Eight batches of MTBD samples prepared with different herb sources were determined by using the above mature method. The herb formulation of each batch is listed in Table S3. There is an indication of the fact that the concentrations of 19 compounds varied significantly in MTBD extracts; the content of flavonoids was the highest, followed by saponins (Figure S4), which attracted the attention of herb quality in picking as well as in circulating during the market. It can be seen from the quantitative research results of different batches of MTBD that we need to strictly control the quality of herb because this is the guarantee of their clinical efficacy and safety.

4. Discussion

Although the isolation and purification before biological activity evaluation are a traditional strategy of exploring material basis in TMM, the time-consuming and labor-intensive characteristics cannot be neglected. In quantitative experiments, Ultraviolet (UV) detector is exceedingly common for flavonoids, phenylpropanoids, and other UV-absorbing compounds [32], while it is not applicable to the analysis of saponin. Although the detection of saponin could be enabled by evaporative light scattering detector (ELSD), the sensitivity during the test procedure should also be taken into account [33]. Herein, in order to shorten the analysis time, improve the analysis sensitivity, and simultaneously determine UV-absorbing compounds and non-UV-absorbing compounds, high performance liquid chromatography coupled with mass spectrometry (HPLC-Q-Exactive MS/MS spectrometer) approach [34], as a high efficiency, is employed in this study to separate and identify the material basis in MTBD. Additionally, the existence of isomer (ICGAA with 1,5-DQA, GE with APG, LT with KPF) in MTBD increases the difficulty of separation and analysis [35]. The chromatographic conditions in quantitative analysis need to be optimized carefully during the present research.

In order to achieve better separation effect for three pairs of isomers in MTBD, the mobile phase was screened in this experiment. The peak of each component was with

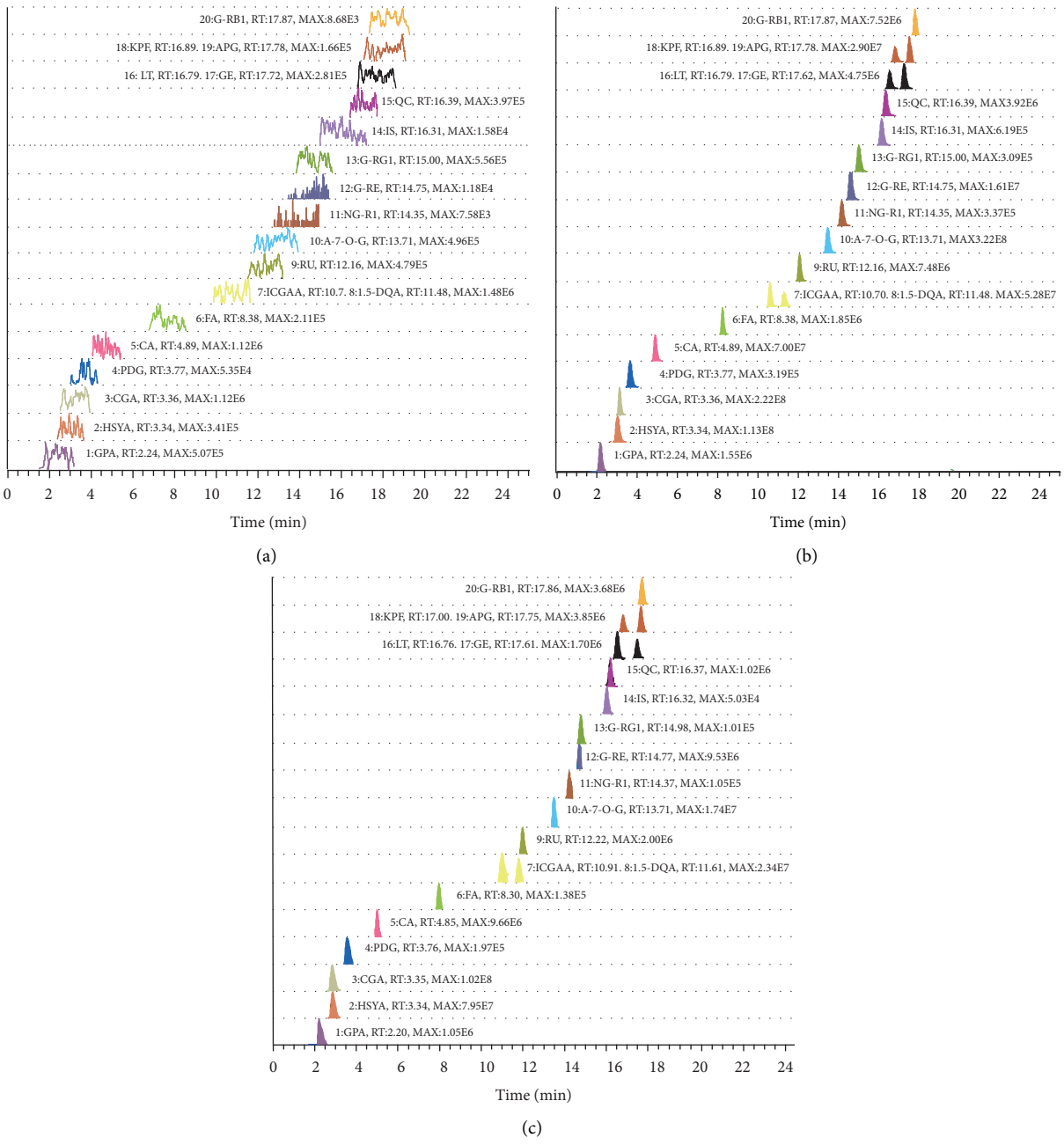

Figure 4: Representative chromatograms of (a) blank, (b) 19 standard samples, and (c) 19 compounds in MTBD.

symmetrical shape and no tailing phenomenon. Additionally, the influence of column temperature and flow rate was considered, and a better separation was achieved under column temperature of 30°C and flow rate of 0.3 mL/min. A variety of chromatographic columns were also optimized in this study. Compared with ACE C18-PFP column (100 × 3.0 mm ID, 3 μm), Grace Alltima C18 column (250 mm × 4.6 nm, 5 μm), HITACHI LaChrom C18 column (250 mm × 4.6 mm ID, 5 μm), and Thermo ODS-2 HYPERSIL column (250 mm × 4.6 mm, 5 μm), ACE C18-PFP column had better separation and resolution, especially for the three isomers.

It was found through analysis that the contents of the 19 components differ in MTBD prepared from different batches of crude drugs; this might be because the crude drugs of different batches were different in origin, growing environments, and harvest time. This has aroused our attention in all aspects of picking and transportation. The presence of moisture will affect the determination of the content of the active ingredients in the medicinal materials. Therefore, the near-infrared method was used in the study to detect the moisture content in the relevant medicinal materials to ensure the final quantitative accuracy of the effective ingredients [36]. Refluxing was used

Table 2: Calibration curves, linear range, r^2, and LOQs of 19 compounds in MTBD.

Compound	Calibration curves	Linear range (μg/mL)	r^2	LLOQ (μg/mL)
ICGAA	$y = 647.937x + 1.476$	4.800–192.000	0.9994	4.800
1,5-DQA	$y = 364.018x - 0.810$	6.100–244.000	0.9991	6.810
GE	$y = 22386.297x - 0.191$	0.023–0.920	0.9982	0.025
APG	$y = 29960.140x - 0.562$	0.065–2.600	0.9989	0.073
LT	$y = 15454.517x - 0.090$	0.015–0.600	0.9986	0.015
KPF	$y = 9208.139x - 0.051$	0.010–0.400	0.9983	0.010
QC	$y = 8437.051x - 0.062$	0.011–0.440	0.9989	0.011
A-7-O-G	$y = 6901.196x + 11.968$	4.200–168.000	0.9962	4.200
RU	$y = 2560.803x - 0.093$	0.230–9.200	0.9992	0.250
HSYA	$y = 1104.734x - 0.935$	9.830–392.000	0.9984	10.930
NG-R_1	$y = 8.300x - 0.016$	2.400–96.000	0.9964	2.400
G-Re	$y = 730.821x + 0.137$	1.010–40.400	0.9963	1.010
G-Rg_1	$y = 21.700x + 0.029$	6.500–260.000	0.9983	6.700
G-Rb_1	$y = 93.320x + 0.128$	5.660–226.400	0.9979	5.830
CA	$y = 183840.263x - 8.999$	0.260–10.400	0.9985	0.260
FA	$y = 2322.874x - 0.525$	0.390–15.600	0.9992	0.410
GPA	$y = 119.544x - 0.011$	0.800–32.000	0.9987	0.800
CGA	$y = 3414.355x - 5.245$	5.500–220.000	0.9978	5.660
PDG	$y = 10.556x - 0.018$	2.180–87.200	0.9987	2.180

Table 3: Precision, repeatability, stability, and accuracy of 19 compounds in MTBD.

Compound	Interday precision (RSD, $n = 3$)			Intraday precision (RSD, $n = 3$)			Repeatability	Stability	Accuracy ($n = 6$, %)	
	Low	Middle	High	Low	Middle	High	(RSD, $n = 6$, %)	(RSD, $n = 4$, %)	Recovery	RSD
ICGAA	4.74	5.61	6.45	1.24	2.34	3.39	2.62	3.13	107.36	1.76
1,5-DQA	3.37	4.31	5.18	1.13	0.59	1.63	6.26	3.48	106.46	2.11
GE	2.42	7.24	4.87	2.29	2.79	0.90	2.30	2.68	106.41	2.06
APG	3.34	5.34	3.64	3.22	2.58	2.82	1.70	2.18	106.73	2.23
LT	4.05	7.84	4.53	3.13	2.81	1.09	4.75	3.92	98.21	3.01
KPF	9.47	9.00	7.98	2.18	1.54	5.51	4.94	3.60	103.12	2.37
QC	8.67	6.94	5.52	6.66	2.25	1.35	4.68	2.81	103.42	4.10
A-7-O-G	4.17	3.42	7.38	4.15	3.05	3.13	2.09	2.38	104.56	1.87
RU	4.03	3.23	3.42	1.86	1.92	2.57	2.99	2.34	105.39	0.92
HSYA	3.81	4.97	5.67	2.25	1.13	4.78	3.40	2.56	104.80	1.13
NG-R1	8.22	4.19	5.85	1.63	2.07	4.55	4.05	0.75	104.87	2.81
G-Re	6.50	3.92	5.41	3.17	1.38	2.47	4.02	3.23	107.35	1.73
G-Rg_1	6.10	7.59	6.12	5.08	4.64	4.80	3.27	2.26	104.64	1.59
G-Rb_1	10.62	3.37	3.61	2.94	2.71	3.47	4.50	2.99	106.94	2.54
CA	6.29	5.83	4.08	5.45	3.62	4.31	2.15	2.43	101.10	0.53
FA	8.76	7.21	7.61	3.90	4.15	2.40	2.94	3.74	105.71	2.10
GPA	8.36	6.89	10.52	2.64	0.54	4.11	3.82	3.59	107.60	3.01
CGA	2.74	5.12	2.82	2.52	1.25	3.50	2.99	2.24	106.59	2.11
PDG	6.95	7.32	7.71	2.69	2.78	4.11	2.67	1.97	92.08	4.57

to prepare the MTBD in the present study [37]. Furthermore, some literatures [38–42] have carried out assays on HSYA, RU, QC, G-Rb_1, G-RG_1, NG-R_1, G-Re, FA, LT, KPF, APG, and GE; but the HPLC-Q-Exactive MS/MS spectrometer approach displayed distinct superiority with desirable resolution and Lower LLOQ. The previous literature [43, 44] measured the content of CA, 1.5-DQA, GPA, PDG, and CGA, but it took too long (60 minutes) and restricted its modern development. Some studies [45, 46] have shown the contents of ICGGA and A-7-O-G; on this basis, we can have a wider linear range and have greater reference value for the formulation of the content of different batches of samples.

5. Conclusions

Based on HPLC-Q-Exactive MS/MS spectrometer with FSCIF approach to rapid detection of structure fragment and quantification of major representative components in MTBD, 143 compounds with seven chemical categories were unambiguously or tentatively identified. This study not only enriched the cleavage law of MTBD compounds but also established an approach for the accurate search and discovery of active components from complex mixtures. The repeatability, accuracy, stability, linearity, recoveries, and reproducibility of quantitative analysis all meet the criteria for acceptability of quantitative studies.

The determination of 19 compounds in MTBD extracts in different batches was obtained to monitor the quality of each prescription, which facilitates the better development of quality evaluation technique in MTBD and will help for further exploration of quality control of MTBD. The 19 compounds determined based on the qualitative and quantitative results are the major components of the MTDB. This experiment can provide a research foundation for subsequent pharmacokinetic studies and formulation of quality standards.

All in all, we compared the differences in the content of the same compound in the same herbs. Our quantitative method can determine 19 compounds in a short time (25 minutes), with a wider linear range and lower LLOQ. On the other hand, we compared the content difference of the same compound in different herbs, and the content fluctuation range is relatively large, which may be related to the processing, compatibility, and the changes in the decocting process of herbs. The content range of the 19 compounds that we have measured can provide the fluctuation range of the compound content when formulating quality standards in the future and help formulate content determination standards for preparations. This qualitative and quantitative analysis of MTBD could provide a new tool for the quality control of this preparation or its related TCM.

Data Availability

The methodological data and structural data used to support the findings of this study are included within the article. The cleavage pathways data used to support the findings of this study are included within the Supplementary Materials.

Disclosure

This article has become a preprint: https://doi.org/10.21203/rs.3.rs-829266/v1.

Conflicts of Interest

The authors declare that there are no conflicts of interest regarding the publication of this paper.

Authors' Contributions

Yu Zhao and Xin Dong contributed equally to this work. All authors read and approved the final manuscript.

Acknowledgments

This work was financially supported by the National Natural Science Foundation of China (81860756 and 81960758), Student Innovation and Entrepreneurship Fund Project of China (202010132003 and 202110132029), Innovation Guide Project (02039001), and Inner Mongolia Autonomous Region Higher Education Science Research Project (NJZY19099).

Supplementary Materials

Table S1: the final concentration of 19 standard solutions. Table S2: the content of 19 compounds in the MTBD medicinal measure (μg, $X \pm$ SD, $n = 3$). Table S3: different sources of medicinal materials. Table S4: quality control concentration levels of 19 compounds. Figure S1: structures of 143 compounds. (A) Structure of flavonoids. (B) Structure of phenylpropanoids. (C) Structure of lignans. (D) Structure of iridoids. (E) Structure of polyphenol. (F) Structure of saponins. (G) Structure of other type compounds. Figure S2: the cracking pathways of (A) ginsenoside Rb_1, (B) notoginsenoside R_1, and (C) 3-(β-D-glucopyranosyl-β-D-glucopyranosyl)-20-O-(6-O-malonyl-β-D-glucopyranosyl-β-D-glucopyranosyl)-3β,12β, 20(S)-trihydroxydammar-24-ene. Figure S3: the cracking pathways of (A) rutin, (B) chlorogenic acids, (C) deacetyl asperulosidic acid. Figure S4: the content of eight batches of medicinal materials. (*Supplementary Materials*)

References

[1] J. Q. Wang, X. Dong, F. X. Ma et al., "Metabolomics profiling reveals Echinops latifolius Tausch improves the trabecular micro-architecture of ovariectomized rats mainly via intervening amino acids and glycerophospholipids metabolism," *Journal of Ethnopharmacology*, vol. 260, Article ID 113018, 2020.

[2] J. H. Xie, Z. Y. Tan, Y. M. Guo, H. Yang, and G. Y. Hu, "Quality standard control of Modified Tabusen-2 decoction and TLC identification method of Eucommia-containing preparations," *Chinese Patent Medicines*, vol. 3, pp. 632–636, 2017.

[3] F. Yang, X. Dong, F. Ma et al., "The interventional effects of Tubson-2 Decoction on ovariectomized rats as determined by a combination of network pharmacology and metabolomics," *Frontiers in Pharmacology*, vol. 11, Article ID 581991, 2020.

[4] J. Y. Li and H. C. Song, "Orthogonal design to optimize the extraction and molding process of Yushang Jiegu capsules," *Journal of Medicine & Pharmacy of Chinese Minorities*, vol. 5, no. 5, pp. 53–55, 2010.

[5] L. Gao and Q. Shi, "Determination of ursolic acid in yushang jiegu capsules by HPLC," *Chinese Traditional Patent Medicine*, vol. 29, no. 29, pp. 398-399, 2006.

[6] J. Zhao, C. Y. Dong, J. P. Shi et al., "Micro-histomorphometry study of Mongolian medicine echinops sphaerocephalus L. on postmenopausal osteoporosis," *Chinese Journal of Osteoporosis*, vol. 26, no. 7, pp. 972–977, 2020.

[7] M. Liu, G. Ye, Y. J. Cui, A. Y. Zhang, Y. Y. Zhao, and D. A. Guo, "Study on the chemical constituents of the aboveground parts of Huadong Echinops latifolius Tausch," *Chinese Traditional and Herbal Drugs*, vol. 33, no. 1, pp. 18–20, 2002.

[8] J. Q. Wang, *Study on the Mechanism of Mongolian Medicine Nitraria Glabra against Osteoporosis Based on Network Pharmacology*, Inner Mongolia Medical University, Hohhot, China, 2019.

[9] X. Gong, Q. Luan, X. Zhou, Y. Zhao, and C. Zhao, "UHPLC-ESI-MS/MS determination and pharmacokinetics of pinoresinol glucoside and chlorogenic acid in rat plasma after oral administration of *Eucommia ulmoides* Oliv extract," *Biomedical Chromatography*, vol. 31, no. 11, 2017.

[10] C. Y. Wang, L. Tang, J. W. He, J. Li, and Y. Z. Wang, "Ethnobotany, phytochemistry and pharmacological properties of eucommia ulmoides: a review," *The American Journal of Chinese Medicine*, vol. 47, no. 2, pp. 259–300, 2019.

[11] M. He, J. Jia, J. Li et al., "Application of characteristic ion filtering with ultra-high performance liquid chromatography quadrupole time of flight tandem mass spectrometry for rapid detection and identification of chemical profiling in *Eucommia ulmoides* Oliv," *Journal of Chromatography A*, vol. 1554, no. 54, pp. 81–91, 2018.

[12] L. L. Zhang, K. Tian, Z. H. Tang et al., "Phytochemistry and pharmacology of *carthamus tinctorius* L," *The American Journal of Chinese Medicine*, vol. 44, no. 2, pp. 197–226, 2016.

[13] X. Duan, L. Pan, D. Peng et al., "The analysis of the active components and metabolites of taohong siwu decoction based on ultra performance liquid chromatography quadrupole time-of-flight mass spectrometry," *Journal of Separation Science*, vol. 43, no. 22, pp. 4131–4147, 2020.

[14] Z. Ju, J. Li, Q. Lu, Y. Yang, L. Yang, and Z. Wang, "Identification and quantitative investigation of the effects of intestinal microflora on the metabolism and pharmacokinetics of notoginsenoside Fc assayed by liquid chromatography/electrospray ionization tandem mass spectrometry," *Journal of Separation Science*, vol. 42, no. 9, pp. 1740–1749, 2019.

[15] Y. Ma, B. X. Huang, W. W. Tang, P. Li, and J. Chen, "Characterization of chemical constituents and metabolites in rat plasma after oral administration of San Miao Wan by ultra-high performance liquid chromatography tandem Q-Exactive Orbitrap mass spectrometry," *Journal of Chromatography B*, vol. 2021, Article ID 122793, 2021.

[16] J. Zhang, Z. H. Huang, X. H. Qiu, Y. M. Yang, D. Y. Zhu, and W. Xu, "Neutral fragment filtering for rapid identification of new diester-diterpenoid alkaloids in roots of Aconitum carmichaeli by ultra-high-pressure liquid chromatography coupled with linear ion trap-orbitrap mass spectrometry," *PLoS One*, vol. 7, no. 12, p. e52352, 2012.

[17] X. Qiao, X.-H. Lin, S. Ji et al., "Global profiling and novel structure discovery using multiple neutral loss/precursor ion scanning combined with substructure recognition and statistical analysis (MNPSS): characterization of terpene-conjugated curcuminoids in curcuma longa as a case study," *Analytical Chemistry*, vol. 88, no. 1, pp. 703–710, 2016.

[18] B. J. Waldner, R. Machalett, S. Schönbichler, M. Dittmer, M. M. Rubner, and D. Intelmann, "Fast evaluation of herbal substance class composition by relative mass defect plots," *Analytical Chemistry*, vol. 92, no. 19, pp. 12909–12916, 2020.

[19] L. L. Fu, H. Ding, and L. F. Han, "Simultaneously targeted and untargeted multicomponent characterization of erzhi pill by offline two-dimensional liquid chromatography/quadrupole-orbitrap mass spectrometry," *Journal of Chromatography A*, vol. 1584, no. 84, pp. 87–96, 2019.

[20] L. L. He, H. Jiang, T. H. Lan et al., "Chemical profile and potential mechanisms of huo-tan-chu-shi decoction in the treatment of coronary heart disease by UHPLC-Q/TOF-MS in combination with network pharmacology analysis and experimental verification," *The Journal of Chromatography B Analytical Technologies in the Biomedical and Life Sciences*, vol. 15, no. 1175, Article ID 122729, 2021.

[21] X. G. Liu, J. S. Li, S. X. Feng et al., "A high-resolution MS/MS based strategy to improve xenobiotic metabolites analysis by metabolic pathway extension searching combined with parallel reaction monitoring: flavonoid metabolism in wound site as a case," *The Journal of Chromatography B Analytical Technologies in the Biomedical and Life Sciences*, vol. 1162, Article ID 122470, 2021.

[22] J. H. Xie, Z. Y. Tan, Y. M. Guo, H. Yang, and G. Y. Hu, "Quality standard control of lanhong capsules and TLC identification method of eucommia-containing preparations," *Chinese Traditional Patent Medicine*, vol. 03, no. 39, pp. 194–198, 2017.

[23] X. W. Hua, *Lanhong Capsule Quality Standard and Study on the Fingerprint of Lancitou*, Xinjiang Medical University, Ürümqi, China, 2014.

[24] X. W. Hua, Y. Li, X. M. Cheng, H. Yang, G. Y. Hu, and C. H. Wang, "Quality control method of *Panax notoginseng* in lanhong capsules," *Chinese Traditional Patent Medicine*, vol. 36, no. 7, pp. 1497–1501, 2014.

[25] Y. Ling and Q. Zhang, "Structural characterisation and screening of triterpene saponins in the bark of Ilex rotunda using high-performance liquid chromatography coupled to electrospray ionisation and quadrupole time-of-flight mass spectrometry," *Phytochemical Analysis*, vol. 32, no. 3, pp. 395–403, 2021.

[26] M. Yoshikawa, T. Morikawa, K. Yashiro, T. Murakami, and H. Matsuda, "Bioactive saponins and glycosides. XIX. Notoginseng(3):immunological adjuvant activity of notoginsenosides and related saponins: structures of notoginsenosides-L, -M, and -N from the roots of *Panax notoginseng* (Burk.) F. H. Chen," *Chemical and Pharmaceutical Bulletin*, vol. 49, no. 11, pp. 1452–1456, 2001.

[27] W. Z. Yang, X. J. Shi, C. L. Yao et al., "A novel neutral loss/product ion scan-incorporated integral approach for the untargeted characterization and comparison of the carboxyl-free ginsenosides from panax ginseng, panax quinquefolius, and panax notoginseng," *Journal of Pharmaceutical and Biomedical Analysis*, vol. 2020, Article ID 112813, 2020.

[28] B. Vanholme, I. El Houari, and W. Boerjan, "Bioactivity: phenylpropanoids' best kept secret," *Current Opinion in Biotechnology*, vol. 56, pp. 156–162, 2019.

[29] X. Wang, W. Wu, J. Zhang et al., "An integrated strategy for holistic quality identification of Chinese patent medicine: liuwei Dihuang Pills as a case study," *Phytochemical Analysis*, vol. 32, no. 2, pp. 183–197, 2021.

[30] X. Wang, C. Wu, M. Xu, C. Cheng, Y. Liu, and X. Di, "Optimisation for simultaneous determination of iridoid glycosides and oligosaccharides in Radix Rehmannia by microwave assisted extraction and HILIC-UHPLC-TQ-MS/MS," *Phytochemical Analysis*, vol. 31, no. 3, pp. 340–348, 2020.

[31] F. Shi, C. Tong, C. He, S. Shi, Y. Cao, and Q. Wei, "Diagnostic ion filtering targeted screening and isolation of anti-inflammatory iridoid glycosides from Hedyotis diffusa," *Journal of Separation Science*, vol. 44, no. 13, pp. 2612–2619, 2021.

[32] T. H. Sani, M. Hadjmohammadi, and M. H. Fatemi, "Extraction and determination of flavonoids in fruit juices and vegetables using Fe_3O_4/SiO_2 magnetic nanoparticles modified with mixed hemi/admicelle cetyltrimethylammonium bromide and high performance liquid chromatography," *Journal of Separation Science*, vol. 43, no. 7, pp. 1224–1231, 2020.

[33] P. Yang, M. Zhou, C. Zhou, Q. Wang, F. Zhang, and J. Chen, "Separation and purification of both tea seed polysaccharide and saponin from camellia cake extract using macroporous resin," *Journal of Separation Science*, vol. 38, no. 4, pp. 656–662, 2015.

[34] M. Teich, M. Schmidtpott, D. van Pinxteren, J. Chen, and H. Herrmann, "Separation and quantification of imidazoles in atmospheric particles using LC-Orbitrap-MS," *Journal of Separation Science*, vol. 43, no. 8, pp. 577–589, 2020.

[35] N. Li, X. Dong, F. Ma et al., "Pharmacokinetics study of 16 active ingredients from Tabson-2 decoction in normal and d-galactose induced osteoporosis rats by liquid chromatography-tandem mass spectrometry," *Journal of Separation Science*, vol. 43, no. 18, pp. 3702–3713, 2020.

[36] Y. F. Zhou, Z. X. Yang, and L. Y. Dong, "Rapid determination of moisture and ethanol extract content in Panax notoginseng by NIRS," *Drug Evaluation Research*, vol. 41, no. 11, pp. 1994–1999, 2018.

[37] M. C. Wei, Y. C. Yang, H. F. Chiu, and H. Hong, "Development of a hyphenated procedure of heat-reflux and ultrasound-assisted extraction followed by RP-HPLC separation for the determination of three flavonoids content in Scutellaria barbata D. Don," *Journal of Chromatography B: Analytical Technologies in the Biomedical and Life Sciences*, vol. 940, pp. 126–134, 2013.

[38] J. Wu, H. J. Yang, and P. Zhou, "Determination of 5 components in *Carthamus tinctorius* L," *Asia-Pacific Traditional Medicine*, vol. 15, no. 11, 2019.

[39] C. L. Yao, W. Z. Yang, and W. Y. Wu, "Simultaneous quantitation of five *Panax notoginseng* saponins by multi heart-cutting two-dimensional liquid chromatography: method development and application to the quality control of eight Notoginseng containing Chinese patent medicines," *Journal of Chromatography A*, vol. 1402, pp. 71–81, 2015.

[40] Y. Z. Wang, "Simultaneous determination of paeoniflorin, hydroxysafflor yellow A and ferulic acid in Xielong Liquor by HPLC," *Chinese Traditional Patent Medicine*, vol. 34, no. 10, pp. 1925–1928, 2012.

[41] J. J. Wang, X. M. Zhang, and H. L. Wang, "Simultaneous determination of quercetin, luteolin, kaempferol and apigenin in *plantago asiatica* L. by reversed-phase high performance liquid chromatography," *Chinese Traditional Patent Medicine*, vol. 31, no. 5, pp. 772–775, 2009.

[42] J. B. Wang, P. Guo, X. B. Zhao, and Y. H. Xie, "Determination of genistein in *fructus sophorae* extract by RP-HPLC," *Chinese Traditional and Herbal Drugs*, vol. 35, no. 4, pp. 402-403, 2004.

[43] J. Sun, Y. Lu, W. Y. Xiang, X. Cao, Z. P. Gong, and A. M. Wang, "Simultaneously determines the content of 6 active ingredients in *Eucommia ulmoides* Olivers by UPLC," *Natural Product Research and Development*, vol. 28, pp. 874–879, 2016.

[44] J. P. Gao, L. Yang, N. Yang et al., "Study on quality of Mongolia medicinal materials flos echinopsis based on HPLC characteristic chromatogram and determination of four caffeic acid derivatives," *Journal of Chinese Medicinal Materials*, vol. 41, no. 7, pp. 1641–1645, 2018.

[45] M. Hua, W. Bi, J. Chen et al., "The determination of isochlorogenic acid A, B, and C in *Lonicera japonica* by HPLC," *Journal of West China Forestry Science*, vol. 46, no. 4, pp. 73–78, 2017.

[46] Y. N. He, Y. G. Zhao, D. L. Yang, D. G. Zhang, and C. M. Wang, "Determination and comparison of luteoloside, apigenin-7-*O*-*β*-*D*-glucosidase, and luteolin in *Humulus scandens* from different habitats in Hebei province," *Chinese Traditional and Herbal Drugs*, vol. 47, no. 20, pp. 3707–3711, 2016.

Hindawi
Evidence-Based Complementary and Alternative Medicine
Volume 2021, Article ID 4512755, 17 pages
https://doi.org/10.1155/2021/4512755

Research Article

Analysis of the Efficacy and Pharmacological Mechanisms of Action of Zhenren Yangzang Decoction on Ulcerative Colitis Using Meta-Analysis and Network Pharmacology

Guosheng Xing,[1,2] Yufeng Zhang,[3] Xinlin Wu,[2] Hua Wang,[2] Yan Liu,[4] Zhen Zhang,[1,2] Mingxing Hou,[1,2] and Haibing Hua[5]

[1]*Nanjing University of Chinese Medicine, Nanjing, Jiangsu 210008, China*
[2]*Department of General Surgery, The Affiliated Hospital of Inner Mongolia Medical University, Hohhot, Inner Mongolia 010050, China*
[3]*Department of Respiratory Medicine, Jiangyin Hospital of Traditional Chinese Medicine, Jiangyin Hospital Affiliated to Nanjing University of Chinese Medicine, Jiangyin, Jiangsu 214400, China*
[4]*Department of Traditional Chinese Medicine, The Affiliated Hospital of Inner Mongolia Medical University, Hohhot, Inner Mongolia 010050, China*
[5]*Department of Gastroenterology, Jiangyin Hospital of Traditional Chinese Medicine, Jiangyin Hospital Affiliated to Nanjing University of Chinese Medicine, Jiangyin, Jiangsu 214400, China*

Correspondence should be addressed to Mingxing Hou; 15354878601@163.com and Haibing Hua; hhbjytcm@163.com

Received 31 August 2021; Revised 20 November 2021; Accepted 13 December 2021; Published 28 December 2021

Academic Editor: Lifeng Han

Objective. We analyzed the efficacy and pharmacological mechanisms of action of Zhen Ren Yang Zang decoction (ZRYZD) on ulcerative colitis (UC) using meta-analysis and network pharmacology. *Methods*. The major databases were searched for randomized controlled trials of ZRYZD for the treatment of UC. Meta-analysis of the efficacy of ZRYZD on UC was conducted using RevMan software. Active compounds and target genes were acquired using the Traditional Chinese Medicine Systems Pharmacology Database and Analysis Platform. UC-related genes were searched using the GeneCards database. Gene Ontology (GO) functional enrichment and Kyoto Encyclopedia of Genes and Genomes (KEGG) pathway enrichment analyses were performed using RGUI. A compound-target network was constructed using Cytoscape software, and a protein-protein interaction network was constructed using the STRING database. Molecular docking simulations of the macromolecular protein targets and their corresponding ligand compounds were performed using the AutoDock tool and AutoDock Vina software. *Results*. Meta-analysis revealed that the total effective rate and recovery rate of clinical efficacy were significantly higher in the experimental group than those of the control group. The screening identified 169 active compounds and 277 active target genes for ZRYZD. The 277 active target genes were compared with the 4,798 UC-related genes. This identified 187 active target genes of ZRYZD for UC that correlated with 138 active compounds. GO functional enrichment and KEGG pathway enrichment analyses were performed, and compound-target and protein-protein interaction networks were constructed. The key compounds and key target proteins were then selected. Finally, target protein binding with the corresponding compound was analyzed using molecular docking. *Conclusion*. Our findings demonstrate the effectiveness and safety of ZRYZD for the treatment of UC and provide insight into the underlying pharmacological mechanisms of action. Furthermore, key compounds were identified, laying the foundation for future studies on ZRYZD for the treatment of UC.

1. Introduction

Ulcerative colitis (UC) is a common chronic intestinal disease of unknown etiology and is associated with multifactorial, multilevel, and nonspecific inflammation [1]. The clinical manifestations of UC include diarrhea, abdominal pain, and stool containing mucus, pus, and/or blood. The incidence of UC is 1.2–20.3 per 100,000 persons per year, and its prevalence is 7.6–246.0 per 100,000 per year [2].

The lesions in UC involve the rectum and sigmoid colon, sometimes throughout the whole colon, mainly invading the colorectal mucosa and submucosa and showing phased and diffuse distribution, resulting in a propensity for relapse [3]. Mesalazine, immunosuppressants, and corticosteroids are clinically used to treat UC; however, these drugs are needed chronically and can cause adverse reactions, and relapse is common after cessation [4, 5]. Traditional Chinese medicine (TCM) has a long history of treating diarrhea and dysentery and is compliant with the concept of individualized treatment [6]. Recently, TCM has been used to treat UC, with positive outcomes [7–9].

Zhen Ren Yang Zang decoction (ZRYZD), first used during the Song Dynasty as the basic prescription for the treatment of diarrhea, primarily consists of yingsuke, roudoukou, hezi, rougui, dangshen, baizhu, danggui, baishao, muxiang, and gancao (scientific names: *Pericarpium Papaveris* (PP), *Semen Myristicae* (SM), *Fructus Chebulae* (FC), *Cortex Cinnamomi* (CC), *Radix Codonopsis* (RC), *Rhizoma Atractylodis Macrocephalae* (RAM), *Radix Angelicae Sinensis* (RAS), *Radix Paeoniae Alba* (RPA), *Radix Aucklandiae* (RA), and *Radix Glycyrrhizae* (RG), respectively) [10]. According to TCM theory, PP, SM, and FC are monarch and minister herbs and are regarded as the main components of ZRYZD.

ZRYZD acts as an intestinal astringent, has antidiarrheal properties, and warms the spleen and kidney. Several clinical studies have reported that the clinical effect of ZRYZD in the treatment of UC is remarkable [10–12]. Previous basic research studies suggest that ZRYZD can ameliorate colonic mucosal dysfunction and that it has a favorable therapeutic action in trinitrobenzene sulfonic acid-induced colitis [13]. Therefore, the clinical efficacy and pharmacology of ZRYZD for the treatment of UC merit further investigation.

In this study, we analyzed the efficacy and pharmacological mechanisms of action of ZRYZD for the treatment of UC using meta-analysis and network pharmacology. First, we screened randomized controlled trials (RCTs) that investigated the clinical efficacy of ZRYZD for UC and performed a meta-analysis to assess clinical efficacy and safety. Next, we identified the active compounds in ZRYZD and its target genes and compared them with UC-related genes to identify the active target genes involved in the therapeutic action of ZRYZD for UC. Subsequently, Gene Ontology (GO) functional enrichment and Kyoto Encyclopedia of Genes and Genomes (KEGG) pathway enrichment analyses were performed. The compound-target, key compound-target, and protein-protein interaction (PPI) networks were constructed, and the key compounds and key target proteins were selected. Finally, target protein binding with the corresponding compound was analyzed using molecular docking analysis.

2. Materials and Methods

2.1. Screening of RCTs of the Efficacy of ZRYZD in the Treatment of UC. PubMed, the Cochrane Central Register of Controlled Trials, Chinese National Knowledge Infrastructure, Wanfang Data, the Chongqing VIP database, and the Chinese Biomedical Literature database, from the establishment of each database to August 15, 2021, were searched using the terms "Zhen Ren Yang Zang decoction" and "ulcerative colitis." These terms were searched in titles, abstracts, and the full text. We also checked references and citations in the identified studies manually to include other potentially eligible trials until no additional articles could be identified.

The inclusion criteria included the following: the study was designed as a RCT, the participants had a diagnosis of UC, ZRYZD was used in the experimental group, the control group used conventional therapy without TCM therapy, and there were clear outcome indicators. Exclusion criteria included the following: the outcome data of the study were incomplete and the ZRYZD prescription lacked the main components.

2.2. Data Extraction, Quality Assessment, and Meta-Analysis. Two reviewers independently extracted the information from the included studies. The main information included the first author, year of publication, number of patients in each group, methods of intervention in the experimental and control groups, and outcome data.

The Cochrane Reviewers' Handbook of guidelines was used to assess the risk of bias. The following seven criteria were used: random sequence generation; allocation concealment; patient blinding; assessor blinding; incomplete outcome data; selective outcome reporting; other risks of bias [14].

These main data were input into the Cochrane Collaboration's RevMan 5.3 software for meta-analysis to analyze the efficacy of ZRYZD on UC.

2.3. Screening of Active Compounds in ZRYZD. The compounds in the ten component herbs (PP, SM, FC, CC, RC, RAM, RAS, RPA, RA, and RG) were obtained using the Traditional Chinese Medicine Systems Pharmacology Database and Analysis Platform (TCMSP) (https://tcmspw.com/tcmsp.php) [15]. TCMSP is a unique systems pharmacology platform of Chinese herbal medicines that captures the relationships between drugs, targets and diseases. Oral bioavailability (OB) and drug-likeness (DL) are commonly used in network pharmacology to define active compounds. OB represents the rate the compound is absorbed into the body, and DL represents the degree to which a compound contains specific functional groups or has physical characteristics similar to existing drugs [16]. We used $OB \geq 30\%$ and $DL \geq 0.18$ to screen for the active compounds (the DLs of compounds in CC are generally low, and we, therefore, set $DL \geq 0.10$ as the filter criteria) [17].

2.4. Screening of the Target Genes of Active Compounds. The corresponding target genes of the active compounds were also retrieved from the TCMSP. Setting the search format as "homo sapiens," the target genes were imported into the UniProt Knowledgebase, a comprehensive resource for protein sequences and annotation data (https://www.uniprot.org/) [18]. Then, the human official gene symbols were identified and were considered the active target genes of ZRYZD.

2.5. Acquisition of UC-Related Genes and Identification of Active Target Genes of ZRYZD Acting on UC. "Ulcerative colitis" was used as the keyword in the GeneCards database (https://www.genecards.org/). The GeneCards database is a searchable, integrative database providing comprehensive, user-friendly information on all annotated and predicted human genes [19], from which the UC-related genes were searched and acquired. Then, the active target genes of ZRYZD were compared with the UC-related genes, and the intersecting genes were defined as the active target genes of ZRYZD acting on UC.

2.6. GO Functional Enrichment and KEGG Pathway Enrichment Analyses. The RGUI 3.6.1 and org.Hs.eg.db packages were used to obtain the entrezIDs of the active target genes. Then, RGUI and the clusterProfiler package were used to perform the GO functional enrichment analyses, which included the biological process (BP), molecular function (MF), cellular component (CC) analysis, and the KEGG pathway enrichment analysis [20].

2.7. Construction of the Compound-Target Network. Cytoscape 3.6.0 software and its NetworkAnalyzer tool function were used to construct and analyze the compound-target network. Nodes represent compounds and target genes, and edges represent the relationships between them. According to the degree of connection between the compound and the target gene (the more the connections, the higher the degree value), the compounds and target genes in the network were subject to further analysis [21].

2.8. Construction of the PPI Network. A PPI network was constructed after introducing the active target genes into the STRING database. The STRING database supports functional discovery in genome-wide experimental datasets (https://string-db.org/) [22]. Defining the research species as "homo sapiens" and the lowest interaction score of 0.4, a PPI network was obtained. Then, the PPI network data were used to perform topology analysis, and the key target proteins of ZRYZD acting on UC were selected according to the degree values of each target protein (the more the connections, the higher the degree value) using Cytoscape 3.6.0 software and its NetworkAnalyzer tool [21].

2.9. Verification of Molecular Docking. The binding of the target protein with its corresponding compound was analyzed using molecular docking. The structures of the target proteins were obtained from the RCSB PDB database (https://www.rcsb.org/), and the compounds were obtained from the PubChem database (https://pubchem.ncbi.nlm.nih.gov/). Molecular docking simulations of target proteins with their corresponding compounds were performed using AutoDockTool 1.5.6 and AutoDock Vina software [23, 24].

2.10. Statistical Analysis. RevMan 5.3 software was used for meta-analysis, and dichotomous data were expressed as the odds ratio (OR) with 95% confidence interval (CI), and continuous data were expressed as mean difference (MD) with 95% CI. Heterogeneity was assessed with the Q-test (P-value and I^2), and $P < 0.10$ indicated heterogeneity across studies. Studies with $I^2 < 50\%$ were considered to have no heterogeneity, and those with $I^2 \geq 50\%$ were considered to have heterogeneity. If no heterogeneity was detected, the fixed effects model was used as the pooling method; otherwise, the random effects model was used [25, 26]. $P < 0.05$ was considered statistically significant.

Using the bioinformatics tools of the platforms and software mentioned above, some statistical analyses for network pharmacology were performed automatically. In the GO functional enrichment and KEGG pathway enrichment analyses, an adjusted P (q-value) < 0.05 was considered statistically significant.

3. Results

3.1. Screened RCTs Investigating the Efficacy of ZRYZD for the Treatment of UC. A total of 118 studies were retrieved through database searching, and 36 studies were retained after removing duplication. According to the inclusion and exclusion criteria, a total of 31 studies were excluded after reading the title, abstract, and full text. Five RCTs [11, 12, 27–29] were included for further evaluation. The literature screening process is shown in Figure 1.

3.2. Description of Included RCTs and Assessment of the Methodological Quality. Five eligible RCTs [11, 12, 27–29] were identified. The five RCTs were all conducted in China and included 356 patients. The five studies were all single-center studies. The basic features of the included studies are outlined in Table 1.

One RCT [28] employed the odd and even numbers method of random sequence generation; none of the RCTs introduced allocation concealment; none of the RCTs described blindness; all the RCTs had complete outcome data; and for all studies, we were unable to determine whether they selectively reported data (Table 2, Figures S1 and S2).

Four RCTs [11, 12, 27, 28] assessed the total effective rate of clinical efficacy, four RCTs [11, 12, 27, 28] assessed the recovery rate of clinical efficacy, and one RCT [12] assessed the recovery rate of clinical efficacy. One RCT [28] evaluated the serum cytokines interleukin- (IL-) 6 and IL-8 and tumor necrosis factor- (TNF-) α, and one RCT [29] evaluated serum IL-6 and TNF-α. Two RCTs [28, 29] analyzed the total syndrome score of TCM, one RCT [28] assessed diarrhea,

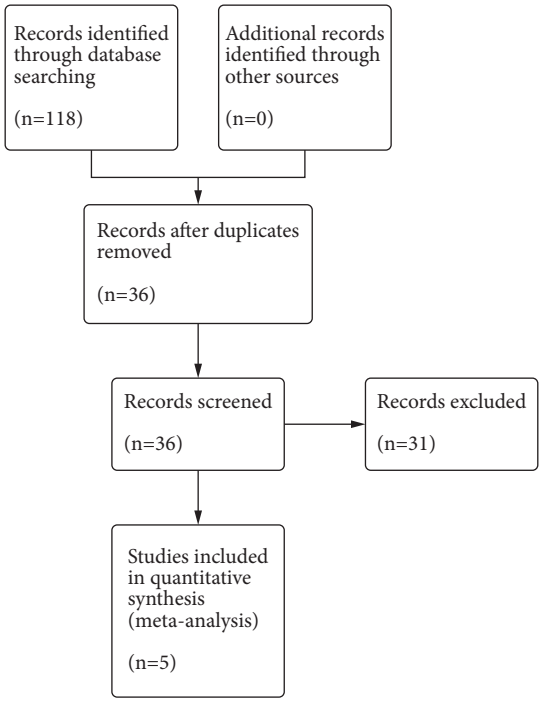

Figure 1: Flowchart of the study selection process.

Table 1: Summary of RCTs of ZRYZD for UC.

Study year [ref]	Country	Sample size (experimental/control)	Mean age (years) (experimental/control)	Experimental	Control	Duration
Yuan JY, 2009 [11]	China	88 (44/44)	35.4/33.6	ZRYZD	SASP	6 months
Zhao KH, 2010 [12]	China	35 (19/16)	39.8 ± 14.0/40.2 ± 15.0	ZRYZD	SASP	6 months
Wang L, 2015 [27]	China	80 (40/40)	33.4/34.6	ZRYZD	SASP	4 weeks
Han Y, 2019 [28]	China	63 (32/31)	38.7 ± 7.9/36.6 ± 9.2	ZRYZD	Mesalazine bowel-soluble tablets	6 weeks
Dai AC, 2021 [29]	China	90 (45/45)	39.8 ± 3.16/39.91 ± 3.22	ZRYZD	Mesalazine bowel-soluble tablets	6 weeks

RCT: randomized controlled trial; ZRYZD: Zhen Ren Yang Zang decoction; UC: ulcerative colitis; SASP: sulfasalazine.

Table 2: Risk of bias in the five included RCTs.

Study year[ref]	Random sequence generation	Allocation concealment	Blinding of patient	Blinding of assessor	Incomplete outcome data	Selective reporting	Other bias
Yuan JY, 2009 [11]	U	U	H	H	L	U	L
Zhao KH, 2010 [12]	U	U	H	H	L	U	L
Wang L, 2015 [27]	U	U	H	H	L	U	L
Han Y, 2019 [28]	H	U	H	H	L	U	L
Dai AC, 2021 [29]	U	U	H	H	L	U	L

RCT: randomized controlled trial; L: low risk of bias; H: high risk of bias; U: unclear (uncertain risk of bias).

abdominal pain, mucopurulent bloody stool, and tenesmus score, and one RCT [28] compared Sutherland disease activity indexes. Adverse reactions were mentioned in three studies [11, 28, 29], while the other two studies [12, 27] did not mention whether there were adverse reactions. The main outcomes and results are presented in Table 3.

3.3. Meta-Analysis

3.3.1. Clinical Efficacy. The four studies [11, 12, 27, 28] that compared the total effective rate of clinical efficacy included a total of 266 participants—135 in the experimental groups and 131 in the control groups. The four studies showed homogeneity of the data (heterogeneity test, $\text{Chi}^2 = 0.37$, $P = 0.95$, $I^2 = 0\%$). When the fixed effects model was used to merge OR values, the pooled OR was 3.11 (95% CI 1.50–6.46, $Z = 3.05$, $P = 0.002$). This indicated that the total effective rate of clinical efficacy was significantly higher in the experimental group than that in the control group (Figure 2(a)).

The four studies [11, 12, 27, 28] that compared the recovery rate of clinical efficacy included a total of 266 participants—135 in the experimental groups and 131 in the control groups. The four studies showed homogeneity (heterogeneity test, $\text{Chi}^2 = 2.76$, $P = 0.43$, $I^2 = 0\%$). When the fixed effects model was used to merge OR values, the pooled OR was 3.32 (95% CI 1.91–5.78, $Z = 4.26$, $P < 0.0001$). This indicated that the recovery rate of clinical efficacy was significantly higher in the experimental group than that in the control group (Figure 2(b)).

3.3.2. Serum Cytokines. The two studies [28, 29] that compared serum IL-6 included a total of 153 participants—77 in the experimental group and 76 in the control group. The two studies showed homogeneity of the data (heterogeneity test, $\text{Chi}^2 = 1.53$, $P = 0.22$, $I^2 = 35\%$). When the fixed effects model was used to merge MD values, the pooled MD was −15.74 [95% CI (−17.95)–(−13.53), $Z = 13.96$, $P < 0.00001$]. This indicated that serum IL-6 was significantly lower in the experimental group than that in the control group (Figure S3A).

The two studies [28, 29] that compared serum TNF-α included a total of 153 participants—77 in the experimental group and 76 in the control group. The two studies showed homogeneity (heterogeneity test, $\text{Chi}^2 = 0.23$, $P = 0.64$, $I^2 = 0\%$). When the fixed effects model was used to merge MD values, the pooled MD was −26.21 [95% CI (−29.37)–(−23.05), $Z = 16.25$, $P < 0.00001$]. This indicated that serum TNF-α was significantly lower in the experimental group than that in the control group (Figure S3B).

3.3.3. Syndrome Scores of TCM. The two studies [28, 29] that compared the total syndrome score TCM included a total of 153 participants—77 in the experimental group and 76 in the control group. The two studies showed heterogeneity (heterogeneity test, $\text{Chi}^2 = 2.45$, $P = 0.12$, $I^2 = 59\%$). When the random effects model was used to merge MD values, the pooled MD was −2.98 [95% CI (−3.73)–(−2.23), $Z = 7.81$, $P < 0.00001$]. This indicated that the total syndrome score of TCM was significantly lower in the experimental group than that in the control group (Figure S4).

3.3.4. Adverse Reactions. The three studies [11, 28, 29] that compared the incidence of adverse reactions included a total of 241 participants—121 in the experimental group and 120 in the control group. The three studies showed homogeneity of the data (heterogeneity test, $\text{Chi}^2 = 0.03$, $P = 0.87$, $I^2 = 0\%$). When the fixed effects model was used to merge OR values, the pooled OR was 0.12 (95% CI 0.03–0.54, $Z = 2.76$, $P = 0.006$). This indicated that the incidence of adverse reactions was significantly lower in the experimental group than in the control group (Figure 3).

3.4. Screening of Active Compounds in ZRYZD. A total of 24 compounds were obtained from PP, 64 from SM, 41 from FC, 100 from CC, 134 from RC, 55 from RAM, 125 from RAS, 85 from RPA, 106 from RA, and 280 from RG using the TCMSP (Supplementary File 1). By setting the filter criteria as OB ≥ 30% and DL ≥ 0.18, 11 active compounds from PP, 9 from SM, 8 from FC, 10 from CC (setting DL ≥ 0.10), 21 from RC, 7 from RAM, 2 from RAS, 13 from RPA, 6 from RA, and 92 from RG were obtained. Finally, 169 active compounds in ZRYZD remained after the exclusion of duplicates. The basic information on the active compounds in ZRYZD is shown in Table S1.

3.5. Screened Active Target Genes of ZRYZD. The corresponding target genes of the 169 active compounds were also obtained from the TCMSP, in which 19 compounds did not have corresponding targets. Then, the corresponding gene symbols were screened by setting the format as "homo sapiens" from the UniProt Knowledgebase. Finally, 277 active target genes of the 150 active compounds in ZRYZD were identified (Supplementary File 2).

3.6. Acquired UC-Related Genes and Identified Active Target Genes of ZRYZD Acting on UC. We used "ulcerative colitis" as the keyword to search in the GeneCards database, which retrieved 4,798 UC-related genes (Supplementary File 3). The 277 active target genes of ZRYZD were compared with the 4,798 UC-related genes, which identified 187 active target genes of ZRYZD acting on UC (Figure 4, Table S2).

3.7. GO Functional Enrichment and KEGG Pathway Enrichment Analyses. The entrezIDs of the active target genes of ZRYZD acting on UC were obtained using RGUI and org.Hs.eg.db (Table S2). Then, GO functional enrichment and KEGG pathway enrichment analyses were performed using RGUI and clusterProfiler.

The GO BP functional enrichment analysis showed that the active target genes of ZRYZD acting on UC were significantly enriched in cellular response to chemical stress, response to lipopolysaccharides, response to molecules of

Table 3: Main outcomes in the included RCTs.

Study year [ref]	Main outcomes	Main results (effect size)	Adverse events
Yuan JY, 2009 [11]	(1) Clinical efficacy		No adverse reactions
	Total effective rate	OR, 3.32 [0.63, 17.43]	
	Recovery rate	OR, 3.10 [1.24, 7.79]	
	Recurrence rate	OR, 0.18 [0.05, 0.61]	
Zhao KH, 2010 [12]	(1) Clinical efficacy		n.r.
	Total effective rate	OR, 4.15 [0.39, 44.57]	
	Recovery rate	OR, 2.86 [0.72, 11.31]	
Wang L, 2015 [27]	(1) Clinical efficacy		n.r.
	Total effective rate	OR, 2.43 [0.81, 7.30]	
	Recovery rate	OR, 8.22 [2.16, 31.27]	
Han Y, 2019 [28]	(1) Clinical efficacy		Experimental: nausea ($n = 3$) Control: nausea ($n = 3$) somnolence ($n = 1$) vomit ($n = 2$)
	Total effective rate	OR, 3.95 [0.96, 16.35]	
	Recovery rate	OR, 1.97 [0.67, 5.73]	
	(2) Syndrome score of TCM		
	Total score	MD, −3.45 [−4.30, −2.60]	
	Diarrhea score	MD, −0.71 [−0.84, −0.58]	
	Abdominal pain score	MD, −0.73 [−0.85, −0.61]	
	Mucopurulent bloody stool score	MD, −1.24 [−1.55, −0.93]	
	Tenesmus score	MD, −0.77 [−1.03, −0.51]	
	(3) Sutherland disease activity indexes	MD, −1.32 [−1.69, −0.95]	
	(4) Serum cytokines		
	IL-6	MD, −14.14 [−17.50, −10.78]	
	IL-8	MD, −48.60 [−52.96, −44.24]	
	TNF-α	MD, −27.06 [−31.80, −22.32]	
Dai AC 2021 [29]	(1) Syndrome score of TCM		Experimental: nausea ($n = 1$) Control: nausea ($n = 3$) somnolence ($n = 2$) vomit ($n = 3$)
	Total score	MD, −2.67 [−3.16, −2.18]	
	(2) Serum cytokines		
	IL-6	MD, −16.96 [−19.89, −14.03]	
	TNF-α	MD, −25.52 [−29.76, −21.28]	

RCT: randomized controlled trial; TCM: traditional Chinese medicine; IL: interleukin; TNF: tumor necrosis factor; OR: odds ratio; MD: mean difference; n.r.: not reported.

bacterial origin, response to oxidative stress, response to reactive oxygen species, and other processes. The GO CC functional enrichment analysis showed that the active target genes of ZRYZD acting on UC were significantly enriched in membrane rafts, cyclin-dependent protein kinase holoenzyme complex, membrane microdomains, membrane regions, serine/threonine protein kinase complex, and other functions. The GO MF functional enrichment analysis showed that the active target genes of ZRYZD acting on UC were significantly enriched in nuclear receptor activity, ligand-activated transcription factor activity, DNA-binding transcription factor binding, RNA polymerase II-specific DNA-binding transcription factor binding, steroid hormone receptor activity, and other functions (Supplementary File 4). The top 10 GO functional enrichments ranked by q-value are shown in Figure 5(a).

The KEGG pathway enrichment analysis showed that the active target genes of ZRYZD acting on UC were significantly enriched in lipid and atherosclerosis, receptor for advanced glycation end products (AGE)-receptor for AGE (RAGE) signaling pathway in diabetic complications, fluid shear stress and atherosclerosis, hepatitis B, prostate cancer, chemical carcinogenesis-receptor activation, pancreatic cancer, bladder cancer, IL-17 signaling pathway, hepatitis C, and other pathways (Supplementary File 5). The top 30 KEGG pathway enrichments ranked by count values are shown in Figure 5(b).

3.8. Construction of Compound-Target Network. A compound-target network was constructed using Cytoscape software and analyzed using the NetworkAnalyzer tool. As some compounds had no correspondence to an overlapping target gene, the 187 overlapping active target genes correlated with 138 active compounds. There were 325 nodes (138 compound nodes and 187 target gene nodes) and 1,418 edges in the network (Supplementary File 6; Figure 6). Using the NetworkAnalyzer tool, the compounds ranked by the degree in the network are shown in Table S3.

PP, SM, and FC are monarch and minister herbs, which are regarded as the main active herbs in ZRYZD. We selected the compounds in PP, SM, and FC in the network for further analysis, as they can be considered the key compounds in ZRYZD acting on UC. The basic information for the key compounds, ranked by degree, with the 2D structure obtained from the PubChem database, is shown in Table 4.

We organized the data in Table 4, removed the compounds without a structure in the PubChem database, merged the same compounds, and used the most commonly used names in PubChem for the compounds with multiple names. The key compounds included ellipticine, ellagic acid, isoguaiacin, beta-sitosterol, (S)-laudanine, protopine, codeine, papaverine, cheilanthifoline, noscapine, peraksine,

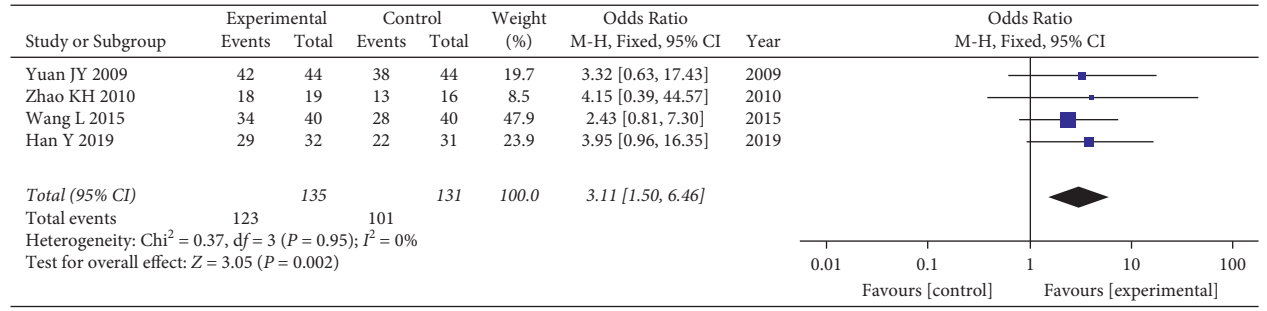

(a)

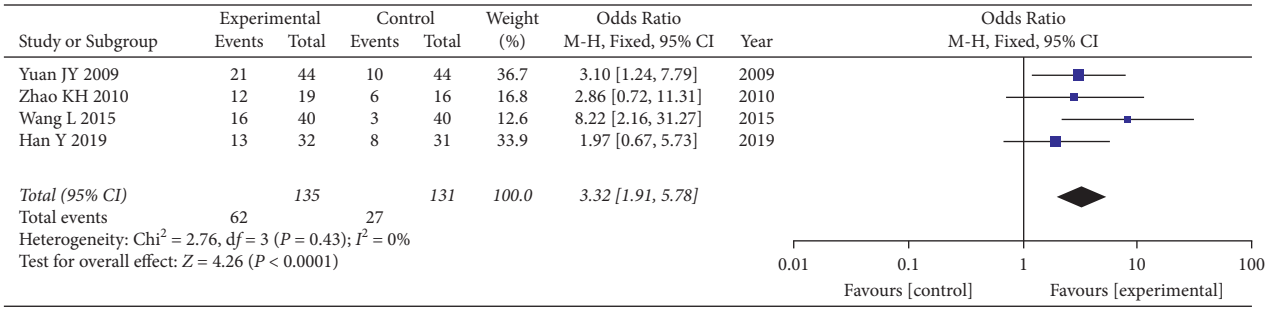

(b)

Figure 2: Forest plot of clinical efficacy. (a) The fixed effects model was used to merge OR values, and the pooled OR was 3.11 (95% CI 1.50–6.46, $P = 0.002$). The total effective rate of clinical efficacy was statistically significantly higher in the experimental group than that in the control group. (b) The fixed effects model was used to merge OR values, and the pooled OR was 3.32 (95% CI 1.91–5.78, $P < 0.0001$). The recovery rate of clinical efficacy was significantly higher in the experimental group than that in the control group.

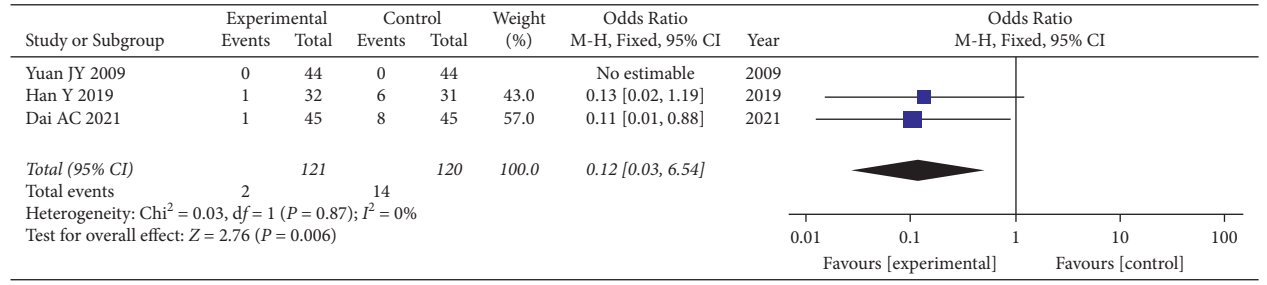

Figure 3: Forest plot of the incidence of adverse reactions. The fixed effects model was used to merge OR values, and the pooled OR was 0.12 (95% CI 0.03–0.54, $P = 0.006$). The incidence of adverse reactions was significantly lower in the experimental group than in the control group.

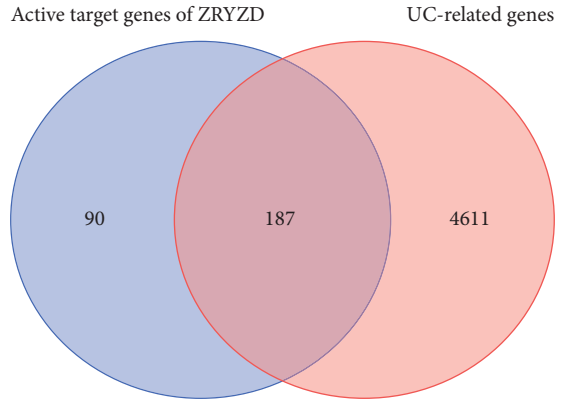

Figure 4: Active target genes of ZRYZD acting on UC. The 277 active target genes of ZRYZD were compared with the 4,798 UC-related genes, and 187 active target genes of ZRYZD acting on UC were identified.

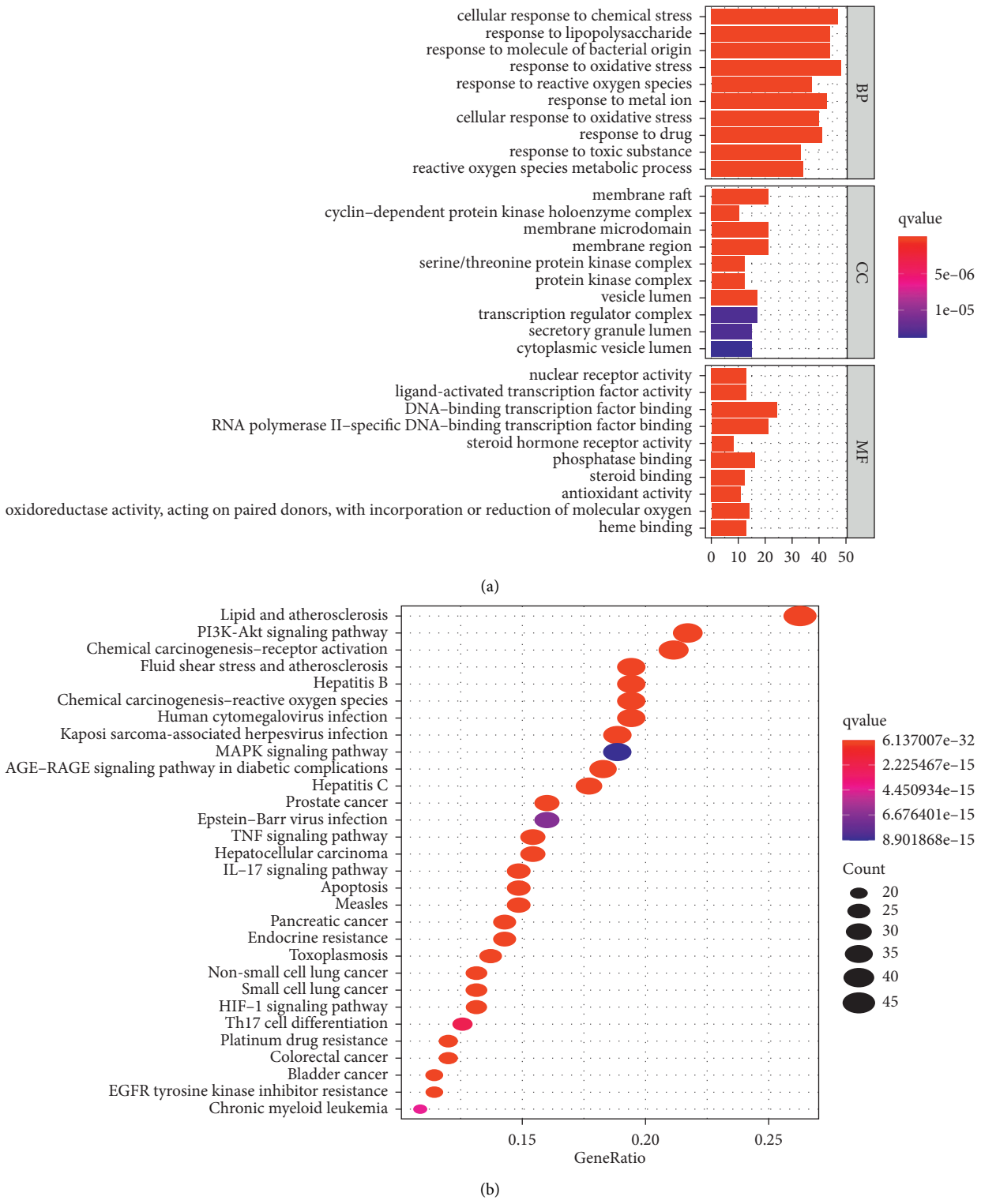

Figure 5: GO functional enrichment and KEGG pathway enrichment. (a) GO functional enrichment of active target genes. The smaller the q-value, the more significant the enrichment. (b) KEGG pathway enrichment of active target genes. The smaller the q-value and the greater the count, the more significant the enrichment.

myricanone, norswertianin, tetrahydrofuroguaiacin B, narceine, permethrin, galbacin, cryptogenin, and chebulic acid.

After introducing the key compounds and their 60 corresponding target genes into Cytoscape software, a key compound-target network was constructed. There were 79

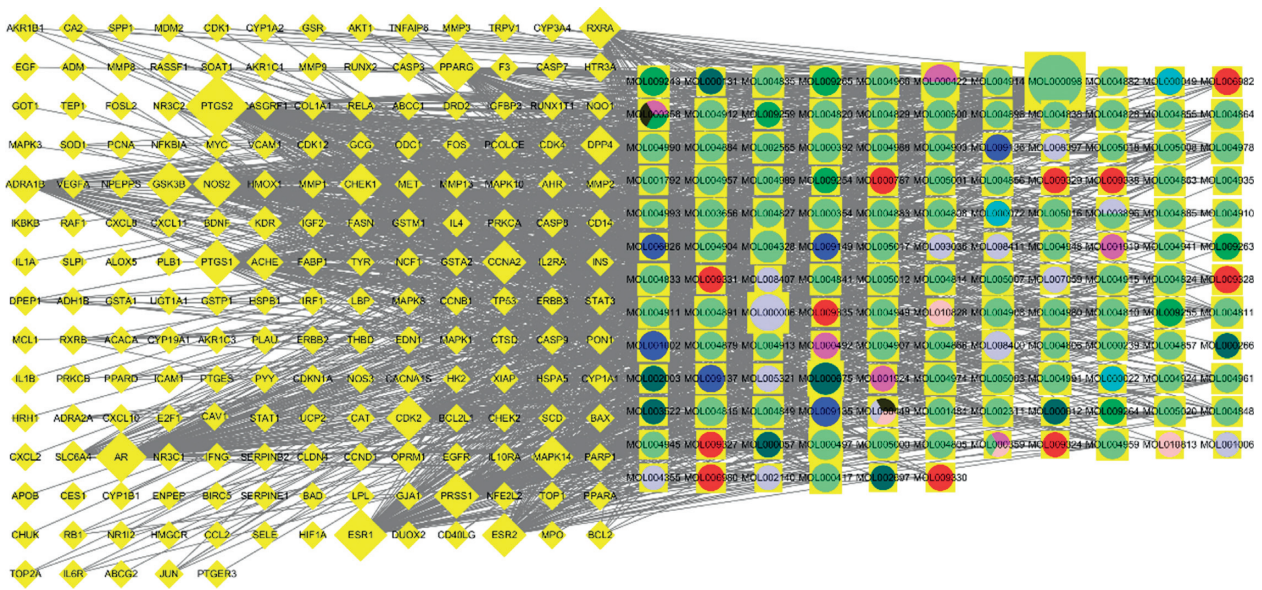

Figure 6: Compound-target network. There were 325 nodes (138 compound nodes and 187 target gene nodes) and 1,418 edges in the network. Circles represent active compounds (different colors represent different compounds), diamonds represent active target genes, and the edges represent links between the nodes. The more the connections between the compound and the target gene, the higher the degree value.

Table 4: Key compounds in ZRYZD acting on UC.

Compound name	Compound ID	Pubchem CID	Molecular formula	2D structure (from PubChem)	Degree	Herb
Ellipticine	MOL009135	3213	$C_{17}H_{14}N_2$	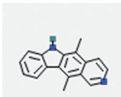	18	FC
Ellagic acid	MOL001002	5281855	$C_{14}H_6O_8$	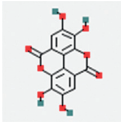	16	FC
Isoguaiacin	MOL009243	10314441	$C_{20}H_{24}O_4$	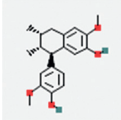	14	SM
Threo-austrobailignan-5	MOL009265	N/A	N/A	N/A	13	SM
Beta-sitosterol	MOL000358	222284	$C_{29}H_{50}O$	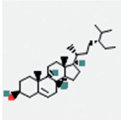	13	SM
5-[[(1S)-6,7-Dimethoxy-2-methyl-3,4-dihydro-1H-isoquinolin-1-yl]methyl]-2-methoxyphenol ((S)-Laudanine)	MOL009328	821396	$C_{20}H_{25}NO_4$	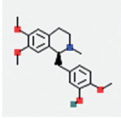	10	PP
5-[(2S,3S)-7-Methoxy-3-methyl-5-[(E)-prop-1-enyl]-2,3-dihydrobenzofuran-2-yl]-1,3-benzodioxole	MOL009255	N/A	N/A	N/A	10	SM
(R)-(6-Methoxy-4-quinolyl)-[(2R,4R,5S)-5-vinylquinuclidin-2-yl]methanol	MOL009137	N/A	N/A	N/A	10	FC
Fumarine (protopine)	MOL000787	4970	$C_{20}H_{19}NO_5$	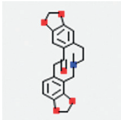	8	PP

Table 4: Continued.

Compound name	Compound ID	Pubchem CID	Molecular formula	2D structure (from PubChem)	Degree	Herb
Codeine	MOL006982	5284371	$C_{18}H_{21}NO_3$	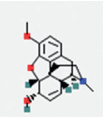	8	PP
Papaverine	MOL006980	4680	$C_{20}H_{21}NO_4$	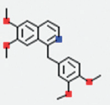	8	PP
Cheilanthifoline	MOL009149	5117621	$C_{19}H_{19}NO_4$	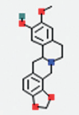	7	FC
Noscapine	MOL009330	275196	$C_{22}H_{23}NO_7$	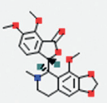	6	PP
Peraksine	MOL009136	78146432	$C_{19}H_{22}N_2O_2$	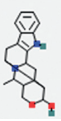	6	FC
Noskapin (noscapine)	MOL009327	275196	$C_{22}H_{23}NO_7$	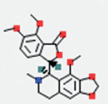	5	PP
Saucernetindiol	MOL009263	N/A	N/A	N/A	5	SM
Erythroculine	MOL009335	N/A	N/A	N/A	4	PP
Myricanone	MOL009331	161748	$C_{21}H_{24}O_5$		4	PP
Norswertianin	MOL009338	5281658	$C_{13}H_8O_6$	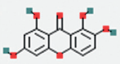	3	PP
Tetrahydrofuroguaiacin B	MOL009264	13870572	$C_{20}H_{24}O_5$	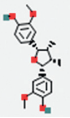	3	SM
Narcein (narceine)	MOL009329	8564	$C_{23}H_{27}NO_8$	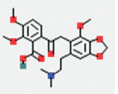	2	PP
Kudos (permethrin)	MOL009259	40326	$C_{21}H_{20}Cl_2O_3$	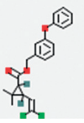	2	SM
Galbacin	MOL009254	234441	$C_{20}H_{20}O_5$	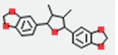	2	SM

Table 4: Continued.

Compound name	Compound ID	Pubchem CID	Molecular formula	2D structure (from PubChem)	Degree	Herb
Cryptogenin	MOL009324	21117640	$C_{27}H_{42}O_4$	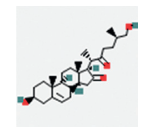	1	PP
Chebulic acid	MOL006826	71308174	$C_{14}H_{12}O_{11}$	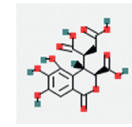	1	FC

ZRYZD: Zhen Ren Yang Zang decoction; UC: ulcerative colitis; PP: *pericarpium papaveris*; SM: *semen myristicae*; FC: *fructus chebulae.*

nodes (19 compound nodes and 60 target gene nodes) and 132 edges in the network (Supplementary File 7; Figure 7). Using the NetworkAnalyzer tool, the top six target genes, ranked by degree, were PTGS2, PTGS1, ADRA1B, RXRA, OPRM1, and SLC6A4.

3.9. Construction of the PPI Network. The 60 corresponding target genes were mapped into the STRING database, and the PPI network was obtained. In the network, 59 target proteins had interactions, and 456 edges represented the interactions between the proteins when the lowest interaction score was set to 0.40 (Supplementary File 8; Figure 8).

The top 10 target genes ranked by the degree in the PPI network are shown in Table 5; these can be considered the key target proteins of ZRYZD acting on UC.

3.10. Molecular Docking Analysis. The 3D structures of the compounds were obtained from the PubChem database, and the target proteins from the RCSB PDB database. Molecular docking simulations of the target proteins and their corresponding compounds were performed using AutoDockTool and AutoDock Vina software. The binding of the target proteins with their corresponding compounds was analyzed using molecular docking. The molecular docking simulations of TP53-ellipticine are shown in Figure 9.

4. Discussion

According to TCM theory, UC belongs to the category of "dysentery" and is characterized by dampness and heat accumulation, qi and blood disorder, and visceral food accumulation. The disease location of UC is in the intestine, and kidney qi insufficiency, spleen deficiency, endogenous dampness, and heat are considered the primary causes of this disease. Accordingly, TCM theory suggests that the treatment of patients should be based on supplementing the spleen and kidney, invigorating qi and warming yang [30]. From the perspective of modern medicine, the pathogenesis of UC is primarily related to chronic nonspecific inflammation, which is the result of the interaction of the host response, genetic factors, and immune imbalance.

ZRYZD, which consists of PP, SM, FC, CC, RC, RAM, RAS, RPA, RA, and RG as the main components, has the effect of consolidating and astringing the intestine, and nourishing the spleen and kidney. PP, SM and FC, which are considered monarch and minister herbs, can be used as intestinal astringents to stop diarrhea. CC, RC, and RAM can warm the spleen and kidney. RAS, RPA, and RA can regulate qi and blood. RG can replenish qi and reconcile all the other herbs [10].

Several clinical studies have reported that ZRYZD improves clinical outcomes in the treatment of UC. Therefore, we first evaluated the effectiveness and safety of ZRYZD for UC using an evidence-based analytical approach. We screened five RCTs that investigated the efficacy of ZRYZD for UC and performed a meta-analysis. Meta-analysis indicated that the total effective rate and recovery rate of clinical efficacy were statistically significantly higher in the experimental group than those in the control group and that the incidence of adverse reactions was significantly lower in the experimental group than that in the control group. This analysis demonstrates the effectiveness and safety of ZRYZD for UC from the perspective of evidence-based medicine, providing a foundation for further investigation of its pharmacological mechanisms of action. Furthermore, meta-analysis indicated that serum IL-6 and TNF-α were significantly lower in the experimental group compared with the control group, suggesting that the therapeutic effectiveness of ZRYZD for UC may be associated with a reduction in inflammation.

Network pharmacology is widely used in the study of TCM. The network pharmacology approach and platform could make the systematic study of herbal medicines achievable and advance pharmacodynamic substance discovery and could also provide a new strategy for translating TCM from an experience-based to an evidence-based medical system [31, 32]. Recently, guidelines for the network pharmacology evaluation method were drafted, allowing many technical and analysis-related problems to be resolved, permitting a more scientific approach for TCM network pharmacology research [33]. Network pharmacology advocates a multicomponent therapeutic approach, which is consistent with the multicomponent, multitarget, and multipathway characteristics of TCM [34, 35]. Hence, we used the network pharmacology approach to investigate the pharmacological mechanisms of action of ZRYZD for UC. In this study, 187 active target genes of ZRYZD acting on UC

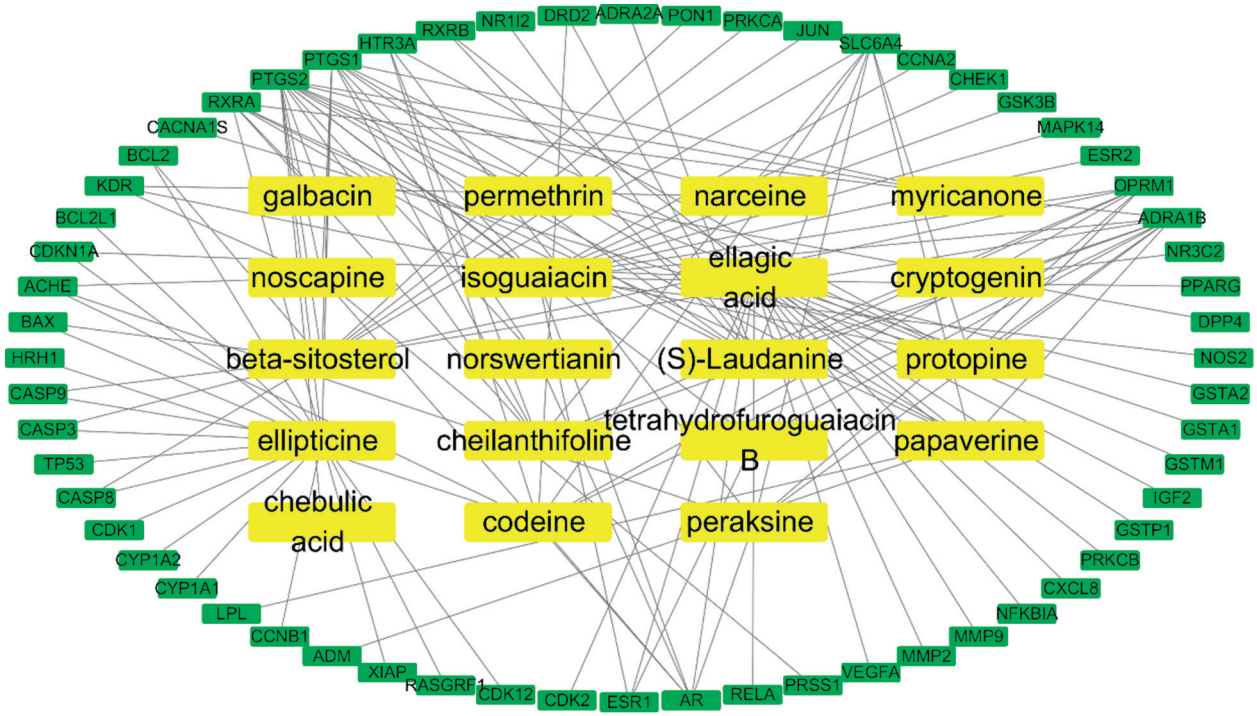

Figure 7: Key compound-target network. There were 79 nodes (19 compound nodes and 60 target gene nodes) and 132 edges in the network. The more the connections between the compound and the target gene, the higher the degree value.

were identified. The GO BP functional enrichment analysis suggested that the active target genes of ZRYZD acting on UC were significantly enriched in the cellular response to chemical stress, response to lipopolysaccharides, response to molecules of bacterial origin, and other processes. The GO CC functional enrichment analysis revealed that the active target genes of ZRYZD acting on UC were significantly enriched in membrane rafts, cyclin-dependent protein kinase holoenzyme complex, membrane microdomains, and other functions. The GO MF functional enrichment analysis showed that the active target genes of ZRYZD acting on UC were significantly enriched in nuclear receptor activity, ligand-activated transcription factor activity, DNA-binding transcription factor binding, and other functions. These functions are closely related to inflammation and immune regulation, which are in turn closely related to the etiopathogenesis of UC [36–38].

The KEGG pathway enrichment analysis showed that many pathways were closely related to the pathogenesis of UC. The primary pathways included lipid and atherosclerosis, AGE-RAGE signaling pathway in diabetic complications, fluid shear stress and atherosclerosis, hepatitis B, prostate cancer, chemical carcinogenesis-receptor activation, pancreatic cancer, bladder cancer, IL-17 signaling pathway, and hepatitis C. Some of these pathways have been reported to be closely related to UC. IL-17 is upregulated in inflamed mucosa from UC patients, and IL-17 levels in peripheral blood mononuclear cells are correlated with disease severity in UC patients [39]. IL-17 is produced mainly by *T* helper 17 cells and is considered to be a key pathophysiological mediator and plays an important role in regulating the intestinal immune response [40]. In UC, AGE and IL-17 are highly expressed and participate in nuclear factor- (NF-) κB pathway activation [41, 42]. These observations suggest that ZRYZD may ameliorate UC via multiple pathways related to inflammation and the immune response. These pathways and relevant target genes are worthy of further study.

A network of a compound-target network was constructed, and the compounds of ZRYZD acting on UC were identified. The 187 overlapping active target genes correlated with 138 active compounds. We found that these 138 compounds correspond to each herb in ZRYZD, and we can argue that every herb in ZRYZD plays a role in acting on UC. We also found that the importance of active compounds in PP, SM, and FC in the compound-target network is obvious. These findings are in agreement with TCM theory. PP, SM, and FC are monarch and minister herbs and are regarded as the main active herbs in ZRYZD. Therefore, we selected the compounds in PP, SM, and FC in the network for further study, and we constructed a key compound-target network to identify the key compounds. The key compounds were ellipticine, ellagic acid, isoguaiacin, beta-sitosterol, (S)-laudanine, protopine, codeine, papaverine, cheilanthifoline, noscapine, peraksine, myricanone, norswertianin, tetrahydrofuroguaiacin B, narceine, permethrin, galbacin, cryptogenin, and chebulic acid. *Ficus carica* aqueous extract containing ellagic acid can ameliorate UC-associated acute functional gastrointestinal disorder in rats [43]; A study verified the ethnomedical use of *Cornus mas* L. for the treatment of UC, in which ellagic acid was identified in extracts and its amount quantified [44]. A study provided evidence for the therapeutic effectiveness of *Canna x generalis* L.H. Bailey rhizome extract for the treatment of UC

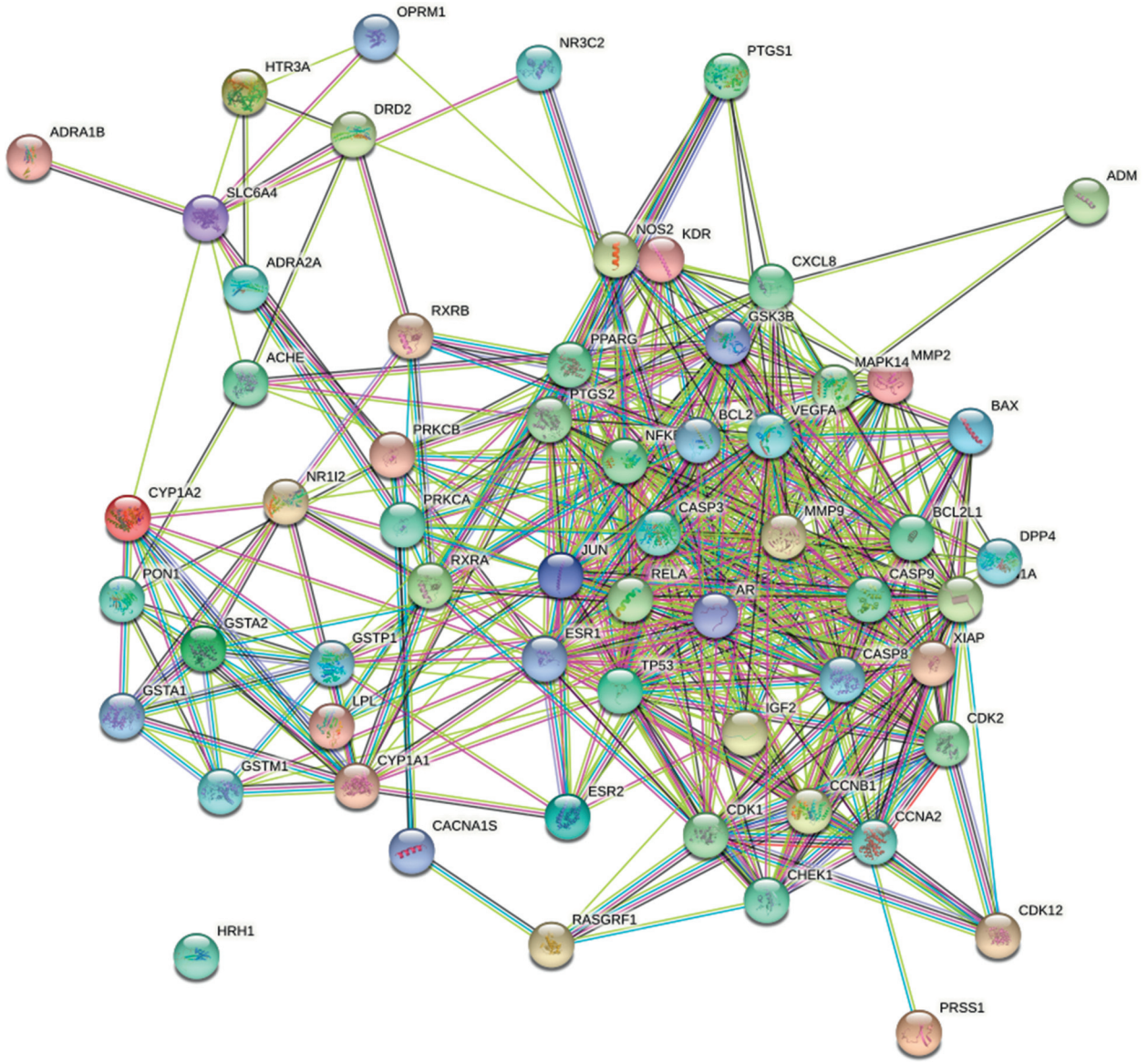

Figure 8: The PPI network. In the network, 23 target proteins had an interaction, and the 90 edges represent the interactions between the proteins, when the lowest interaction score was set to 0.40. The more the connections, the higher the degree value.

and discovered beta-sitosterol as one of the major identified constituents [45], which was shown to improve experimental colitis in mice by targeting pathogenic bacteria [46]. Prostaglandin synthetase activity in rectal biopsy specimens from patients with UC has been shown to fall on treatment with sulfasalazine, local steroids, and codeine phosphate [47]. Papaverine adjuvant can treat microcirculatory disturbance in severe UC complicated with cytomegalovirus infection [48]. These studies reveal an effect on the regulation of inflammation and immune function. Therefore, the action of ZRYZD on UC could be the result of the interaction of multiple compounds. However, there are only a few studies on the effect of individual constituent compounds on UC, which therefore requires further investigation.

The PPI network showed that the action of ZRYZD on UC was related to multiple targets. The key target proteins were TP53, VEGFA, JUN, CASP3, ESR1, PTGS2, MMP9, PPARG, BCL2L1, and CASP8. A previous study showed that alterations in p53 may be an early biomarker of a progressor colon and that p53 is upregulated early in UC-related carcinogenesis [49]. In UC patients, p53 enhances VEGF expression and subsequent production of proinflammatory TNF-α and IL-6 [50]. *Berberis lycium* fruit extract can attenuate oxidative/inflammatory stress and promote mucosal healing by downregulating NF-κB/c-Jun/MAPK signaling and augmenting splenic Treg proliferation in a murine model of dextran sulfate sodium-induced UC [51]. Analysis of biopsies from UC patients and normal controls demonstrates that disease-associated occludin downregulation is accompanied by and correlated with reduced caspase-3 expression [52]. Inactivation through methylation of the putative tumor suppressor gene ESR1 may not be associated with colorectal carcinogenesis in UC [53]. Amentoflavone inhibits PTGS2 expression and

Table 5: Key target proteins of ZRYZD acting on UC.

Key target	Entry	Entry name	Protein names	Degree
TP53	P04637	P53_HUMAN	Cellular tumor antigen p53	37
VEGFA	P15692	VEGFA_HUMAN	Vascular endothelial growth factor A	35
JUN	P05412	JUN_HUMAN	Transcription factor AP-1	35
CASP3	P42574	CASP3_HUMAN	Caspase-3	34
ESR1	P03372	ESR1_HUMAN	Estrogen receptor	33
PTGS2	P35354	PGH2_HUMAN	Prostaglandin G/H synthase 2	30
MMP9	P14780	MMP9_HUMAN	Matrix metalloproteinase-9	30
PPARG	P37231	PPARG_HUMAN	Peroxisome proliferator-activated receptor gamma	28
BCL2L1	Q07817	B2CL1_HUMAN	Bcl-2-like protein 1	27
CASP8	Q14790	CASP8_HUMAN	Caspase-8	27

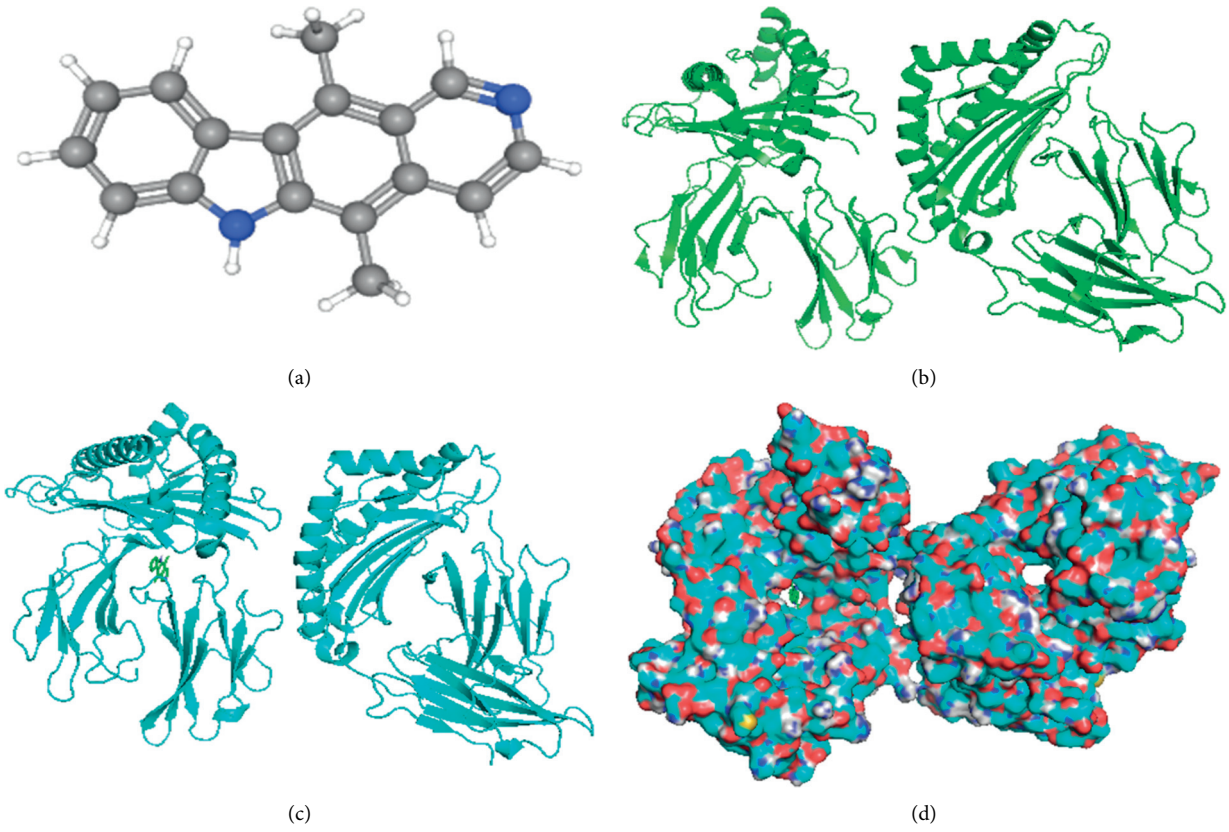

Figure 9: Molecular docking of TP53 and ellipticine. (a) 3D structures of ellipticine from the PubChem database. (b) 3D structures of TP53 from the RCSB PDB database. (c) Molecular docking simulation. (d) Molecular docking simulation displaying the protein surface.

modulates cytokine profile and NF-κB signal transduction pathways in rats with UC [54]. In patients with active UC, MMP2, MMP9, and inflammatory factors are significantly increased [55]. Gliclazide attenuates acetic acid-induced colitis via the modulation of PPARG, NF-κB, and MAPK signaling pathways [56]. HSPA6 is a UC susceptibility factor that is induced by cigarette smoke and protects intestinal epithelial cells by stabilizing antiapoptotic Bcl-XL [57]. Cyclosporine upregulates transforming growth factor-β in colonic tissue and inhibits caspase-8 activity in epithelial cells [58]. These studies demonstrate the relationship between these genes and UC, facilitating the further exploration of the therapeutic mechanisms of action.

Molecular docking was also performed to analyze specific interactions between key compounds and their protein targets, which could improve the robustness of the network model. The preliminary molecular docking results showed that the key active compounds in ZRYZD had high binding activities with their corresponding protein targets. These active compounds may mediate the therapeutic action of ZRYZD for UC via related signaling pathways. Compounds related to the corresponding target proteins can also be investigated in future studies.

The pharmacological mechanisms of action of ZRYZD for UC were investigated using a network pharmacology approach, and the binding of the target to the corresponding compound was analyzed using molecular docking. However,

there are some limitations to using these approaches. First, the active compounds and target genes of ZRYZD were searched using the TCMSP database. The screening criteria and definition of the active compounds were fixed, and the UC-related genes were obtained from the GeneCards database. Although these databases are currently relatively comprehensive, some compounds and target genes may have been omitted. In addition, not all the compounds that enter the circulation may contribute to the efficacy of ZRYZD. Second, while the GO functional enrichment and KEGG pathway enrichment analyses were performed, and a PPI network was constructed to investigate the target genes and pathways of ZRYZD acting on UC, the potential target genes and pathways require further study using empirical analyses. Third, only preliminary molecular docking analyses were conducted in this study, and more in-depth analyses of the molecular docking of small-molecule compounds and macromolecular protein targets are needed.

5. Conclusion

The effectiveness and safety of ZRYZD for the treatment of UC were evaluated with an evidence-based approach. Using network pharmacology, we investigated the relationships between the active compounds, target genes, and signaling pathways, which revealed the involvement of multiple compounds, multiple targets, and multiple pathways. Finally, key compounds and their predicted target proteins were used for molecular docking analyses, which provided further evidence that these compounds may be important mediators of the therapeutic action of ZRYZD against UC.

Data Availability

The data used to support this study are included in the supplementary files.

Conflicts of Interest

The authors declare no conflicts of interest.

Authors' Contributions

Guosheng Xing, Yufeng Zhang, Mingxing Hou, and Haibing Hua conceived and designed the study and wrote the manuscript. Guosheng Xing, Xinlin Wu, Hua Wang, Yan Liu, and Zhen Zhang were responsible for data collation and extraction and performed the data analysis. Mingxing Hou and Haibing Hua performed supervision and project administration. Guosheng Xing, Yufeng Zhang, and Haibing Hua performed the revision of the article. All the authors read and approved the final manuscript. Guosheng Xing and Yufeng Zhang contributed equally to the article.

Acknowledgments

The authors would like to acknowledge the web database platform and software for data analyses. This study was partially supported by the Science and Technology Project of Inner Mongolia Medical University (YKD2020KJBW(LH) 014) and the Inner Mongolia Natural Science Foundation (2021MS08097) to Xing, and the fifth phase of the "333 project" scientific research funded project to Hua. The authors thank Barry Patel, PhD, from Liwen Bianji (Edanz) (https://www.liwenbianji.cn/), for editing the English text of a draft of this manuscript.

Supplementary Materials

Figure S1: Risk of bias graph. Figure S2: risk of bias summary. Figure S3: forest plot of comparison of serum cytokines. Figure S4: forest plot of comparison of the total syndrome score of TCM. Table S1: basic information on the active compounds in ZRYZD. Table S2: gene symbols and entrezID of active target genes. Table S3: compounds ranked by the degree in the network. Supplementary File 1: compounds of ZRYZD from TCMSP. Supplementary File 2: corresponding target genes of ZRYZD. Supplementary File 3: UC-related target genes. Supplementary File 4: GO functional enrichment analysis. Supplementary File 5: KEGG pathway enrichment analysis. Supplementary File 6: data of compound-target networks. Supplementary File 7: data of key compound-target networks. Supplementary File 8: data of PPI network. (*Supplementary Materials*)

References

[1] R. Ungaro, S. Mehandru, P. B. Allen, L. Peyrin-Biroulet, and J.-F. Colombel, "Ulcerative colitis," *The Lancet*, vol. 389, no. 10080, pp. 1756–1770, 2017.

[2] S. Danese and C. Fiocchi, "Ulcerative colitis," *New England Journal of Medicine*, vol. 365, no. 18, pp. 1713–1725, 2011.

[3] T. Tanaka, T. Kobunai, Y. Yamamoto et al., "Assessment of the changes in mitochondrial gene polymorphism in ulcerative colitis and the etiology of ulcerative colitis-associated colorectal cancer," *Anticancer Research*, vol. 40, no. 1, pp. 101–107, 2020.

[4] C. Bello, J. Belaiche, E. Louis, and C. Reenaers, "Evolution and predictive factors of relapse in ulcerative colitis patients treated with mesalazine after a first course of corticosteroids," *Journal of Crohns & Colitis*, vol. 5, no. 3, pp. 196–202, 2011.

[5] M. Salice, F. Rizzello, C. Calabrese, L. Calandrini, and P. Gionchetti, "A current overview of corticosteroid use in active ulcerative colitis," *Expert Review of Gastroenterology & Hepatology*, vol. 13, no. 6, pp. 557–561, 2019.

[6] X. Zhou, R. Gao, X. Zhang, T. Shen, and K. Xu, "Efficacy of xianglian pill for antibiotic-associated diarrhea: a protocol for systematic review and meta-analysis," *Traditional Medicine Research*, vol. 6, no. 5, p. 43, 2021.

[7] P. Wan, H. Chen, Y. Guo, and A. P. Bai, "Advances in treatment of ulcerative colitis with herbs: from bench to bedside," *World Journal of Gastroenterology*, vol. 20, no. 39, pp. 14099–14104, 2014.

[8] Z. Shen, Q. Zhou, Y. Ni, W. He, H. Shen, and L. Zhu, "Traditional Chinese medicine for mild-to-moderate ulcerative colitis: protocol for a network meta-analysis of randomized controlled trials," *Medicine (Baltimore)*, vol. 98, no. 33, Article ID e16881, 2019.

[9] Z. X. Yan, Y. M. Liu, T. Ma et al., "Efficacy and safety of retention enema with traditional Chinese medicine for ulcerative colitis: a meta-analysis of randomized controlled

trials," *Complementary Therapies in Clinical Practice*, vol. 42, Article ID 101278, 2021.

[10] J. Qi, Y. N. Tang, Y. F. Zhang, Q. Q. Xia, and W. L. Jiang, "Zhenren yangzang decoction in treatment of ulcerative colitis: a systematic review," *Liaoning Journal of Traditional Chinese Medicine*, vol. 43, no. 1, pp. 16–19, 2016.

[11] J. Y. Yuan and D. H. Li, "Clinical observation of 44 cases of zhenren yangzang decoction in treatment of ulcerative colitis," *China Journal of Traditional Chinese Medicine and Pharmacy*, vol. 24, no. S1, pp. 117-118, 2009.

[12] K. H. Zhao, "Warming and astringent method treating 19 cases of ulcerative colitis with deficiency of spleen and kidney yang," *Henan Traditional Chinese Medicine*, vol. 30, no. 1, pp. 63-64, 2010.

[13] H. Wang, S. H. Li, Y. Zhang et al., "Therapeutic efficacy and mechanism of Zhenrenyangzang decoction in rats with experimental ulcerative colitis," *International Journal of Clinical and Experimental Medicine*, vol. 8, no. 9, pp. 15254–15261, 2015.

[14] J. P. Higgins, D. G. Altman, P. Jüni et al., "The Cochrane collaboration's tool for assessing risk of bias in randomised trials," *BMJ (Clinical research ed.)*, vol. 343, Article ID d5928, 2011.

[15] J. Ru, P. Li, J. Wang et al., "TCMSP: a database of systems pharmacology for drug discovery from herbal medicines," *Journal of Cheminformatics*, vol. 6, no. 1, p. 13, 2014.

[16] Q. Xia, M. Liu, H. Li, L. Tian, J. Qi, and Y. Zhang, "Network pharmacology strategy to investigate the pharmacological mechanism of Huang Qi Xi Xin decoction on cough variant asthma and evidence-based medicine approach validation," *Evidence-based Complementary and Alternative Medicine: ECAM*, vol. 2020, Article ID 3829092, 15 pages, 2020.

[17] W. Jiang, Y. Zhang, M. Liu et al., "A network pharmacology approach to explore the mechanism of kangguan decoction in the treatment of coronavirus disease 2019 with preliminary verification," *TMR Integrative Medicine*, vol. 5, Article ID e21025, 2021.

[18] C. T. UniProt, "UniProt: the universal protein knowledgebase," *Nucleic Acids Research*, vol. 46, no. 5, p. 2699, 2018.

[19] G. Stelzer, N. Rosen, I. Plaschkes et al., "The genecards suite: from gene data mining to disease genome sequence analyses," *Current Protocols in Bioinformatics*, vol. 54, pp. 1–33, 2016.

[20] G. Yu, L.-G. Wang, Y. Han, and Q.-Y. He, "ClusterProfiler: an *R* package for comparing biological themes among gene clusters," *OMICS: A Journal of Integrative Biology*, vol. 16, no. 5, pp. 284–287, 2012.

[21] P. Shannon, A. Markiel, O. Ozier et al., "Cytoscape: a software environment for integrated models of biomolecular interaction networks," *Genome Research*, vol. 13, no. 11, pp. 2498–2504, 2003.

[22] D. Szklarczyk, A. L. Gable, D. Lyon et al., "STRING v11: protein-protein association networks with increased coverage, supporting functional discovery in genome-wide experimental datasets," *Nucleic Acids Research*, vol. 47, no. D1, pp. D607–D613, 2019.

[23] M. F. Sanner, "Python: a programming language for software integration and development," *Journal of Molecular Graphics & Modelling*, vol. 17, no. 1, pp. 57–61, 1999.

[24] D. Jiang, X. Wang, L. Tian, and Y. Zhang, "Network pharmacology strategy to investigate the pharmacological mechanism of siwu decoction on primary dysmenorrhea and molecular docking verification," *Evidence-based Complementary and Alternative Medicine*, vol. 2021, Article ID 6662247, 13 pages, 2021.

[25] J. P. T. Higgins and S. G. Thompson, "Quantifying heterogeneity in a meta-analysis," *Statistics in Medicine*, vol. 21, no. 11, pp. 1539–1558, 2002.

[26] J. P. T. Higgins, S. G. Thompson, J. J. Deeks, and D. G. Altman, "Measuring inconsistency in meta-analyses," *BMJ*, vol. 327, no. 7414, pp. 557–560, 2003.

[27] L. Wang and D. M. Liu, "Treatment of 40 cases of ulcerative colitis with deficiency of spleen and kidney yang by zhenren yangzang decoction and sini decoction," *Hunan Journal of Traditional Chinese Medicine*, vol. 31, no. 10, pp. 43-44, 2015.

[28] Y. Han, Y. Zhang, D. F. Yang et al., "Clinical efficacy of dongbin organ-nourishing decoction in ulcerative colitis patients regarding disease activity and serum inflammatory cytokines," *Journal of Clinical and Experimental Medicine*, vol. 18, no. 9, pp. 936–939, 2019.

[29] A. C. Dai, L. J. Chu, C. X. Zhang, N. H. Guo, Y. Y. Liang, and Z. Y. Wu, "Effect of zhenren yangzang decoction on micro inflammatory state and disease degree of ulcerative colitis," *Journal of Practical Traditional Chinese Medicine*, vol. 37, no. 7, pp. 1118-1119, 2021.

[30] Z. F. Chen and H. Y. Liu, "Research progress of traditional Chinese medicine in ulcerative colitis," *Journal of Changchun University of Chinese Medicine*, vol. 34, no. 1, pp. 196–198, 2018.

[31] B. Zhang, X. Wang, and S. Li, "An integrative platform of TCM network pharmacology and its application on a herbal formula, Qing-Luo-Yin," *Evidence-based Complementary and Alternative Medicine: ECAM*, vol. 2013, Article ID 456747, 12 pages, 2013.

[32] S. Li and B. Zhang, "Traditional Chinese medicine network pharmacology: theory, methodology and application," *Chinese Journal of Natural Medicines*, vol. 11, no. 2, pp. 110–120, 2013.

[33] S. Li, "Network pharmacology evaluation method guidance-draft," *World Journal of Traditional Chinese Medicine*, vol. 7, no. 1, pp. 146–154, 2021.

[34] J. Yuan, J. Hao, and D. Chen, "Network pharmacology: an important breakthrough in traditional Chinese medicine research," *TMR Integrative Medicine*, vol. 2, no. 3, pp. 92–98, 2018.

[35] T.-T. Luo, Y. Lu, S.-K. Yan, X. Xiao, X.-L. Rong, and J. Guo, "Network pharmacology in research of Chinese medicine formula: methodology, application and prospective," *Chinese Journal of Integrative Medicine*, vol. 26, no. 1, pp. 72–80, 2020.

[36] M. Wei, H. Li, Q. Li et al., "Based on network pharmacology to explore the molecular targets and mechanisms of gegen qinlian decoction for the treatment of ulcerative colitis," *Biomed Research International*, vol. 2020, Article ID 5217405, 18 pages, 2020.

[37] L. Xu, J. Zhang, Y. Wang, Z. Zhang, F. Wang, and X. Tang, "Uncovering the mechanism of Ge-Gen-Qin-Lian decoction for treating ulcerative colitis based on network pharmacology and molecular docking verification," *Bioscience Reports*, vol. 41, no. 2, 2021.

[38] B. Shi, S. Liu, A. Huang et al., "Revealing the mechanism of friedelin in the treatment of ulcerative colitis based on network pharmacology and experimental verification," *Evidence-Based Complementary and Alternative Medicine*, vol. 2021, Article ID 4451779, 14 pages, 2021.

[39] Y. Iboshi, K. Nakamura, K. Fukaura et al., "Increased IL-17A/IL-17F expression ratio represents the key mucosal *T* helper/regulatory cell-related gene signature paralleling disease activity in ulcerative colitis," *Journal of Gastroenterology*, vol. 52, no. 3, pp. 315–326, 2017.

[40] A. Ueno, L. Jeffery, T. Kobayashi, T. Hibi, S. Ghosh, and H. Jijon, "Th17 plasticity and its relevance to inflammatory bowel disease," *Journal of Autoimmunity*, vol. 87, pp. 38–49, 2018.

[41] J. Tobon-Velasco, E. Cuevas, and M. Torres-Ramos, "Receptor for AGEs (RAGE) as mediator of NF-kB pathway activation in neuroinflammation and oxidative stress," *CNS & Neurological Disorders-Drug Targets*, vol. 13, no. 9, pp. 1615–1626, 2014.

[42] H. Zhang, B. Xia, J. Li et al., "Expression and clinical significance of IL-17 and IL-17 receptor in ulcerative colitis," *Journal of Huazhong University of Science and Technology [Medical Sciences]*, vol. 36, no. 1, pp. 37–40, 2016.

[43] K. Rtibi, D. Grami, D. Wannes et al., "Ficus carica aqueous extract alleviates delayed gastric emptying and recovers ulcerative colitis-enhanced acute functional gastrointestinal disorders in rats," *Journal of Ethnopharmacology*, vol. 224, pp. 242–249, 2018.

[44] I. Süntar, C. K. Cevik, A. O. Çeribaşı, and A. Gökbulut, "Healing effects of cornus mas L. in experimentally induced ulcerative colitis in rats: from ethnobotany to pharmacology," *Journal of Ethnopharmacology*, vol. 248, Article ID 112322, 2020.

[45] T. N. Mahmoud, W. H. El-Maadawy, Z. A. Kandil, H. Khalil, N. M. El-Fiky, and A. T. El, "Canna x generalis L.H. bailey rhizome extract ameliorates dextran sulfate sodium-induced colitis via modulating intestinal mucosal dysfunction, oxidative stress, inflammation, and TLR4/NF-B and NLRP3 inflammasome pathways," *Journal of Ethnopharmacology*, vol. 269, Article ID 113670, 2021.

[46] K. Ding, Y. Y. Tan, Y. Ding et al., "β-sitosterol improves experimental colitis in mice with a target against pathogenic bacteria," *Journal of Cellular Biochemistry*, vol. 120, no. 4, pp. 5687–5694, 2019.

[47] P. R. Smith, D. J. Dawson, and C. H. Swan, "Prostaglandin synthetase activity in acute ulcerative colitis: effects of treatment with sulphasalazine, codeine phosphate and prednisolone," *Gut*, vol. 20, no. 9, pp. 802–805, 1979.

[48] Y. Tian, Y. Zheng, J. Dong, J. Zhang, and H. Wang, "Papaverine adjuvant therapy for microcirculatory disturbance in severe ulcerative colitis complicated with CMV infection: a case report," *Clinical Journal of Gastroenterology*, vol. 12, no. 5, pp. 407–413, 2019.

[49] M. Friis-Ottessen, E. Burum-Auensen, A. R. Schjolberg et al., "TP53/p53 alterations and aurora A expression in progressor and non-progressor colectomies from patients with long-standing ulcerative colitis," *International Journal of Molecular Medicine*, vol. 35, no. 1, pp. 24–30, 2015.

[50] N. D. Zdravkovic, I. P. Jovanovic, G. D. Radosavljevic et al., "Potential dual immunomodulatory role of VEGF in ulcerative colitis and colorectal carcinoma," *International Journal of Medical Sciences*, vol. 11, no. 9, pp. 936–947, 2014.

[51] A. Sharma, N. V. Tirpude, P. M. Kulurkar, R. Sharma, and Y. Padwad, "Berberis lycium fruit extract attenuates oxi-inflammatory stress and promotes mucosal healing by mitigating NF-κB/c-Jun/MAPKs signalling and augmenting splenic treg proliferation in a murine model of dextran sulphate sodium-induced ulcerative colitis," *European Journal of Nutrition*, vol. 59, no. 6, pp. 2663–2681, 2020.

[52] W.-T. Kuo, L. Shen, L. Zuo et al., "Inflammation-induced occludin downregulation limits epithelial apoptosis by suppressing caspase-3 expression," *Gastroenterology*, vol. 157, no. 5, pp. 1323–1337, 2019.

[53] R. P. Arasaradnam, K. Khoo, M. Bradburn, J. Mathers, and S. Kelly, "DNA methylation of ESR-1 and N-33 in colorectal mucosa of patients with ulcerative colitis (UC)," *Epigenetics*, vol. 5, no. 5, pp. 422–426, 2010.

[54] K. M. Sakthivel and C. Guruvayoorappan, "Amentoflavone inhibits iNOS, COX-2 expression and modulates cytokine profile, NF-κB signal transduction pathways in rats with ulcerative colitis," *International Immunopharmacology*, vol. 17, no. 3, pp. 907–916, 2013.

[55] X. Bai, G. Bai, L. Tang, L. Liu, Y. Li, and W. Jiang, "Changes in MMP-2, MMP-9, inflammation, blood coagulation and intestinal mucosal permeability in patients with active ulcerative colitis," *Experimental and Therapeutic Medicine*, vol. 20, no. 1, pp. 269–274, 2020.

[56] E. A. Arafa, W. R. Mohamed, D. M. Zaher, and H. A. Omar, "Gliclazide attenuates acetic acid-induced colitis via the modulation of PPAR gamma, NF-kappaB and MAPK signaling pathways," *Toxicology and Applied Pharmacology*, vol. 391, Article ID 114919, 2020.

[57] A. Regeling, F. Imhann, H. H. Volders et al., "HSPA6 is an ulcerative colitis susceptibility factor that is induced by cigarette smoke and protects intestinal epithelial cells by stabilizing anti-apoptotic Bcl-XL," *Biochimica et Biophysica Acta (BBA)-Molecular Basis of Disease*, vol. 1862, no. 4, pp. 788–796, 2016.

[58] Y. Satoh, Y. Ishiguro, H. Sakuraba et al., "Cyclosporine regulates intestinal epithelial apoptosis via TGF-β-related signaling," *American Journal of Physiology-Gastrointestinal and Liver Physiology*, vol. 297, no. 3, pp. G514–G519, 2009.

Hindawi
Evidence-Based Complementary and Alternative Medicine
Volume 2021, Article ID 7677392, 10 pages
https://doi.org/10.1155/2021/7677392

Research Article

Biomarkers and Mechanism Analysis for Polygoni Multiflori Radix Preparata-Induced Liver Injury by UHPLC-Q-TOF-MS-Based Metabolomics

Liming Wang,[1] Zhida Wang,[2] Yanchao Xing,[1] Erwei Liu,[1] Xiumei Gao,[1] Linlin Wang,[3] and Zhifei Fu[1]

[1]*State Key Laboratory of Component-based Chinese Medicine, Tianjin University of Traditional Chinese Medicine, 10 Poyanghu Road, Jinghai, Tianjin 301617, China*
[2]*NHC Key Laboratory of Hormones and Development, Tianjin Key Laboratory of Metabolic Diseases, Chu Hsien-I Memorial Hospital & Tianjin Institute of Endocrinology, Tianjin Medical University, Tianjin 300070, China*
[3]*Second Affiliated Hospital of Tianjin University of Traditional Chinese Medicine, Tianjin 300250, China*

Correspondence should be addressed to Linlin Wang; lynnwlin@yeah.net and Zhifei Fu; fuzhifei@tjutcm.edu.cn

Received 2 September 2021; Accepted 12 October 2021; Published 23 November 2021

Academic Editor: Li-Ping Kang

Background. Polygonum Multiflorum Radix Preparata (PMP), prepared from *Polygonum multiflorum* Thunb. (PM), is traditionally valued for its liver and kidney-tonifying effects. However, the previous studies showed that PMP was hepatotoxic, which limited its clinical use. Unfortunately, the potential hepatotoxic ingredients and the molecular mechanism are still uncertain. *Objective*. The aim of this study was to find out potential biomarkers of hepatotoxicity using metabolomics profile. *Materials and Methods*. 60% ethanol extract of PMP (PMPE) was prepared. Subsequently, an untargeted metabolomics technology in combination with ROC curve analysis method was applied to investigate the alteration of plasma metabolites in rats after oral administration of PMPE (40 g/kg/d) for 28 days. *Results*. Compared to the control group, the significant difference in metabolic profiling was observed in the PMPE-induced liver injury group, and sixteen highly specific biomarkers were identified. These metabolites were mainly enriched into bile acids, lipids, and energy metabolisms, indicating that PMPE-induced liver injury could be related to cholestasis and dysregulated lipid metabolism. *Conclusions*. This study is contributed to understand the potential pathogenesis of PMP-induced liver injury. The metabonomic method may be a valuable tool for the clinical diagnosis of PMP-induced liver injury.

1. Introduction

Polygoni Multiflori (PM, Heshouwu in Chinese), derived from the roots of *Polygonum multiflorum* Thunb., is a widely used Chinese medicinal material in clinic. Raw PM (RPM) has the effects of detoxicating, eliminating carbuncle, cutting off malaria, loosening bowel, and relieving constipation. A few of ancient books of traditional Chinese medicine, such as "ben cao hui yan," recorded that RPM is poisonous [1]. To reduce toxicity and enhance tonic effect, RPM was usually processed by black bean sauce or by nine cycles of steaming and sun drying to obtain the processed PM (PMP) [2]. PMP demonstrates the functions of nourishing the liver, kidney, and blood, strengthening the muscles and bones, and blackens hair [3–6]. Interestingly, RMP steamed with black soybeans for nine cycles was safe. However, modern processing technologies, usually steamed with the black soybean juice once, still exhibit obvious hepatotoxicity [7, 8]. PMP-related liver injury has been reported in many countries and regions, such as South Korea, Japan, and UK [9]. Recently, the National Medical Products Administration in China has also warned of the risk of liver injury from the extracts of RPM and PMP [10]. Unfortunately, although extensive experiments have been performed in recent years, the

potential toxic mechanisms that cause liver injury remain unclear. Therefore, it is particularly urgent and important to establish a method for the early warning of liver injury of PMP.

Metabolome is located downstream of gene regulation and protein network and could provide terminal information of biology. Metabolomics is the study of endogenous metabolite alterations associated with maintaining the normal function and development of organisms after the stimulation or disturbance of biological systems [11]. It has been widely applied in various fields of life sciences and represents a powerful tool for interpreting life phenomena and exploring mechanisms of disease [12]. Chromatography combined with mass spectrometry (such as LC-MS and GC-MS) and nuclear magnetic resonance (NMR) spectroscopy is widely applied in metabolomics studies, and LC-MS is the most popular used methodology in untargeted metabolomics research. Ultrahigh performance liquid chromatography-mass spectrometry technology provides a rapid, concise, and high-throughput approach for the analysis of biological fluids or tissues [13]. Combined with multivariate statistical analysis methods, it provides an effective method for the discovery of metabolic pathways. The targeted and untargeted methods in MS-based metabolomics were used to detect changes in the processing technologies of Polygoni Multiflori Radix [14]. In conclusion, metabolomics has been extensively used for the discovery of biomarkers and the research on the metabolic mechanism [15].

The hepatotoxicity components of PMP have always been the subject of controversy. In our previous study [16], we performed a comparative study on the chemical components in the aqueous extract and 60% ethanol extract of PMP (PMPE). The results showed that the different components were attributed to anthraquinones, such as emodin, rhein, and physcion. Furthermore, the pharmacokinetics characters of these main components in rats were studied. The $t_{1/2(h)}$ of those components of the PMPE was longer compared to the aqueous extract of PMP and increased with the increasing of dosage of PMPE. Anthraquinone components (such as emodin) which has higher content in PMPE are regarded as potential liver damage components [16]. Based on our previous research and literature review, the PMPE showed a degree of hepatotoxicity [4, 16, 17]; therefore, we selected PMPE to investigate the components and mechanism of potential liver injury of PMP. The study aimed to further explore the potential hepatotoxicity mechanism of PMPE using the LC-MS-based metabolomics method. The reliability of discriminated metabolite was further screened by receiver operating characteristic (ROC) curve analysis, and the related metabolic pathways were clarified. Combined with biochemical indicators, our work could further clarify the potential mechanism of PMPE-induced liver injury.

2. Materials and Methods

2.1. Chemicals and Reagents. HPLC grade methanol (ME) and acetonitrile (ACN) were provided by Thermo Fisher Scientific Co., Ltd. (Pittsburgh, PA, USA). Ultrapure water was obtained from Watsons Food&Beverage Co., Ltd. (Guangdong, China). PMP was purchased from Anguo Shengshan Pharmaceutical Co., Ltd. (Hebei, China).

2.2. Sample Preparation. PMP (10 kg) was extracted with 60% ethanol (v/v) to yield 1.7 kg extract (PMPE), stored at 4°C for further use. The main constituents in PMPE were profiled and reported by our previous research [16].

2.3. Animal and Experiment Design. Sprague Dawley (SD) rats (6–8 weeks) were purchased from HFK Bioscience Co., Ltd. (Beijing, China). All animals were kept under the same breeding room conditions with a temperature between 20 and 25°C and given standard laboratory water and food. The procedures involving animals and their care were conformed to the Guiding Principles for the Care and Use of Laboratory Animals of China. The rats were kept in the breeding room for 7 days and then randomly divided into different groups ($n = 7$ for each group).

Animals were randomly divided into the blank control group (BC, equivalent physiological saline) and PMPE treatment group; based on our previous studies [16], the dosage was set at 40 g/kg per day (amount of crude drug weight of rat/day). The clinical syndromes of animals were observed every day. The animal's body weight was monitored once a week after intragastric administration.

Rats were fasted for 12 hours after oral administration of PMPE for 28 days, and blood sample of rat was collected from the abdominal aorta. One part with no anticoagulant samples remained for 2 hours, 3500 × g was centrifuged for 10 min, and then serum was obtained for analysis of the serum biochemical index. The remaining serum with anticoagulant was centrifuged under 3000 × g for 10 min, and finally, the plasma was obtained and frozen in the refrigerator at −80°C for further analysis. The liver of each rat was taken for histological examination, and the organ index was calculated.

2.4. Serum Biochemical Analysis. The serum biochemical indexes, including alanine aminotransferase (ALT), aspartate aminotransferase (AST), total bile acid (TBA), alkaline phosphatase (ALP), total bilirubin (T-BIL), and triglyceride (TG), were measured dynamically using a Hitachi 7020 automatic biochemistry analyzer (Tokyo, Japan).

2.5. Liver Histopathology Assessment. The liver samples were fixed with 10% neutral formalin for 48–72 h, embedded in paraffin after fixation, continuously sectioned at a thickness of 5 μm, stained with hematoxylin and eosin (H&E), and evaluated using a microscope.

2.6. Plasma Preparation and UHPLC/Q-TOF-MS Analysis. An amount of 100 μL of plasma was added into 400 μL of acetonitrile to precipitate protein. All the samples were vortexed for 5 min and centrifuged at 14000 × g for 10 min under 4°C. The supernatant was transferred into 1.5 mL tube

and dried under a nitrogen stream. All samples were redissolved in 100 μL of methanol-water (80 : 20, v/v). Each reconstituted sample was centrifuged at 14000 × g for 10 min under 4°C, and then the supernatant was transferred into sample vials for analysis using UHPLC/Q-TOF-MS. The quality control (QC) samples were prepared by adding equal amounts of all analytes. During the research process, QC was carried out every five samples to verify the stability and accuracy of the system.

LC analysis was conducted on an Agilent 1290 UHPLC system equipped with an ACQUITY UPLC HSS T_3 column (2.1 × 100 mm, 1.8 μm, Waters, Ireland) under the temperature of 35°C. The mobile phase consisted of 0.1% formic acid in water (A) and acetonitrile (B). The gradient of elution conditions was as follows: 0–13 min, 3–100% B, 13–17 min, 100% B. The flow rate was 0.4 mL·min^{-1}, and the injection volume was 2 μL.

The mass spectrometry analysis was performed on an Agilent 6520 Accurate-Mass Q-TOF/MS system. The conditions of the ESI source were drying gas flow rate, 8.0 L·min^{-1}; drying gas temperature, 350°C; nebulizer, 30 psi; capillary voltage (Vcap), 4000 V in positive ion mode, and 3500 V in negative ion mode; fragmentor voltage, 150 V and 175 V in positive and negative ion modes, respectively. Collision energy was 20 V and 40 V, and the scanning range of the mass analyzer was m/z 50–1000.

2.7. MS Data Processing Analysis. Data collection and procession were performed using the following software and databases: Agilent Mass Hunter Workstation software (version B.04.00) and Agilent MSC software (version B.07.00). Metabolites were identified through precise molecular weight, retention time, MS/MS fragmentation, the Metlin database (http://metlin.scripps.edu/index.php), and HMDB database (https://hmdb.ca/). The precursor ion mass tolerance was set to 10 ppm.

All data were normalized using the sum method. Subsequently, multivariate data analysis was conducted using the SIMCA-P (V 14.1, Umetrics, Sweden), including principal component analysis (PCA), partial least squares discriminant analysis (PLS-DA), and orthogonal partial least squares discriminant analysis (OPLS-DA). Permutation test was used to evaluate whether the established model was overfitting. A cross-validated analysis of variance was used to evaluate the reliability of the OPLS-DA model.

2.8. Statistical Analysis. All data were expressed as mean ± standard deviation, and the data were analyzed using GraphPad Prism version 8.01 (GraphPad Software Inc., La Jolla, CA, USA). Student's t-test was used to assign significance ($p < 0.05$).

3. Results

3.1. Clinical Observation after Treatment of PMPE. Compared with the BC group, the weekly growth of the body weight in PMPE-treated rats significantly reduced (Figure 1(a)), whereas the liver index of PMPE-treated rats significantly increased ($p < 0.05$) (Figure 1(b)). Liver pathology revealed liver cell degeneration, necrosis, and inflammatory cell infiltration after administration PMPE (Figure 1(c)).

3.2. Hepatotoxicity Assessment of the PMPE. Compared with the BC group, the levels of ALP, TAB, and TBIL increased significantly ($p < 0.05$), and the content of ALT, TG, and AST also showed increasing tendency (Figure 2).

3.3. Metabolomic Profile Analysis of PMPE-Induced Liver Injury. A total of 1827 and 992 features in plasma were extracted in the positive and negative ion mode, respectively. A representative plasma total ion current (TIC) chromatogram of the blank control group and the PMPE group are shown in Supplementary Figure S1.

3.4. Precision and System Stability Analysis. In order to estimate the precision and stability of the analytical method, QC samples were included into the entire analysis process, and the peak areas of the 6 characteristic ions were selected as evaluation indicators. As shown in Supplementary Table S1, the relative standard deviation (RSD) values of the peak area of the six characteristic ions of the QC samples were all less than 10%.

3.5. Identification of Potential Liver Injury Biomarker and Pathway Analysis. PCA was used for visualizing group clustering and visualizing possible outliers. The BC group and PMPE group were obviously separated in the positive and negative ion mode (positive: $R^2 = 0.433$, $Q^2 = 0.177$; negative: $R^2 = 0.559$, $Q^2 = 0.344$), indicating that there was a significant difference between the BC and the PMPE groups (Figure 3). PLS-DA and permutation analysis were performed to evaluate the reliability of the model (positive: $R^2 = 0.487$, $Q^2 = 0.96$; negative: $R^2 = 0.605$, $Q^2 = 0.99$). The model validation of PLS-DA was performed at 200 permutations analysis (Supplementary Figure S1), and the results indicated that the PLS-DA model was credible and had no overfitting. OPLS-DA was carried out to reveal the differences of metabolites among groups as a supervised classification analysis method (positive: $R^2 = 0.568$, $Q^2 = 0.952$; negative: $R^2 = 0\ .605$, $Q^2 = 0.987$). Scatter plots and S-plot are shown in Figure 4. Variable important in projection (VIP) was used to evaluate the strength and explanatory power of the expression pattern of metabolites on the classification and discrimination of each group of samples. Differential metabolites were screened according to the VIP (VIP > 1.0) and P values of Student's t-test ($p < 0.05$). A total of 342 differential characteristic ions from positive and negative ion patterns were selected. Based on the exact molecular ion mass, retention time of reference compounds, and metabolites database (METLIN, LIPID MAPS, and HMDB database), a total of 39 metabolites were identified as biomarker candidates of PMPE-induced liver injury finally. All candidate biomarkers were presented in Supplementary Table S2.

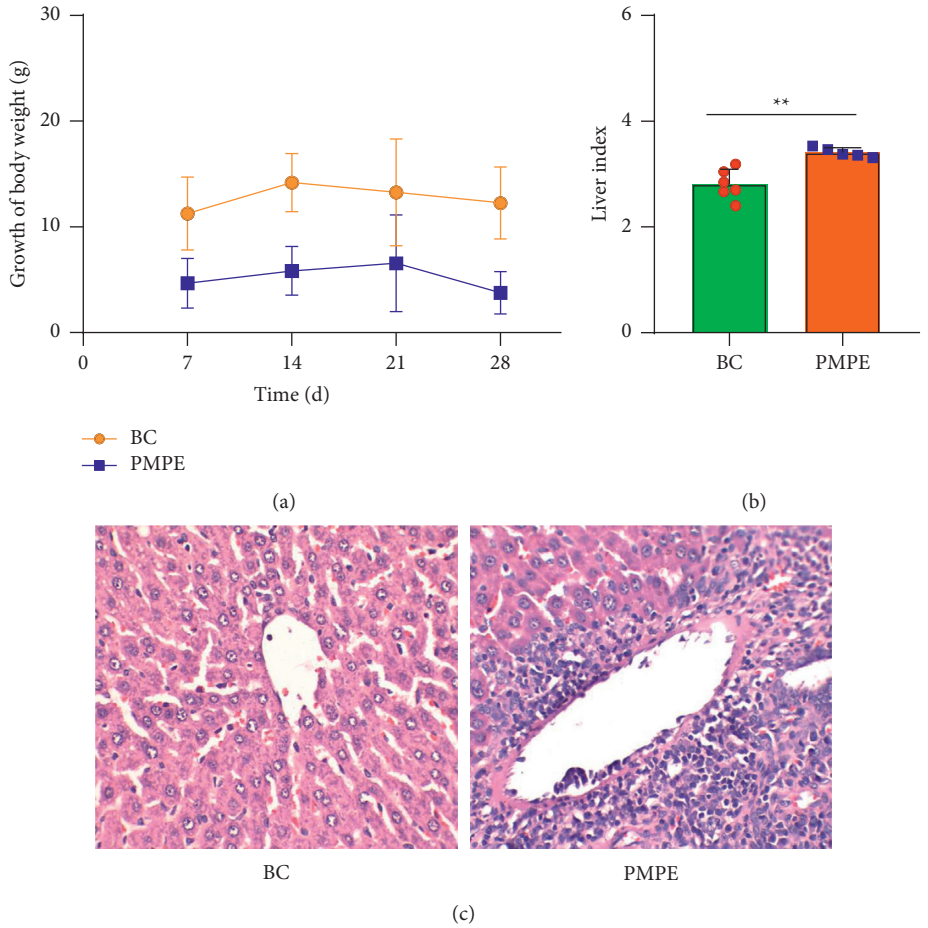

Figure 1: The weight curve within 28 days of rats (a), liver index (b), and (c) Pathological sections of liver of rats after 28 days of administration of 60% ethanol extract of PMP (400 times under light microscope) in Blank Control (BC) and 60% ethanol extract of PMP (PMPE) groups $^{*}p < 0.05$, compared with the control group, $^{**}p < 0.01$, compared with the control group.

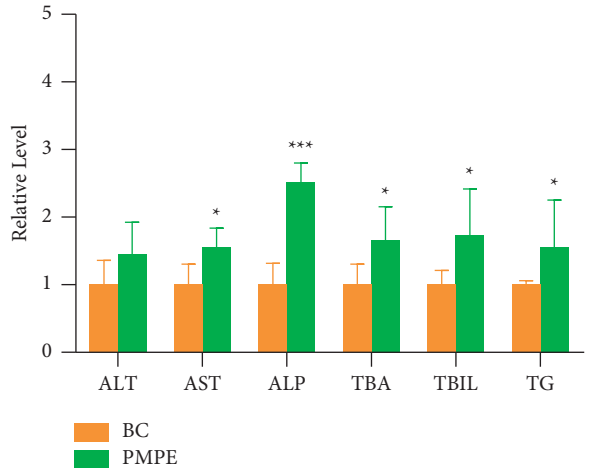

Figure 2: Serum relative levels of ALT, AST, ALP, TG, TBA, and TBIL in BC and PMPE groups, $^{*}p < 0.05$, $^{***}p < 0.0001$ compared with the control group. ALT, alanine aminotransferase; AST, aspartate aminotransferase; ALP, alkaline phosphatase; TG, triglyceride; TBA, total bile acid; TBIL total bilirubin.

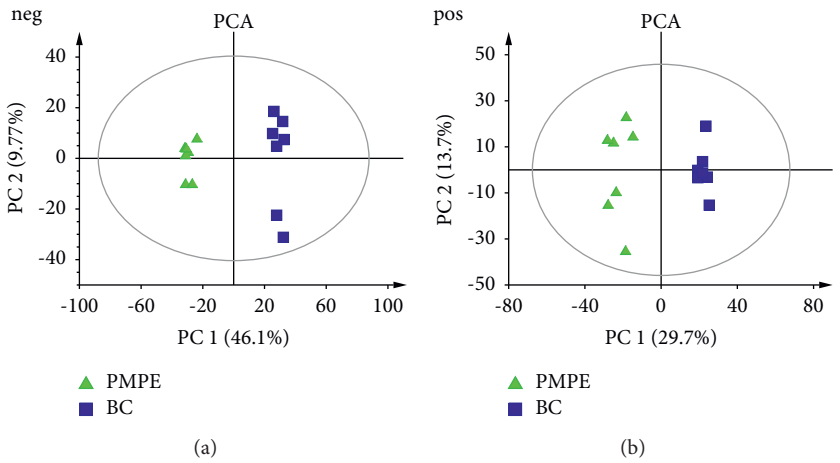

Figure 3: PCA score plots of the LC-MS spectra from plasma. Negative (left) and Positive (right).

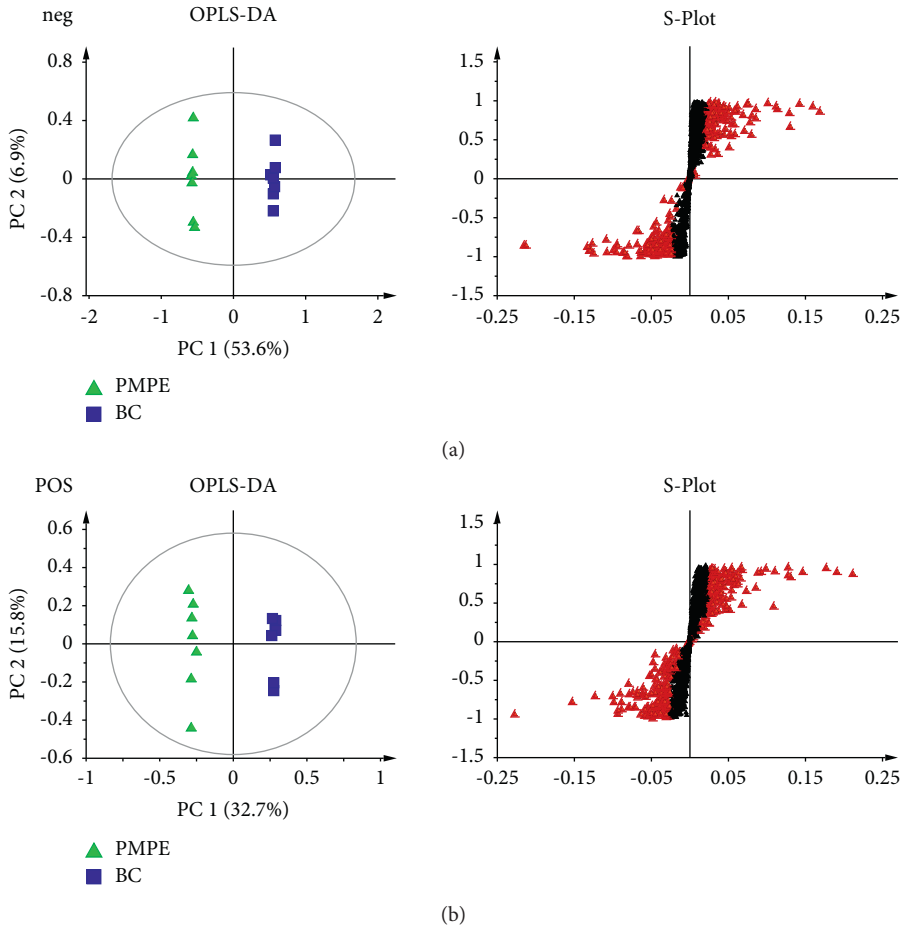

Figure 4: OPLS-DA analysis (left) and S-Plot (right) of the rat plasma from LC–MS spectra negative mode and positive mode.

The ROC curves were performed for the analysis of sorting out the potential diagnostic metabolites with high specificity and sensitivity to distinguish between the BC and PMPE groups. The diagnostic values were assessed by the area under the ROC curve (AUC), which was carried out using GraphPad Prism (version 8.0 San Diego, USA). The AUCs of candidate liver injury biomarkers which were higher than 0.8 were regarded as potential biomarkers (Figure 5 and Supplementary Table S3). The results manifested that these biomarkers had better discrimination ability for healthy rats and liver injury rats. A total of 16 potential biomarkers were reconfirmed from the positive

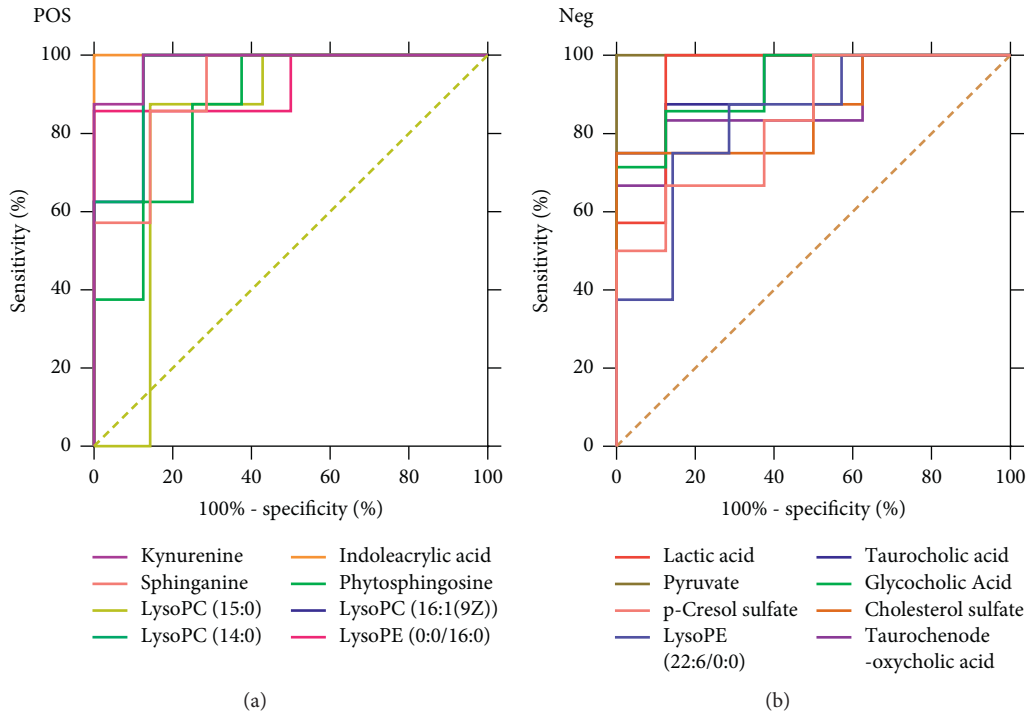

Figure 5: Potential biomarker ROC curve analysis. Positive (left) and Negative (right).

and negative ion patterns in rat plasma (8 for negative and 8 for positive). Potential biomarkers are summarized in Table 1. Six metabolites were significantly decreased in the PMPE group compared with those in the BC group, including kynurenine, lactic acid, pyruvate, sphinganine, phytosphingosine, and indoleacrylic acid (Figure 6).

To further elucidate the metabolic pathways of specific metabolites associated with PMPE-induced liver injury, we used the MetaboAnalyst4.0 (https://www.metaboanalyst.ca/) for enrichment and topological analysis of the KEGG signaling pathway. The most affected metabolic pathways were primary bile acid biosynthesis, sphingolipid metabolism, energy metabolism, glycerophospholipid metabolism, and tryptophan metabolism (Figure 7 and Supplementary Figure S2). In order to exhibit the results clearly, we constructed a network of potential metabolic pathways based on biomarkers in rat plasma (Figure 8).

4. Discussion

Biliary cholestasis and bile duct injury are the main clinical manifestations of cholestasis caused by drugs. Serum biochemical parameters ALP is preferred in clinical diagnosis. According to the above results, the levels of ALP, TBA, and TBIL showed significantly increased accompanied by liver cell degeneration, necrosis, and inflammatory cell infiltration, indicating that the PMPE-induced hepatotoxicity may be related to cholestasis. Meanwhile, the levels of taurochenodeoxycholic acid, taurocholic acid, and glycocholic acid were significantly increased in plasma of hepatotoxicity rats. Pathway enrichment and topology analysis also indicated that the biosynthesis pathway of bile acids was disrupted or interfered. In the process of generation, formation, transportation, and discharge of bile acid, any failure in those steps could cause cholestasis. Bile acid, especially hydrophobic toxic bile acids accumulation in liver cells, could induce inflammatory reactions by damaging mitochondria and lead to endoplasmic reticulum stress. These changes could directly destroy membranes of cell and organelle by virtue of detergent action and lead to hepatocyte injury finally. When hepatocytes are damaged, bile acid metabolism is impaired and reversely flows into blood [18, 19]. These explain the mechanisms of serum TBA increased in rat with PMPE-induced liver injury.

As the endogenous ligand of FXR (farnesoid X receptor), bile acid is not only an important substance in lipid digestion and absorption but also serves as a signal molecule to transmit information through FXR-mediated signaling pathways and participate in the regulation of lipid metabolism in the body. FXR could monitor the metabolism of triglycerides and fatty acids through a variety of mechanisms. Generally, when FXR was activated by bile acids, SREPB-1c (sterol regulatory element-binding protein-1c), which is a major transcription factor involved in fat synthesis genes, was downregulated by SHP (recombinant small heterodimer partner) signal pathway in order to inhibit lipid synthesis. The activity of LDLR (low-density lipoprotein receptor) and VLDLR (very low-density lipoprotein receptor) was upregulated to increase lipid oxidation consumption and reduced lipid accumulation in the liver thereby [20]. Thus, lipids will accumulate in the liver when the activity of FXR was downregulated in the condition of disordered intrahepatic bile acid metabolism.

Table 1: Biomarker candidates of PMPE-induced liver injury.

	VIP	FC	m/z	Formula	Biomaker	HMDB	KEGG	*P*-value
Pos	4.98	0.72	188.06905	$C_{11}H_9NO_2$	Indoleacrylic acid	HMDB00734	-	5.62E-05
	1.99	0.47	209.09043	$C_{10}H_{12}N_2O_3$	Kynurenine*	HMDB0000684	C00328	2.84E-04
	1.41	0.79	302.30336	$C_{18}H_{39}NO_2$	Sphinganine	HMDB0000269	C00836	4.11E-02
	1.62	0.76	318.29862	$C_{18}H_{39}NO_3$	Phytosphingosine	HMDB0004610	C12144	3.47E-02
	1.62	1.82	454.29073	$C_{21}H_{44}NO_7P$	LysoPE(0 : 0/16 : 0)	HMDB0011473	-	1.10E-02
	2.62	2.58	468.30649	$C_{22}H_{47}NO_7P$	LysoPC(14 : 0)	HMDB0010379	C04230	2.33E-03
	1.07	1.65	482.32192	$C_{23}H_{48}NO_7P$	LysoPC(15 : 0)	HMDB0010381	C04230	4.79E-03
	3.74	2.35	494.32224	$C_{24}H_{49}NO_7P$	LysoPC(16 : 1(9Z))	HMDB0010383	C04230	4.65E-02
Neg	1.39	0.30	87.00888	$C_3H_4O_3$	Pyruvate*	HMDB0000243	C00022	3.10E-07
	5.7	0.47	89.02465	$C_3H_6O_3$	Lactic acid	HMDB0000190	C00256	1.02E-02
	2.49	1.54	187.00644	$C_7H_8O_4S$	p-Cresol sulfate	HMDB11635	C06677	4.23E-02
	2.05	2.38	464.30076	$C_{26}H_{43}NO_6$	Glycocholic acid	HMDB0000138	C01921	1.22E-02
	1.14	2.30	465.30223	$C_{27}H_{46}O_4S$	Cholesterol sulfate	HMDB0000653	C18043	1.42E-02
	2.33	1.80	496.27305	$C_{26}H_{45}NO_7S$	Taurocholic acid	HMDB0000036	C05122	3.02E-02
	3.8	2.23	498.28706	$C_{26}H_{45}NO_6S$	Taurochenodeoxycholic acid	HMDB0000951	C05465	3.30E-02
	1.05	1.50	524.27794	$C_{27}H_{44}NO_7P$	LysoPE (22 : 6/0 : 0)	HMDB0011526	-	6.14E-03

Pos: positive; Neg: negative; FC: fold change; HMDB: human metabolome database; KEGG: Kyoto encyclopedia of genes and genomes. *: compared with the reference standards.

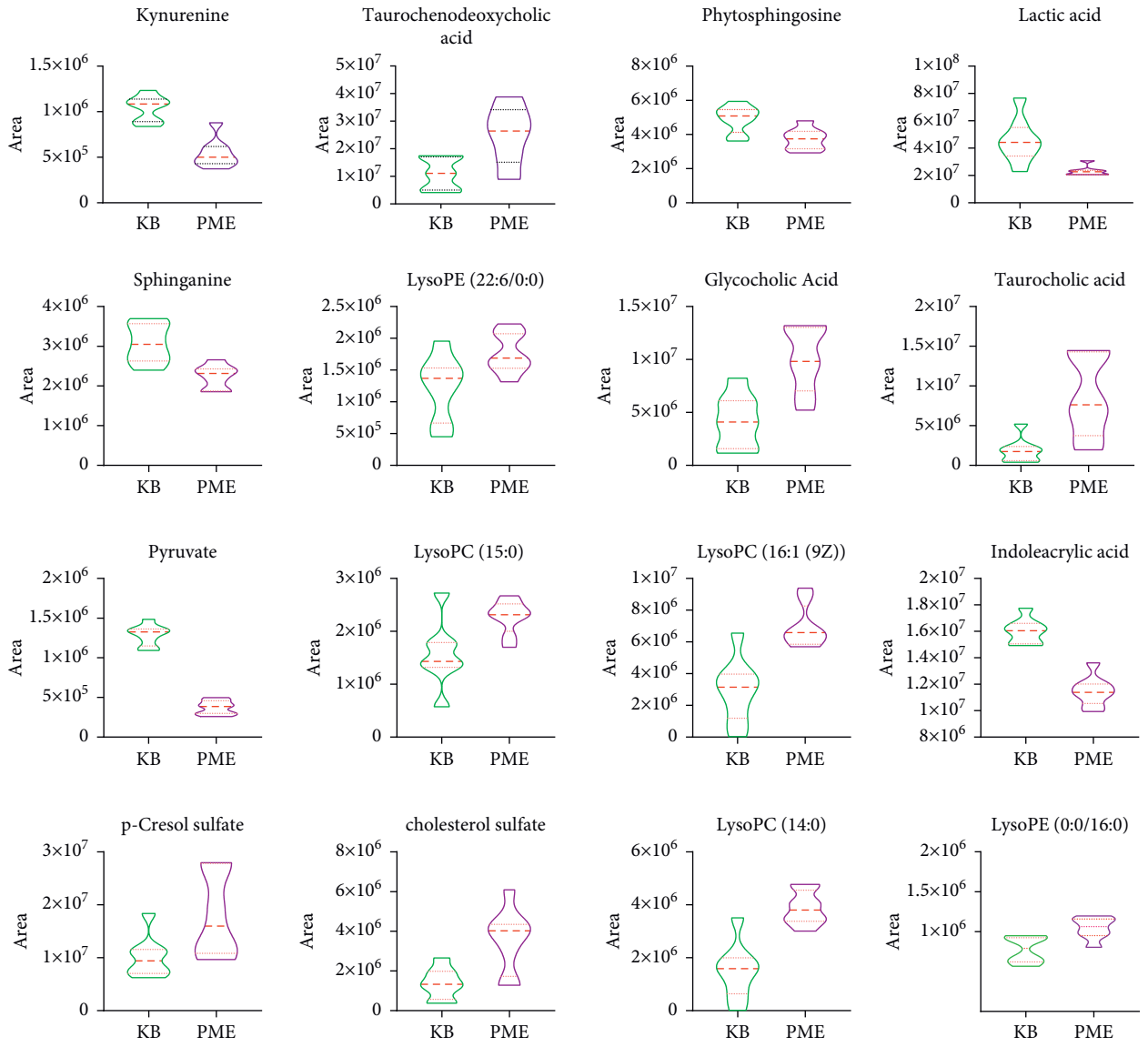

Figure 6: The relative level of potential biomarker content.

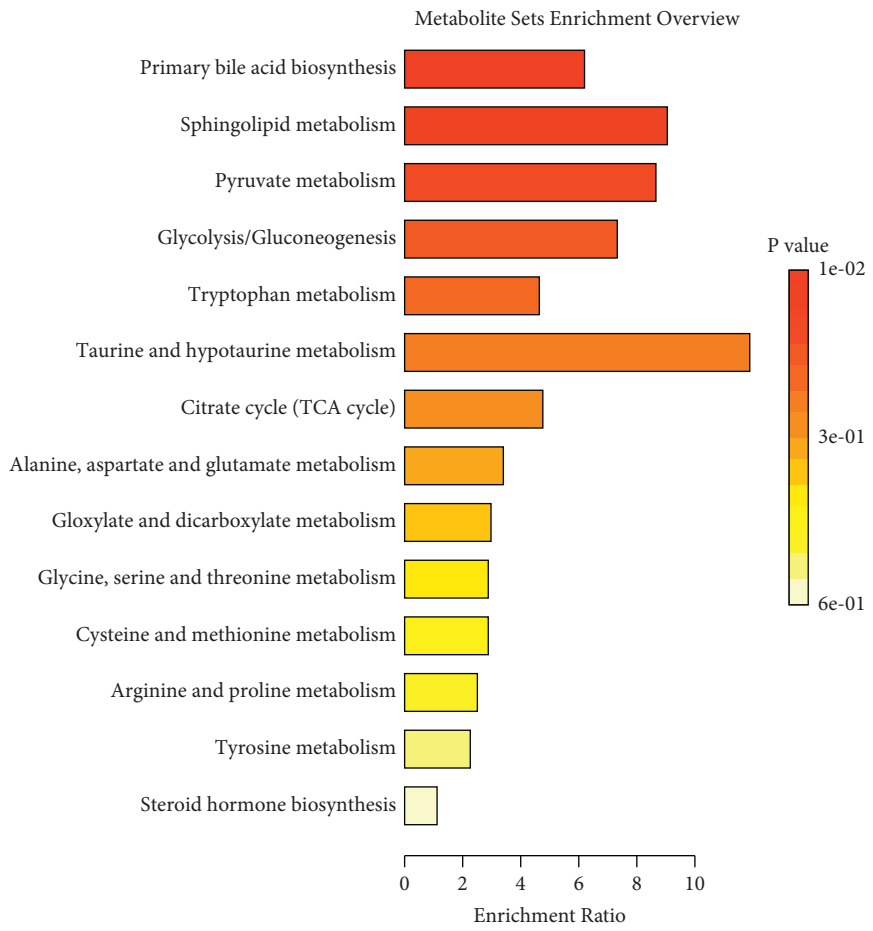

Figure 7: Differential metabolites pathway enrichment analysis of PMPE-induced liver injured.

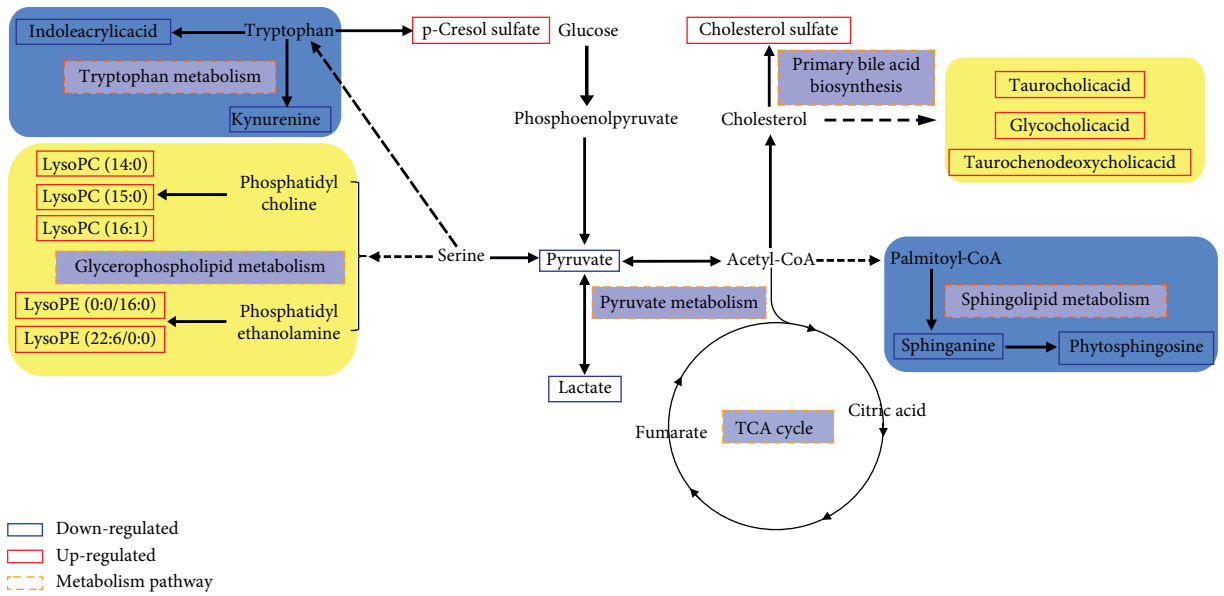

Figure 8: Potential metabolic pathway of PME-induced liver injured.

Phosphatidylcholine (PC) and phosphatidylethanolamine (PE), two most affluent glycerophospholipids, play a pivotal biological function in regulating lipoprotein metabolism [21]. They can be metabolized by phospholipase A2 (PLA2) into LPC (lysophosphatidylcholine), LPE (lysophosphatidylethanolamine), and arachidonic acid, which plays a very important role in lipid inflammation [22]. Metabolic disorders of these lipids result in changes in membrane lipid composition and affect the physical properties and functional integrity of the membrane. These could lead to hepatocellular apoptosis, inflammation, and the progression of liver disease. In addition, studies have reported that LPC has a certain proinflammatory function and is a new type of inflammatory lipids [23]. The experimental studies *in vivo* have shown that LPC can induce hepatitis which is harmful to the liver. It can also induce hepatocyte lipid apoptosis by activating GPCRs (G protein-coupled receptors) and depolarization of mitochondrial membrane [24]. Many researches have shown that the incubation of primary hepatocytes with LPC could induce cell death by apoptosis [25]. In our study, LPC and LPE were the most increased lipids in the oral administration group of PME, and the accumulation of these metabolites caused hepatocyte dysfunction. Sphingolipids are an important ingredient of the biofilm structure. As the important active molecules in organisms, sphingolipids and their metabolites have been identified as new biomarkers of chronic hepatopathy disease and hepatocellular carcinoma (HCC) [26].

As the site of gluconeogenesis and glycogen synthesis, the liver plays an important role in regulating blood sugar levels. Bile acids could regulate glucose metabolism through FXR-SHP or bile acid-TGR5 (Takeda G protein-coupled receptor 5) signal pathway [27]. Some representative important metabolites related to energy metabolism and tryptophan metabolism were detected in this study, such as pyruvic acid, lactic acid, kynurenine, and indoleacrylic acid. These metabolites were significantly reduced. The low level of kynurenine is closely related to abnormal liver function and energy metabolism. It has been reported that drug-induced liver injury is related to the mitochondrial function and energy homeostasis [28]. Moreover, the decrease of indoleacrylic acid is related to the disorder of tryptophan metabolism in the liver. The parallels with our findings are striking. These results indicated that liver injury affected the disorder of these metabolic pathways. In conclusion, all results indicated that PMP affected metabolic disorder of bile acids, lipids, and glucose metabolism; impaired liver function; and could induce liver injury finally.

Compared with the control group, the content of p-cresol sulfate in the PME group was significantly increased. Cholesterol sulfate is a representative substance of uremic toxin produced by tyrosine. The results suggested that the kidney may be damaged in different degrees, which may be attributed to the aggravation of kidney metabolism after liver injury. In addition, the disorder of bilirubin metabolism and blood circulation could also lead to renal function decline (hepatorenal syndrome) [29].

5. Conclusion

In summary, LC-MS-based plasma metabolomics analysis combined with ROC curve analysis method provides an integrated view of the metabolic features of PMP-induced hepatoxicity. The differential metabolites were identified. Metabolic pathway analysis indicated that the bile acid biosynthesis pathway was the main pathways affected by PMP, which may be the cause of liver injury. The sphingolipid metabolism, energy metabolism, glycerophospholipid metabolism, and tryptophan metabolism pathway were also involved. These discriminating metabolites may help to understand the pathogenesis of liver injury and provide a good prospect for the clinical diagnosis of PMPE-induced liver injury.

Abbreviations

PMP:	Polygonum Multiflorum Radix Preparata
PM:	Polygoni Multiflori
PMPE:	60% ethanol extract of PMP
ROC:	Receiver operating characteristic
UHPLC-Q-TOF-MS:	Ultrahigh performance liquid chromatography coupled with quadrupole time-of-flight mass spectrometry
QC:	Quality control
RSD:	Relative standard deviation.

Data Availability

Data are available from the corresponding author upon request.

Conflicts of Interest

The authors declare that they have no conflicts of interest.

Authors' Contributions

Liming Wang and Zhida Wang contributed equally to this work. They performed the experiment and wrote the manuscript. Yanchao Xing analyzed the data. Erwei Liu and Xiumei Gao revised the manuscript. Manuscript editing and review were performed by Linlin Wang and Zhifei Fu. All authors read and approved the final manuscript.

Acknowledgments

This work was supported by the Innovation Team and Talents Cultivation Program of National Administration of Traditional Chinese Medicine (ZYYCXTD-C-202009), National Key R&D Program of China (2018YFC1704500), Important Drug Development Fund, Ministry of Science and Technology of China (2019ZX09201005-002-007), Science and Technology Program of Tianjin, China (19ZYPTJC00060), and Education Commission Research Program of Tianjin, China (2019KJ079).

Supplementary Materials

Table S1: the relative standard deviation (RSD) values of the peak area of the six characteristic ions of the QC samples.

Table S2: biomarker candidates of PMPE-induced liver injury in positive and negative mode. Table S3: the AUC values of candidate liver injury biomarkers. Figure S1: TIC of the LC-MS spectra, PLS-DA analysis, and permutations analysis in negative mode and positive mode. Figure S2: analysis of metabolic pathways related to liver injury. (*Supplementary Materials*)

References

[1] H. Yu, L. Wang, Y. He et al., "Advances in the study of the potential hepatotoxic components and mechanism of polygonum multiflorum," *Evidence-based Complementary and Alternative Medicine*, vol. 2020, Article ID 6489648, 12 pages, 2020.

[2] China Pharmacopoeia Committee, *Pharmacopoeia of the People's Republic of China*, China Pharmacopoeia Committee, Beijing, China, 2020.

[3] L. Lin, B. Ni, H. Lin et al., "Traditional usages, botany, phytochemistry, pharmacology and toxicology of Polygonum multiflorum Thunb.: a review," *Journal of Ethnopharmacology*, vol. 159, pp. 158–183, 2015.

[4] T. Teka, L. Wang, J. Gao et al., "Polygonum multiflorum: recent updates on newly isolated compounds, potential hepatotoxic compounds and their mechanisms," *Journal of Ethnopharmacology*, vol. 271, Article ID 113864, 2021.

[5] J. Y. Shin, Y.-H. Choi, and J. Kim, "Polygonum multiflorum extract support hair growth by elongating anagen phase and abrogating the effect of androgen in cultured human dermal papilla cells," *BMC Complementary Medecine Therapies*, vol. 20, no. 1, p. 144, 2020.

[6] M. Han, J. Lu, G. Zhang et al., "Mechanistic studies on the use of polygonum multiflorum for the treatment of hair graying," *BioMed Research International*, vol. 2015, Article ID 651048, 8 pages, 2015.

[7] H. Wang and X. Li, "Clinical analysis of 33 cases of drug induced liver injury caused by Polygonum multiflorum Thunb and its preparations," *Chinese Journal of Integrated Traditional and Western Medicine on Liver Diseases*, vol. 28, no. 1, pp. 25–27, 2018.

[8] Y. Zhu, Y. Li, Y. Wang et al., "Analysis of clinical characteristics in 595 patients with Herb-induced liver injury," *Chinese Journal of Integrated Traditional and Western Medicine*, vol. 36, no. 1, pp. 44–48, 2016.

[9] J. Hoofnagle, J. Serrano, and J. Knoben, "LiverTox: a website on drug-induced liver injury," *Hepatology*, vol. 57, no. 3, pp. 873-874, 2013.

[10] National Medical Products Administration, *ZTZL-2014-10354. 2014 -07-16*, National Medical Products Administration, Beijing, China, 2014.

[11] A. C. Schrimpe-Rutledge, S. G. Codreanu, S. D. Sherrod, and J. A. McLean, "Untargeted metabolomics strategies—challenges and emerging directions," *Journal of the American Society for Mass Spectrometry*, vol. 27, no. 12, pp. 1897–1905, 2016.

[12] F. R. Pinu, D. J. Beale, A. M. Paten et al., "Systems biology and multi-omics integration: viewpoints from the metabolomics research community," *Metabolites*, vol. 9, no. 4, p. 76, 2019.

[13] S. Forcisi, F. Moritz, B. Kanawati et al., "Liquid chromatography–mass spectrometry in metabolomics research: mass analyzers in ultra high pressure liquid chromatography coupling," *Journal of Chromatography A*, vol. 1292, pp. 51–65, 2013.

[14] L. Liang, J. Xu, W. Zhou et al., "Integrating targeted and untargeted metabolomics to investigate the processing chemistry of Polygoni Multiflori Radix," *Frontiers in Pharmacology*, vol. 9, p. 934, 2018.

[15] Y. Huang, X. Zhao, Z. Zhang, S. Chen, S. Li, and Z. Shi, "Metabolomics profiling and diagnosis biomarkers searching for drug-induced liver injury implicated to polygonum multiflorum: a cross-sectional cohort study," *Frontiers in Medecine*, vol. 7, Article ID 592434, 2020.

[16] L. Wang, M. Sang, E. Liu et al., "Rapid profiling and pharmacokinetic studies of major compounds in crude extract from Polygonum multiflorum by UHPLC-Q-TOF-MS and UPLC–MS/MS," *Journal of Pharmaceutical and Biomedical Analysis*, vol. 140, pp. 45–61, 2017.

[17] Y. Xing, L. Wang, C. Wang et al., "Pharmacokinetic studies unveiled the drug-drug interaction between trans-2,3,5,4'-tetrahydroxystilbene- 2-O-β-d-glucopyranoside and emodin that may contribute to the idiosyncratic hepatotoxicity of Polygoni Multiflori Radix," *Journal of Pharmaceutical and Biomedical Analysis*, vol. 164, pp. 672–680, 2019.

[18] Q. Dong, N. Li, Q. Li et al., "Screening for biomarkers of liver injury induced by Polygonum multiflorum: a targeted metabolomic study," *Frontiers in Pharmacology*, vol. 6, p. 217, 2015.

[19] D. Sokolovic, J. Nikolic, G. Kocic, T. Jevtovic-Stoimenov et al., "The effect of ursodeoxycholic acid on oxidative stress level and DNase activity in rat liver after bile duct ligation," *Drug and Chemical Toxicology*, vol. 36, no. 2, pp. 141–148, 2013.

[20] B. Goodwin, S. Jones, R. Price et al., "A regulatory cascade of the nuclear receptors FXR, SHP-1, and LRH-1 represses bile acid biosynthesis," *Molecular Cell*, vol. 6, no. 3, pp. 517–526, 2000.

[21] G. Drin, "Topological regulation of lipid balance in cells," *Annual Review of Biochemistry*, vol. 83, pp. 51–77, 2014.

[22] E. A. Dennis and P. C. Norris, "Eicosanoid storm in infection and inflammation," *Nature Reviews Immunology*, vol. 15, no. 8, pp. 511–523, 2015.

[23] S. Law, M. Chan, G. K. Marathe, F. Parveen, C. Chen, and L. Ke, "An updated review of lysophosphatidylcholine metabolism in human diseases," *International Journal of Molecular Sciences*, vol. 20, no. 5, p. 1149, 2019.

[24] V. B. O'Donnell, J. Rossjohn, and M. J. O. Wakelam, "Phospholipid signaling in innate immune cells," *Journal of Clinical Investigation*, vol. 128, no. 7, pp. 2670–2679, 2018.

[25] K. Kakisaka, S. Cazanave, C. Fingas et al., "Mechanisms of lysophosphatidylcholine-induced hepatocyte lipoapoptosis," *American Journal of Physiology - Gastrointestinal and Liver Physiology*, vol. 302, no. 1, pp. 77–84, 2012.

[26] A. D. Patterson, O. Maurhofer, D. Beyoğlu et al., "Aberrant lipid metabolism in hepatocellular carcinoma revealed by plasma metabolomics and lipid profiling," *Cancer Research*, vol. 71, no. 21, pp. 6590–6600, 2011.

[27] D. Duran-Sandoval, B. Cariou, F. Percevault et al., "The farnesoid X receptor modulates hepatic carbohydrate metabolism during the fasting-refeeding transition," *Journal of Biological Chemistry*, vol. 280, no. 33, pp. 29971–29979, 2005.

[28] M. Cuykx, C. Beirnaert, R. Rodrigues, K. Laukens, T. Vanhaecke, and A. Covaci, "Untargeted liquid chromatography-mass spectrometry metabolomics to assess drug-induced cholestatic features in HepaRG® cells," *Toxicology and Applied Pharmacology*, vol. 379, Article ID 114666, 2019.

[29] Y. Yan, N. Shi, X. Han, G. Li, B. Wen, and J. Gao, "UPLC/MS/MS-based metabolomics study of the hepatotoxicity and nephrotoxicity in rats induced by Polygonum multiflorum Thunb," *ACS Omega*, vol. 5, no. 18, pp. 10489–10500, 2020.